Physics Reports 819 (2019) 1–105

Contents lists available at ScienceDirect

Physics Reports

journal homepage: www.elsevier.com/locate/physrep

Network dynamics of coupled oscillators and phase reduction techniques

Bastian Pietras [a,b,1], Andreas Daffertshofer [a,*]

[a] Amsterdam Movement Science & Institute for Brain and Behavior Amsterdam, Faculty of Behavioral and Movement Sciences, Vrije Universiteit Amsterdam, van der Boechorststraat 9, 1081 BT Amsterdam, The Netherlands
[b] Department of Physics, Lancaster University, Lancaster LA1 4YB, United Kingdom

ARTICLE INFO

Article history:
Received 2 July 2018
Received in revised form 11 March 2019
Accepted 4 June 2019
Available online 25 June 2019
Editor: Massimo Vergassola

Keywords:
Oscillator networks
Phase reduction
Synchronization
Collective behavior

ABSTRACT

Investigating the dynamics of a network of oscillatory systems is a timely and urgent topic. Phase synchronization has proven paradigmatic to study emergent collective behavior within a network. Defining the phase dynamics, however, is not a trivial task. The literature provides an arsenal of solutions, but results are scattered and their formulation is far from standardized. Here, we present, in a unified language, a catalogue of popular techniques for deriving the phase dynamics of coupled oscillators. Traditionally, approaches to phase reduction address the (weakly) perturbed dynamics of an oscillator. They fall into three classes. (i) Many phase reduction techniques start off with a Hopf normal form description, thereby providing mathematical rigor. There, the caveat is to first derive the proper normal form. We explicate several ways to do that, both analytically and (semi-)numerically. (ii) Other analytic techniques capitalize on time scale separation and/or averaging over cyclic variables. While appealing for their more intuitive implementation, they often lack accuracy. (iii) Direct numerical approaches help to identify oscillatory behavior but may limit an overarching view how the reduced phase dynamics depends on model parameters. After illustrating and reviewing the necessary mathematical details for single oscillators, we turn to networks of coupled oscillators as the central issue of this report. We show in detail how the concepts of phase reduction for single oscillators can be extended and applied to oscillator networks. Again, we distinguish between numerical and analytic phase reduction techniques. As the latter dwell on a network normal form, we also discuss associated reduction methods. To illustrate benefits and pitfalls of the different phase reduction techniques, we apply them point-by-point to two classic examples: networks of Brusselators and a more elaborate model of coupled Wilson–Cowan oscillators. The reduction of complex oscillatory systems is crucial for numerical analyses but more so for analytical estimates and model prediction. The most common reduction is towards phase oscillator networks that have proven successful in describing not only the transition between incoherence and global synchronization, but also in predicting the existence of less trivial network states. Many of these predictions have been confirmed in experiments. As we show, however, the phase dynamics depends to large extent on the employed phase reduction technique. In view of current and future trends, we also provide an overview of various methods for augmented phase reduction as well as for phase–amplitude reduction. We

* Corresponding author.
E-mail addresses: bastian.pietras@bccn-berlin.de (B. Pietras), a.daffertshofer@vu.nl (A. Daffertshofer).
[1] Current address: Bernstein Center for Computational Neuroscience, 10115 Berlin, Germany and Institute of Mathematics, Technical University Berlin, 10623 Berlin, Germany.

https://doi.org/10.1016/j.physrep.2019.06.001

indicate how these techniques can be extended to oscillator networks and, hence, may allow for an improved derivation of the phase dynamics of coupled oscillators.

Contents

List of Symbols

$\mathbb{N}$	Set of positive integers
$\mathbb{R}$	Set of real numbers
$\mathbb{C}$	Set of complex numbers
$\mathbb{S}^1 = \mathbb{T}$	Circle of all phases $[0, 2\pi)$
$\boldsymbol{x}, x, y$	Real-valued state variable (non bold-face = scalar)
z	Complex-valued state variable
$\mathcal{X} \subset \mathbb{R}^n$	State space
$n \in \mathbb{N}$	Dimension of state space
$\mathcal{F}$	Vector field
ϕ	Flow
$\boldsymbol{f}, f$	Nonlinear function prescribing the internal dynamics (non bold-face = scalar)
$\boldsymbol{g}, g$	Nonlinear coupling function (non bold-face = scalar)
$\boldsymbol{L}$	Jacobian matrix
$\boldsymbol{J}$	Diagonalized Jacobian
$\lambda = \varrho + i\omega$	Eigenvalues of the Jacobian
μ	Bifurcation parameter

κ	Coupling strength
$\boldsymbol{p}$	Perturbation
t	Time
τ	Slow time
$\mathcal{C}$	Limit cycle
$\boldsymbol{x}^c, x^c, y^c$	State variable on the limit cycle
θ^c	Phase on the limit cycle
R_k	Amplitude of oscillation (radius of the limit cycle)
$\boldsymbol{\rho}_k, r_k$	Amplitude (distance to the limit cycle)
$\mathcal{B}$	Basin of attraction
$\mathcal{I}$	Isochron
$\Theta\colon \mathcal{X} \to \mathbb{S}^1$	(Asymptotic) phase map
θ	Phase
ψ	Phase difference
ω	Natural frequency
$g(\omega)$	Natural frequency distribution
T	Period
$\mathcal{Q}\colon \mathbb{S}^1 \to \mathbb{R}$	Infinitesimal phase response curve
$G\colon \mathbb{S}^1 \times \mathbb{R}^n \to \mathbb{R}$	Phase response function
$\mathbf{Z}\colon \mathbb{S}^1 \to \mathbb{R}^n$	Phase sensitivity function in n real dimensions
$Z\colon \mathbb{S}^1 \to \mathbb{C}$	Phase sensitivity function in one complex dimension
H	Phase interaction function
a_n, b_n	Amplitudes of phase interaction function
$\boldsymbol{C} = \{C_{jk}\}_{j,k}$	Adjacency matrix, where $j, k = 1, \ldots, N$
$N \in \mathbb{N}$	Network size
R	Kuramoto order parameter (real-valued)
Ψ	Mean phase
$w \in \mathbb{C}$	Normal form variable
$M \in \mathbb{N}$	Order of normal form
$\sigma_m = u_m + iv_m$	Coefficients of Hopf normal form
$\alpha, \beta, \gamma, \delta \in \mathbb{C}$	Coefficients of the Hopf normal form of an oscillator network
$\lambda^{\text{intra}}, \lambda^{\text{inter}}$	Eigenvalue associated with intra-, intercluster perturbations
$\boldsymbol{I}_n, Id_n$	Identity matrix in $\mathbb{R}^{n\times n}$
$\bar{z}$	Complex conjugate of complex-valued variable z
$\langle\cdot\rangle$	Temporal average (over one period)
$\langle\cdot,\cdot\rangle$	Inner product on $\mathbb{R}^n$, also used in dot-notation
$[\cdot,\cdot]$	Lie bracket
S^1	Rotation group on $\mathbb{C}^N$
S_N	Permutation group on $\mathbb{C}^N$
$\mathcal{L}$	Linear operator

1. Introduction

Oscillatory behavior of complex networks abounds on all scales. Examples range from pendulum clocks [1] to the interaction between organ pipes [2], from electronic circuits [3] and coupled Josephson junctions [4] to cardiac pacemakers [5] and circadian rhythms [6], from flashing fireflies [7], animal flocking [8], and fish schooling [9] to rhythmic applause [10] and the behavior in social networks [11], from chemical oscillations [12] over biological oscillations [13] to neural oscillations in the human brain [14–17]. Over the years, mesoscopic and macroscopic models have been designed and developed that describe different kinds of interactions between oscillatory systems. Understanding the collective behavior in complex networks and how interaction gives rise to emergent phenomena is as always an urgent topic at the frontiers of all of science, from neurobiology to statistical physics.

Exploring complex networks is an inherently difficult task. The complexity of a network emanates from its structure and its dynamics. The interplay between structural and dynamical complexity complicates an accessible characterization of (the state of) a network. On top of that, the structure, or topology, of a network may change dynamically, adding further to its complexity. But already for a static and non-evolving topology, the dynamics on complex networks may be all but

trivial. The crucial question from a nonlinear dynamics point of view is: how will a network of interacting dynamical systems behave collectively, given the individual (nodal) dynamics and the coupling structure? In this report, we focus on describing, characterizing, and predicting the collective behavior of complex networks whose individual nodes exhibit oscillatory dynamics.

Among the mechanisms that lead to emergent collective dynamics, synchronization certainly plays a major role. The large-scale organization of a complex network occurs as pairs or groups of nodes synchronize their individual dynamics [18–25]. For complex networks of coupled oscillators, the concept of *phase synchronization* has become a paradigm to investigate emergent collective phenomena. The phase dynamics of interacting oscillators are indicative for their synchronization behavior. At the same time, the notion of phase allows for a direct and unique identification of the state of a presumably high-dimensional oscillator in terms of a one-dimensional variable, thus facilitating an analytic approach to the dynamics of complex networks.

Phase synchronization is believed crucial for information processing and information transfer in networks, especially in the human brain [26–31]. A vast amount of literature accumulated about modeling synchronization phenomena of cortical oscillations using network models of phase oscillators [32–40]. The brain is but one field of application for complex networks of coupled phase oscillators. Dörfler and Bullo [41] provided an extensive survey of how phase models have found their way into various other areas relevant in both sciences and engineering; they focused on control systems such as vehicle coordination, electric power networks, and clock synchronization in decentralized networks. The success of the seminal Kuramoto model [12,42–45] underlines the popularity of coupled phase oscillator models across fields.

We will highlight how such Kuramoto-like networks of coupled phase oscillators can be derived from complex oscillator networks. A mathematically rigorous derivation from the underlying dynamics to an accurate phase model can be laborious. For this reason, it is tempting to introduce phase models based on heuristic arguments rather than through rigorous mathematics. By avoiding a careful derivation, however, the phase description of the oscillatory dynamics is, strictly speaking, bereft of its fundamental basis, and the link from the actual dynamics to the phase model may be spurious, rendering the validity of the latter questionable. We advocate a mathematically rigorous phase reduction. It can add to the significance of the network analysis and, more importantly, to its impact in the scientific world.

Phase reduction has traditionally been applied to oscillators subject to (weak) perturbations, e.g., from external sources or through coupling to other oscillators. Describing every oscillator of a network by its associated phase dynamics allows for assessing the collective dynamics in terms of their phase relationships. Phase reduction, however, is arbitrarily more intricate when deriving the phase dynamics of multiple oscillators simultaneously, as in the case of an oscillator network. The literature about phase reduction of coupled oscillators is vast but scattered. As of yet, there is no comprehensive formulation of different approaches and their respective methodologies. Here, we provide an overview over different mathematically sound techniques for the phase reduction of oscillator networks. Using a unified language, we prepare for an insightful comparison between reduction techniques and complement them, when missing, with mathematical proofs, in particular with respect to nonlinear coupling schemes between oscillators. We will guide the reader along different ways how to distill the phase dynamics of oscillator networks and determine their (phase) synchronization properties. By this, we hope to offer an accessible approach to complex networks of coupled oscillators.

Weakly coupled oscillators

Recorded signals from oscillator networks often stand out for their dynamical richness, which is typically manifested in non-trivial or complex macroscopic dynamics. In networks with a given connectivity structure, macroscopic complexity emerges through an interplay of the activity of individual nodes. The interaction between the nodes can hence be considered crucial for the complexity of the network as a whole. To provide a dynamical account of this macroscopic behavior, one typically introduces phases and amplitudes at every node, even if the precise oscillator dynamics are unknown. This dynamics might already be very complicated. But if phase–amplitude interactions are negligible at the nodal level, the respective phase and amplitude dynamics decouple from one another. Then, it suffices to focus on the first and the macroscopic network dynamics can eventually be expressed in terms of nodal phases only. The separation of phase and amplitude dynamics at the nodal level is a typical characteristic of weakly connected networks, or, more specific, *weakly coupled oscillators*. The attribute ‘weak’ implies that at every node, perturbations through external forcing or internal coupling are sufficiently small when compared to the size of the state variable of the unperturbed, single-node dynamics. Large perturbations may induce a qualitative change in the network dynamics beyond mere quantitative adjustments. Weak perturbations allow an oscillator to asymptotically return to its state prior to the perturbation. Put differently, there is a critical strength of perturbation at which the network undergoes a transition from one macroscopic behavior to a qualitatively distinct macroscopic behavior. This critical value is arguably reached whenever a bifurcation in the dynamics occurs in, at least, one of the nodes. Then, dynamical systems theory does no longer allow for describing the node evolution by linear approximation. We will hence assume that this critical perturbation strength will not be exceeded through the coupling with other nodes. That is, the oscillators are weakly coupled.

For illustration, we sketch a network of five weakly coupled oscillators in Fig. 1.1. Every node shows oscillatory behavior in the two-dimensional state variables $\boldsymbol{x}_k = (x_k, y_k) \in \mathbb{R}^2$, $k = 1, \ldots, 5$. For each of the five nodes, we find a closed orbit, the *limit cycle* (depicted in blue), which describes the nodal dynamics in the absence of coupling. The weak coupling between the oscillators will ‘kick’ the dynamics away from the closed orbit, but only so far that the convergence toward

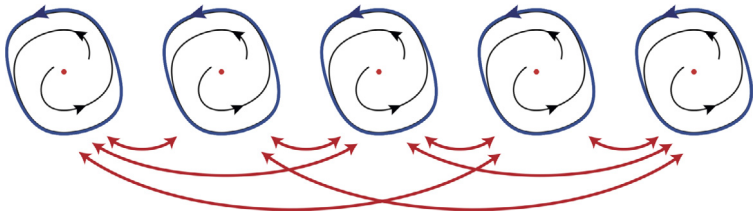

Fig. 1.1. A network of weakly coupled planar limit cycle oscillators. Each oscillator $k = 1, \ldots, N = 5$, is described in the two-dimensional state variables $\boldsymbol{x}_k = (x_k, y_k)$. The coupling between oscillators is indicated by red arrows. Without coupling, each oscillator follows the blue limit-cycle trajectory. Upon perturbation, the oscillator will be kicked away from the limit cycle and follows a trajectory that leads exponentially fast towards the globally attracting limit cycle. Globally attracting implies that the basin of attraction spans the whole x–y plane except for the unstable origin (red). Two trajectories from within the basin of attraction are shown in black.

it is sufficiently fast (see the two exemplary trajectories in black within the limit cycle). This allows for identifying the state of each oscillator $\boldsymbol{x}_k$ with a circular variable, the phase $\theta_k \in \mathbb{S}^1$. Deriving the dynamics $\dot{\theta}_k$ of the phase variables from the network dynamics $\dot{\boldsymbol{x}}_k$ is central to this report. Given the phase dynamics $\dot{\theta}_k$, we can infer the collective behavior of the full network by means of the nodes' phase synchronization.

Throughout this report, we will stay within the framework of weakly coupled oscillators. We briefly sketch why this is beneficial for a concise presentation of the theory, and will properly introduce all required definitions later at due time. The governing dynamics of a network of $N \gg 1$ interacting oscillators shall be of the form

$$\dot{\boldsymbol{x}}_k = \boldsymbol{f}_k(\boldsymbol{x}_k; \mu_k) + \kappa \boldsymbol{g}_k(\boldsymbol{x}_1, \boldsymbol{x}_2, \ldots, \boldsymbol{x}_N) \ , \quad k = 1, \ldots, N. \tag{1.1}$$

The functions $\boldsymbol{f}_k$ determine the node-specific and uncoupled dynamics, whereas $\boldsymbol{g}_k$ comprises all coupling effects on oscillator $\boldsymbol{x}_k$ through the other nodes $\boldsymbol{x}_{j\neq k}$. The coupling strength is denoted by $\kappa \in \mathbb{R}$ and μ_k are bifurcation parameters. We guarantee weak coupling by assuming the coupling strength to be sufficiently small, $\kappa \ll 1$. Furthermore, we assume that the oscillators are nearly identical and that the coupling structure is pairwise, i.e. the coupling function $\boldsymbol{g}_k$ can be decomposed into the sum of pairwise interactions. Hence, one can rewrite (1.1) as

$$\dot{\boldsymbol{x}}_k = \boldsymbol{f}(\boldsymbol{x}_k; \mu) + \kappa \sum_{j=1}^{N} \boldsymbol{g}_{kj}(\boldsymbol{x}_k, \boldsymbol{x}_j) \tag{1.2}$$

with μ being the only bifurcation parameter. Phase reduction implies transforming (1.2) into the phase model

$$\dot{\theta}_k = \omega + \kappa \sum_{j=1}^{N} H_{kj}(\theta_k - \theta_j) \ , \quad k = 1, \ldots, N. \tag{1.3}$$

In particular, the state $\boldsymbol{x}_k$ of every oscillatory node will be characterized by a phase variable θ_k. The corresponding phase dynamics comprises a *natural frequency* term ω and contributions from the other oscillators. The latter add up by means of *phase interaction functions* H_{kj} that depend on the pairwise phase differences $\theta_k - \theta_j$ of oscillators k and j. As we will show, the shape of H_{kj} is decisive for the collective behavior. It is hence crucial to derive the phase interaction function between oscillators with great precision. We will elaborate on derivations of the phase dynamics (1.3) from the network dynamics (1.2). Moreover, we will characterize collective behavior of complex networks by means of phase dynamics. By this, we can ultimately bridge the gap between the dynamics of individual nodes and the emergent synchronization phenomena of interacting oscillators with a given coupling structure.

Phase reductions and weakly coupled oscillators

There already exists abundant literature covering approaches to phase reduction. To name but a few, the textbooks by Hoppensteadt and Izhikevich [46], Izhikevich [47] and Ermentrout and Terman [48] provide thorough mathematical concepts to discuss the dynamics of coupled oscillators in terms of their phases. Yet, it seems that conceptual misunderstandings still prevail when phase reduction is employed to explain observed macroscopic dynamics of an oscillatory network given the underlying micro- and mesoscopic dynamics at the network's nodes. We seek to pinpoint frequent caveats and highlight sensitive issues in the derivation of phase models from both an analytic and numerical point of view. In the following, we will review the details of the most commonly used reduction techniques in a unified language. Subsequently, we will compare their outcomes using two classic examples from the fields where phase reduction was introduced and applied originally: coupled chemical oscillators [12,49–51] and coupled neural oscillators [52–64]; cf. also the review by Schwemmer and Lewis [65] as the introductory chapter to a collection of articles on applications of phase reduction and phase response analysis for neural networks [66]. Specifically, we will consider networks of Brusselators and coupled Wilson–Cowan oscillators.

The Brusselator is an exemplary chemical oscillator and one of the most discussed reaction–diffusion systems [67]. This excitable system displays a broad spectrum of complex phenomena. Despite its rich dynamical behavior, the model is comparably 'easy' to analyze given its polynomial form. As such, the Brusselator serves perfectly to illustrate the benefits and pitfalls of the different phase reduction techniques. The Wilson–Cowan neural mass model [68,69] can be considered a raw model introducing biophysical realism in macroscopic neural dynamics. Its archetypical form has also been applied to model, e.g., gene networks, see [70]. As such, it may be seen as a universal and representative nonlinear model exhibiting complex oscillatory dynamics across disciplines. While the Wilson–Cowan model is often believed to 'just' resemble the Kuramoto model [32,39], we will show that, due to its higher-order nonlinearities, it is a challenge to properly define the corresponding phase dynamics.

Analytic and numerical phase reduction techniques

The different approaches to phase reduction can broadly be classified as analytic and numerical reduction techniques. By and large, numerical approaches tend to approximate the actual phase dynamics better. However, computations rely on software implementations and the relation between the parameters in the underlying oscillator model and those in the resulting phase model may remain unclear. In contrast, analytic approaches can provide a rigorous representation of the model parameters in the reduced phase dynamics. They usually capitalize on generic normal forms in order to extract meaningful phases. It is, hence, essential to first rewrite the dynamics of nonlinear oscillators in a particular dynamic regime in the desired form. We thus complement our report with a review of normal form and center manifold reductions. An immediate and important question, however, arises about the validity of reduced phase models. A useful phase model should provide proper predictions about the network behavior of the underlying model of coupled oscillators. However, and to anticipate our main finding, different phase reduction techniques do not necessarily yield consistent results. While the reduced phase dynamics may differ only quantitatively in some parameter regions, e.g., in close vicinity to a bifurcation boundary, for other parameters these quantitative differences can become large and lead to qualitatively different predictions. Here, we strive for providing instructive answers as to which reduction techniques perform more adequately to describe the macroscopic properties of the network dynamics. In any case, phase reduction techniques always have to be applied with great care, and their choice crucially depends on the particular parameter region and dynamical regime as well as on the targeted macroscopic observable. After a brief historical note, we begin with the phase description of a single oscillator and show how the phase dynamics can be derived. Subsequently, we will extend these ideas to oscillator networks and explicate the various phase reduction techniques.

A historical note

Algorithms to derive the phase dynamics of coupled nonlinear oscillators and their phase interaction function have independently been introduced by Ioel Gil'evich Malkin [46,71,72], by John C. Neu [49–51] and by Bard Ermentrout and Nancy Kopell [53–55]. When implemented numerically, they can be applied to the underlying oscillatory dynamics in a straightforward way. First analytic considerations to determine the phase dynamics of a perturbed nonlinear oscillator go back to Arthur Winfree [73] and Yoshiki Kuramoto [12]. The idea is to distill the characterizing properties of the oscillator in terms of their phase response and thereby tie the effect of the perturbation (e.g., through coupling to another oscillator) to the current state of the oscillator in phase space. Two prevailing analytic techniques of phase reduction are based on the concepts of isochrons and Floquet eigenvectors, respectively. Another analytic technique has been promoted by Peter Ashwin and Ana Rodrigues [74]. It allows to directly deduce the phase model of an oscillator network and is therefore worth being compared against. Building upon equivariant normal form theory, however, it dwells on specific symmetry properties of the network. In order to derive the phase dynamics analytically, it is thus crucial that the underlying oscillatory dynamics have a generic form, a so-called normal form. This can be achieved via center manifold and normal form reductions [75–80]. The oscillations are required to be close to a bifurcation, that is, they can be thought to have emerged via this bifurcation. Seminal for this is a supercritical Hopf bifurcation, where the dynamics can be transformed into an Andronov–Hopf oscillator, also known as a Stuart–Landau oscillator. In fact, there are different methods to obtain the Hopf normal form. We focus on three analytic techniques: a perturbation-based approach introduced by Kuramoto [12], a normal form reduction via nonlinear transforms going back to Henri Poincaré [81] that has been popularized by Yuri A. Kuznetsov [82], and an algebraic approach based on the ideas of Poincaré and Floris Takens [81,83,84].

Normal form reduction is a prerequisite for analytic phase reductions. We will consequently refer to analytic phase reduction techniques as the two-step approaches that retrieve the phase dynamics analytically from the underlying oscillatory dynamics via an intermediate transformation in Hopf normal form. As an alternative to the more elaborate reduction techniques that include normal forms, a more traditional technique is worth of note which dwells on averaging [75,85]. Hermann Haken popularized the combination of a rotating wave approximation and a slowly varying amplitude approximation [86–88], which originally turned out particularly useful in the physics of nonlinear optics, for characterizing the phase dynamics of complex oscillatory networks.

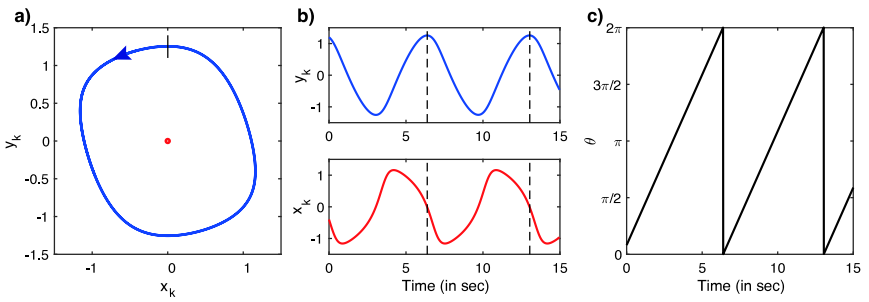

Fig. 2.1. An uncoupled planar limit cycle oscillator. (a) The two-dimensional state variable $\boldsymbol{x}_k = (x_k, y_k)$ follows a closed periodic orbit in the x–y plane, the oscillator's limit cycle. (b) The state variables $x_k(t) = x_k(t+T)$ and $y_k(t) = y_k(t+T)$ are periodic in time. (c) The corresponding phase θ of the oscillator increases monotonically between 0 and 2π during one period T. We choose a reference point on the limit cycle where the value of y_k is maximal, see the dashed lines in (a) and (b). Whenever the oscillatory crosses this point, the phase is reset to $\theta = 0$.

Outline

We will start with the phase dynamics of a single oscillator and introduce all definitions necessary for an adequate phase description of oscillatory dynamics in Section 2. In Section 3, we present the commonly used phase reduction techniques. As analytic phase reduction techniques crucially rely on generic forms of the underlying dynamics, we highlight the link between phase reductions and normal forms in Section 4. Particular emphasis lies on Hopf normal forms and their reduction. We complement the section with an exemplary application of the previously presented phase reduction techniques to a single oscillator in Hopf normal form.

Next, we address phase reduction of complex oscillatory networks. After a brief introduction to networks of coupled oscillators, Section 5 is devoted to a comprehensive description of oscillator networks in terms of phase variables. We outline how collective behavior of oscillator networks can be characterized and assessed in form of their phase synchronization properties. In Section 6, we extend the phase reduction techniques for a single oscillator to networks of coupled oscillators. Malkin's Theorem plays a key role here and deserves its own sub-section. We explicitly distinguish between numerical and analytic phase reduction techniques for oscillator networks. Analytic techniques capitalize on a *network Hopf normal form*, which we will present and motivate in due course. Moreover, we will illustrate phase reductions of an oscillator network in Hopf normal form in great detail. In Section 7, we review two reduction techniques of the Hopf normal form of an oscillator network. These network normal form reductions take up and extend the ideas of Hopf normal form reductions for individual oscillators, and are essential for analytic phase reduction techniques.

For illustration, we apply the presented phase reduction techniques and compare them along two exemplary network models. In Section 8, we study weakly coupled Brusselators. Moving from chemical oscillators to neurobiology, we investigate the phase dynamics of weakly coupled Wilson–Cowan neural masses in Section 9.

Finally, we discuss the main assumptions on phase reduction of complex oscillatory systems in Section 10 and provide an overview over augmented phase reduction and phase–amplitude reduction methods in a unified language in Section 11.

2. Phase and amplitude description of a single oscillator

Oscillatory dynamics manifests through activity that is periodic in time. Such oscillatory behavior can occur on a network level, and at the level of the individual nodes. In this *Section*, we concentrate on a single node that shows oscillatory activity. To illustrate a single oscillator $\boldsymbol{x}_k$ with dynamics in two real dimensions, i.e. $\boldsymbol{x}_k = (x_k, y_k) \in \mathbb{R}^2$, in Fig. 2.1 we depict the (blue) closed orbit in the coordinate plane[2] spanned by the two state variables x_k and y_k. In the absence of coupling or, more general, perturbations, the nodal dynamics will converge towards a stable limit cycle in the x–y plane. The state variables are periodic in time, $x_k(t) = x_k(t+T)$ and $y_k(t) = y_k(t+T)$ for some period $T > 0$. On the limit cycle, one can introduce a phase $\theta^c = \theta^c(t)$ that increases monotonically from 0 to 2π during one period T after which it is reset to zero. Throughout this *Section*, the superscript c indicates that the variables are evaluated exactly on the limit cycle. A perturbation can 'kick' the oscillator away from its limit cycle. If the perturbation is weak enough and the oscillator remains in the so-called basin of attraction of the limit cycle, the oscillator's trajectory will spiral back into the limit cycle; see Fig. 2.2 (panel a). As will be shown below, also in this case a monotonically increasing 2π-periodic phase can be defined that we will denote as $\theta = \theta(t)$.

Next to the phase, one can define an amplitude variable r_k that describes the distance to the limit cycle. Alternatively, we can describe the amplitude R_k of oscillator k as the (Euclidean) distance to the center of oscillation, which we typically

[2] Usually, this coordinate space is called the *phase space*. In two dimensions, it is also referred to as the phase plane of x_k and y_k. However, to avoid confusion between the 'phase as a state' and the 'phase as function of time', we stick to the notion of *coordinate plane*. For the same reason we do not adopt the notion of *phase transitions* but rather refer to 'qualitative changes in macroscopic behavior' to describe the transition from one dynamical regime of the collective dynamics to another.

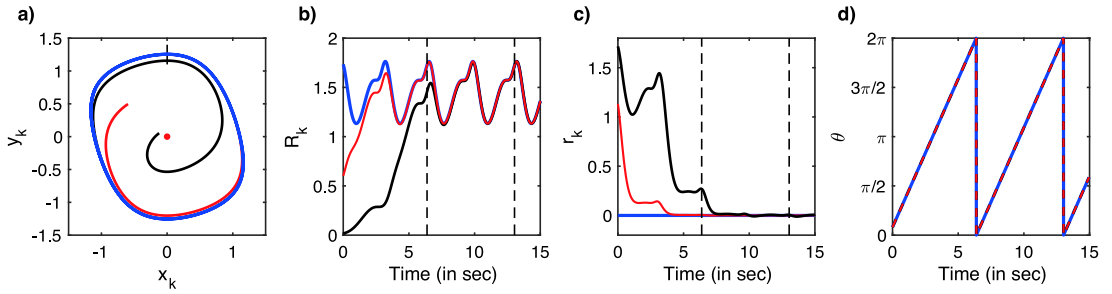

Fig. 2.2. Amplitude and phase description. (a) Two trajectories (black, red) converge to the oscillator's limit cycle (blue). (b) The amplitudes of oscillation $R_k^2 = x_k^2 + y_k^2$ are the distance from the center. (c) The amplitudes $r_k = R_k^c - R_k$ denote the distance from the limit cycle $\mathcal{C}$. (d) The respective phases θ of the two trajectories coincide for all times $t \geq 0$.

set to the origin, such that $R_k^2 = x_k^2 + y_k^2$; see Fig. 2.2 (panel b). While the amplitude of the limit cycle oscillation R_k^c wobbles steadily around a non-zero value, the amplitude R_k approaches R_k^c after a short transient. Equivalently, the amplitude variable r_k representing the distance to the limit cycle, i.e. $r_k = R_k^c - R_k$, converges to zero as the oscillator reaches the stable limit cycle; see Fig. 2.2 (panel c). One can convert the amplitude variable r_k to the actual amplitude of oscillation R_k and vice versa. In this report, we will use the distance to the limit cycle r_k to describe the amplitude dynamics unless stated otherwise.

Phase and amplitude descriptions can be extended to oscillatory dynamics in more than two dimensions. If oscillators approach their respective limit cycles exponentially fast, one can focus solely on the phase dynamics. The different time scales at which fast amplitudes and rather slow phases evolve allow for time scale separation. If the perturbations are sufficiently weak so that the oscillators will not be too far off the limit cycle trajectory, the amplitude values will converge to their asymptotic value in a fraction of a period; cf. Fig. 2.2. In this case, one may consider the amplitudes constant and approximate them with their asymptotic values. In consequence, one can represent a high-dimensional dynamics at every node by its one-dimensional phase dynamics only. Of course, this greatly facilitates the study of synchronization and other complex collective phenomena in oscillator networks. As the phase description is central to our study, we will first introduce all necessary definitions for establishing an oscillator's phase dynamics.

2.1. Oscillators, phases & isochrons

The form of oscillators may vary substantially within and between networks under study. To define phases of oscillators, the underlying dynamics are required to exhibit self-sustaining limit cycle oscillations. We consider a single oscillator as the dynamical system

$$\begin{aligned} \dot{\boldsymbol{x}} &= \mathcal{F}_x(\boldsymbol{x}, \boldsymbol{p}; \mu) \,, \\ \dot{\boldsymbol{p}} &= \mathcal{F}_p(\boldsymbol{x}, \boldsymbol{p}; \mu) \,, \end{aligned} \tag{2.1}$$

where the vector $\boldsymbol{x} = \boldsymbol{x}(t) \in \mathcal{X} \subset \mathbb{R}^n$ represents the state variables $x_1, x_2, \ldots, x_n \in \mathbb{R}$ that evolve according to a vector field $\mathcal{F}_x$. This dynamics is subject to perturbations $\boldsymbol{p} = \boldsymbol{p}(t) \in \mathbb{R}^n$, whose evolution is governed by a vector field $\mathcal{F}_p$. The parameter $\mu \in \mathbb{R}$ is a general bifurcation parameter that we will drop in this section whenever possible to ease legibility. If we consider merely additive perturbations, the first equation in (2.1) reduces to

$$\dot{\boldsymbol{x}} = \boldsymbol{f}(\boldsymbol{x}) + \kappa \boldsymbol{p}(t) \,, \tag{2.2}$$

where the perturbations are scaled by the parameter $\kappa \in \mathbb{R}$, which is typically considered small. In anticipation of the network dynamics of coupled oscillators, the external perturbations $\boldsymbol{p}$ are given by the intrinsic network coupling.

Oscillators. If a solution $\boldsymbol{x}(t)$ of (2.1) is periodic in time, $\boldsymbol{x}(t) = \boldsymbol{x}(t+T)$ for some constant $T > 0$, then (2.1) describes oscillatory dynamics. For a given vector field $\mathcal{F} = (\mathcal{F}_x, \mathcal{F}_p)$ one can associate the flow $\phi(t)$ determined by $\mathcal{F}$ and starting at some initial state $\boldsymbol{x}_0 \in \mathcal{X}$ with $\boldsymbol{x}(t) = \phi(t; \boldsymbol{x}_0, \boldsymbol{p})$. If (2.1) exhibits a stable time-periodic dynamics without external perturbations, $\boldsymbol{p} \equiv \boldsymbol{0}$, then the dynamical system $\dot{\boldsymbol{x}} = \mathcal{F}_x(\boldsymbol{x}, \boldsymbol{0}) = \boldsymbol{f}(\boldsymbol{x})$ describes an oscillator and the corresponding flow will be denoted by $\boldsymbol{x}(t) = \phi(t; \boldsymbol{x}_0)$.

Limit cycles & basin of attraction. The stable, non-constant, time-periodic solution $\boldsymbol{x}^c(t) = \boldsymbol{x}^c(t+T)$ of an oscillator $\dot{\boldsymbol{x}} = \boldsymbol{f}(\boldsymbol{x})$ follows a trajectory along a closed periodic orbit $\mathcal{C} \subset \mathcal{X}$. This stable periodic orbit is referred to as the oscillator's limit cycle. If we choose an initial condition $\boldsymbol{x}(t_0) = \boldsymbol{x}_0^c \in c$ on the limit cycle, then the unperturbed flow $\phi(t; \boldsymbol{x}_0^c)$ will stay on $\mathcal{C}$ for all times $t \geq t_0$. One can parametrize the limit cycle as the set

$$\mathcal{C} := \left\{ \boldsymbol{x}^c \in \mathcal{X} \mid \boldsymbol{x}^c = \phi(t; \boldsymbol{x}_0^c), \ t \in [0, T) \right\} \,. \tag{2.3}$$

The smallest positive constant $T > 0$ such that $\mathcal{C}$ in (2.3) is a closed orbit is called the *period*. The corresponding angular *frequency* ω of the oscillator $\boldsymbol{x}^c$ will be $\omega = 2\pi/T$. We always consider the limit cycle $\mathcal{C}$ to be hyperbolically stable and without self-crossings.

A *hyperbolically stable limit cycle* $\mathcal{C}$ attracts all solutions with initial conditions $\boldsymbol{x}_0 \in \mathcal{B}$ in a close vicinity $\mathcal{B} = \mathcal{B}(\mathcal{C})$ of $\mathcal{C}$. The maximal open set of these initial points is the *basin of attraction*. Formally, it can be given by $\mathcal{B}(\mathcal{C}) := \{\boldsymbol{x}_0 \in \mathcal{X} \mid \lim_{t\to\infty} \mathrm{dist}(\phi(t;\boldsymbol{x}_0), \mathcal{C}) = 0\}$, where $\mathrm{dist}(\boldsymbol{x}, \mathcal{C}) := \inf_{\boldsymbol{x}^c\in\mathcal{C}} \|\boldsymbol{x} - \boldsymbol{x}^c\|_2$ is the distance from $\boldsymbol{x} \in \mathcal{X}$ to the set $\mathcal{C} \subset \mathcal{X}$ in the Euclidean norm $\|\cdot\|_2$ on $\mathbb{R}^n$.

Phase. The limit cycle $\mathcal{C}$ is a one-dimensional manifold in $\mathbb{R}^n$. Every one-dimensional manifold can be parametrized by a scalar variable. In the case of limit cycle oscillations, the most appropriate variable is a linearly growing phase θ that results from a smooth bijective phase map $\Theta\colon \mathcal{C} \to \mathbb{S}^1$, where $\Theta(\boldsymbol{x}^c) = \theta^c$. Such a phase-reparametrization of the limit cycle (2.3) can be achieved by introducing $\theta = \omega t$ where the frequency $\omega = 2\pi/T$ defines the uniform growth rate. While in the remainder of the report we solely consider smooth oscillators, we briefly add an approach to tackle the non-smooth case.

Phase of non-smooth oscillators. Naturally, for limit-cycle oscillations in the x–y plane with the center at the origin, a general 'phase'-parameterization of the limit cycle trajectory $\big(x(t), y(t)\big)$ can be achieved by $\tilde\theta(t) = \arctan\big(y(t)/x(t)\big)$. We call $\tilde\theta$ the *protophase* as it stems from a smooth bijective transformation $\mathcal{C} \to \mathbb{S}^1$, but does not grow uniformly, $\dot{\tilde\theta} \neq const$. The concept of protophase can be generalized for limit-cycle oscillators $\boldsymbol{x}$ in arbitrary dimension $n > 2$ by constructing a two-dimensional embedding, e.g., by using the Hilbert transform $\hat y$ of a (monotonically increasing) scalar observable $y = f(\boldsymbol{x})$ and computing $\tilde\theta = \arctan\big(\hat y/y\big)$ [89,90]. Given the protophase $\tilde\theta$, we can eventually compute the (uniformly increasing) phase θ by

$$\theta = \omega \int_0^{\tilde\theta} \frac{d\tilde\theta'}{\dot{\tilde\theta}(\theta')} \,. \tag{2.4}$$

The protophase is useful to define a phase for non-smooth oscillators. As an example, we consider so-called integrate-and-fire dynamics: a scalar state variable x monotonically increases according to $\dot x = f(x)$ between two thresholds $v_r < v_f$ with $f(x) > 0$ for $x \in [v_r, v_f]$. When reaching the upper (firing) threshold v_f, the state will be instantaneously reset to the lower (reset) threshold v_r and start integrating again. In that case, one can define the phase map Θ as the bijective change of variables [59]

$$\Theta(x)\colon x \mapsto \omega \int_{v_r}^{x} \frac{1}{f(y)} dy \,, \tag{2.5}$$

with the threshold values v_r and v_f mapped to $\theta = 0$ and $\theta = 2\pi$, respectively. Importantly, (2.5) and (2.4) are of very similar nature. By identifying $\tilde\theta$ with the state x on the integrate-and-fire dynamics and setting the zero-phase $\theta = 0$ at $x = v_r$, we find the phase θ by integrating the inverse of $\dot{\tilde\theta} = \dot x = f(x)$ from v_r to the actual state.

Asymptotic phase. The notion of phase can be extended to the limit cycle's basin of attraction $\mathcal{B}(\mathcal{C})$. This is an important statement because it underlies all of the to-be-discussed mathematical descriptions of phase dynamics. We briefly show that this is true: Without loss of generality, we consider a reference point $\boldsymbol{x}_0^c$ of zero phase by putting $\Theta(\boldsymbol{x}_0^c) = 0$. In the absence of external perturbations, the phase θ^c increases constantly on the limit cycle $\mathcal{C}$. In particular, we have $\theta^c = \Theta\big(\phi(t;\boldsymbol{x}_0^c)\big) = \omega t + \Theta(\boldsymbol{x}_0^c) = \omega t$ and $\dot\theta^c = \omega$. Within the basin of attraction, one can define the unique asymptotic phase θ of the oscillator $\boldsymbol{x} \in \mathcal{B}(\mathcal{C})$ as

$$\theta := \Theta(\boldsymbol{x}) \in [0, 2\pi) \tag{2.6}$$

such that $\lim_{t\to\infty} \|\phi(t;\boldsymbol{x}) - \phi\big(t;\phi(\theta/\omega;\boldsymbol{x}_0^c)\big)\|_2 = 0$ holds. The asymptotic phase θ increases along all unperturbed trajectories by means of $\theta = \omega t + \Theta(\boldsymbol{x})$ at the same constant rate ω. This enables us to use $\boldsymbol{x}^c(t)$ and $\boldsymbol{x}^c(\theta)$ interchangeably when parametrizing the time $t = \theta/\omega$ along the limit cycle. We can therefore rephrase the condition above that defines the asymptotic phase more intuitively as

$$\lim_{t\to\infty} \big|\boldsymbol{x}(t) - \boldsymbol{x}^c\big(\theta(t)\big)\big| = 0 \,. \tag{2.7}$$

Isochrons. Sets of points $\boldsymbol{x} \in \mathcal{B}(\mathcal{C})$ with the same asymptotic phase $\Theta(\boldsymbol{x}) = \theta$ are called isochrons. Accordingly, (2.7) can be regarded as the *isochron condition*. As to a rigorous definition, the isochron $\mathcal{I}(\theta)$ associated with the phase θ is the set $\mathcal{I}(\theta) := \{\boldsymbol{x} \in \mathcal{B}(\mathcal{C}) \mid \Theta(\boldsymbol{x}) = \theta\}$, which is a co-dimension one sub-manifold in $\mathcal{B}(\mathcal{C})$ that crosses the periodic orbit $\mathcal{C}$ transversally, that is, at a finite angle.

We illustrate the concept of isochrons and the asymptotic phase map in Fig. 2.3. There, the isochrons transversally cross the (blue) limit cycle. In general, isochrons can be shown to exist for any stable hyperbolic periodic orbit and their union covers the whole basin of attraction $\mathcal{B}(\mathcal{C})$ [91,92]. In mathematical terms, they define a so-called fibration of $\mathcal{B}(\mathcal{C})$.

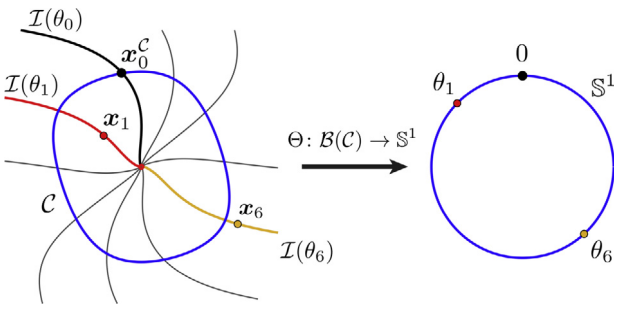

Fig. 2.3. Phase map $\Theta\colon \mathcal{B}(\mathcal{C}) \to \mathbb{S}^1$ associates to each point x_j in the neighborhood $\mathcal{B}(\mathcal{C})$ of the limit cycle $\mathcal{C}$ an asymptotic phase $\theta_j \in \mathbb{S}^1$. The set of all points in $\mathcal{B}(\mathcal{C})$ that are mapped onto the same phase θ forms the isochron $\mathcal{I}(\theta)$ associated with phase θ. Shown are ten isochrons associated to the phases $\theta_n = 2\pi n/10$, $n = 0, \ldots, 9$. An arbitrarily chosen reference point $\boldsymbol{x}_0^c \in \mathcal{C}$ serves as the initial phase $\theta = 0$.

2.2. Phase response

Phase response curve. The *phase response curve* or phase resetting curve is a crucial determinant for the interaction between oscillators. It measures the extent to which an external perturbation $\boldsymbol{p}(t)$ advances or pushes back the asymptotic phase of an oscillator. A perturbation thus leads to a phase advance or a phase delay, respectively. Given a trajectory $\boldsymbol{x}^c(t)$ along the limit cycle subject to a pulse-like perturbation $\boldsymbol{p}(t)$ during an infinitesimal time interval $\mathcal{T} = \lim_{\delta\to 0}(t_0-\delta, t_0+\delta)$, i.e. $\boldsymbol{p}(t \in \mathcal{T}) \neq 0$, an immediate strategy to identify the corresponding phase response $G(\theta, \boldsymbol{p})$ at phase $\theta_0 = \Theta(\boldsymbol{x}^c(t_0))$ reads:

(i) determine the perturbed point $\lim_{\delta\to 0}\tilde{\boldsymbol{x}}(t_0+\delta) \in \mathcal{B}(\mathcal{C})$ and its corresponding asymptotic phase $\Theta(\tilde{\boldsymbol{x}})$;
(ii) take the difference between the perturbed asymptotic phase and the unperturbed phase $\Theta(\boldsymbol{x}^c) = \theta_0$;
(iii) repeat (i) and (ii) for all phases $\theta_0 = \theta \in \mathbb{S}^1$ in order to determine the *phase response curve*

$$G(\theta; \boldsymbol{p}) = \Theta\left(\tilde{\boldsymbol{x}}\right) - \Theta\left(\boldsymbol{x}^c\right) = \Theta\left(\boldsymbol{x}^c + \boldsymbol{p}\right) - \theta \ . \tag{2.8}$$

One can determine the phase response curve also for arbitrary perturbations during finite time intervals $\mathcal{T} = (t_0, t_1)$ with $t_1 > t_0$. For this, the first step (i) above has to be modified slightly:

(i_a) determine the perturbed point $\tilde{\boldsymbol{x}}(t_1) = \phi(t_1; \tilde{\boldsymbol{x}}(t_0), \boldsymbol{p}) = \phi(t_1; \boldsymbol{x}^c(t_0), \boldsymbol{p})$ and the unperturbed one $\boldsymbol{x}^c(t_1) = \phi(t; \boldsymbol{x}^c(t_0))$, as well as the corresponding (asymptotic) phases $\Theta(\tilde{\boldsymbol{x}}(t_1))$ and $\Theta(\boldsymbol{x}^c(t_1))$.

The dynamics has to be integrated to determine both the perturbed and unperturbed state at time $t = t_1$. One can continue integrating for longer times, ideally for $t \to \infty$ and, subsequently, estimate the asymptotic phase difference according to

$$G(\theta; \boldsymbol{p}) = \Theta\left(\lim_{t\to\infty} \phi\big(t; \boldsymbol{x}^c(t_0), \boldsymbol{p}\big)\right) - \Theta\left(\lim_{t\to\infty} \phi\big(t; \boldsymbol{x}^c(t_0)\big)\right) \ .$$

Note that this definition coincides with

$$G(\theta; \boldsymbol{p}) = \Theta\left(\phi\big(t_1; \boldsymbol{x}^c(t_0), \boldsymbol{p}\big)\right) - \Theta\left(\phi\big(t_1; \boldsymbol{x}^c(t_0)\big)\right) \ .$$

In the following we will only consider pulse-like perturbations $\boldsymbol{p}(t)$ that are non-zero at the time instant t_0 of the pulse and therefore omit the explicit time-dependence of $\boldsymbol{p}$.

Infinitesimal phase response curve. If the perturbation is pulse-like, i.e. $\mathcal{T} \to \delta(t_0)$, and sufficiently weak, $|\boldsymbol{p}| \ll 1$, then it is convenient to express the phase response in terms of the infinitesimal phase response curve.[3] Using the directional derivative $D\Theta(\boldsymbol{x})[\boldsymbol{y}] := \lim_{h\to 0}[\Theta(\boldsymbol{x} + h\boldsymbol{y}) - \Theta(\boldsymbol{x})]/h$, one can define the *infinitesimal phase response curve* as a map $Q : \mathbb{S}^1 \to \mathbb{R}$ with

$$Q(\theta) := D\,\Theta\left(\boldsymbol{x}^c\right)\left[\partial_{\boldsymbol{p}}\mathcal{F}\left(\boldsymbol{x}^c, \boldsymbol{0}\right)\right] = \nabla_x\Theta\left(\boldsymbol{x}^c\right)\cdot\partial_{\boldsymbol{p}}\mathcal{F}\left(\boldsymbol{x}^c, \boldsymbol{0}\right) \ .$$

Here, we expressed the directional derivative as the inner product in $\mathbb{R}^n$. $\nabla_x\Theta(\boldsymbol{x}^c)$ denotes the gradient of the asymptotic phase map Θ evaluated on the limit cycle $\mathcal{C}$, and $\partial_{\boldsymbol{p}}\mathcal{F}(\boldsymbol{x}^c, \boldsymbol{0})$ corresponds to an infinitesimal perturbation from the limit cycle trajectory $\boldsymbol{x}^c$ at phase θ.

[3] Several papers refer to this as *infinitesimal phase resetting curve* or *phase response function*.

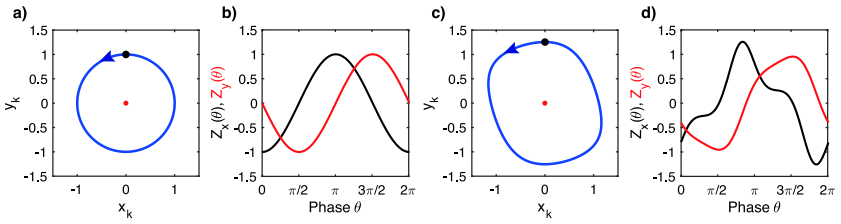

Fig. 2.4. Phase response of limit-cycle oscillators. (a) Circular limit cycle of the Stuart–Landau oscillator $\dot{z} = z - (1+i)|z|^2 z$ with $z = x + iy$ and (b) the two sinusoidal components of the phase sensitivity function $\boldsymbol{Z} = (Z_x, Z_y)$, characterizing the response to infinitesimal perturbations in the x- and y-direction, respectively. (c) The Rayleigh oscillator $\dot{x} = y, \dot{y} = -\omega + (1 - x^2)y$ and (d) its phase sensitivity function.

Phase sensitivity function. The afore-introduced gradient, now written as

$$\boldsymbol{Z}(\theta) = \nabla_x \Theta\big(\boldsymbol{x}^c(\theta)\big) = \nabla \Theta(\boldsymbol{x})\big|_{\boldsymbol{x}=\boldsymbol{x}^c(\theta)} , \tag{2.9}$$

can serve to determine the phase response. $\boldsymbol{Z}: \mathbb{S}^1 \to \mathbb{R}^n$ is commonly referred to as *phase sensitivity function* or linear response function [73]. It is closely related to the infinitesimal phase response curve Q: If $\partial_{\boldsymbol{p}} \mathcal{F}(\boldsymbol{x}^c, \boldsymbol{0})$ is a unit vector $\boldsymbol{e}_j$ along the jth direction, then we have $Q(\theta) = Z_j(\theta)$. This follows immediately from the dynamics (2.2) with uni-directional additive perturbation $\kappa \boldsymbol{p} = \kappa \boldsymbol{e}_j$. The phase response curve (2.8) can always be computed using $Q(\theta)$ since the definitions (2.9) and (2.8) imply

$$Z_j(\theta) = \lim_{p \to 0} \frac{G\big(\theta, p\,\boldsymbol{e}_j\big)}{p} . \tag{2.10}$$

In Fig. 2.4, we depict the phase sensitivity functions of two classic examples, the Stuart–Landau oscillator and the Rayleigh oscillator. The components of $\boldsymbol{Z} = (Z_x, Z_y)$ describe the effect of infinitesimal perturbations in the x- and y-direction, respectively. While the phase sensitivity function of the Stuart–Landau oscillator is sinusoidal in both components, the slightly angular limit cycle dynamics of the Rayleigh oscillator results in more complicated phase responses as indicated by the phase sensitivity function.

2.3. Phase dynamics

For infinitesimal perturbations $|\boldsymbol{p}| \ll 1$, the phase response curve (2.8) can be linearly approximated by the aforementioned phase sensitivity function (2.9) in terms of

$$G(\theta; \boldsymbol{p}) \cong \boldsymbol{Z}(\theta) \cdot \boldsymbol{p} . \tag{2.11}$$

Whenever the dynamics stays close to the limit cycle $\mathcal{C}$, one may further approximate each $\boldsymbol{x}$ by its corresponding value $\boldsymbol{x}^c$ on $\mathcal{C}$ such that the reduced phase dynamics can be given by

$$\dot{\theta} = \omega + G(\theta; \boldsymbol{p}) = \omega + \varepsilon \boldsymbol{Z}(\theta) \cdot \boldsymbol{p} . \tag{2.12}$$

In (2.12) we used the parameter $\kappa = \varepsilon \ll 1$ to indicate that the perturbation is very small. In other words, the phase response to a weak, pulse-like perturbation $\boldsymbol{p}$ at phase θ^c can be approximated by the product $\boldsymbol{Z}(\theta^c) \cdot \boldsymbol{p}$. That is, small perturbations $|\boldsymbol{p}| \ll 1$ do not move the oscillator too far away from the limit cycle $\mathcal{C}$ and the dynamics $\boldsymbol{x}$ can be approximated sufficiently well by the value on the periodic orbit, $\boldsymbol{x}(t) \approx \boldsymbol{x}^c(t)$, see Fig. 2.2. One can formally expand the dynamics $\dot{\boldsymbol{x}} = \mathcal{F}(\boldsymbol{x}, \boldsymbol{p})$ for small $\boldsymbol{p}$ around the unperturbed dynamics $\boldsymbol{f}(\boldsymbol{x})$, i.e., $\mathcal{F}(\boldsymbol{x}, \boldsymbol{p}) = \boldsymbol{f}(\boldsymbol{x}) + \partial_{\boldsymbol{p}} \mathcal{F}(\boldsymbol{x}, \boldsymbol{0}) \boldsymbol{p} + \mathcal{O}^2(\boldsymbol{p})$. Taken together, we obtain the asymptotic phase dynamics

$$\dot{\theta} = \frac{d}{dt} \Theta(\boldsymbol{x}) = \nabla_x \Theta(\boldsymbol{x}) \cdot \dot{\boldsymbol{x}} \approx \nabla_x \Theta\left(\boldsymbol{x}^c\right) \cdot \dot{\boldsymbol{x}}^c \approx \nabla_x \Theta\left(\boldsymbol{x}^c\right) \cdot \left[\boldsymbol{f}(\boldsymbol{x}^c) + \partial_{\boldsymbol{p}} \mathcal{F}\left(\boldsymbol{x}^c, \boldsymbol{0}\right) \boldsymbol{p}\right]$$

and, because $\dot{\theta}^c = \nabla_x \Theta(\boldsymbol{x}^c) \cdot \boldsymbol{f}(\boldsymbol{x}^c) = \omega$ holds, this form reduces at first order to (2.12).

The phase dynamics (2.12) of a single oscillator forms an essential building block to determine the phase dynamics of an oscillator network. Deriving the individual terms in (2.12) thus poses the first main challenge. In the following section, we will briefly introduce several different methodologies along which such a derivation can be achieved.

3. Phase reduction techniques for a single oscillator

A first and direct way to quantify the phase response to a (small or large) stimulus $\boldsymbol{p}$ of the limit cycle trajectory $\boldsymbol{x}^c(t)$ at a particular phase θ dates back to the work by Glass, Mackey and co-workers [93] in the early 1980s. Their method leads to the phase response function $G(\theta, \boldsymbol{p})$ as introduced in Section 2, where we also presented how the method can be

implemented experimentally. Despite its simplicity, such an experimental procedure is not very accurate when it comes to infinitesimal perturbations.

As fundamental it is to properly derive the phase dynamics of a single oscillator $\boldsymbol{x}$, as many ways there are to achieve a phase reduction. The important concepts to do so – limit cycle $\mathcal{C}$, basin of attraction $\mathcal{B}(\mathcal{C})$, asymptotic phase map Θ, isochrons $\mathcal{I}(\theta)$, infinitesimal phase response curve $\mathcal{Q}$, phase sensitivity function $\boldsymbol{Z}$ – have been introduced in the previous section. In the following, we will briefly collect different methodologies how to establish the phase dynamics and the necessary properties of the limit cycle to define (2.12),

$$\dot{\theta} = \omega + G(\theta; \boldsymbol{p}) = \omega + \varepsilon \boldsymbol{Z}(\theta) \cdot \boldsymbol{p}$$
$$\boldsymbol{Z} = \nabla_x \Theta(\boldsymbol{x}^c)$$

for an infinitesimal, pulse-like perturbation $\boldsymbol{p}$.

3.1. Winfree's reduction via isochrons

The idea behind the reduction via isochrons dwells on explicit expressions of the asymptotic phase map $\Theta(\boldsymbol{x})$ along the isochrons $\mathcal{I}(\theta)$ and of the limit cycle $\mathcal{C}$. Once these expressions have been obtained, the phase sensitivity function $\boldsymbol{Z}$ can be determined as the gradient of the asymptotic phase map evaluated on the limit cycle, that is, $\boldsymbol{Z} = \nabla_x \Theta(\boldsymbol{x}^c)$. In principle, this approach can be applied to every dynamical system that exhibits stable limit cycle oscillations. However, it is essential to include explicit expressions of Θ and $\mathcal{C}$, which, unfortunately, cannot be obtained analytically in the majority of cases.

3.2. Kuramoto's reduction via Floquet eigenvectors

Explicit analytic expressions of the asymptotic phase map $\Theta(\boldsymbol{x})$ and of the isochrons can only be derived for selected examples of oscillators. However, one can exploit the relationship between the asymptotic phase of an oscillator $\boldsymbol{x}$ and the eigenvectors associated with the linearized part of $\boldsymbol{f}(\boldsymbol{x})$ about its periodic limit cycle solution $\boldsymbol{x}^c$. The underlying theory of first-order linear systems with periodic coefficients is called Floquet theory [94] and has been promoted by Kuramoto to being applied for phase reductions [12]. This technique can be applied to any dynamical system with stable limit cycle oscillations. While it does not rely on the explicit form of the phase map Θ, it requires an explicit expression of the limit cycle $\mathcal{C}$.

To briefly revise the idea of Floquet eigenvectors for deriving the phase sensitivity function $\boldsymbol{Z}$, we consider an oscillator $\dot{\boldsymbol{x}} = \boldsymbol{f}(\boldsymbol{x})$ with a stable T-periodic limit cycle solution $\boldsymbol{x}^c$. For small deviations $\boldsymbol{u}(t)$ off $\boldsymbol{x}^c(t)$, we find for $\boldsymbol{x}(t) = \boldsymbol{x}^c(t) + \boldsymbol{u}(t)$ the linear system

$$\dot{\boldsymbol{u}} = \boldsymbol{L}(t)\boldsymbol{u} \ , \quad \text{with} \quad \boldsymbol{L}(t) = \nabla \boldsymbol{f}(\boldsymbol{x})\big|_{\boldsymbol{x}=\boldsymbol{x}^c(t)} \tag{3.1}$$

with $\boldsymbol{L}(t)$ being a T-periodic $n \times n$-matrix. A general solution of (3.1) takes on the form $\boldsymbol{u}(t) = \boldsymbol{S}(t)\mathrm{e}^{\boldsymbol{\Lambda} t}\boldsymbol{u}(0)$, where $\boldsymbol{S}(t)$ is a T-periodic matrix with initial condition $\boldsymbol{S}(0) = \boldsymbol{I}$ and $\boldsymbol{\Lambda}$ is a time-independent matrix. The matrix exponential $\exp(\boldsymbol{\Lambda} t)$ is defined in the usual way.[4] The normalized left and right eigenvectors of $\boldsymbol{\Lambda}$ associated with eigenvalue λ_j will be denoted by $\boldsymbol{v}_j$ and $\boldsymbol{u}_j$. The limit cycle solution $\boldsymbol{x}^c$ being stable implies $\mathrm{Re}(\lambda_j) \leq 0$. While one eigenvalue $\lambda_0 \equiv 0$ vanishes, which corresponds to (phase) disturbances along the periodic orbit $\mathcal{C} = \{\boldsymbol{x}^c(t) \mid t \in \mathbb{R}\}$, the other eigenvalues $\lambda_1, \ldots, \lambda_{n-1}$ are assumed to have negative real parts. It is true that $\boldsymbol{u}_0 = \dot{\boldsymbol{x}}^c(0)$. That is, $\boldsymbol{u}_0$ is a tangent vector of $\mathcal{C}$ at point $\boldsymbol{x}^c(0)$ and has the same direction as that of the infinitesimal phase disturbances. Moreover, $\boldsymbol{u}_0$ satisfies $\boldsymbol{S}(t)\boldsymbol{u}_0 = \dot{\boldsymbol{x}}^c(t)$.[5] Next, we use the facts that the phase sensitivity function $\boldsymbol{Z}(\theta)$ is normal to the tangent space $T(\theta)$ of the isochron $\mathcal{I}(\theta)$ at point $\theta(t) = \boldsymbol{x}^c(\theta(t))$ and that $T(0)$ is free from the zero-eigenvector component, cf. [Chapter 3.4, 12]. This means that $\boldsymbol{Z}(0)\boldsymbol{u}_j = 0$ for all $j > 0$. Hence, $\boldsymbol{Z}(0)$ must be proportional to the left zero-eigenvector $\boldsymbol{v}_0$. Since $\boldsymbol{Z}(\theta)$ has been introduced as the gradient of the asymptotic phase map $\Theta(\boldsymbol{x})$ evaluated on the limit cycle, we can differentiate $\Theta(\boldsymbol{x}^c) = \theta^c(t)$ on the limit cycle and find $\boldsymbol{Z}(\theta) \cdot \dot{\boldsymbol{x}}^c(t) = \omega$, when using $\dot{\theta}^c = \omega = 2\pi/T$. By identifying $\boldsymbol{Z}(t)$ with $\boldsymbol{Z}(\theta)$ via $\theta \mapsto t/\omega$, we can combine our findings and arrive at

$$\boldsymbol{Z}(t) = \omega \boldsymbol{v}_0 \boldsymbol{S}(t)^{-1} \ . \tag{3.2}$$

---

4 $\mathrm{e}^{\boldsymbol{\Lambda} t} = \sum_{k=0}^{\infty} \frac{1}{k!} \boldsymbol{\Lambda}^k t^k = \boldsymbol{I}_n + \boldsymbol{\Lambda} t + \frac{\boldsymbol{\Lambda}^2 t^2}{2!} + \cdots$.

5 Indeed, differentiating $\dot{\boldsymbol{x}}_0(t) = \boldsymbol{f}(\boldsymbol{x}_0(t))$ on both sides results in

$$\frac{d}{dt}\dot{\boldsymbol{x}}^c(t) = \frac{d}{dt}\boldsymbol{f}(\boldsymbol{x}^c(t)) = \nabla \boldsymbol{f}(\boldsymbol{x})\big|_{\boldsymbol{x}=\boldsymbol{x}^c(t)} \cdot \dot{\boldsymbol{x}}^c(t) = \boldsymbol{L}(t)\dot{\boldsymbol{x}}^c(t) \ .$$

So $\dot{\boldsymbol{x}}^c(t)$ is a particular solution of $\dot{\boldsymbol{u}} = \boldsymbol{L}(t)\boldsymbol{u}$. Thus, we can write $\dot{\boldsymbol{x}}^c(t) = \boldsymbol{S}(t)\mathrm{e}^{\boldsymbol{\Lambda} t}\dot{\boldsymbol{x}}^c(0)$. Using the definition of the matrix exponential together with $\boldsymbol{\Lambda}\boldsymbol{u}_0 = \lambda_0 \boldsymbol{u}_0 = 0$, the right-hand side reduces to $\boldsymbol{S}(t)\boldsymbol{u}_0$ as wanted.

3.3. Direct method

Most direct methods, such as the experimental procedure by Glass, Mackey and co-workers mentioned above, suffer from numerical deficits when computing the phase sensitivity function $\boldsymbol{Z}$ via $G(\theta, \boldsymbol{p})$ in the limit of infinitesimal perturbations $\|\boldsymbol{p}\| \ll 1$. An exception presents the recently proposed method by Novičenko and Pyragas. They proposed an algorithm based on the same idea to capture the oscillator's response to short finite pulses at different phases of the limit cycle [95], hence the name "direct method". Conceptually, their adaptation exploits the linearized dynamics about the limit cycle $\mathcal{C}$. The here-presented method is a convenient reformulation of Kuramoto's reduction via Floquet eigenvectors of the previous subsection that allows for a straightforward numerical implementation.

As before in (3.1), we let $\boldsymbol{u}(t)$ denote small deviations from the limit cycle trajectory $\boldsymbol{x}^c(t)$ such that $\dot{\boldsymbol{u}} = \boldsymbol{L}(t)\boldsymbol{u}$ holds where $\boldsymbol{L}(t) = \nabla \boldsymbol{f}(\boldsymbol{x})\big|_{\boldsymbol{x}=\boldsymbol{x}^c(t)}$ and with initial condition $\boldsymbol{x}(0) = \boldsymbol{x}^c(\theta)$ for the initial phase θ. To obtain the jth component Z_j of the phase sensitivity function $\boldsymbol{Z}$, we choose the initial condition $\boldsymbol{u}(0) = (u_1(0), \ldots, u_n(0))^\intercal$ with $u_k(0) = \delta_{kj}$ where δ_{kj} denotes the Kronecker-δ. Because of the asymptotic stability of the limit cycle, the vector $\boldsymbol{u}(pT)$ with $p \in \mathbb{N}$ and T the oscillator's period becomes parallel to the velocity vector $\dot{\boldsymbol{x}}^c(\theta)$ as $p \to \infty$ [95]. That is, $\lim_{p\to\infty} \boldsymbol{u}(pT) = \dot{\boldsymbol{x}}^c(\theta) Z_j(\theta)$ by definition of the phase sensitivity function $\boldsymbol{Z}$. Applying the pseudo-inverse of $\dot{\boldsymbol{x}}^c(\theta)$, we obtain for the phase sensitivity function

$$Z_j(\theta) = \lim_{p\to\infty} \frac{\dot{\boldsymbol{x}}^c(\theta) \cdot \boldsymbol{u}(pT)}{\dot{\boldsymbol{x}}^c(\theta) \cdot \dot{\boldsymbol{x}}^c(\theta)} \,. \tag{3.3}$$

For more details, e.g., how to improve this algorithm by replacing the vector $\boldsymbol{u}$ by the fundamental matrix $\boldsymbol{\Phi}$ so that $\boldsymbol{Z}$ can directly be extracted from $\boldsymbol{\Phi}$, we refer to Novičenko's and Pyragas' instructive work [95].

3.4. Adjoint method

The adjoint method is nowadays the standard technique to determine the phase sensitivity function $\boldsymbol{Z}$ of an oscillator $\boldsymbol{x}$ [46,48,53,55,64]. Computing $\boldsymbol{Z}(\theta)$ in a direct way as the gradient of the (asymptotic) phase map $\Theta(\boldsymbol{x})$ evaluated on the limit cycle $\mathcal{C} = \{\boldsymbol{x}^c(t) : t \in \mathbb{R}\}$ can become arbitrary difficult, as one has to find analytic expressions for the phase map Θ. As it turns out, the function $\boldsymbol{Z}(\theta)$ is the solution to the adjoint problem associated with the dynamics $\dot{\boldsymbol{x}} = \boldsymbol{f}(\boldsymbol{x})$ when linearized about the unperturbed limit cycle $\mathcal{C}$. For an infinitesimal perturbation $\boldsymbol{p}$ the perturbed trajectory $\boldsymbol{x}(t) = \boldsymbol{x}^c(t) + \boldsymbol{u}(t)$ stays arbitrarily close to the T-periodic limit cycle trajectory $\boldsymbol{x}^c(t)$, such that the dynamics of $\boldsymbol{u}(t)$ can be assumed linear, that is, $\dot{\boldsymbol{u}} = \boldsymbol{L}(t)\boldsymbol{u}$ with $\boldsymbol{L}(t) = \nabla \boldsymbol{f}(\boldsymbol{x})\big|_{\boldsymbol{x}=\boldsymbol{x}^c(t)}$ as before. Solutions to the linearized equation satisfy

$$\left(\tfrac{d}{dt} - \boldsymbol{L}(t)\right)\boldsymbol{y}(t) =: \left(\mathcal{L}\boldsymbol{y}\right)(t) = 0 \,,$$

where $\mathcal{L}$ is a linear operator on the space of $\mathbb{R}^n$-valued T-periodic functions. We define the standard inner product $\langle \cdot, \cdot \rangle$ on T-periodic functions in $\mathbb{R}^n$ as

$$\langle \boldsymbol{u}(t), \boldsymbol{v}(t) \rangle = \int_0^T \boldsymbol{u}(t) \cdot \boldsymbol{v}(t) dt \,.$$

Then, the adjoint linear operator $\mathcal{L}^*$ satisfies $\langle \boldsymbol{u}, \mathcal{L}\boldsymbol{v} \rangle = \langle \mathcal{L}^*\boldsymbol{u}, \boldsymbol{v} \rangle$. In particular, we find that

$$\left(\mathcal{L}^*\boldsymbol{y}\right)(t) = -\dot{\boldsymbol{y}}(t) - \boldsymbol{L}(t)^\intercal \boldsymbol{y}(t) \,. \tag{3.4}$$

When determining the phase shift between the asymptotic phase $\theta_p = \Theta(\boldsymbol{x}^c + \boldsymbol{p})$ after an infinitesimal perturbation $\boldsymbol{p} = \boldsymbol{u}(t)$ at time t_0 and the unperturbed phase $\theta^c = \Theta(\boldsymbol{x}^c)$, we note that for the phase shift $\Delta\theta = \theta_p - \theta^c$ one has

$$\Delta\theta = \left\langle \boldsymbol{Z}(t), \boldsymbol{x}^c(t) + \boldsymbol{u}(t) - \boldsymbol{x}^c(t) \right\rangle + \mathcal{O}(|\boldsymbol{u}|^2) \,.$$

The phase shift $\Delta\theta$ is independent of time after the perturbation at $t = t_0$. Hence,

$$\begin{aligned} 0 &= \frac{d}{dt}\left\langle \boldsymbol{Z}(t), \boldsymbol{u}(t) \right\rangle = \left\langle \frac{d\boldsymbol{Z}(t)}{dt}, \boldsymbol{u}(t) \right\rangle + \left\langle \boldsymbol{Z}(t), \frac{d\boldsymbol{u}(t)}{dt} \right\rangle = \left\langle \frac{d\boldsymbol{Z}(t)}{dt}, \boldsymbol{u}(t) \right\rangle + \left\langle \boldsymbol{Z}(t), \boldsymbol{L}(t)\boldsymbol{u}(t) \right\rangle \\ &= \left\langle \frac{d\boldsymbol{Z}(t)}{dt}, \boldsymbol{u}(t) \right\rangle + \left\langle \boldsymbol{L}(t)^\intercal \boldsymbol{Z}(t), \boldsymbol{u}(t) \right\rangle = \left\langle \frac{d\boldsymbol{Z}(t)}{dt} + \boldsymbol{L}(t)^\intercal \boldsymbol{Z}(t), \boldsymbol{u}(t) \right\rangle = \left\langle -\left(\mathcal{L}^*\boldsymbol{Z}\right)(t), \boldsymbol{u}(t) \right\rangle. \end{aligned}$$

Since the perturbation $\boldsymbol{u}(t)$ was assumed arbitrary, it follows that

$$\mathcal{L}^*\boldsymbol{Z}(t) = 0 \,. \tag{3.5}$$

With $\Theta(\boldsymbol{x}^c(\theta)) = \theta$ and taking the time derivative on both sides, we use $\dot{\theta} = \omega$ to find

$$\dot{\Theta}\left(\boldsymbol{x}^c(\theta)\right) = \boldsymbol{Z}(t) \cdot \frac{d\boldsymbol{x}^c(\theta)}{dt} = \omega \,. \tag{3.6}$$

This normalization is required such that $\boldsymbol{Z}(t)$ is the unique solution to (3.4)–(3.6).

Numerical implementation in XPPAUT and Matcont

For arbitrary limit cycle oscillators, one can solve $\mathcal{L}^*\boldsymbol{y} = 0$ numerically. As numerical procedures do not rely on a critical distance to a bifurcation point, the adjoint method can provide a valuable reference to monitor accuracy, and, by this, the validity of analytic phase reduction techniques as a system gradually moves away from a bifurcation point. We will exploit this capacity in the forthcoming Sections 8 and 9.

The numerical exploration of the phase sensitivity function $\boldsymbol{Z}$ as the solution to the adjoint problem (3.4)–(3.6) may present a problem in itself. The solution $\boldsymbol{Z}(T) = \boldsymbol{Z}(0)$ of (3.5) is periodic, so that we encounter a boundary value problem. While a direct (forward) integration is not feasible, one can integrate (3.5) backward in time [96]. As long as the limit cycle is asymptotically stable, backward integration retrieves the periodic solution of the adjoint equation and cancels possible higher harmonics out. The adjoint method is efficiently automated in Ermentrout's software package XPPAUT [97]. The implemented algorithm, however, relies on a numerical interpolation of the Jacobian matrix being evaluated at the limit cycle solution. Moreover, the procedure shows a slow convergence of the adjoint solution towards the phase sensitivity function $\boldsymbol{Z}$ when the limit cycle is only weakly stable. Govaerts and Sautois [98] proposed an alternative numerical approach to solve the adjoint problem. Their algorithm solves the corresponding boundary value problem using an orthogonal collocation method with Gauss collocation points. As a by-product, they obtain the phase sensitivity function $\boldsymbol{Z}$. This method is fast, rendering it particularly useful when a large number of phase sensitivity functions are needed, e.g., for the evolution of limit cycles if one parameter of the system is changed. This method is implemented in the Matlab software package MatCont [99].

3.5. Haken's reduction via averaging

An alternative and more ad-hoc approach to reduce the phase dynamics of a (perturbed) oscillator has been promoted by Haken and applies averaging. The idea is to average the oscillatory dynamics over one cycle when assuming that its amplitude and phase change slowly as compared to the oscillator's frequency. Following a three-step approach, first the time-dependent amplitude and phase are fixed. The system is subsequently integrated over one period to remove all harmonic oscillations; see also [86,87] for a rigorous reasoning. Last, amplitude and phase are considered again to be time-dependent [33,75]. Haken popularized this procedure as a combination of rotating wave and slowly varying amplitude approximations [88]. While this technique is usually applied to weakly nonlinear oscillations described by second-order differential equations, see for an overview, e.g., [100,101], it can also be applied to systems of first-order differential equations, as will be illustrated below.

As averaging is applied to the linearized dynamics about an unstable fixed point within a stable limit cycle solution $\boldsymbol{x}^c$ (in contrast to the linearized dynamics about $\boldsymbol{x}^c$ as in the previous subsections), this technique loses accuracy for large-amplitude oscillations. Still, it provides a straightforward phase model whose parameters are directly linked to those of the underlying oscillatory model, and presents a valuable addition to the variety of phase reduction techniques.

Applying Haken's reduction technique to an oscillator requires stable limit cycle oscillations that can be transformed into a (nearly) circular shape by an appropriate change of variables.[6] In the following we will assume a planar oscillator $\dot{\boldsymbol{x}} = \boldsymbol{f}(\boldsymbol{x};\mu)$ subject to (additive) perturbations $\varepsilon\boldsymbol{p}$ where the state vector is given by $\boldsymbol{x} = (x, y) \in \mathbb{R}^2$. The unperturbed dynamics lead to a stable circular limit cycle around the unstable fixed point $\boldsymbol{x}_0 = (0, 0)$. We can perform a polar coordinate transformation $x = R\cos(\theta), y = R\sin(\theta)$ with $\theta = \omega t + \phi$, where ϕ denotes a slowly varying phase deviation due to the perturbation. Moreover, we have $R^2 = x^2 + y^2$ and $\theta = \tan^{-1}(y_k, x_k)$; $\tan^{-1}$ is the quadrant-corrected inverse tangent.[7] The (central) frequency ω, however, has to be determined, e.g., as the (absolute value of the) imaginary part of the complex conjugate pair of eigenvalues of the Jacobian of $\boldsymbol{f}$, that is, $\omega = \mathrm{Im}(\lambda_+)$ with $\lambda_\pm \in \mathbb{C}$ the pair of complex eigenvalues.

Assuming that R, ϕ hardly change over one period of oscillation, $T = 2\pi/\omega$, i.e.

$$\left|\dot{R}/R\right| \ll \omega \quad \text{and} \quad \left|\dot{\phi}/\phi\right| \ll \omega \,, \tag{3.7}$$

one can average the dynamics over the interval $[0, T)$ by means of $\langle f(s)\rangle := \frac{1}{T}\int_0^T f(s)ds$. Exploiting trigonometric identities, the (averaged) dynamics $\dot{\phi}$ and $\dot{R}$ can be expressed in the state variables x, y as[8]

$$\dot{\phi} = -\omega + \left\langle \frac{1}{R^2}\left(x\dot{y} - y\dot{x}\right)\right\rangle \tag{3.8a}$$

---

6 Such a coordinate change is always possible for, e.g., oscillations that emerge through a Hopf bifurcation. Away from that point, higher order corrections might be in place; for a corresponding approximation scheme see [86].

7 Note that θ_k rather takes the form of the protophase than the phase. For circular oscillations, however, the phase and protophase are (nearly) the same.

8 The averaging in (3.8) is sound also from a time-scale separation argument. The assumption (3.7) implies that $\phi = \phi(\tau)$ and $R = R(\tau)$ depend on a slower time $\tau = \varepsilon t$. As a result, we obtain the dynamics of the phase deviation ϕ and of the slowly varying amplitude R by averaging over the period $T = 2\pi/\omega$. Indeed, using polar coordinates in the angular brackets of (3.8) one can see that all terms at least of order $\mathcal{O}(R)$. Close to, e.g., a supercritical Hopf bifurcation, $0 < R \ll 1$ is small so that this averaging is appropriate.

$$\dot{R} = \left\langle \frac{x\dot{x} + y\dot{y}}{R} \right\rangle . \tag{3.8b}$$

We retrieve the (full) phase dynamics by inserting (3.8a) into $\dot{\theta} = \omega + \dot{\phi}$. Note that the system (3.8) describes both phase and amplitude dynamics, which can be reduced further if we assume that the (non-trivial) fixed point solution of (3.8b) approximates the (time-varying) amplitude R sufficiently well. Upon inserting the (stationary) solution R into (3.8a), we eventually find the reduced phase dynamics $\dot{\phi}$, which will split into a natural frequency part of order $\mathcal{O}(1)$ and a part of order $\mathcal{O}(\varepsilon)$. The latter may further decompose into the product of the phase sensitivity function $\boldsymbol{Z}$ and the perturbation $\boldsymbol{p}$. The inherent averaging of this reduction method, however, is detrimental for assessing the effect of an infinitesimal perturbation. By contrast, the method becomes more insightful when considering a network of weakly coupled oscillators. In the weak coupling limit, averaging is instrumental for computing the phase deviations due to the coupling. Replacing $\boldsymbol{p}$ by the respective coupling terms with the other oscillators, the interaction terms of the reduced phase dynamics can be regarded as the product of phase sensitivity function $\boldsymbol{Z}$ and coupling terms averaged over one period T.

4. Phase reductions and normal forms

Although the phase reduction techniques presented in the previous section slightly differ in their approach how to derive the phase dynamics, they all have in common that they rely on the exact forms of the limit cycle and of the (linearized) dynamics around it. All the presented phase reduction techniques are equivalent and lead to identical results. We will analytically demonstrate that this is true along one particular example for which it is possible to indicate the explicit expressions of the limit cycle trajectory and of the linearized dynamics around it.

Numerical phase reduction techniques. General oscillatory dynamics cannot be treated analytically and one has to rely on numerical assessments. The required properties for phase reduction, such as the limit cycle and the linearized dynamics around it, are then computed, stored and exploited numerically. The adjoint method presented in Section 3.4 has become a standard phase reduction technique due to its algorithmic implementation in the software packages XPPAUT [97] and MatCont. The direct method in Section 3.3 serves as a powerful alternative. We refer to these two methods as *numerical phase reduction techniques*.

Analytic phase reduction techniques. Analytic approaches typically build on so-called canonical forms of the oscillatory dynamics. Center manifold and normal form reductions have proven very helpful to simplify the dynamics, in particular if oscillations have emerged through particular bifurcations. The transformed, simplified dynamics allow to retrieve explicit analytic forms of the limit cycle trajectory as well as of the linearized dynamics around it so that the phase dynamics can be obtained analytically following either of the techniques in Section 3. In the following, we will refer to these two-step approaches that combine a preceding normal form reduction with a subsequent phase reduction as *analytic phase reduction techniques*.

A direct consequence of such two-step reductions is that the accuracy of the analytically obtained phase dynamics typically scales with the distance to the bifurcation point. The reason is that the transformations made in the first step result in simplified dynamics that are given in the form of a truncated power series. While the corresponding residual is negligibly small in the direct vicinity of the bifurcation point, the error may become larger the farther away from the bifurcation point. Hence, also the reduced phase dynamics become less accurate for growing distances from the bifurcation point. That is why analytic phase reduction techniques require a careful assessment of the underlying dynamics with respect to their bifurcation structure. On top of that, different center manifold and normal form reduction methods may also differ as in how the dependence on the distance to the bifurcation point is respected in the simplified dynamics. Below we will illustrate these differences in more detail, as they are fundamental for a possible mismatch between different analytic reduction techniques. In short, analytic two-step phase reduction techniques may appear daunting both in their rather intricate application of subsequent transformations, and in their restricted validity away from bifurcation boundaries. Still, they establish an explicit link between original model parameters and the resulting phase dynamics, which numerical phase reduction techniques can only provide through an extensive scanning of the parameter space. As such, they retain their grand appeal by allowing for an analytic intuition that may get lost along numerical approaches.

Oscillations and bifurcations. The above mentioned transformations as the first step of an analytic phase reduction may be applied to any kind of dynamics exhibiting stable oscillatory behavior. For the sake of legibility, however, we will restrict ourselves to oscillatory dynamics that have emerged through a so-called supercritical Hopf bifurcation, i.e. at the transition where oscillations with a finite frequency emerge or vanish. The Hopf bifurcation allows to rigorously derive a canonical model. It is the only type of bifurcation that allows a step-by-step reduction of the phase dynamics without rough heuristics. The seminal work by Eric Shea–Brown and co-workers [64] provides a nice account of phase reductions of the four simplest, co-dimension one bifurcations that lead to oscillatory dynamics: *Hopf*, *Bautin*, *SNIC* (saddle–node on an invariant circle) and *homoclinic*. The global character[9] of the SNIC and homoclinic bifurcations, however, requires

[9] Bifurcations are typically classified as 'local' or 'global'. A local bifurcation is characterized through the loss of stability or the disappearance of an equilibrium. Qualitative changes of the system's dynamical behavior are localized in a small neighborhood. Outside this neighborhood the dynamics remains qualitatively identical unless other bifurcations occur there simultaneously. If one cannot confine the qualitative changes through a bifurcation to a (small) neighborhood, one speaks of a global bifurcation. Examples for local bifurcations are saddle–node, pitchfork, transcritical or Hopf bifurcations, while homoclinic and SNIC bifurcation are of global character.

an educated guess about the limit cycle trajectories away from the respective fixed points undergoing the particular bifurcation, so that the corresponding phase sensitivity function cannot be parametrized in terms of the original oscillator dynamics. The Bautin bifurcation (or generalized Hopf bifurcation) has the normal form that agrees with that of the Hopf bifurcation except for the sign of the parameter of the cubic term is different. This leads to a subcritical Hopf bifurcation, whose branch of unstable periodic orbits becomes stable at a saddle–node bifurcation of periodic orbits. Given the similarity of their normal forms, it appears reasonable to restrict our considerations on phase reductions of oscillatory dynamics that emerge through a Hopf bifurcation.

4.1. Canonical models, center manifolds and normal forms

Oscillator dynamics on the limit cycle are similar across models if these oscillations emerge through the same particular type of bifurcation. This similarity gives rise to *canonical models* for every type of bifurcation, which capture the essence of the dynamics near the bifurcation point. All dynamical systems with similar dynamical behavior can be transformed into a canonical model. The insights from a canonical model can be very fruitful for identifying the phase dynamics, as for systems close to the same bifurcation it suffices to consider canonical models of the corresponding dynamical systems [46]. Even without knowing the exact equations of the canonical model, the phase sensitivity function $\boldsymbol{Z}$ can often be anticipated to have a particular form that is characteristic for the type of bifurcation, see, e.g., [64,102]. However, determining the exact form of the limit cycle and of the dynamics around it crucially depends on the equations of the canonical model. Unfortunately, there is a caveat. As Hoppensteadt and Izhikevich properly remarked in their textbook [46], there does not exist a general algorithm for deriving canonical models. Normal form and center manifold theories have proven successful candidates to obtain simplified equations and to reduce their dimension, respectively. We here clarify the intricate link between these theories and indicate how to apply them for subsequent phase reductions.

The concepts of center manifolds and of normal forms are so closely related that many textbooks do not bother to distinguish between them. Often, the *center manifold reduction* of a dynamical system is computed first in order to reduce the dimension of the system. Afterwards, this simplified, lower-dimensional system is brought into normal form. However, there is a subtle conceptual difference to the actual *normal form reduction*. A normal form reduction is characterized through smooth, consecutive transformations or changes of coordinates, which preserve the essential characteristics of the underlying dynamical system and which do not reduce its dimension. Via coordinate transformations a normal form reduction yields a thorough picture of the dynamics in terms of the system's stable, unstable and center manifolds. Normal form reductions even provide the stable and unstable fibrations over the center manifold [77]. In this sense, normal forms can be considered more general because the reduced analytic expressions accurately describe the dynamics also away from bifurcation points.

Center manifold. Whenever a dynamical system passes through a bifurcation, there is a sudden qualitative change in the system's behavior. For instance, a fixed point solution of the dynamical system switches its stability. This change in stability is represented in the spectrum of the linearized dynamics about the fixed point: the real part of at least one eigenvalue changes signs and becomes zero at the critical bifurcation point. The *center manifold* is an invariant manifold corresponding to the eigenvectors associated with the eigenvalues with zero real part.[10] The dynamics on the center manifold is slower than that on the stable and unstable manifolds, corresponding to the eigenvalues with negative and positive non-vanishing real parts, respectively. The attraction towards the stable manifold as well as the repulsion from the unstable manifold are exponentially fast. Hence, one can determine the entire dynamics via the center, or critical, modes, i.e. through the variables $\boldsymbol{x}_{\text{slow}}$ corresponding to the slow flow along the center manifold. More formally, the local behavior of the fast variables $\boldsymbol{x}_{\text{fast}}$ around the fixed point can be expressed as

$$\boldsymbol{x}_{\text{fast}} = \boldsymbol{C}\left(\boldsymbol{x}_{\text{slow}}\right) \ . \tag{4.1}$$

Importantly, the function $\boldsymbol{C}$, albeit arbitrary, only contains terms of second and higher order. The expression (4.1) characterizes the center manifold locally with the corresponding dynamics given by

$$\dot{\boldsymbol{x}}_{\text{slow}} = \boldsymbol{L}\boldsymbol{x}_{\text{slow}} + \boldsymbol{N}\left(\boldsymbol{x}_{\text{slow}}, \boldsymbol{C}\left(\boldsymbol{x}_{\text{slow}}\right)\right) \ . \tag{4.2}$$

The real parts of all the eigenvalues of the matrix $\boldsymbol{L}$ vanish and $\boldsymbol{N}$ contains all the nonlinear terms. This *center manifold reduction* effectively reduces the dimensionality of the system to the number of eigenvalues with vanishing real part. One may interpret this dimensionality reduction in that the fast variables $\boldsymbol{x}_{\text{fast}}$ are prescribed by the slow ones $\boldsymbol{x}_{\text{slow}}$, which in the physics literature is often referred to as Haken's *slaving principle* [88,103].

In the case of a supercritical Hopf bifurcation, a stable fixed point loses stability as a pair of complex conjugate eigenvalues crosses the imaginary axes and stable limit-cycle oscillations emerge. Hence, we have two eigenvalues with zero real part, and the corresponding center manifold is two-dimensional.

[10] The eigenvectors associated with the eigenvalues with vanishing real part span the center eigenspace of the respective fixed point. The center manifold has the same dimension as the center eigenspace and is tangential to it at the fixed point.

Normal form. The normal form of a bifurcation is the 'simplest', reduced equation (4.2) that exhibits the qualitative features of the bifurcation type. The dimension of the normal form coincides with the number of critical modes, and hence with the dimension of the center manifold. The normal form can be achieved, e.g., by removing all non-resonant terms in the nonlinear function $\boldsymbol{C}$.[11]

Although the nomenclature appears somewhat misleading, normal form reductions do not necessarily result in the normal form of a bifurcation as defined above. This is only true close to bifurcations of dynamical systems where all eigenvalues have zero real part, e.g., as in the case of a Hopf bifurcation in a two-dimensional dynamical system. The reason for this is that normal form reductions yield a simplified equation – a 'normal form' in the strict sense – of the same dimension as that of the underlying dynamical system. As such, a normal form reduction is a rigorous transformation of a dynamical system into a simplified equation without reducing its dimension, whereas a center manifold reduction reduces the dimension without simplifying the equation.[12] Interestingly, given the normal form through a normal form reduction, the critical center modes will 'miraculously' decouple from the fast variables and the normal form of the bifurcation on the center manifold is retained [77,104]. In the following we will refer to the 'normal form of a bifurcation' simply as *normal form* unless stated otherwise.

A bit of history. Normal form theory goes back to Poinaré's work [81] and has ever since attracted attention as a technique of transforming nonlinear differential equations to generic and simpler standard forms near a (local) bifurcation point. The precise normal form can be determined in different ways. While coordinate transformations have been frequently used, addressing normal form calculations more categorically involves a matrix representation method, an adjoint method and a method based on the representation theory of the Lie algebra $\mathrm{sl}(2,\mathbb{R})$. All these methods are strongly connected and, as mentioned earlier, based on the ideas of Takens [83,84]. The resulting normal form can be expressed as lying in the kernel of an adjoint linear operator on the space of homogeneous polynomials [75–77]. Alternatively, a perturbation technique has been proposed by Nayfeh [78] and Yu [105], which dwells on the methods of multiple time scales [100] and of intrinsic harmonic balancing [106]. The reductive perturbation approach of Kuramoto in Section 4.3.1 also uses a two time-scale separation.

More recent developments. Other approaches to derive normal forms can be subsumed into time averaging [75,85], a Lyapunov–Schmidt reduction method [79], and a singular point value method [107,108]. The latter were originally meant to determine focus, or focal, values of a (degenerated Hopf) critical point to prove the existence (and the maximal amount of multiple) limit cycle(s), but this requires the computation of higher-order normal forms [80]. The idea behind the singular point value method is to introduce formal power series and recursive forms to calculate singular point quantities. The Lyapunov–Schmidt reduction approach, on the other hand, elegantly reformulates the problem of proving the existence of periodic solutions emerging from Hopf bifurcations as that of finding a family of solutions of an abstract equation in a functional space of periodic functions. Its reformulation in terms of functional analysis allows for a generalization of the problem in infinite-dimensional space, cf. [82]. Essentially, one projects the entire system under study into the subspace that is spanned by the eigenvectors associated with the pair of purely imaginary eigenvalues at the Hopf point. This results into a set of algebraic equations while the other approaches yield differential equations [80]. By projecting the system into a specific subspace, also the methods of time averaging and of multiple time scales fall in the same category. For time averaging, one transforms the original autonomous system $\dot{\boldsymbol{x}} = \boldsymbol{f}(\boldsymbol{x};\mu)$ into a non-autonomous one via $\boldsymbol{y} = \exp(t\boldsymbol{J})\boldsymbol{x}$. Here, $\boldsymbol{J}$ is the Jacobian of the vector field $\boldsymbol{f}(\boldsymbol{x};\mu)$ at $\boldsymbol{x} = 0$. The domain $\Omega \subset \mathbb{R}^n$ of $\boldsymbol{x} \in \Omega$ is invariant under the Lie group $\boldsymbol{\Gamma} = \{\exp(t\boldsymbol{J}) \mid t \in \mathbb{R}\}$. The time-dependent system is subsequently solved using the conventional averaging method [85,109,110]. It is important to realize that most of these methods rely on a 'preprocessing' and a dimensionality reduction following center manifold theory, which assures the existence of an *amplitude equation* and also indicates its order. For instance, the singular point value method first applies a center manifold reduction to the original dynamics, which yields a two-dimensional center manifold associated with the Hopf bifurcation. The perturbation method, by contrast, does not necessarily require such a center manifold reduction [80,111,112].

4.2. Hopf normal form

Whenever a single oscillatory dynamics emerges through a (supercritical) Hopf bifurcation, it is possible to transform it into *Hopf normal form*

$$\dot{w} = f(w;\mu) = \sum_{m=0}^{M-1} (-1)^m \sigma_m |w|^{2m} w + \mathcal{O}^{2M}(w)\,, \quad w \in \mathbb{C}\,. \tag{4.4}$$

[11] In consequence, the normal form will contain only *resonant monomials* $w_1^{m_1} \cdot \ldots \cdot w_n^{m_n}$ with $m_j \in \mathbb{N}, j = 1,\ldots,n$, satisfying

$$m_1 + \cdots + m_n = k \quad \text{and} \quad m_1\lambda_1 + \cdots + m_n\lambda_n - \lambda_k = 0, \quad \text{for each } k \geq 2. \tag{4.3}$$

For pure imaginary eigenvalues λ_j of the dynamic's Jacobian, the second equation of (4.3) becomes indeed a resonance among frequencies in the usual sense. This resonance property can be proven in a straightforward way for the semi-simple normal form style, cf. Theorem §2.1.5 in [76]; see also below.

[12] A center manifold reduction may even lead to the loss of some important nonlinear properties of the system under study that are linked to the dynamics on the stable and unstable manifolds.

Here, $\sigma_m = \sigma_m(\mu) \in \mathbb{C}$ are complex-valued coefficients, the parameter $\mu \in \mathbb{R}$ denotes the bifurcation parameter and can be interpreted as the distance to the Hopf bifurcation at $\mu = \tilde{\mu} = 0$. The integer $M \in \mathbb{N}$ defines the order of the Hopf normal form. For second order, i.e. for $M = 2$, (4.4) takes on the form of a complex *Stuart–Landau oscillator*:

$$\dot{w} = \alpha w - \beta |w|^2 w$$

with $\alpha \equiv \sigma_0 = u_0 + iv_0$ and $\beta \equiv \sigma_1 = u_1 + iv_1$. Setting $u_0(\mu) = \mu$ while keeping the other parameters fix with $u_1 > 0$, circular oscillations emerge at $\mu = 0$ with radius $R = \sqrt{\mu/u_1} \propto \sqrt{\mu}$. Here, μ indeed denotes the distance to the Hopf bifurcation.

4.3. Hopf normal form reductions

We consider the dynamical system

$$\dot{\boldsymbol{x}} = \boldsymbol{f}(\boldsymbol{x}; \mu)$$

with state vector $\boldsymbol{x} \in \mathbb{R}^n$ and vector field $\boldsymbol{f} = (f_1, \ldots, f_n): \mathbb{R}^n \to \mathbb{R}^n$. The system has a stable fixed point solution $\tilde{\boldsymbol{x}}$, i.e. $\boldsymbol{f}(\boldsymbol{x} = \tilde{\boldsymbol{x}}; \mu) = \boldsymbol{0}$ for small values of the bifurcation parameter $\mu \in \mathbb{R}$. At a given parameter value $\mu = \tilde{\mu}$ the fixed point $\tilde{\boldsymbol{x}}$ undergoes a supercritical Hopf bifurcation: For $\mu < \tilde{\mu}$, the dynamics $\dot{\boldsymbol{x}} = \boldsymbol{f}(\boldsymbol{x}; \mu)$ has a stable fixed point, which loses stability at $\mu = \tilde{\mu}$, and stable oscillations emerge for $\mu > \tilde{\mu}$. Without loss of generality we translate the fixed point to the origin, i.e. $\tilde{\boldsymbol{x}} = \boldsymbol{0}$, and assume that $\tilde{\mu} = 0$. Then, for $\mu > 0$, stable limit cycle oscillations emerge with natural frequency $\omega \neq 0$ and amplitude $R = \mathcal{O}(\varepsilon)$ where $\varepsilon = \sqrt{\mu}$.

In the following subsections we will illustrate three different ways how to reduce $\dot{\boldsymbol{x}} = \boldsymbol{f}(\boldsymbol{x}; \mu)$ to the Hopf normal form (4.4). In Section 4.3.1 we will present a physically motivated, reductive perturbation approach promoted by Kuramoto [12]. Its inherent separation of time-scales lets this approach resemble a center manifold reduction. A mathematical approach of a Hopf normal form reduction using nonlinear, so-called Poincaré transformations will be subject in Section 4.3.2. For simplicity, we will consider a two-dimensional system so that the dimension of the phase space already coincides with the one of the expected center manifold. While this approach is hence kept as mathematically exact as possible, the concept extends naturally to general n-dimensional systems, where the governing equations restricted to the center manifold can be computed with a projection method as outlined in [Chapter 5.4, 82]. Ultimately, we will provide a rather general normal form reduction approach in Section 4.3.3 that goes back to early ideas of Takens [84] and utilizes an adjoint linear operator expressed in a Lie bracket formalism. To compare it against the two other methods, we have applied it exemplarily to a two-dimensional system in Appendix A.4, where we also provide the computations of Hopf normal forms of higher order.

The different Hopf normal form reductions to be presented below vary not only in their methodical approach, but also in their accuracy. While, e.g., the reductive perturbation approach in Section 4.3.1 discards any higher order dependence on μ, the nonlinear transforms approach, Section 4.3.2, respects this μ-dependence at all times. The differences between the reduction techniques[13] may be negligible for small-amplitude oscillations, that is, close to the Hopf bifurcation point with $0 < \mu \ll \mu_0 \ll 1$. But the resulting normal form techniques will diverge drastically when the amplitudes of oscillation become larger. These differences eventually become evident in the reduced phase dynamics and may cause qualitatively different collective dynamics.

4.3.1. Kuramoto's reductive perturbation

To outline Kuramoto's early approach to derive the Hopf normal form we adopt the reasoning of Chapter 2 in his seminal book "Chemical Oscillations, Turbulence, and Waves" [12]. The approach belongs to the general group of *reductive perturbation methods*, which include all related techniques using stretched space–time coordinates. It builds on the method of multiple scales via a small parameter expansion, much related to bifurcation theory [113]. As has already been noted by Haken and Kuramoto [114,115], the method lacks some precision in its mathematical theory, but has nonetheless proven to be of indisputable utility in practice.

The goal of the reductive perturbation approach is to derive a so-called amplitude equation, which coincides with the canonical model of an oscillator close to a supercritical Hopf bifurcation. We consider the n-dimensional dynamics $\dot{\boldsymbol{x}} = \boldsymbol{f}(\boldsymbol{x}; \mu)$ which has a stable fixed point solution $\boldsymbol{x} = \boldsymbol{0}$ that undergoes a Hopf bifurcation at $\mu = 0$, giving rise to stable limit-cycle oscillations with amplitude $R = \mathcal{O}(\varepsilon)$ where $\varepsilon = \sqrt{\mu}$. In the following we will only consider $\mu > 0$. Next, we expand $\boldsymbol{f}(\boldsymbol{x}; \mu) = \boldsymbol{f}(\boldsymbol{x}; \varepsilon^2)$ around $\boldsymbol{x} = 0$ in terms of

$$\boldsymbol{f}(\boldsymbol{x}; \varepsilon^2) = \boldsymbol{n}_1(\boldsymbol{x}; \varepsilon^2) + \boldsymbol{n}_2(\boldsymbol{x}, \boldsymbol{x}; \varepsilon^2) + \boldsymbol{n}_3(\boldsymbol{x}, \boldsymbol{x}, \boldsymbol{x}; \varepsilon^2) + \mathcal{O}^4(\boldsymbol{x}) \ ,$$

[13] The accuracy of the reductive perturbation method is at first order in μ. The accuracy of the nonlinear transform approach is at the same order in μ as the order M of the normal form. As to the third approach based on Takens, it is possible to achieve the same accuracy as with the nonlinear transform approach. To do so, one assumes the parameter μ to be an additional variable and consider the $n + 1$-dimensional, so-called extended system. The subsequent transformations then become parameter-dependent and can be implemented in the corresponding algorithm, see Section 4.3.3 and [104]. For the sake of simplicity, however, we present only the non-extended system, thereby providing another normal form with the same accuracy as the reductive perturbation approach.

where the functions $\boldsymbol{n}_k$ are given by

$$\boldsymbol{n}_k(\boldsymbol{u}^{(1)}, \boldsymbol{u}^{(2)}, \dots, \boldsymbol{u}^{(k)}; \varepsilon^2) = \sum_{i_1,\dots,i_k=1}^{n} \frac{1}{k!} \left(\frac{\partial^k \boldsymbol{f}(\boldsymbol{x}; \varepsilon^2)}{\partial x_{i_1} \partial x_{i_2} \dots \partial x_{i_k}} \right)_{\boldsymbol{x}=\boldsymbol{0}} u_{i_1}^{(1)} u_{i_2}^{(2)} \dots u_{i_k}^{(k)}$$

with $\boldsymbol{u}^{(j)} = \left(u_1^{(j)}, \dots, u_n^{(j)}\right)^\intercal \in \mathbb{R}^n$. We further expand $\boldsymbol{n}_k$ with respect to ε^2 and immediately obtain

$$\boldsymbol{f}(\boldsymbol{x}; \varepsilon^2) = \hat{\boldsymbol{L}}_0 \boldsymbol{x} + \varepsilon^2 \hat{\boldsymbol{L}}_1 \boldsymbol{x} + \boldsymbol{n}_2(\boldsymbol{x}, \boldsymbol{x}) + \boldsymbol{n}_3(\boldsymbol{x}, \boldsymbol{x}, \boldsymbol{x}) + \mathcal{O}^4(\boldsymbol{x}) \,, \tag{4.5}$$

where $\boldsymbol{n}_2(\boldsymbol{x}, \boldsymbol{x}) = \boldsymbol{n}_2(\boldsymbol{x}, \boldsymbol{x}; \varepsilon^2 = 0)$ and a similar expression for $\boldsymbol{n}_3$; see also Appendix A.2.1. In (4.5) we omitted all $\mathcal{O}(\varepsilon^2)$ terms in $\boldsymbol{n}_2$ and $\boldsymbol{n}_3$. Since we assumed $\boldsymbol{x}$ to undergo a Hopf bifurcation, the operator $\hat{\boldsymbol{L}}_0$ has a pair of purely imaginary eigenvalues $\pm i\omega_0$, while the other $n-2$ eigenvalues have non-vanishing real part. Let $\boldsymbol{u}$ and $\boldsymbol{v}$ denote the right and left eigenvectors of $\hat{\boldsymbol{L}}_0$, respectively, corresponding to the eigenvalue $+i\omega_0$. That is, $\hat{\boldsymbol{L}}_0 \boldsymbol{u} = i\omega_0 \boldsymbol{u}$ and $\boldsymbol{v}\hat{\boldsymbol{L}}_0 = i\omega_0 \boldsymbol{v}$. They are normalized as $\boldsymbol{v}\boldsymbol{u} = v_1 u_1 + \dots + v_n u_n = 1$ and fulfill $\boldsymbol{v}\bar{\boldsymbol{u}} = \bar{\boldsymbol{v}}\boldsymbol{u} = 0$. Furthermore, let $\boldsymbol{x}_0$ denote the solution to the linearized system, $\dot{\boldsymbol{x}} = \hat{\boldsymbol{L}}_0 \boldsymbol{x}$, which can be given as

$$\boldsymbol{x}_0(t) = w \mathrm{e}^{i\phi(t)} \boldsymbol{u} + \bar{w} \mathrm{e}^{-i\phi(t)} \bar{\boldsymbol{u}} \,. \tag{4.6}$$

w is an arbitrary complex number (the "complex amplitude"), and $\phi(t) = \omega_0 t$. In general, however, a solution $\boldsymbol{x}(t)$ that satisfies the full (non-linearized) dynamics $\dot{\boldsymbol{x}} = \boldsymbol{f}(\boldsymbol{x}; \varepsilon^2)$ will deviate from $\boldsymbol{x}_0(t)$. When introducing a rescaled time, $\tau = \varepsilon^2 t$, and considering $w = w(\tau)$ to be time-dependent (on the slower time scale), we can describe the time-asymptotic behavior of $\boldsymbol{x}(t)$ in the form

$$\begin{aligned} \boldsymbol{x} &= \boldsymbol{x}_0(w, \bar{w}, \phi) + \boldsymbol{\rho}(w, \bar{w}, \phi) \,, \\ \dot{w} &= f(w, \bar{w}) \,. \end{aligned} \tag{4.7}$$

The functions $\boldsymbol{\rho}$ and f are to be determined perturbatively, i.e., by considering a 'small' deviation from the exact solution $\boldsymbol{x} = \boldsymbol{x}_0$ and expanding the dynamics around it. Eq. (4.7) is referred to as the *amplitude equation*. The explicit form of $f(w, w')$ in lowest order is

$$f(w, \bar{w}) = \alpha w - \beta |w|^2 w \,, \tag{4.8}$$

where the complex-valued coefficients α and β satisfy

$$\begin{aligned} \alpha &= \boldsymbol{v}\hat{\boldsymbol{L}}_1 \boldsymbol{u} \,, \\ \beta &= -3\boldsymbol{v}\boldsymbol{n}_3(\boldsymbol{u}, \boldsymbol{u}, \bar{\boldsymbol{u}}) + 4\boldsymbol{v}\boldsymbol{n}_2\left(\boldsymbol{u}, \hat{\boldsymbol{L}}_0^{-1} \boldsymbol{n}_2(\boldsymbol{u}, \bar{\boldsymbol{u}})\right) + 2\boldsymbol{v}\boldsymbol{n}_2\left(\bar{\boldsymbol{u}}, (\hat{\boldsymbol{L}}_0 - 2i\omega_0 \boldsymbol{I})^{-1} \boldsymbol{n}_2(\boldsymbol{u}, \boldsymbol{u})\right) \,. \end{aligned} \tag{4.9}$$

$\boldsymbol{I}$ denotes an n-dimensional identity matrix; cf. Eqs. (2.2.17–20) in [12]. The exact derivation with all mathematical details can be found in Appendix A.2.1.

4.3.2. Poincaré's reduction via nonlinear transforms

Instead of employing perturbation theory, one can alternatively derive the Hopf normal form via nonlinear transforms, as already used by Poincaré. We follow closely the line of argument in Kuznetsov's textbook [Chapter 3, 82] and consider the dynamics $\dot{\boldsymbol{x}} = \boldsymbol{f}(\boldsymbol{x}; \mu)$ as in the previous subsection. To simplify notation, we restrict our case to only two real dimensions $\boldsymbol{x} = (x, y), \boldsymbol{x}' = (x', y') \in \mathbb{R}^2$.[14] As usual, for $\mu = 0$ the fixed point $\boldsymbol{x} = \boldsymbol{0}$ undergoes a supercritical Hopf bifurcation. We can decompose $\boldsymbol{f}$ into a linear and nonlinear part,

$$\boldsymbol{f}(\boldsymbol{x}) = \boldsymbol{L}(\mu)\boldsymbol{x} + \boldsymbol{F}(\boldsymbol{x}; \mu) \,,$$

where $\boldsymbol{L}(\mu) = \nabla \boldsymbol{f}(\boldsymbol{x}; \mu)\big|_{\boldsymbol{x}=\boldsymbol{0}}$ has eigenvalues $\lambda(\mu) = \varrho(\mu) \pm i\omega(\mu)$ that satisfy $\varrho(0) = 0$ and $\omega(0) = \omega_0 > 0$. The goal is then to rewrite the dynamics in a generic form (4.4) and to provide an instruction how to determine the corresponding complex-valued parameters with a sequence of near-identity transformations. The transformation of $\boldsymbol{f}(\boldsymbol{x}; \mu)$ into the desired Hopf normal form $\alpha(\mu)w - \beta(\mu)|w|^2 w$ can finally be achieved using the strategy sketched below. We refer to Appendix A.3 for all mathematical details. In brief:

(i) We write the dynamics $\dot{\boldsymbol{x}} = \boldsymbol{f}(\boldsymbol{x}; \mu)$ in complex form

$$\dot{z} = \lambda z + \tilde{f}(z, \bar{z}; \mu) \,, \tag{4.10}$$

where the transformation $\boldsymbol{x} \in \mathbb{R}^2 \mapsto z \in \mathbb{C}$ in the complex plane is determined by the eigenvectors of the Jacobian $\boldsymbol{L}$.

[14] A straightforward extension to n-dimensional dynamical systems using a projection method can be found in [Chapter 5, 82].

(ii) Provided that the right-hand side of (4.10) can be approximated in polynomial from up to third order, that is,

$$\dot{z} = \lambda z + \sum_{2\le k+l\le 3} f_{kl} z^k \bar{z}^l + \mathcal{O}^4(z) \,,$$

we can achieve the Hopf normal form for a single oscillator $\dot{w} = \lambda w - \beta |w|^2 w + \mathcal{O}^4(w)$ via a *Poincaré transformation*, i.e. a nonlinear near-identity coordinate transform

$$z = \psi(w) = w + \sum_{2\le k+l\le 3} h_{kl} w^k \bar{w}^l \,. \tag{4.11}$$

The coefficients h_{jk} depend on λ and the f_{kl} and can be identified through introducing a local inverse transform and a subsequent comparison of coefficients, see Appendix A.3.

Note that there is a prevailing and inherent dependence of all coefficients on the bifurcation parameter μ. Evaluating the resulting formulas at the bifurcation point, $\mu = 0$, reveals the similarity to the *reductive perturbation approach*, cf. Section 4.3.1. For instance, we can determine the parameter $\beta(0) = \beta(\mu = 0)$ that relates to the cubic term in the normal form as

$$\beta(0) = -\tfrac{i}{2\omega_0}\left(f_{20} f_{11} - 2|f_{11}|^2 - \tfrac{1}{3}|f_{02}|^2\right) - \frac{1}{2} f_{21} \,.$$

This closely resembles equation (4.9) in Section 4.3.1.

4.3.3. Takens' reduction via Lie brackets

This admittedly more abstract, yet frequently used technique to compute the Hopf normal form has been introduced by Leung and co-workers [116,117] but is coined according to Takens' corresponding work [84]. The approach belongs to the class of the so-called matrix representation methods. It allows for determining arbitrary higher-order Hopf normal forms, though the resulting normal form is of the same order of accuracy as the reductive perturbation technique in Section 4.3.1.[15] We again start off with dynamics $\dot{\boldsymbol{x}} = \boldsymbol{f}(\boldsymbol{x}; \mu)$ in the vicinity of the fixed point $\boldsymbol{x} = 0$ with $|\mu| \ll 1$ sufficiently small. After diagonalizing the Jacobian $\boldsymbol{L}(\mu) = \nabla \boldsymbol{f}(\boldsymbol{x}; \mu)\big|_{\boldsymbol{x}=\boldsymbol{0}} = D\boldsymbol{f}(\boldsymbol{x}; \mu)\big|_{\boldsymbol{x}=\boldsymbol{0}}$ evaluated at $\mu = 0$, one finds the dynamics in Jordan normal form

$$\dot{\boldsymbol{z}} = \boldsymbol{J}\boldsymbol{z} + \boldsymbol{F}(\boldsymbol{z}) \,, \tag{4.12}$$

with $\boldsymbol{J} = \mathrm{diag}(\lambda_1, \ldots, \lambda_n)$, where $\lambda_j \in \mathbb{C}, j = 1, \ldots, n$, are the complex eigenvalues of $\boldsymbol{L}(0)$, and $\boldsymbol{F}$ comprises all nonlinear terms in $\boldsymbol{z}$. The goal is to establish a transformation

$$\boldsymbol{z} = \boldsymbol{P}(\boldsymbol{w}) = \boldsymbol{w} + \boldsymbol{p}(\boldsymbol{w}) \tag{4.13}$$

that removes all irrelevant terms (up to a given order) from the Taylor series of

$$\dot{\boldsymbol{w}} = (D\boldsymbol{P}(\boldsymbol{w}))^{-1}\left[\boldsymbol{J}\boldsymbol{P}(\boldsymbol{w}) + \boldsymbol{F}\big(\boldsymbol{P}(\boldsymbol{w})\big)\right] \,. \tag{4.14}$$

The transformation (4.13) is nearly-identical due to its linear part. We expand the nonlinear function $\boldsymbol{F}(\boldsymbol{z})$ as a series of homogeneous polynomials

$$\boldsymbol{F}(\boldsymbol{z}) = \boldsymbol{F}_2(\boldsymbol{z}) + \boldsymbol{F}_3(\boldsymbol{z}) + \cdots + \boldsymbol{F}_r(\boldsymbol{z}) + \mathcal{O}^{r+1}(\boldsymbol{z}) \,, \quad \boldsymbol{F}_k \in \mathcal{P}_k \,, \tag{4.15}$$

where $r \in \mathbb{N}$ and $\mathcal{P}_k$ is the set of homogeneous polynomials of order k, and introduce an adjoint operator $L_J : \mathcal{P}_k \to \mathcal{P}_k$ via

$$L_J(\boldsymbol{Y})(\boldsymbol{z}) = [\boldsymbol{Y}, \boldsymbol{J}\boldsymbol{z}](\boldsymbol{z}) = \boldsymbol{J}\boldsymbol{Y}(\boldsymbol{z}) - (D\boldsymbol{Y}(\boldsymbol{z}))\boldsymbol{J}\boldsymbol{z} \,, \tag{4.16}$$

where $[\cdot, \cdot]$ denotes the Lie bracket [84]. With this definition one can immediately use *Takens' normal form theorem* [75,84,116]: Given a system $\dot{\boldsymbol{z}} = \boldsymbol{J}\boldsymbol{z} + \boldsymbol{F}(\boldsymbol{z})$ of differential equations, where $\boldsymbol{F} = \boldsymbol{F}_2 + \boldsymbol{F}_3 + \ldots$ as in (4.15) is truncated at order r and $\boldsymbol{F}(\boldsymbol{0}) = \boldsymbol{0}$, choose a complement $\mathcal{H}_k$ of $L_J(\mathcal{P}_k)$, such that $\mathcal{P}_k = L_J(\mathcal{P}_k) \oplus \mathcal{H}_k$. Then, there is an analytic change of coordinates in a neighborhood of the origin which transforms the system above to $\dot{\boldsymbol{w}} = \boldsymbol{h}(\boldsymbol{w}) = \boldsymbol{h}_1(\boldsymbol{w}) + \boldsymbol{h}_2(\boldsymbol{w}) + \cdots + \boldsymbol{h}_r(\boldsymbol{w}) + \boldsymbol{R}_r$ with $\boldsymbol{h}_1(\boldsymbol{w})$ being the linear term and $\boldsymbol{h}_k \in \mathcal{H}_k$ for $k = 2, \ldots, r$, and residual $\boldsymbol{R}_r = \mathcal{O}^{r+1}(\boldsymbol{w})$. The proof of this theorem is constructive and by induction, using a series of coordinate transforms $\boldsymbol{z} = \boldsymbol{w} + \boldsymbol{p}_k(\boldsymbol{w})$ with $\boldsymbol{p}_k$ homogeneous polynomials of degree k with $k = 1, \ldots, r$. The coefficients of $\boldsymbol{p}_k$ are to be determined in each step such that

$$\boldsymbol{F}_k(\boldsymbol{w}) + L_J(\boldsymbol{p}_k)(\boldsymbol{w}) \in \mathcal{H}_k \,. \tag{4.17}$$

Details of the proof and further examples can be found in [75,77,78,84,116,117].[16] Since we address classical, first-level normal forms only, the entire transformation procedure is based on the Jacobian, that is, on the linearized dynamics near

[15] The technique presented here applies only to vector fields that have a single zero eigenvalue or a single pair of purely imaginary eigenvalues [75]. Moreover, we restrict the theory to the semi-simple case only, that is, the dynamics have a diagonizable linear part.

[16] $\boldsymbol{J}$ is semi-simple, so the complement $\mathcal{H}_k$ will be chosen as $\mathcal{H}_k = \ker\big(L_J(\mathcal{P}_k)\big)$ as mentioned above. In this case, a direct calculation shows that $\mathcal{H}_k$ is spanned by all resonant monomials of order k for each $k \ge 2$, from which (4.3) follows.

the bifurcation point. If the bifurcation possesses certain symmetries, they become apparent in the Jacobian and are thus induced on the nonlinear part of the computed normal form. In particular, systems near a Hopf bifurcation are mapped by a polynomial transformation to a normal form that has circular symmetry.

A practical application of this computational approach to a two-dimensional system $\boldsymbol{z} = (z_1, z_2)$ near the Hopf bifurcation can be found in Appendix A.4 including further mathematical details. Unfortunately, the complexity of computing the coefficients for higher-order normal forms increases rapidly as the determination of parameters builds recursively upon each other and on the lower-order near-identity transformations $\boldsymbol{p}_k$, $k \leq 4$. It hence becomes necessary to implement efficient algorithms in symbolic computation software. An arithmetic algorithm including the computation of normal forms up to order eleven has been presented in [117].

4.4. Example: Phase reductions of a single oscillator in Hopf normal form

The general Mth-order *Hopf normal form* of a single oscillator in the vicinity of a (supercritical) Hopf bifurcation has been introduced in (4.4). It reads

$$\dot{w} = f(w;\mu) = \sum_{m=0}^{M-1} (-1)^m \sigma_m |w|^{2m} w + \mathcal{O}^{2M}(w)\,, \quad w \in \mathbb{C}\,,$$

with complex-valued coefficients $\sigma_m = \sigma_m(\mu) \in \mathbb{C}$ and bifurcation parameter $\mu \in \mathbb{R}$ indicating the distance to the Hopf bifurcation at $\mu = 0$. The complex-valued variable $w \in \mathbb{C}$ can be written in polar coordinates (R, θ) as $w = Re^{i\theta}$, or in planar coordinates $\boldsymbol{x} = (x, y) \in \mathbb{R}^2$ as $w = x + iy$. The amplitude, or radius, $R \geq 0$ and angle $\theta \in \mathbb{S}^1$ satisfy $R = \sqrt{x^2 + y^2}$ and $\theta = \tan^{-1}(y, x)$ with $\tan^{-1}$ the quadrant-corrected inverse tangent. The Hopf normal form (4.4) in polar coordinates reads

$$\dot{R} = \sum_{m=0}^{M-1} (-1)^m u_m R^{2m+1} = R \cdot \Re\,, \quad \dot{\theta} = \sum_{m=0}^{M} (-1)^n v_m R^{2m} = \Im\,, \tag{4.18}$$

with $\sigma_m = u_m + iv_m$ and real-valued $u_m, v_m \in \mathbb{R}$, where we abbreviated

$$\Re = \sum_{m=0}^{M-1} (-1)^m u_m R^{2m}\,, \quad \Im = \sum_{m=0}^{M} (-1)^n v_m R^{2m}\,.$$

The corresponding planar dynamics of (4.4) reads

$$\dot{\boldsymbol{x}} = \begin{pmatrix} \Re & -\Im \\ \Im & \Re \end{pmatrix} \boldsymbol{x}\,. \tag{4.19}$$

In (4.18) the radial dynamics $\dot{R}$ decouples from the angular dynamics $\dot{\theta}$. If the parameters $\sigma_m = u_m + iv_m$ are such that $\dot{R}$ has a stable non-trivial solution R^c, then there exists a T-periodic circular limit-cycle solution of (4.4),

$$w^c(t) = x^c(t) + iy^c(t) = R^c e^{i\theta^c}\,, \quad \text{or} \quad \boldsymbol{x}^c(t) = \begin{pmatrix} x^c(t) \\ y^c(t) \end{pmatrix} = R^c \begin{pmatrix} \cos\theta^c \\ \sin\theta^c \end{pmatrix}$$

with constant radius R^c and constantly increasing phase $\theta^c(t) = \omega t + \theta_0$. The period $T = 2\pi/\omega$ is defined through the frequency ω. Note that both R^c and ω depend on the normal form coefficients σ_m or (u_m, v_m), respectively, with $m = 0, \ldots, M-1$.[17] Without loss of generality, we set $\theta_0 = 0$ so that θ^c is uniquely defined through the frequency ω.

Winfree's reduction via isochrons

As mentioned above, Winfree's reduction via isochrons heavily depends on whether explicit expressions of the limit cycle $\mathcal{C}$ and the asymptotic phase map Θ along the isochrons are available. For an oscillator in Hopf normal form (4.4) of second order, $M = 2$, this is indeed the case. Expressed in polar coordinates, (4.18) has a globally attracting limit cycle

$$w^c(t) = R^c e^{i\omega t}$$

with radius $R^c = \sqrt{c_2}$ and frequency $\omega = v_0 - v_1 c_2$ with $c_2 = u_0/u_1$. The asymptotic phase map $\theta = \Theta(w)$ defined in Section 2.1 for $\boldsymbol{x} = (\mathrm{Re}(w), \mathrm{Im}(w))$ in $\mathbb{R}^2 \setminus \{\boldsymbol{0}\}$ fulfills $\dot{\theta} = \omega$. Its explicit form reads

$$\Theta\Big(w = Re^{i\phi}\Big) = \arg w - \frac{v_1}{u_1} \ln\left|\frac{w}{w^c}\right| = \phi - \frac{\beta_I}{\beta_R} \ln\left|\frac{R}{R^c}\right|\,.$$

[17] For second order Hopf normal forms, i.e. $M = 2$, $R^c = \sqrt{u_0/u_1}$ and $\omega = v_0 - u_0 v_1/u_1$ if $u_0, u_1 > 0$. For third order, $M = 3$, $R^c > 0$ solves $u_0 - u_1 R^2 + u_2 R^4 = 0$ if $u_0, u_1, u_2 > 0$ and $u_1^2 - 4u_0 u_2 \geq 0$. The frequency ω then depends on $u_0, u_1, u_2, v_0, v_1, v_2$.

The phase sensitivity function $\boldsymbol{Z}(\theta) = \big(Z_x(\theta), Z_y(\theta)\big) = \nabla\Theta(w)\big|_{w=w^c}$ is the gradient of the phase map Θ evaluated at the limit cycle w^c. For infinitesimally small and pulse-like perturbations $\boldsymbol{p} = x_p + iy_p$, we can compute $\boldsymbol{Z}$ also via the phase response function $G(\theta, \boldsymbol{p} = x_p + iy_p) = \Theta(w^c(\theta) + \boldsymbol{p}) - \theta$ according to (2.10) as

$$\boldsymbol{Z}(\theta) = \begin{pmatrix} Z_x(\theta) \\ Z_Y(\theta) \end{pmatrix} = \begin{pmatrix} \partial_x G(\theta, \boldsymbol{p}) \\ \partial_y G(\theta, \boldsymbol{p}) \end{pmatrix}_{x_p = y_p = 0}$$

The explicit forms of $\boldsymbol{Z}(\theta) \in \mathbb{R}^2$ as well as of the corresponding complex-valued form $Z(\theta) = Z_x(\theta) + iZ_y(\theta)$ are

$$\boldsymbol{Z}(\theta) = \frac{1}{R^c}\begin{pmatrix} -\sin\theta - c_2\cos\theta \\ -c_2\sin\theta + \cos\theta \end{pmatrix} \quad \text{and} \quad Z(\theta) = \frac{-c_2 + i}{R^c}\mathrm{e}^{i\theta} \,. \tag{4.20}$$

Kuramoto's reduction via Floquet eigenvectors

Despite the simplicity of Winfree's reduction via isochrons, deriving the explicit form for the asymptotic phase map Θ becomes challenging already for Hopf normal forms (4.4) beyond second order. Alternatively, one can use Kuramoto's reduction via Floquet eigenvectors to derive the phase sensitivity function $\boldsymbol{Z}$. In view of (3.2), we therefore have to determine $\boldsymbol{v}_0$ and $\boldsymbol{S}(t)$. To do so, we consider a stable limit cycle solution $w^c(t) = R^c\mathrm{e}^{i\omega t}$ in the polar coordinate dynamics (4.18) as before. By introducing a small deviation $z(t)$ off the limit-cycle trajectory $w^c(t)$ as $w(t) = w^c(t)[1 + z(t)]$, the linearized dynamics of (4.18) satisfies

$$\dot{z} = \left(\sum_{m=0}^{M-1}(-1)^m(u_m + iv_m)(R^c)^{2m}m\right)(z + \bar{z}) + \mathcal{O}^2(z) =: (\varsigma_R + i\varsigma_I)(z + \bar{z}) + \mathcal{O}^2(z) \,. \tag{4.21}$$

Separating real and imaginary parts in terms of $z = \xi + i\eta$, we can simplify (4.21) in matrix form as

$$\frac{d}{dt}\begin{pmatrix} \xi \\ \eta \end{pmatrix} = \boldsymbol{\Lambda}\begin{pmatrix} \xi \\ \eta \end{pmatrix} \quad \text{where} \quad \boldsymbol{\Lambda} = -2\varsigma_R\begin{pmatrix} 1 & 0 \\ c_2 & 0 \end{pmatrix} \tag{4.22}$$

with $c_2 = \varsigma_I/\varsigma_R$. Usually, $c_2 = c_2^M$ depends on the order of the Hopf normal form.[18] The eigenvalues of $\boldsymbol{\Lambda}$ are $\lambda_0 = 0$ and $\lambda_1 = -2\varsigma_R$ with corresponding left and right eigenvectors

$$\begin{aligned} \boldsymbol{u}_0 &= R^c\omega\begin{pmatrix} 0 \\ 1 \end{pmatrix}, & \boldsymbol{u}_1 &= \begin{pmatrix} 1 \\ c_2 \end{pmatrix}, \\ \boldsymbol{v}_0 &= \frac{1}{R^c\omega}(-c_2, 1), & \boldsymbol{v}_2 &= (1, 0); \end{aligned} \tag{4.23}$$

the factor $R^c\omega$ is for consistency with $\boldsymbol{u}_0 = \dot{\boldsymbol{x}}^c(0)$. Moreover, we find the matrix $\boldsymbol{S}(t)$ by linking the deviations ξ, η from w^c in the complex plane with deviations $\boldsymbol{u} \in \mathbb{R}^2$ of the corresponding planar limit cycle solution $\boldsymbol{x}^c$ via

$$\boldsymbol{u}(t) = R^c\boldsymbol{S}(t)\begin{pmatrix} \xi(t) \\ \eta(t) \end{pmatrix} \quad \text{where } \boldsymbol{S}(t) = \begin{pmatrix} \cos(\omega t) & -\sin(\omega t) \\ \sin(\omega t) & \cos(\omega t) \end{pmatrix} \,. \tag{4.24}$$

According to (3.2), the phase sensitivity function is given by

$$\boldsymbol{Z}(t) = \omega\boldsymbol{v}_0\boldsymbol{S}(t)^{-1} = \frac{1}{R^c}\begin{pmatrix} -\sin(\omega t) - c_2\cos(\omega t) \\ -c_2\sin(\omega t) + \cos(\omega t) \end{pmatrix} \tag{4.25}$$

By the change of variables $t \mapsto \theta/\omega$, we arrive at the same form (4.20) as in the previous paragraph. Interestingly, the shape of the phase sensitivity function $\boldsymbol{Z}(\theta)$ does not change when incorporating higher order terms in the Hopf normal form (4.4).

Direct method

The numerically implemented adaptation of the direct method by Novičenko and Pyragas builds on the same theoretical concepts as Kuramoto's reduction via Floquet eigenvectors. The mathematical arguments how to apply this method to an oscillator in Hopf normal thus coincide with the previous subsection, and result in the same form of the phase sensitivity function $\boldsymbol{Z}$.

---

[18] For second ($M = 2$) and third order ($M = 3$) Hopf normal forms

$$\dot{\omega} = \sum_{m=0}^{M-1}(-1)^m\sigma_m|\omega|^{2m}\omega \,, \quad \text{with} \quad \sigma_m = u_m + iv_m \,,$$

we have

$$c_2^2 = \frac{v_1}{u_1} \,, \quad \text{and} \quad c_2^3 = \frac{v_2}{u_2}\left(1 - u_1\left[u_1^2 - 4v_0u_2\right]^{-1/2}\right) + v_1\left[u_1^2 - 4u_0u_2\right]^{-1/2} \,.$$

Adjoint method

The adjoint method reveals the phase sensitivity function $\boldsymbol{Z}$ as the unique solution to the adjoint problem (3.4)–(3.6). For an oscillator in Hopf normal form (4.4), it is convenient to consider the dynamics in polar coordinates (4.18), which we write as

$$\frac{dR}{dt} = G(R), \quad \frac{d\theta}{dt} = H(R) \,. \tag{4.26}$$

This is the typical polar coordinate representation of $\lambda - \omega$ systems [48,118]. The corresponding adjoint problem reads in the general form

$$\frac{d}{dt}\begin{pmatrix} \frac{\partial}{\partial R}\Theta\left(\boldsymbol{x}^c(t)\right) \\ \frac{\partial}{\partial \theta}\Theta\left(\boldsymbol{x}^c(t)\right) \end{pmatrix} = -\boldsymbol{L}(t)^{\mathsf{T}} \begin{pmatrix} \frac{\partial}{\partial R}\Theta\left(\boldsymbol{x}^c(t)\right) \\ \frac{\partial}{\partial \theta}\Theta\left(\boldsymbol{x}^c(t)\right) \end{pmatrix} \tag{4.27}$$

where $\boldsymbol{L}(t) = \nabla \boldsymbol{f}(\boldsymbol{x})\big|_{\boldsymbol{x}=\boldsymbol{x}^c(t)}$ as before. In polar coordinates, we have

$$\boldsymbol{L}(t)^{\mathsf{T}} = \begin{pmatrix} G'(R^c) & H'(R^c) \\ 0 & 0 \end{pmatrix}$$

where the prime denotes differentiation with respect to R. A solution to (4.27) is given by

$$\left(\tfrac{\partial}{\partial R}\Theta\left(\boldsymbol{x}^c(t)\right), \tfrac{\partial}{\partial \theta}\Theta\left(\boldsymbol{x}^c(t)\right)\right) = \left(-\tfrac{H'(R^c)}{G'(R^c)}, 1\right) \,. \tag{4.28}$$

Transforming (4.28) back into Cartesian coordinates $(x, y) = (R\cos\theta, R\sin\theta)$, the phase sensitivity function becomes

$$\boldsymbol{Z}(\theta) = \frac{1}{R^c}\begin{pmatrix} -\sin\theta - c_2\cos\theta \\ -c_2\sin\theta + \cos\theta \end{pmatrix} \,, \tag{4.29}$$

with $c_2 = c_2^M = R^c H'(R^c)/G'(R^c)$. For instance, considering the second order Hopf normal form, $M = 2$, we have $R^c = \sqrt{u_0/u_1}$ and

$$c_2^2 = R^c \frac{-2v_1 R^c}{u_0 - 3u_1(R^c)^2} = \frac{-2v_1}{-2u_0}\frac{u_0}{u_1} = \frac{v_1}{u_1} \,,$$

as already found in the previous paragraphs.

Haken's reduction via averaging

As Haken's reduction method dwells on averaging over one cycle, this method is not appropriate for deriving the phase sensitivity function $\boldsymbol{Z}$. Averaging over a pulse-like perturbation $\boldsymbol{p}$ cannot lead to a meaningful result. However, the method becomes more effective when reducing the phase dynamics of weakly coupled oscillators, as averaging is inherent to the framework of weak coupling.

5. Phase description of an oscillator network

The characterization of complex networks has attracted a literal boost of attention in recent decades [119–126]. In general, and as mentioned in the *Introduction*, complex networks can be characterized with respect to their structure and dynamics [127–129]. The *structure* of a network refers to its underlying topology, that is, the connectivity between the elements, or nodes, of the network [130]. Typically, statistical indicators such as, e.g., the degree distribution, shortest path length, clustering, assortativity, or modularity, are used to describe the structural properties of a network [131]. Noteworthy, the network structure has a non-trivial effect on the network dynamics [132]. And, it can also change over time [133,134]. The *dynamics* of complex networks, on the other hand, refers to dynamical processes of the individual nodes, the (dynamic) interaction between these nodal dynamics, and the emergent collective dynamics on the (global) network level [23,135–138]. This report focuses on the dynamics of complex oscillator networks, where we assume the dynamics of each node to be oscillatory. For simplicity, we further assume the network structure to be given and static over time. When speaking about the macroscopic dynamics, i.e., the *collective behavior* of a network, we here refer to the emergence of collective phenomena and large-scale organization through the particular dynamics of each node and between nodes [20,23,88,139,140]. It is convenient to introduce macroscopic variables, or observables, that characterize the collective behavior. One example of such an observable is the Kuramoto order parameter [12], which will be introduced in more detail below. Its absolute value is a real number between 0 and 1, which indicates the degree of similarity, or of synchronization, between the phases of the oscillatory nodes. Naturally, it is possible to adapt and use other statistical indicators, e.g., the clustering coefficient, for assessing not only the structure [141], but also the (dynamical) collective behavior of a network. This allows for a more detailed description of how similar the dynamical (micro-) processes of different nodes are. E.g., one can distinguish between particular groups, or clusters, of nodes that share similar dynamical features within each group, such as having the same phase dynamics, but these phase dynamics differ from those of the other groups [142–145].

Can the results and insights about the phase description of a single oscillator be applied and extended to multiple interacting oscillators? The subsequent sections are devoted to answer this question. Not only we will present different techniques to derive the phase dynamics of an oscillator network. But we will also pinpoint limitations and pitfalls of the existing theory.

5.1. Networks of coupled oscillators

We assume that the network consists of $N \gg 1$ nodes, whose dynamical state is given by the vector $\boldsymbol{x}_k = \boldsymbol{x}_k(t) \in \mathcal{X}$, $k = 1, \ldots, N$, where $\mathcal{X} \subset \mathbb{R}^n$ is an n-dimensional state space. The evolution of the state vector is governed by the dynamical system $\dot{\boldsymbol{x}}_k = \mathcal{F}_k(\boldsymbol{x}_1, \ldots, \boldsymbol{x}_N; \mu_k)$, which shall be of the form (1.1),

$$\dot{\boldsymbol{x}}_k = \boldsymbol{f}_k(\boldsymbol{x}_k; \mu_k) + \kappa \boldsymbol{g}_k(\boldsymbol{x}_1, \boldsymbol{x}_2, \ldots, \boldsymbol{x}_N) \ .$$

The vector field $\mathcal{F}_k = \mathcal{F}_k(\boldsymbol{x}_1, \ldots, \boldsymbol{x}_N, t)$, and hence also $\boldsymbol{f}_k = \boldsymbol{f}_k(\boldsymbol{x}_K, t)$ and $\boldsymbol{g}_k = \boldsymbol{g}_k(\boldsymbol{x}_1, \ldots, \boldsymbol{x}_N, t)$, may explicitly depend on time t. For the sake of conciseness, however, we consider here only autonomous individual dynamics $\boldsymbol{f}_k$ and state-dependent coupling $\boldsymbol{g}_k$ without further time variations and refer to Section 10 for a corresponding discussion. Assuming nearly identical oscillators and a pairwise coupling structure, leads to the dynamics (1.2),

$$\dot{\boldsymbol{x}}_k = \boldsymbol{f}(\boldsymbol{x}_k; \mu) + \kappa \sum_{j=1}^{N} \boldsymbol{g}_{kj}\big(\boldsymbol{x}_k, \boldsymbol{x}_j\big) \ .$$

This is similar to the dynamics (2.2) of a single oscillator with additive perturbations $\boldsymbol{p}$, but we replaced $\boldsymbol{p}$ by the sum over all pairwise coupling terms $\boldsymbol{g}_{kj}\big(\boldsymbol{x}_k, \boldsymbol{x}_j\big)$ with the respective other oscillators $\boldsymbol{x}_j, j \neq k$. As before, the parameter $\mu \in \mathbb{R}$ is a general bifurcation parameter that we will drop whenever possible. The parameter $\kappa \in \mathbb{R}$ denotes the coupling strength and scales the coupling/interaction between oscillators.

Analogously to Section 2, the goal is to identify the (presumably) high-dimensional state $\boldsymbol{x}_k$ of each individual oscillator by a one-dimensional phase variable θ_k and describe the corresponding phase dynamics. A phase reduction of an oscillator network is, however, arbitrarily more intricate than that of a single oscillator. The reason for this intricacy is twofold: First, the phases of all oscillators have to be determined simultaneously. And second, the coupling term(s) do not only depend on the phase, or phase sensitivity function, respectively, of only one oscillator, but on the phases of multiple oscillators. In consequence, deriving the phase dynamics of an oscillator network can be a laborious undertaking. So, why should we bother such an endeavor? Besides referring to the phase dynamics, there exist other ways to determine whether coupled oscillators synchronize or not. Synchronization, moreover, is but one of many possible network states. If, for instance, one is interested in the character of collective oscillations emerging from a network of coupled dynamical elements, there is a range of phase reduction approaches to derive the dynamics of a global (macroscopic) phase variable and to predict the robustness of such collective oscillations with respect to perturbations of individual nodes of the network [146–163]. Nonetheless, deriving the phase dynamics of each oscillatory node of the network including the corresponding coupling dynamics between them, reveals invaluable information about the whole network, from which also the state of the network can readily be inferred. In addition, individual parameters of the underlying dynamics can be identified, e.g., for playing a key role in synchronization mechanisms, or leading to clustering effects in particular parts of the network. Such insights are crucial when control schemes are to be applied to promote or prevent synchrony.

In the following subsections, we will present the ideas behind phase reduction of an oscillator network and how the reduced phase dynamics can be used to identify and predict network states and collective dynamics. In the next Section 6 we provide more details about various techniques of the actual phase reduction of an oscillator network.

5.2. Phase dynamics of oscillator networks

The phase model (2.12) can be extended to a network of oscillators $\boldsymbol{x}_1, \ldots, \boldsymbol{x}_N$ with dynamics (1.2). Assuming identical oscillators, in the uncoupled case, i.e. for $\kappa = 0$, each of the systems $\dot{\boldsymbol{x}}_k = \boldsymbol{f}(\boldsymbol{x}_k)$ has the same hyperbolically stable limit cycle $\mathcal{C}$ with period $T > 0$ and frequency $\omega = 2\pi/T$. Starting again with defining phase variables θ_k according to the isochron condition (2.7) and following the same reasoning as in the single oscillator case, we end up with

$$\dot{\theta}_k = \omega + \kappa \boldsymbol{Z}(\theta_k) \cdot \sum_{j=1}^{N} \boldsymbol{g}_{kj}(\theta_k, \theta_j) \ ; \tag{5.1}$$

here, we abbreviated $\boldsymbol{g}_{kj}(\theta_k, \theta_j) = \boldsymbol{g}_{kj}(\boldsymbol{x}^c(\theta_k), \boldsymbol{x}^c(\theta_j))$. The dynamics (5.1) directly corresponds to (2.12), but has now been extended to an oscillator network and the perturbation $\boldsymbol{p}$ has been replaced by (the sum over) the coupling terms $\boldsymbol{g}_{kj}$. For the derivation of (5.1) we again assumed that the oscillators $\boldsymbol{x}_k$ are not moved too far away from their respective limit cycles $\mathcal{C}$ through the coupling. This guarantees that we can approximate the dynamics by their respective values on the limit cycle, that is, $\boldsymbol{x}_k(t) \approx \boldsymbol{x}_k^c(t)$ for all $k = 1, \ldots, N$.

Weak coupling and averaging. If the coupling is sufficiently weak, one can make use of *averaging*. For this, we introduce *relative phase* variables ϕ_k via

$$\theta_k = \phi_k + \omega t \ , \tag{5.2}$$

so that the ϕ_k denote deviations from the natural (unperturbed) dynamics along the limit cycle with frequency ω. The relative phases ϕ_k can be found to evolve slowly in time according to

$$\dot{\phi}_k = \kappa \, \boldsymbol{Z}\,(\phi_k + \omega t) \cdot \sum_{j=1}^{N} \boldsymbol{g}_{kj}\big(\phi_k + \omega t, \phi_j + \omega t\big) \tag{5.3}$$

with $0 < \kappa \ll 1$. Due to the weak coupling assumption, the slow dynamics (5.3) of the relative phases ϕ_k capture the effects of the coupling entirely. In order to apply averaging properly, the phases ϕ_k have to be slow variables such that they do not vary (significantly) within a period. In fact, the smallness of κ implies not only that ϕ_k are slowly varying – by contrast, the term ωt varies rapidly with time –, but also that the coupling can only have small effects on an oscillator's dynamics over any given period $T = 2\pi/\omega$. Still, these small effects can accumulate over time and lead to, e.g., phase synchronization in the network. Suppose that all oscillators get synchronized at some point. This synchronized state will be sustained over times of order $1/\kappa$, which, for κ small, is assumed to be longer than any other characteristic timescale in the dynamics. During this time, the term ωt will undergo a large number of changes, which is of order ω/κ. Hence, over one period T, the ϕ_k can be expected almost time independent. Then, one can average the right-hand side of (5.3) over one period T by considering ϕ_k to be constant (with respect to the integral over T); to make this averaging procedure more rigorous by averaging theory, see, e.g., [55,75]. Combining the averaged dynamics with (5.2), yields the sought-for phase dynamics (1.3) in the ordinary phase variables θ_k,

$$\dot{\theta}_k = \omega + \kappa \sum_{j=1}^{N} H_{kj}(\theta_k - \theta_j)\,,$$

with the *phase interaction function*

$$H_{kj}(\psi) = \frac{1}{2\pi} \int_0^{2\pi} \boldsymbol{Z}(\varphi + \psi) \cdot \boldsymbol{g}_{kj}(\varphi + \psi, \varphi)\, d\varphi\,. \tag{5.4}$$

More detailed derivations can be found in, e.g., Kuramoto's seminal book [Chapter 5, 12] or Ermentrout and Terman's textbook [Chapter 8.3, 48]; see also the recent reviews by Schwemmer and Lewis [65], by Nakao [164] as well as by Gherardini, Gupta and Ruffo [165].

In what follows, the network (1.2) and its phase dynamics (1.3) will be our central equations. We will show how to determine the phase interaction function H_{kj} as given in (5.4).

5.3. Collective behavior

The emergence of collective dynamics of a network can be captured by appropriate observables. What is more, the form of the previously introduced phase interaction function(s) H_{kj} can indicate whether two or more interacting oscillators synchronize and form clusters. We here present conventional observables to describe various kinds of collective behavior and highlight the link to the phase interaction function.

To begin, we introduce slightly simplified oscillator network dynamics and their corresponding phase dynamics, considering a pairwise coupling structure. That is, rather than the general form of coupling as in (1.2), we use

$$\dot{\boldsymbol{x}}_k = \boldsymbol{f}(\boldsymbol{x}_k; \mu) + \frac{\kappa}{N} \sum_{j=1}^{N} C_{kj} \boldsymbol{g}(\boldsymbol{x}_k, \boldsymbol{x}_j) \tag{5.5}$$

with connectivity matrix $\boldsymbol{C} = \big\{C_{kj}\big\}_{k,l}$.[19] The pairwise coupling structure in (5.5) leads to the phase dynamics

$$\dot{\theta}_k = \omega + \frac{\kappa}{N} \sum_{j=1}^{N} C_{kj} H\left(\theta_k - \theta_j\right)\,, \tag{5.6}$$

where H is the phase interaction function. Comparing (5.6) with (1.3), we have replaced H_{kj} with $C_{kj}H$. Obviously, we have to determine the phase interaction function H only once and not for each pair of oscillators separately as in (5.4). Moreover, the function H is periodic with period $T = 2\pi/\omega$. Hence, it can be expressed as a Fourier series

$$H(\psi) = \sum_{n \geq 0} a_n \cos(n\psi) + b_n \sin(n\psi)\,. \tag{5.7}$$

The (number of) Fourier components a_n and b_n insinuate the 'degree of complexity' in the phase dynamics. As will be shown below, the first harmonics ($n = 1$) play a dominant role for the synchronization behavior of the oscillator network. Including higher harmonics ($n > 1$) may give rise to clustering of phases, or even to switching behavior between clusters.

[19] If the coupling, or connectivity, matrix $\boldsymbol{C}$ has only binary entries, $C_{kj} = 0$ or 1, it is also referred to as *adjacency matrix*.

5.3.1. Synchronization

Synchronization alludes to the correlated, coherent dynamics of individual oscillators. Synchronous collective behavior is opposed to uncorrelated, incoherent behavior of the various single oscillators. In case of two coupled oscillators 1 and 2 with $C_{12} = C_{21} = 1$, the conditions for synchronization can be stated explicitly. If the oscillators have identical natural frequencies, $\omega_1 = \omega_2$, if the frequency mismatch $\Delta = \omega_1 - \omega_2$ vanishes, then the oscillators will synchronize in-phase with $\theta_1(t) = \theta_2(t)$ for large enough t. In fact, when defining $\Gamma(\psi) = H(\psi) - H(-\psi)$ as the odd part of the phase interaction function H, that is, $\Gamma(\psi) = 2\sum_{n\geq 1} \sin(n\psi)$, and $\psi := \theta_1 - \theta_2$, one finds $\dot{\psi} = \Delta + \kappa\Gamma(\psi) = \kappa\Gamma(\psi)$. The resulting in-phase synchronized solution $\psi = 0$ is stable for $\kappa\Gamma'(0) = 2\kappa H'(0) > 0$. In this case, the phase model hence exhibits *attractive coupling*. On the other hand, the anti-phase solution, $\psi = \pm\pi$, is stable if $\kappa H'(\pm\pi) > 0$. Then one speaks of *repulsive coupling*. For non-identical oscillators, $\omega_1 \neq \omega_2$, i.e. $\Delta \neq 0$, *phase locking*, or *mutual synchronization*, can be observed as long as $\kappa \min \Gamma(\psi) < \Delta < \kappa \max \Gamma(\psi)$ holds.

All these properties can be extended to networks of more than two coupled oscillators. We consider positive coupling strengths $\kappa > 0$ from now on, unless stated otherwise. If $H(\psi)$ only consists of first harmonics, i.e. $a_1, b_1 \neq 0$ but $a_n = b_n = 0$ for all $n > 1$, we retrieve the *Kuramoto–Sakaguchi model*

$$\dot{\theta}_k = \omega_k - \kappa \sum_{j=1}^{N} \sin\big(\theta_k - \theta_j + \alpha\big) \tag{5.8}$$

with phase lag parameter $\alpha \in \mathbb{R}$. In the previous notation of (5.7), we have $C_{kj} = -1$ for all $k \neq j$. The special case $\alpha = 0$ yields the classic Kuramoto model, for which $a_1 = 0$ and $b_1 > 0$. By construction, the Kuramoto model 'only' features attractive coupling. Also, the more general Kuramoto–Sakaguchi model (5.8), whose phase interaction function H is commonly written as $H(\psi) = A\sin(\psi + \alpha)$, exhibits attractive coupling[20] for $|\alpha| \leq \pi/2$. In networks of identical and globally coupled oscillators, the strength of (attractive) coupling can be minimal to let the network synchronize. For non-identical oscillators, the heterogeneity in the natural frequency terms tends to suppress synchronization. Yet, when the coupling exceeds a critical value, a transition to collective synchronization can be observed [12,73].

Stability of the synchronized solution. A convenient approach to assess the network behavior of identical, coupled systems, not necessarily phase oscillators, is based on the *master stability function* (MSF) formalism [166]. The MSF approach is used to determine the stability of the fully synchronized state in terms of the eigenstructure of the connectivity matrix $\boldsymbol{C}$, see also [167]. For the phase model $\dot{\theta}_k = \omega + \kappa \sum_j C_{kj} H(\theta_k - \theta_j)$, we are interested in the stability of the synchronous state $\theta_k = \theta$ for all k, that is, $\theta_k - \theta_j = 0$ for all $j \neq k$. Given that close to full synchrony the phase differences tend to be small, we can expand H around the origin and find at first order $H(\theta_k - \theta_j) \approx H'(0)[\theta_k - \theta_j]$. Writing the phase model in vector form, one can find the Jacobian $\hat{H}$ at the synchronous state $\Theta_0 = (\theta, \ldots, \theta)$ with entries $\hat{H}_{kj}$ having graph-Laplacian structure $\hat{H}_{kj} = \kappa H'(0)\big(C_{kj} - \delta_{kj}\sum_l C_{kl}\big)$. The (linear) stability of the synchronous state here depends on the eigenvalues of $\hat{H}$. We note that one eigenvalue is always zero. If the network is globally coupled, i.e., $C_{kj} = 1$ for all j, k, the synchronized state is stable if $\kappa H'(0) > 0$ and unstable if $\kappa H'(0) < 0$, cf. [168]. Nicosia and co-workers recently used a similar approach to investigate the mechanisms behind remote synchronization behavior [169]. When full synchronization cannot be achieved, network symmetries play a crucial role in establishing functional modules, which do not even require structural connectivity as represented in the connectivity matrix C_{kj}.

5.3.2. Order parameters, observables, and mean field-driven dynamics

Kuramoto order parameter. The degree of network synchronization is commonly measured in terms of the *complex Kuramoto order parameter* defined as

$$Re^{i\Psi} = \frac{1}{N}\sum_{k=1}^{N} e^{i\theta_k} \,. \tag{5.9}$$

The modulus R and the complex argument Ψ represent the amplitude and (mean) phase, respectively, of collective oscillations, that is, of the *mean field* behavior. R takes values between $R = 0$, corresponding to a fully incoherent state, and $R = 1$, corresponding to complete synchronization of all oscillators. In the continuum limit, $N \to \infty$, and for an appropriately chosen distribution $g(\omega)$ of natural frequencies, the Kuramoto model can be solved analytically and the real-valued Kuramoto order parameter R undergoes a pitchfork-bifurcation at a critical coupling strength (which depends on the properties of g) from incoherence to (partial) synchronization, see [12,164,170].

[20] We can use trigonometric identities to write $a_1\cos(\psi) + b_1\sin(\psi) = A\sin(\psi + \alpha)$ with $A^2 = a_1^2 + b_1^2$ and $\alpha = \tan^{-1}(a_1/b_1)$. If we fix the sign of A by imposing $A = \mathrm{sgn}(b_1)[a_1^2 + b_1^2]^{1/2}$, for $b_1 > 0$ we find $\alpha = \tan^{-1}(a_1/b_1) \in (-\pi/2, \pi/2)$, and $|\alpha| > \pi/2$ for $b_1 < 0$. Hence, the coupling is attractive whenever $b_1 > 0$. For $b_1 < 0$, the repulsive character of the coupling can be balanced using negative coupling strengths $\kappa < 0$, so that $\kappa A > 0$. With the convention $\mathrm{sgn}(A) = \mathrm{sgn}(a_1)$, however, synchronization cannot occur for $\kappa A > 0$.

Microscopic and macroscopic observables. The Kuramoto order parameter is a prime example for a macroscopic observable. Here, we took the network average over the different microscopic states. Due to averaging, macroscopic observables are usually more regular than microscopic ones. This is in particular true for very large networks. In a more rigorous way, we can define macroscopic observables as (averaged) properties of the network. To do so, one describes the state of the network by a distribution function of the microscopic variables. In the case of an oscillator network, the main property of interest is the (time-varying) distribution ρ of phases $\theta_k(t)$ of the oscillators, that is, $\rho = \rho(\theta, t)$. Such a distribution can be discrete when the network size $N < \infty$ is finite, or continuous in the limit $N \to \infty$. We can define a typical *microscopic* observable by identifying each oscillator (with phase $\theta \in [0, 2\pi]$) as a point $z \in \mathbb{C}$ on the complex unit-circle, that is, $z = \mathrm{e}^{i\theta}$ is a complex-valued microscopic observable. A first *macroscopic* observable is the mean, or expectation, value[21]

$$\int_{|z|=1} \rho(z, t) z dz = \int_0^{2\pi} \rho(\theta, t) \mathrm{e}^{\mathrm{i}\theta} d\theta \tag{5.10}$$

of the microscopic observables. This macroscopic observable (5.10) is the continuous formulation of the Kuramoto order parameter (5.9), which justifies the nomenclature that the macroscopic variables R and Ψ define the mean field behavior. Naturally, one can generalize (5.10) and consider the (complex) amplitudes of higher Fourier modes

$$Z_m = \int_0^{2\pi} \rho(\theta, t) \mathrm{e}^{\mathrm{i}m\theta} d\theta \ ,$$

which are typically referred to as *Kuramoto–Daido order parameters*; $m = 1$ again leads to the Kuramoto order parameter $Z_1 = R\mathrm{e}^{i\Psi}$. In fact, Z_m are the *moments* $\langle (\mathrm{e}^{i\theta})^m \rangle$ of the microscopic observables $\mathrm{e}^{i\theta}$. It may also be convenient to consider the corresponding *circular cumulants* as alternative macroscopic observables, see, e.g., [171] for more details. For our purposes, however, it will suffice to use either the Kuramoto order parameter, or to consider the full distribution density of phases $\rho(\theta, t)$ when a simple network average does not reveal the sought-for information. This can be the case, e.g., when multiple cluster states emerge.

Mean field-driven dynamics. When assessing the network behavior, it is often convenient to rewrite the phase model (5.6) & (5.7) in the form of a single oscillator that is driven by the mean field variables $R(t)$ and $\Psi(t)$:

$$\dot{\theta}_k = \omega_k + \kappa \sum_{n \geq 0} a_n(R) \cos(\Psi - \theta_k) + b_n(R) \sin(\Psi - \theta_k) \ . \tag{5.11}$$

Here the Fourier amplitudes a_n, b_n now depend on R. Note that this dependence on the mean field can also be nonlinear, which may lead to non-trivial collective behavior.

In [172–174], Rosenblum and Pikovsky investigated a form of the Kuramoto–Sakaguchi model (5.8) where a_1 and b_1 depended on both R and R^3. Due to this nonlinear coupling, a self-consistent partial synchrony solution can arise with $0 < R < 1$ at the border between stability and instability domains for the synchronous state. They reported a mismatch between the time-average frequencies of the oscillators and the frequency of the mean field, which they called self-organized quasiperiodic solutions. This mismatch is an essential property of partial synchrony in that microscopic and macroscopic dynamics differ from one another. Detecting these quasiperiodic states requires a more careful inspection of the network behavior than considering only the (averaged) evolution of the Kuramoto order parameter. Evaluating Poincaré sections can hint at the quasiperiodic character of the mean-field solution, as has been proposed by Rosenblum and Pikovsky [172], but also studying the evolution of the (instantaneous) phases θ in terms of their distribution $\rho(\theta, t)$ may shed light on the actual, no longer trivial collective dynamics.

5.3.3. Clustering, chaos and higher harmonics

Cluster states can be viewed as a generalized form of synchronous behavior. Considering a network of $N > 1$ coupled oscillators, then the asynchronous state (corresponding to a vanishing Kuramoto order parameter, $R = 0$) is characterized by N (independent) groups, or *clusters*, of one oscillator each. By contrast, the fully synchronized network state ($R = 1$) features a single cluster of N oscillators. Both the structure and dynamics of complex networks can lead to clustering effects. The number $M \in \{1, 2, \ldots, N\}$ of clusters can be static, or change over time. Moreover, one speaks of *balanced* cluster states when every cluster consists of the same number of elements. A particular and noteworthy dynamic network state is called a *heteroclinic cycle*. Given a balanced M-cluster state, heteroclinic cycles can be defined as a slow switching behavior of individual oscillators between two clusters. As illustrated in Fig. 5.1 (panel a) for $M = 2$, slow switching is characterized by spontaneous decreases of the real-valued Kuramoto order parameter (top panel).

Cluster states may emerge in oscillator networks already for trivial topology, such as a global (all-to-all) coupling structure, when there are higher harmonics in the phase model. Higher harmonics can also increase the variety of non-trivial network behavior beyond clustering behavior. A first example of higher harmonics in the phase model is a biharmonic phase interaction function H with non-vanishing first and second harmonics, i.e. $a_n, b_n \neq 0$ for $n = 1$ and $n = 2$. The occurrence of balanced two-phase-cluster states is then expected, and has frequently been reported [175–177]. What is more, one can indicate stability boundaries for cluster states according to the eigenvalues associated with

[21] Here we use the integral sign as a generalization of the (possibly discrete) sum over oscillator states.

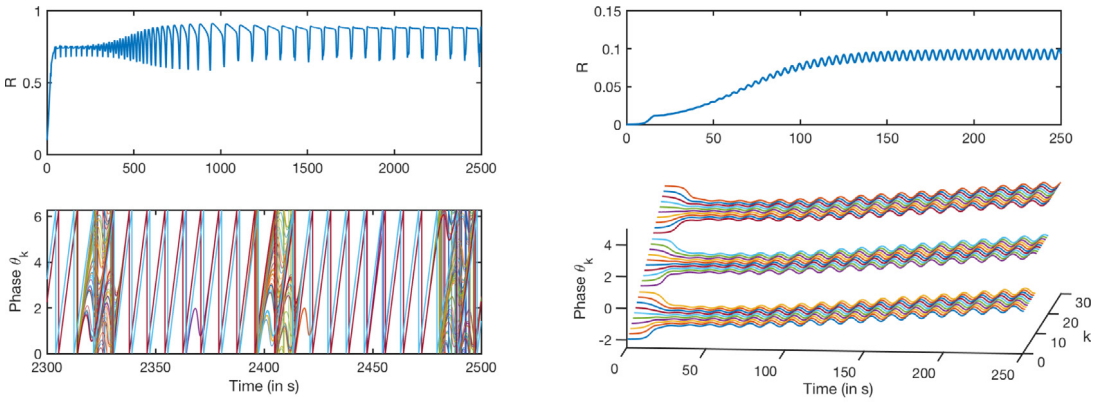

(a) Slow switching (b) Oscillating three-cluster state

Fig. 5.1. (a) Slow switching between two clusters in a network of $N = 1000$ biharmonically coupled phase oscillators. (b) Oscillating three-cluster state for $N = 30$ identical phase oscillators with phase interaction function $H(\psi) = \sqrt{2}\sin(\psi + \pi/4) - 0.09\sin(2\psi) + 0.16\sin(3\psi) - 0.09\sin(4\psi) - 0.03\sin(5\psi) - 0.06\sin(6\psi)$. Top panels: time evolution of the real-valued Kuramoto order parameter. Bottom: time evolution of the individual phases.

intracluster and intercluster perturbations, respectively. The eigenvalues for intracluster perturbations can be computed by $\lambda_n^{\text{intra}} = \sum_{k=1}^{\infty} b_{kn}$ yielding the values for synchronized (one-cluster, λ_1^{intra}) and balanced two-cluster solutions (also called anti-phase cluster, $\lambda_2^{\text{intra}}, \lambda_2^{\text{inter}}$) as $\lambda_1^{\text{intra}} = H'(0)$, $\lambda_2^{\text{intra}} = \frac{1}{2}\left(H'(0) + H'(\pi)\right)$, and $\lambda_2^{\text{inter}} = H'(\pi)$. Hence, the biharmonic phase model will feature:

(i) global synchrony for $\kappa b_1 > 0$,
(ii) a balanced two-cluster state if $\kappa b_1 < 0$ and $\kappa b_2 > 0$,
(iii) heteroclinic cycles if $\kappa b_1 < 0, \kappa b_2 < 0$ and b_1 is comparable to b_2.

In [178,179] Kori and Kuramoto argued that the slow-switching behavior characteristic for heteroclinic cycles may be explained as an effective convergence to an unstable unbalanced two-cluster solution. In the same article, the authors also explored the effect of delay on the robustness of the mechanism. Clusella and co-workers summarized the possible macroscopic dynamics for identical biharmonically coupled phase oscillators in [180]. There, they also reported self-consistent partial synchrony solutions, see also the work by Komarov and Pikovsky for an analytic account of the network behavior for a biharmonic coupling function [181,182].

When further increasing the number of harmonics in the phase interaction function H, even small networks of identical phase oscillators can display very rich collective behavior in terms of the Kuramoto order parameter R. Even macroscopic chaos can occur, e.g., when allowing for interaction functions with up to the fourth harmonics [183]. Numerical simulations may provide more insight into the variety of clustering behavior when more than two harmonics are present; e.g., Okuda found an oscillating three-cluster state in [175]. While the order parameter dynamics can hint at such non-trivial network behavior, it typically fails to provide a clear-cut picture of the (nodal) phase dynamics. The oscillating order parameter in Fig. 5.1 (panel b, top) does not provide any sign that there are actually three oscillating cluster states as revealed by the phase time series (bottom). For that reason, it is important to identify the characteristics of the collective behavior first and subsequently choose an appropriate macroscopic observable that is able to capture the actual dynamics.

6. Phase reduction techniques for an oscillator network

The analysis of the network dynamics of (weakly) coupled oscillators can greatly be simplified by exploiting the reduced phase dynamics. Despite the reduction of dimensionality and, thus, complexity of the network dynamics, the phase dynamics can still reveal a detailed picture of rich collective behavior. The loss of information through the simplification in terms of phase variables, however, has to be minimal. This can only be achieved through a careful phase reduction of the underlying network dynamics. The main goal of this *Section* is hence to review the different (network) phase reduction techniques, to highlight their common features, and to pinpoint their differences. By that we hope to clarify the view on this rather complex challenge of network phase reduction and to aid unifying the concepts and languages from different disciplines.

We will capitalize on the three basic assumptions on the network of coupled oscillators as outlined in the *Introduction*:

(1) The network is weakly coupled , i.e. the coupling strength $\kappa \ll 1$ is sufficiently small.
(2) The oscillators are nearly identical, i.e. the node-specific dynamics can be written as $\boldsymbol{f}_k = \boldsymbol{f} + \varepsilon\tilde{\boldsymbol{f}}_k$ for some small fluctuations $\tilde{\boldsymbol{f}}_k$ with $|\varepsilon| \ll 1$; these fluctuations will be subsumed into the term $\kappa \boldsymbol{g}_k$.

(3) The coupling structure is pairwise, i.e. the coupling function can be decomposed into the sum of pairwise interactions, unless stated otherwise.

By virtue of these assumptions, the underlying network dynamics is given by (5.5),

$$\dot{\boldsymbol{x}}_k = \boldsymbol{f}\,(\boldsymbol{x}_k;\,\mu) + \kappa \sum_{j=1}^{N} C_{kj}\boldsymbol{g}\big(\boldsymbol{x}_k, \boldsymbol{x}_j\big)\ .$$

The network phase reduction then aims at establishing the phase model (5.6),

$$\dot{\theta}_k = \omega + \kappa \sum_{j=1}^{N} C_{kj} H\big(\theta_k - \theta_j\big)\ ,$$

where the natural frequency ω is defined through the function $\boldsymbol{f}$, whereas the phase interaction function H depends on both $\boldsymbol{f}$ and $\boldsymbol{g}$. There is, indeed, a robust mathematical theory that guarantees the reduction of (5.5) into (5.6). This is the theory of *weakly coupled oscillators* and dwells on *Malkin's Theorem*, which we will state below. In particular, assumptions (1) and (2) have to be fulfilled for Malkin's theorem to be applied. The pairwise coupling structure, assumption (3), is not necessarily required but eases the subsequent presentation of (network) phase reduction techniques as the phase interaction function H is identical for all pairs (k, j) of oscillators.

6.1. Malkin's theorem for weakly coupled oscillators

Weak coupling. The notion of weak coupling underlies the mathematical theory of the here presented phase reduction techniques of oscillator networks. The weakness of the coupling manifests as the coupling strength κ is assumed to be small. But, how small is *small*? In fact, the smallness assumption "$\kappa \ll 1$" is a mathematical idealization, which can also be written in the form "$\kappa \to 0$". This idealization simplifies the analysis of the network under study to obtain mathematically rigorous results. Most of the time, the condition $\kappa \to 0$ of *infinitesimal* coupling strength can be loosened to the condition "there is a positive $\kappa_0 > 0$ such that for all $0 \leq \kappa < \kappa_0$ the obtained result is true". Then again, one can ask: how small is κ_0? The answer crucially relies on the dynamics under investigation, and numeric values can only be provided in context. Moreover, it is always possible to rescale functions so that the rescaled (maximal) coupling strength $\tilde{\kappa}$ ($\tilde{\kappa}_0$) can be smaller or bigger than κ (κ_0). Conclusively, the idealized mathematical condition $\kappa \ll 1$ remains a somewhat abstract assumption [46].

Weakly coupled oscillators. As already said, the oscillator networks that we consider throughout this report exhibit weak coupling, or connectivity, between nodes. To be precise, the *theory of weakly coupled oscillators* requires that every node of the network features stable limit cycle oscillations in the absence of coupling, $\kappa = 0$. These oscillations are assumed to have emerged through a bifurcation in the local dynamics, $\dot{\boldsymbol{x}}_k = \boldsymbol{f}_k(\boldsymbol{x}_k;\,\mu_k)$, when the control, or bifurcation, parameter μ_k crosses a critical value $\tilde{\mu}_k$. Without loss of generality, the critical value at the bifurcation[22] can be set to zero, i.e. $\tilde{\mu}_k = 0$. Then, $\mu_k \ll 1$, which moreover is assumed small, denotes the distance of the oscillatory dynamics of node k to its respective bifurcation point. The weak coupling assumption has to ensure that the coupling cannot induce any bifurcation of the nodal dynamics, that is, $0 \leq \kappa \ll \kappa_0 \leq \min_k \mu_k \ll 1$. In case of (nearly) identical oscillators with $\boldsymbol{f}_k = \boldsymbol{f}$ for all k, so that $\mu_k = \mu$, the weak coupling assumption becomes:

$$0 \leq \kappa \ll \mu \ll 1\ .$$

An inherent assumption necessary for a (meaningful) phase reduction is that the perturbations, or coupling effects, do not move any oscillator's trajectory out of the basin of attraction of the respective limit cycle, or bring it close to invariant structures on the boundary of the basin of attraction, see, e.g., [184].

Taken together, it is widely accepted that the notion of "weak coupling" implies that an oscillator's intrinsic dynamics dominates the effects due to coupling at each point in the periodic cycle [65]. Hence, over a period $|\boldsymbol{f}(\boldsymbol{x}_k)|$ should be (at least) an order of magnitude greater than $|\kappa \boldsymbol{g}_k(\boldsymbol{x}_1, \ldots, \boldsymbol{x}_N)|$. For sufficiently small values of κ, the phase model can then capture the dynamics of the full system quantitatively. Nonetheless, the phase model can often provide qualitatively correct predictions about the network dynamics also for moderate coupling strengths [57,63,65,185,186].

Malkin's theorem. Having established a basic understanding of the notion of weak coupling, we present the mathematical backbone of phase reduction techniques for oscillator networks. The theorem below dates back to the work of Malkin [71, 72], who proved it in rather general terms. Hoppensteadt and Izhikevich adopted the theorem for weakly coupled oscillators and provided the corresponding proof in [46], thereby following Blechmann [187], Neu [50], Ermentrout and Kopell [52,53,55]. We here state the theorem in the form for weakly coupled oscillators with identical natural frequencies. There are, however, extensions for non-identical natural frequencies [46] and for general (not necessarily weakly coupled) nonautonomous systems having parametrized families of solutions [72,187].

[22] In principle, the dynamics can be close to multiple bifurcations. In this case, $\tilde{\mu}_k$ refers to the bifurcation point closest to μ_k.

Malkin theorem for weakly coupled oscillators. *Consider a weakly connected system of the form* $\dot{\boldsymbol{x}}_k = \boldsymbol{f}_k(\boldsymbol{x}_k) + \kappa\, \boldsymbol{g}_k(\boldsymbol{x}_1, \ldots, \boldsymbol{x}_N)$ *with* $\boldsymbol{x}_k \in \mathbb{R}^n$ *for* $k = 1, \ldots, N$ *such that each equation in the uncoupled system* $\dot{\boldsymbol{x}}_k = \boldsymbol{f}_k(\boldsymbol{x}_k)$ *has an exponentially orbitally stable T-periodic solution* $\boldsymbol{x}_k^c(t)$ *with frequency* $\omega = 2\pi/T$. *Let* $\tau = \kappa t$ *be slow time and let* $\phi_k(\tau) \in \mathbb{S}^1$ *be the phase deviation from the natural oscillation* $\boldsymbol{x}_k^c(t)$, $t \geq 0$. *Then, the vector of phase deviations* $\phi = (\phi_1, \ldots, \phi_N)^\intercal \in \mathbb{T}^N$ *is a solution to*

$$\phi_k' = H_k(\phi_k - \phi, \kappa)\,, \quad k = 1, \ldots, N\,, \tag{6.1}$$

where $' = d/d\tau$, *the phase vector* $\phi_k - \phi = (\phi_k - \phi_1, \ldots, \phi_k - \phi_N)^\intercal \in \mathbb{T}^N$, *and the function*

$$H_k(\phi_k - \phi, 0) = \frac{1}{T}\int_0^T \boldsymbol{Z}_k(t) \cdot \boldsymbol{g}_k(\boldsymbol{x}_1^c(t + \phi_1 - \phi_k), \ldots, \boldsymbol{x}_N^c(t + \phi_N - \phi_k))\, dt\,, \tag{6.2}$$

with $\boldsymbol{Z}_k(t) \in \mathbb{R}^n$ *the unique nontrivial T-periodic solution to the linear system*

$$\dot{\boldsymbol{Z}}_k(t) = -\left(\nabla \boldsymbol{f}_k(\boldsymbol{x})\big|_{\boldsymbol{x}=\boldsymbol{x}_k^c(t)}\right)^\intercal \boldsymbol{Z}_k(t) \tag{6.3}$$

satisfying the normalization condition

$$\boldsymbol{Z}_k(0) \cdot \boldsymbol{f}_k\big(\boldsymbol{x}_k^c(0)\big) = \omega\,. \tag{6.4}$$

The proof of this theorem builds upon a singular perturbation approach and can be found in Appendix A.1; see also [46] or [65]. Note that the solution $\boldsymbol{Z}_k(t)$ to the adjoint problem (6.3) & (6.4) is exactly the phase sensitivity function of oscillator $\boldsymbol{x}_k$ as introduced in Section 2. The mathematical details how the solution of the adjoint problem $\boldsymbol{Z}$ can be related to the gradient of the asymptotic phase map $\nabla\Theta$ evaluated at the limit cycle, have been depicted in Section 3.4, see also [64].

Application of Malkin's theorem. The theorem summarizes the important ingredients for a phase reduction of an oscillator network. It indicates the (slow) dynamics of phase deviations ϕ_k from the natural oscillations $\boldsymbol{x}_k^c(t)$. The full phase dynamics can be found from (6.1) at first order $\mathcal{O}(\kappa)$ as

$$\dot{\theta}_k = \omega + \kappa\; H_k(\theta_k - \theta, 0)$$

where $\theta = (\theta_1, \ldots, \theta_N)^\intercal \in \mathbb{T}^N$. The phase interaction function H_k given in (6.2) coincides with the one previously introduced in (5.4) when restricting the coupling to only pairwise interactions $\boldsymbol{g}_k(\boldsymbol{x}_1, \ldots, \boldsymbol{x}_N) = \sum_{j=1}^N \boldsymbol{g}_{kj}(\boldsymbol{x}_k, \boldsymbol{x}_j)$. Note that Malkin's Theorem requires identical natural frequencies $\omega_k = \omega$ for all k, but not necessarily identical oscillators. Hence, the individual phase sensitivity functions $\boldsymbol{Z}_k$ may differ from one another, therefore leading to oscillator specific phase interaction functions H_k. In case of identical oscillators, however, that is, $\boldsymbol{f}_k = \boldsymbol{f}$ for all k, the number of adjoint problems (6.3) & (6.4) to be solved, cf. also Section 3.4, reduces from N to 1. Eventually, assuming that the coupling functions $\boldsymbol{g}_{kj}$ coincide up to a connectivity value C_{kj}, i.e. $\boldsymbol{g}_{kj} = C_{kj}\boldsymbol{g}$, we arrive at the desired phase dynamics (5.6),

$$\dot{\theta}_k = \omega + \kappa \sum_{j=1}^N C_{kj} H(\theta_k - \theta_j)\,.$$

For a phase reduction of the form above, we have to determine the natural frequency ω of the oscillators, and the phase interaction function H as the averaged product of the oscillator's phase sensitivity function $\boldsymbol{Z}$ and the coupling function $\boldsymbol{g}$. However, the coupling function $\boldsymbol{g}$ has to be evaluated at the limit cycle $\boldsymbol{x}^c$. It is thus fundamental to know not only the (approximate) shape of the limit cycle, but the explicit trajectory along the limit cycle.

Numerical vs. analytic phase reduction techniques. Setting up the phase model (5.6), both the phase sensitivity function $\boldsymbol{Z}$ and the limit cycle trajectory $\boldsymbol{x}^c(t)$ need to be known explicitly. Given the latter, one can infer $\boldsymbol{Z}$ along one of the different phase reduction techniques for a single oscillator as presented in Section 3. Already there we distinguished between analytic and numerical phase reduction techniques, depending on whether or not explicit expressions of the limit cycle trajectory and of the linearized dynamics around it can be obtained analytically. The following two subsections will review numerical and analytic phase reduction techniques for a network of weakly coupled oscillators.

6.2. Numerical phase reduction techniques

Recall that numerical phase reduction techniques can be distinguished between *adjoint* and *direct methods*. Both methods were introduced in detail for a single oscillator, the direct method in Section 3.3 and the adjoint method in Section 3.4. As Malkin's Theorem capitalizes on the adjoint method to solve for the phase sensitivity function $\boldsymbol{Z}$, the adjoint method is sometimes also referred to as *Malkin's method*. Regarding the accuracy of the different methods, either of them performs equally well given that they exploit the linearized dynamics around the limit cycle as discussed in detail in Section 3. Storing the numeric values of the limit cycle trajectory is a standard routine, so that the evaluation of the coupling functions at the limit cycle does neither hamper nor improve the accuracy of either of the numeric methods when applied to an oscillator network. We tested the algorithms for the direct method against the algorithms of the adjoint method, using the software packages XPPAUT [97] and MatCont [99] as well as our own adjoint solver implemented

in Matlab (The Mathworks Inc., Natwick, MA). We found a very good agreement between all methods, such that we use them interchangeably as "the" numerical method in the following, unless stated otherwise. As a by note, we would like to remark that XPPAUT has conveniently automatized the computation of the phase interaction function H, which can, moreover, be decomposed in a Fourier series as in (5.7). Sections 8 and 9 will provide extensive illustrations of the application and strength of numerical phase reduction techniques.

6.3. Analytic phase reduction techniques

As already discussed in Section 4 for a single oscillator, analytic phase reduction techniques exploit the properties of an oscillator's limit cycle behavior in order to establish an explicit link to its phase dynamics. With respect to networks of the coupled oscillators, analytic phase reduction techniques can be extended to determine the corresponding phase model explicitly in terms of the underlying model equations. Linking the parameters of the original dynamics to those of the phase model allows for predicting reliably how specific model parameters shape the phase dynamics of the network. As we have seen for a single oscillator in Section 4.4, however, only few examples are analytically tractable. A normal form reduction often has to precede the phase reduction. This normal form reduction has a direct effect on the accuracy of the analytically obtained phase dynamics.

When considering an oscillator network, normal form reductions become arbitrarily more involved. The transformations to bring the dynamics of an individual oscillator in a simplified form immediately effect the form of the other oscillators through the coupling terms. Hence, a normal form reduction has to occur for all oscillators of the network simultaneously, giving rise to the notion of a *network normal form*. We focus on networks of (weakly) coupled identical oscillators as introduced in the assumptions (i)-(iii) above, and concentrate on oscillations that have emerged through a Hopf bifurcation.

In the first subsection, we introduce a particular case of the network Hopf normal form. The technical details how the network Hopf normal form can be obtained will be subject of Section 7. Provided that the dynamics of an oscillator network is given in its network Hopf normal form, the phase dynamics can immediately be deduced. In the second subsection, we show explicitly how the various phase reduction techniques for a single oscillator introduced in Section 3 can be applied to this simplified network dynamics. We prove that the various phase reduction techniques (including Haken's reduction via averaging) result in the same phase model, which will be illustrated below for weakly coupled oscillators in second order Hopf normal form. The third subsection presents a phase reduction technique for the (full) network Hopf normal form, which we deem worth reporting for its mathematical elegance.

6.3.1. Hopf normal form of an oscillator network

Extending the notion of Hopf normal form to an oscillator network, we first introduce a rather general network dynamics where each oscillator is given in Hopf normal norm.

Hopf normal form with coupling. When considering an oscillator in Hopf normal form of order $M \in \mathbb{N}$ as one node in a network of oscillators, the governing dynamics may be given as

$$\dot{w}_k = f(w_k;\mu) + \kappa\, g_k(w_1,\dots,w_N) \overset{(4.4)}{=} \sum_{m=0}^{M-1}(-1)^m \sigma_m |w_k|^{2m} w_k + \kappa\, g_k(w_1,\dots,w_N)\,, \tag{6.5}$$

with a coupling function $g_k : \mathbb{C}^N \to \mathbb{C}$ that depends on all other oscillators $w_{j\neq k} \in \mathbb{C}$. As usual, the coupling strength κ is assumed to be small, i.e. $|\kappa| \ll 1$. Capitalizing on the assumption (iii) of exclusively pairwise interactions as in (5.5), this pairwise coupling structure is expected to be preserved in (6.5), too. For simplicity, we further assume that the pairwise coupling functions g_{kj} between oscillators coincide up to an adjacency value $C_{kj} \in \{0, 1\}$ that denotes structural connectivity between nodes. Hence, the coupling simplifies to

$$g_k(w_1,\dots,w_N) = \frac{1}{N}\sum_{j=1}^{N} g_{kj}(w_k, w_j) = \frac{1}{N}\sum_{j=1}^{N} C_{kj} g(w_k, w_j)\,. \tag{6.6}$$

That is, we consider the network dynamics

$$\dot{w}_k = \sum_{m=0}^{M-1}(-1)^m \sigma_m |w_k|^{2m} w_k + \frac{\kappa}{N}\sum_{j=1}^{N} C_{kj} g(w_k, w_j)\,. \tag{6.7}$$

As we will show below, this dynamics allows a phase reduction following the techniques in Section 3.

Three remarks are due at this point: First, thanks to the pairwise coupling structure it suffices to consider only two coupled oscillators w, w' with dynamics

$$\dot{w} = f(w;\mu) + \kappa\, g(w, w')\,, \tag{6.8}$$

and a similar equation holds for w'. The analytic results of (6.8) can be extended to the whole network in an analogous way. Second, the coupling function $g(w, w')$ in (6.8) depends in general also on the complex conjugates of w and w'. We can formally expand $g(w, w') = g(w, \bar{w}, w', \bar{w}')$ as a power series

$$g(w, \bar{w}, w', \bar{w}') = \sum_{k+l+m+n\geq 0} g_{klmn} w^k \bar{w}^l w'^m \bar{w}'^n \tag{6.9}$$

with complex-valued coefficients $g_{klmn} \in \mathbb{C}$. Importantly, not all of these coefficients contribute to the reduced phase dynamics. Only linear and cubic terms provide substantial contributions to the first and second harmonics of the resulting phase model; see the subsequent Section 6.3.3* that builds on [177]. Third, (6.7) is not the network Hopf normal form. In Section 4.3.3, we highlighted the importance of the inherent symmetries in normal forms. Here, however, the circular symmetry of the Hopf normal form is not respected in the coupling terms (6.9).

Hopf normal form of an oscillator network. Considering a network of coupled identical oscillators close to a supercritical Hopf bifurcation, the network Hopf normal form of second order with exclusively pairwise interactions reads[23]

$$\dot{w}_k = \alpha w_k - \beta |w_k|^2 w_k + \frac{\kappa}{N} \sum_{j=1}^{N} C_{kj} \left[\gamma w_j + \delta \bar{w}_k w_j^2 \right] . \tag{6.10}$$

For the sake of legibility we renamed $\sigma_1 = \alpha$ and $\sigma_2 = \beta$, and introduced the complex-valued coupling parameters $\gamma = \gamma_R + i\gamma_I$ and $\delta = \delta_R + i\delta_I$. With the definitions in Section 4.1, (6.10) defines the Hopf normal form of the entire network $w_1, \ldots, w_N$ as the monomials

$$\sum_{j=1}^{N} w_j \quad \text{and} \quad \bar{w}_k \sum_{j=1} w_j^2$$

are the only resonant monomials of the pairwise coupling function (6.6). The circular symmetry of the (individual) Hopf normal form is maintained on the network level. The general network Hopf normal form will be introduced later in Section 6.3.5, for which we also need further, yet basic, definitions of equivariance theory. For our purposes, however, the exemplary network Hopf normal form (6.10) is more than sufficient: On the one hand, it allows for a straightforward phase reduction as depicted in the following subsection. On the other hand, it serves perfectly as the targeted dynamics of two seminal normal form reduction techniques, whose similarities and differences will be illustrated in detail in Section 7.

6.3.2. Example: Phase reductions of an oscillator network in Hopf normal form

Analogous to Section 4.4, we now demonstrate the different phase reduction techniques of Section 3 for the network Hopf normal form (6.10). We will exemplarily use a pair of coupled oscillators,

$$\dot{w}_k = \alpha w_k - \beta |w_k|^2 w_k + \kappa \left(\gamma w_j + \delta \bar{w}_k w_j^2 \right)$$

with $(k, j) = (1, 2)$ or $(2, 1)$, in order to establish the phase dynamics (5.6) & (5.7), which read

$$\dot{\theta}_k = \omega + \kappa \sum_{j=1}^{N} C_{kj} H\left(\theta_k - \theta_j\right), \quad \text{where } H(\psi) = \sum_{n\geq 0} a_n \cos(n\psi) + b_n \sin(n\psi) .$$

The analytic phase reduction techniques present mathematical recipes along which we can determine the frequency ω and the amplitudes a_n, b_n of the Fourier modes in terms of the normal form coefficients $\alpha = u_0 + iv_0$, $\beta = u_1 + iv_1$ as well as $\gamma = \gamma_R + i\gamma_I$ and $\delta = \delta_R + i\delta_I$. The frequency and the Fourier coefficients of first and second harmonics of the reduced phase models will coincide across all analytic phase reduction techniques. The frequency reads $\omega = u_0(c_0 - c_2)$ and the Fourier coefficients are

$$\begin{aligned} a_1 &= \gamma_R(c_1 - c_2) , & b_1 &= -\gamma_R(1 + c_1 c_2) , \\ a_2 &= R^2 \delta_R(c_3 - c_2) , & b_2 &= -R^2 \delta_R(1 + c_2 c_3) , \end{aligned} \tag{6.11}$$

where we abbreviated $c_0 = v_0/u_0$, $c_2 = v_1/u_1$, $c_1 = \gamma_I/\gamma_R$, and $c_3 = \delta_I/\delta_R$, and R denotes the amplitude of oscillation.

Winfree's and Kuramoto's reductions & the direct and the adjoint methods

The common basis for Winfree's and Kuramoto's reduction techniques as well as for the direct and the adjoint methods, is that for weak perturbations, in this case through the weak coupling to other oscillators, the different approaches capitalize on the linearized dynamics around the limit cycle of an uncoupled oscillator. The essential properties of the

[23] Eq. (6.10) is the Hopf normal form of the full network (6.7) with $S_N \times S^1$-equivariance in the weak coupling limit and for large network size $N \gg 1$, see Section 6.3.5 for a rigorous derivation.

limit cycle w^c and the phase sensitivity function $\boldsymbol{Z}$ were derived in Section 4.4 as:

$$\begin{aligned}
&\textit{limit cycle}: && w^c(\theta_k) = R^c \mathrm{e}^{i\theta_k} \quad \text{with } \theta_k = \omega t + \phi_k \\
&\textit{natural frequency}: && \omega = u_0(c_0 - c_2) \\
&\textit{amplitude}: && R^c = \sqrt{u_0/u_1} \\
&\textit{phase sensitivity function}: && Z(\theta) = (-c_2 + i)\mathrm{e}^{i\theta}/R^c \ .
\end{aligned}$$

The phase sensitivity function $Z(\theta) = Z_x(\theta) + iZ_y(\theta)$ can alternatively be written in vector form as $\boldsymbol{Z}(\theta) = \big(Z_x(\theta), Z_y(\theta)\big)^\intercal$ with $Z_x(\theta) = (-\sin\theta - c_2\cos\theta)/R^c$ and $Z_y(\theta) = (-c_2\sin\theta + \cos\theta)/R^c$. From here, we can determine the phase interaction function H by averaging the product of $\boldsymbol{Z}$ with the coupling function $\boldsymbol{g}$ with the arguments evaluated on the limit cycle. In complex notation, we have $g(w_k, w_j) = \gamma w_j + \delta \bar{w}_k w_j^2$, then $g(\theta_k, \theta_j) \coloneqq g\big(w^c(\theta_k), w^c(\theta_j)\big)$. The scalar (vector) product becomes the complex dot product[24] and the phase interaction function can be computed as

$$H(\psi) = \frac{1}{2\pi}\int_0^{2\pi} (-c_2 + i)\mathrm{e}^{i(\psi+\varphi)} \cdot \left(\gamma \mathrm{e}^{i(\psi+\varphi)} + \delta (R^c)^2 \mathrm{e}^{-i(\psi-\varphi)}\right) d\varphi \ .$$

Evaluating the integral leads exactly to the desired Fourier amplitudes (6.11).

Haken's reduction via averaging

Haken's phase reduction approach via averaging serves as an alternative to the previous phase reduction techniques. Although the latter are formulated for rather general oscillatory dynamical systems, their practical application is limited to a few exceptional cases in which either explicit expressions for the limit cycle and the asymptotic phase maps are available, or the dynamics has already been reduced to normal form. This approach is a more direct way to reduce an oscillatory network to its phase dynamics. Although the inherent averaging in this approach does not allow for a rigorous deduction of the phase sensitivity function $\boldsymbol{Z}$, for the same reason it regains its validity (and power) when assessing the phase dynamics of coupled oscillators whose amplitude and phase change slowly as compared to the oscillators' frequency. This is particularly the case for weakly coupled oscillators where averaging is required to compute the phase interaction function H. Below we show in detail that Haken's reduction approach results in the same phase model (5.6) & (5.7) with Fourier amplitudes (6.11) as computed along the other techniques. We would like to remark that Haken's reduction approach can also be applied for oscillatory networks beyond the limit of weak coupling.[25] In fact, it allows to (analytically) reduce oscillatory network dynamics that are induced through (strong) coupling between the (excitable) elements, see, e.g., [33]. However, since averaging is applied to the linearized dynamics around an unstable fixed point within a stable limit cycle solution $\boldsymbol{x}^c$ (in contrast to the linearized dynamics around $\boldsymbol{x}^c$ as in Section 3.2), this technique loses accuracy for large-amplitude oscillations, see also Section 8. Yet, it provides a phase model whose parameters are directly linked to those of the underlying oscillatory model, and presents a valuable addition to the variety of phase reduction techniques.

Haken's reduction approach requires that every node in the network describes stable circular oscillations in the plane. This is given by the network Hopf normal form (6.10). For two coupled oscillators $w_k, w_j \in \mathbb{C}$ as above we consider the dynamics in two-dimensional real-valued coordinates $w_k = x_k + iy_k$ and $w_j = x_j + iy_j$. We first transform the nonlinear coupling terms in real coordinates and use polar coordinates $w_k = R_k \mathrm{e}^{i(\omega t + \phi_k)}$. In particular, we can use the following identities

$$\langle x_k y_k \rangle = 0 \quad \text{and} \quad \langle x_k^2 \rangle = \langle y_k^2 \rangle = \tfrac{1}{2} R_k^2 \ . \tag{6.12}$$

Substituting them and the corresponding (x_k, y_k)-dynamics in (3.8) and defining $\psi = \phi_k - \phi_j$, we arrive at

$$\dot{\phi}_k = -\omega + v_0 - v_1 R_k^2 + \kappa \left[\frac{R_j}{R_k}\Big(\gamma_I \cos\psi - \gamma_R \sin\psi\Big) + R_j^2\Big(\delta_I \cos(2\psi) - \delta_R \sin(2\psi)\Big)\right] \tag{6.13a}$$

$$\dot{R}_k = u_0 R_k - u_1 R_k^3 + \kappa \left[R_j\Big(\gamma_R \cos\psi + \gamma_I \sin\psi\Big) + R_k R_j^2\Big(\delta_R \cos(2\psi) + \delta_I \sin(2\psi)\Big)\right]. \tag{6.13b}$$

In the case of weak coupling, $\kappa \ll 1$, and being close to the Hopf bifurcation, $R_{k,j} \ll 1$, the R_k-dynamics (6.13b) evolves very slowly compared to ϕ_k. Therefore, one can assume that R_k and R_j are constant and do not vanish. We can solve (6.13b) for R_k^2 by adiabatically eliminating the R_k-dynamics, i.e. $\dot{R}_k = 0$, as

$$R_k^2 = \frac{u_0}{u_1} + \frac{\kappa}{u_1}\left[\frac{R_j}{R_k}\Big(\gamma_R \cos\psi + \gamma_I \sin\psi\Big) + R_j^2\Big(\delta_R \cos(2\psi) + \delta_I \sin(2\psi)\Big)\right] \ ,$$

[24] The complex dot product for $a, b \in \mathbb{C}$ is defined as $a \cdot b = (\bar{a}b + a\bar{b})/2$.

[25] Note the change from "oscillator network" to "oscillatory network" as we have introduced "oscillators" in Section 2.1 such that they exhibit stable limit cycle oscillations without external coupling.

which is close to the uncoupled limit cycle radius $R^c = \sqrt{u_0/u_1}$. Substituting R^c into (6.13a) and using $\dot\theta_k = \omega + \dot\phi_k$, we find that

$$\begin{aligned}\dot\theta_k = v_0 - u_0\frac{v_1}{u_1} + \kappa\left\{\left[\left(\gamma_I - \gamma_R\frac{v_1}{u_1}\right)\cos(\theta_k-\theta_j) - \left(\gamma_R + \gamma_I\frac{v_1}{u_1}\right)\sin(\theta_k-\theta_j)\right] + \right.\\ \left. + {R^c}^2\left[\left(\delta_I - \delta_R\frac{v_1}{u_1}\right)\cos\big(2(\theta_k-\theta_j)\big) - \left(\delta_R + \delta_I\frac{v_1}{u_1}\right)\sin\big(2(\theta_k-\theta_j)\big)\right]\right\}\ .\end{aligned} \tag{6.14}$$

This result can immediately be extended to a network of coupled oscillators yielding the phase model (5.7) with Fourier amplitudes (6.11).

*6.3.3. Nonlinear coupling terms in Hopf normal forms**

Allowing for nonlinear coupling terms (6.9) in the network dynamics (6.7), the corresponding phase interaction function H of the reduced phase model includes also higher harmonics, which may hint at richer collective behavior, see Section 5.3.3. Only a few nonlinear terms g_{klmn} contribute to the (averaged) phase interaction function H. In fact, only two terms, g_{0010} and g_{0120}, are the dominant contributors to the first and second harmonics of H at leading order. To demonstrate this, we consider the dynamics (6.8) of two coupled oscillators in Hopf normal form of arbitrary order $M \geq 1$. Without coupling, $\kappa = 0$, we find a stable limit cycle solution $w^c(t) = R^c e^{i\theta^c(t)}$ for the two oscillators; for the sake of legibility we will drop the ^{c} and refer to them as w, w'. The resulting phase model takes then the form $\dot\theta = \omega + \kappa H(\theta - \theta')$, where the phase interaction function H can be expanded in Fourier space as in (5.7). In the complex plane, we can compute H as

$$H(\theta-\theta') = \big\langle Z(\theta)\cdot g(w,\bar w, w', \bar w')\big\rangle\ , \tag{6.15}$$

where $a\cdot b = (\bar a b + a\bar b)/2$ with $a, b \in \mathbb{C}$ is the complex dot product as above. For conciseness, we express the averaging in compressed form as $\langle f(\theta,\theta')\rangle = \frac{1}{2\pi}\int_0^{2\pi} f(\theta+\vartheta, \theta'+\vartheta)\, d\vartheta$.

The assumption of the Hopf normal form implies that $f(w,\bar w)$ consists only of the resonant terms $|w|^n w$ with $n = 0, 1, 2, \ldots$, and that the dynamics $\dot w = f(w,\bar w)$ is rotation invariant. Consequently, both $w(\theta)$ and the phase sensitivity function $Z(\theta)$ are of the form $w = w(0)e^{i\theta}$ and $Z(\theta) = Z(0)e^{i\theta}$. For direct linear coupling $g(w,\bar w, w', \bar w') = g_{0010}w'$ the interaction function $H(\theta-\theta') = \big\langle Z(\theta)\cdot g_{0010}w'(\theta')\big\rangle$ thus contains only first harmonics.

Being near a supercritical Hopf bifurcation, the amplitude of the oscillations reads $R^c = |w| = \mathcal{O}(\sqrt{\mu})$, where μ denotes the distance to the Hopf bifurcation in parameter space. By introducing $\varepsilon^2 = \mu$, we have $R^c = \mathcal{O}(\varepsilon)$ and $Z(\theta) = \mathcal{O}^{-1}(\varepsilon)$. Any higher order term $|w|^n w$ in $f(w,\bar w)$ presents then corrections of order $\mathcal{O}^3(\varepsilon)$ and $\mathcal{O}^1(\varepsilon)$ to $w(\theta)$ and $Z(\theta)$, respectively. In view of the expansion in Fourier space (5.7), these terms lead to corrections of order $\mathcal{O}^2(\varepsilon)$ in a_1 and b_1, but they do not contribute to higher harmonics $a_n, b_n \neq 0$ for $n \geq 2$. For the phase interaction function H to contain higher harmonics, we have to take higher-order terms g_{klmn} in the coupling function $g(w,\bar w, w', \bar w')$ into account. We consider $g(w,\bar w, w', \bar w') = w^k \bar w^l w'^m \bar w'^n$ a single monomial with $k, l, m, n \geq 0$ and $g_{klmn} = \delta_{klmn}$. Then, we have $Z\cdot g = \mathcal{O}^{k+m+n+l-1}(\varepsilon)$. On the other hand,

$$Z\cdot g(w,w') \propto e^{-i\theta}\cdot\big(e^{i\theta}\big)^k\big(e^{-i\theta}\big)^l\big(e^{i\theta'}\big)^m\big(e^{-i\theta'}\big)^n = e^{i(k-l-1)\theta}e^{i(m-n)\theta'}$$

holds. The latter term contributes to the amplitudes a_j and b_j of the jth harmonic ($j > 0$) when it is a function of only $\pm j(\theta-\theta')$. This means that the set (k,l,m,n) has to fulfill $k - l - 1 = \pm j$ and $m - n = \mp j$. The term $\bar w^{j-1}w'^j = \mathcal{O}^{2j-1}(\varepsilon)$ contributes significantly to a_j and b_j. Therefore, the amplitudes of the jth harmonic are of order $\mathcal{O}(Z\cdot g(w,w')) = \mathcal{O}^{(2j-1)-1}(\varepsilon)$, that is,

$$a_j, b_j = \mathcal{O}^{2(j-1)}(\varepsilon)\ . \tag{6.16}$$

Note that this is in line with the coefficient a_0 of the zeroth harmonic, $j = 0$, whose major contributions stem from the monomial $g(w,\bar w, w', \bar w') = w$ and yield a constant increase or decrease of the natural frequency depending on the sign of a_0. For $j > 0$, the term $w^{j+1}\bar w'^j = \mathcal{O}^{2j+1}(\varepsilon)$ gives contributions of order $\mathcal{O}^{2j}(\varepsilon)$ to the jth harmonic. These contributions, however, present only minor corrections as they are smaller than a_j, b_j of two orders of magnitude, and can therefore be neglected. Along these lines, we consider coupling terms of order 3, which yield contributions of order $\mathcal{O}^2(\varepsilon)$ to the phase dynamics. The terms $w^2\bar w'$, $|w|^2 w'$, and $|w'|^2 w'$ contribute to the first harmonics a_1, b_1. Their values differ at one order of magnitude from a_1, b_1, so that their contributions can be neglected. Likewise, $|w|^2 w$ and $w|w'|^2$ contribute negligibly to the zeroth harmonic, namely by less than two orders of magnitude. The only cubic resonant term that affects the phase dynamics is $\bar w w'^2$, which contributes to the second harmonics a_2, b_2 at the same order of magnitude $\mathcal{O}^2(\varepsilon)$. Moreover, we can show that no monomial in $g(w,\bar w, w', \bar w')$ of even order will contribute to H. When evaluating the inner product in (6.15) with $g(w,w') \propto \exp\big(i(k-l)\theta + i(m-n)\theta'\big)$, we obtain

$$\begin{aligned}H(\theta-\theta') &\propto \frac{1}{2\pi}\int_0^{2\pi}\alpha_{klmn}e^{-i(\theta+\vartheta)}e^{i\left((k-l)\theta+(m-n)\theta'+(k-l+m-n)\vartheta\right)} + \beta_{klmn}e^{i(\theta+\vartheta)}e^{-i\left((k-l)\theta+(m-n)\theta'+(k-l+m-n)\vartheta\right)}d\vartheta\\ &\propto \frac{1}{2\pi}\int_0^{2\pi}\alpha_{klmn}e^{i((k-l+m-n-1)\vartheta)} + \beta_{klmn}e^{-i((k-l+m-n-1)\vartheta)}d\vartheta\ ,\end{aligned} \tag{6.17}$$

where $\alpha_{klmn}, \beta_{klmn} \in \mathbb{C}$ are constants. Due to the inherent averaging in (6.17) and as $\exp(in\vartheta)$ is 2π-periodic, $H(\theta - \theta')$ will vanish if $(k-l+m-n)$ is even. This means that only monomials of odd order will contribute to the phase interaction function H.

6.3.4. Equivariant theory and the network Hopf normal form

The full network Hopf normal form becomes more involved without the assumptions of weak coupling and of large network size $N \gg 1$. In fact, the coupling in the full network normal form comprises terms that describe simultaneous interactions between multiple oscillators, and thus is beyond a mere pairwise coupling structure. Here, we briefly present the Hopf network normal form. How a phase model can be reduced while respecting the additional terms, will be subject of the following subjection. There, we will introduce a phase reduction technique proposed by Ashwin and Rodrigues [74] that exploits the symmetry properties of a network of weakly coupled oscillators, see also [188]. This symmetry approach presents an important extension to previous reported reduction techniques, especially when dealing with networks featuring complex coupling functions of multiple interacting oscillators.

Given a network of $N \geq 4$ all-to-all coupled oscillators, where each can be described individually in Hopf normal form as in (4.4), we consider the network dynamics

$$\dot{w}_k = f(w_k; \mu) + \kappa\, g_k(w_1, \ldots, w_N) \tag{6.18}$$

with full *permutation symmetry* S_N and which respects *rotational invariance* S^1. Intuitively, full permutation is given if the dynamics (6.18) can be interchangeably used for any two oscillators $k \neq j$. That is, the network dynamics remains the same for any permutation $\sigma \in S_N$ with

$$\sigma\,(w_1, \ldots, w_N) = \left(w_{\sigma^{-1}(1)}, \ldots, w_{\sigma^{-1}(N)}\right)\ .$$

As f is the same for all oscillators, this means that

$$g_k(w_1, \ldots, w_N) = g_1(w_k, w_2, \ldots, w_{k-1}, w_1, w_{k+1}, \ldots, w_N) \tag{6.19}$$

has to be symmetric under all permutations of the last $N-1$ arguments that fix the first. In particular, we need the network to be globally (all-to-all) coupled with $C_{kj} = 1$ for all $k \neq j$ with the same coupling function for all nodes.

Rotational invariance is fulfilled if both the uncoupled term f and the coupling g are in Hopf normal form. Eq. (6.18) is rotational invariant if the rotation of all variables $w_1, \ldots, w_N$ by the same phase $\theta \in \mathbb{S}^1$ does not change the network dynamics. Formally, the action of the group S^1 on $\mathbb{C}^N$ is defined by

$$\theta(w_1, \ldots, w_N) := \mathrm{e}^{i\theta}(w_1, \ldots, w_N)$$

for any (phase) $\theta \in \mathbb{S}^1$. Indeed, the non-vanishing, resonant polynomial components, i.e. monomials, appearing in the Hopf normal form are exactly those that satisfy the circular S^1 symmetry. While we previously assumed g to be an arbitrary power series in its variables, this power series is here restricted to consist of only resonant monomials. For g with monomials of degree lower than or equal to three, there are at most 11 non-vanishing terms that fulfill the symmetry assumptions [74]. Denoting by $w = (w_1, \ldots, w_N)$ the variable vector with $N \geq 4$, then the admissible coupling terms $\hat{g}_j$ are:

$$\hat{g}_{-1}(w) = \frac{1}{N}\sum_{j=1}^{N} w_j, \qquad \hat{g}_2(w) = w_1^2\frac{1}{N}\sum_{j=1}^{N} \bar{w}_j, \qquad \hat{g}_3(w) = |w_1|^2\frac{1}{N}\sum_{j=1}^{N} w_j,$$

$$\hat{g}_4(w) = w_1\frac{1}{N}\sum_{j=1}^{N} |w_j|^2, \qquad \hat{g}_5(w) = w_1\frac{1}{N^2}\sum_{j,k=1}^{N} w_j\bar{w}_k, \qquad \hat{g}_6(w) = \bar{w}_1\frac{1}{N}\sum_{j=1}^{N} w_j^2,$$

$$\hat{g}_7(w) = \bar{w}_1\frac{1}{N^2}\sum_{j,k=1}^{N} w_j w_k, \qquad \hat{g}_8(w) = \frac{1}{N}\sum_{j=1}^{N} |w_j|^2 w_j, \qquad \hat{g}_9(w) = \frac{1}{N^2}\sum_{j,k=1}^{N} w_j^2\bar{w}_k,$$

$$\hat{g}_{10}(w) = \frac{1}{N^2}\sum_{j,k=1}^{N} w_j|w_k|^2, \qquad \hat{g}_{11}(w) = \frac{1}{N^3}\sum_{j,k,l=1}^{N} w_j w_k \bar{w}_l\ .$$

Combining this with the individual Hopf normal form of second order, $\dot{w}_k = \alpha w_k - \beta|w_k|^2 w_k$, leads to the network Hopf normal form of second order with $S_N \times S^1$-equivariance

$$\dot{w}_k = \alpha w_k - \beta|w_k|^2 w_k + \kappa \sum_j a_j \hat{g}_j(w_k, w_2, \ldots, w_{k-1}, w_1, w_{k+1}, \ldots, w_N)\ . \tag{6.20}$$

The decomposition into the eleven coupling terms in (6.20) holds for any polynomial function $\boldsymbol{g} : \mathbb{C}^N \to \mathbb{C}^N$, $\boldsymbol{g} = (g_1, \ldots, g_N)$, of degree lower than or equal to 3 and which respects the $S_N \times S^1$-equivariance as in (6.19), see [Theorem 4.2, 189]. The proof for the network Hopf normal form, however, is not instructive, but existential: Equivariance theory allows to establish the explicit form (6.20), but it does not provide a "recipe" how to achieve it from some underlying network dynamics of the form $\dot{\boldsymbol{x}}_k = \boldsymbol{f}(\boldsymbol{x}_k; \mu) + \kappa \boldsymbol{g}_x(\boldsymbol{x}_1, \ldots, \boldsymbol{x}_N)$. In the subsequent Section 7 we will provide two (approximate) recipes for the simplified network Hopf normal form as considered before.

6.3.5. Ashwin & Rodrigues' phase reduction via $S_N \times S^1$-symmetry

Given the full network Hopf normal form (6.20) with weak coupling strength $|\kappa| \ll 1$, Ashwin and Rodrigues [74] derived the phase model

$$\dot{\theta}_k = \tilde{\omega}(\theta, \kappa) + \kappa \left(H_k^{(2)}(\theta) + H_k^{(3)}(\theta) + H_k^{(4)}(\theta) \right) \tag{6.21}$$

via equivariant theory. The phase dynamics (6.21) respects the coupling structure of the underlying dynamics (6.20) and allows interactions of up to four oscillators: The functions $H_k^{(j)}$ denote the sums over pairwise, triplet and quadruplet interactions of the phases for $j = 2, 3, 4$, respectively,

$$H_k^{(2)}(\theta) = \frac{1}{N} \sum_{j=1}^{N} H_2(\theta_j - \theta_k)$$

$$H_k^{(3)}(\theta) = \frac{1}{N^2} \sum_{j,l=1}^{N} H_{3,1}(\theta_j + \theta_l - 2\theta_k) + \frac{1}{N^2} \sum_{j,l=1}^{N} H_{3,2}(2\theta_j - \theta_l - \theta_k)$$

$$H_k^{(4)}(\theta) = \frac{1}{N^3} \sum_{j,l,m=1}^{N} H_4(\theta_j + \theta_l - \theta_m - \theta_k)$$

with $\theta = (\theta_1, \ldots, \theta_N)$ denoting the phase vector as before. In Appendix A.5, we provide the explicit expressions of the particular phase interaction functions $H_2, \ldots, H_4$.

In the limit of weak coupling $0 < \kappa \ll \mu \ll 1$ and for reasonably large network size $N \gg 4$, this general network Hopf normal form (6.21) reduces to

$$\dot{\theta}_k = \omega + \kappa \left(\frac{1}{N} \sum_{j=1}^{N} \left[\xi_1^0 \cos\left(\theta_j - \theta_k + \chi_1^0\right) + \varepsilon^2 \xi_2^1 \cos\left(2(\theta_j - \theta_k) + \chi_2^1\right) \right] + \mathcal{O}(\varepsilon^4) \right) \tag{6.22}$$

with $\omega = \alpha_I - \varepsilon^2(\beta_I/\beta_R) + \mathcal{O}(\varepsilon^4)$ and $\varepsilon^2 = \mu$ with $\varepsilon > 0$. In particular, the phase interaction function, i.e. the term in brackets in (6.22), consists of first and second harmonics with merely pairwise interactions. Rearranging terms by using (a) trigonometric identities and (b) the fact that the amplitude R^c of oscillations close to a supercritical Hopf bifurcation scales with $R^c \propto \sqrt{\mu}$, and discarding those terms of order $\mathcal{O}^4(\varepsilon)$, (6.22) coincides with the phase dynamics of the previously established network Hopf normal form (6.10) up to the connectivity values C_{kj}; see also Appendix A.5 for more details.

Following the argumentation in Section 6.3.3*, we already realized that only a specific selection of coupling terms contributes to the phase dynamics (at leading order). In fact, the averaging inherent to determine the phase interaction function H – which is intrinsically tied to the assumption of weak coupling and slowly varying phase deviations [12,46] – distinguished the same coupling terms $\hat{g}_j$ as dominant contributors to the phase dynamics that have been found along Ashwin and Rodrigues' reduction approach of the full network. Hence, averaging can be thought of as imposing those symmetry constraints on the coupling functions g_k that are intrinsic to the Hopf normal form.

For any particular choice of coupling topology other than global, all-to-all coupling, the permutation symmetry S_N cannot be upheld. However, for given coupling functions $\boldsymbol{g} = (g_1, \ldots, g_N)$ and connectivity matrix $\boldsymbol{C} = \{C_{kj}\}_{k,j}$, one can heuristically define a substitution operator $\mathcal{K}$ via the formal convolution $\mathcal{K}_{\boldsymbol{C}}\big(\boldsymbol{g}(w_1, \ldots, w_N)\big) := \big(\boldsymbol{C} \star \boldsymbol{g}\big)(w_1, \ldots, w_N)$ with entries

$$\big(\boldsymbol{C} \star \boldsymbol{g}\big)_j(w_1, \ldots, w_N) = g_j\big(C_{j1}w_1, \ldots, C_{jN}w_N\big) \ .$$

Then, one can first follow Ashwin and Rodrigues' phase reduction approach to derive (6.22), and subsequently apply the convolution $\mathcal{K} \star g$, which reveals the phase model

$$\dot{\theta}_k = \omega + \frac{\kappa}{N} \sum_{j=1}^{N} C_{kj} \left[\xi_1^0 \cos(\theta_j - \theta_k + \chi_1) + R^{c\,2} \xi_2^1 \cos\left(2(\theta_j - \theta_k) + \chi_2\right) \right] \ .$$

Using trigonometric identities, we eventually arrive at the desired phase model (5.7) with Fourier amplitudes (6.11).

7. Hopf normal form reduction of an oscillator network

Normal form reductions for oscillator networks are similar in nature to those for a single oscillator, but they become more involved as the reduction has to occur for all oscillators of the network simultaneously. Despite the mathematically proven existence of the network Hopf normal form, there is, to the best of our knowledge, no general and exact algorithm for deriving such a canonical model. According to Hoppensteadt and Izhikevich, "the process of deriving canonical models is rather an art than a science" [Chapter 4.1, 46]. Two schemes have proven fruitful to retain the simplified network Hopf

normal form (6.10),

$$\dot{w}_k = \alpha w_k - \beta|w_k|^2 w_k + \frac{\kappa}{N}\sum_{j=1}^{N} C_{kj}\left[\gamma w_j + \delta \bar{w}_k w_j^2\right]$$

from the dynamics (5.5),

$$\dot{\boldsymbol{x}}_k = \boldsymbol{f}\,(\boldsymbol{x}_k;\,\mu) + \frac{\kappa}{N}\sum_{j=1}^{N} C_{kj}\boldsymbol{g}\big(\boldsymbol{x}_k, \boldsymbol{x}_j\big)\ .$$

The first one, *Kuramoto's reductive perturbation approach*, is a natural extension of the technique described in Section 4.3.1. The second one, *Poincaré's nonlinear transform approach*, capitalizes on a series of nonlinear transforms as introduced in Section 4.3.2. However, both techniques only approximate the network dynamics to the network Hopf normal form. A mathematically rigorous normal form reduction of the full network $\boldsymbol{X} = \big(\boldsymbol{x}_1, \ldots, \boldsymbol{x}_N\big)$ has to incorporate coordinate transforms of the form $\boldsymbol{X} = \Psi(W)$ where $W = (w_1, \ldots, w_N)$ and $\Psi = (\psi_1, \ldots, \psi_N)$ with $\psi_j = \psi_j(w_1, \ldots, w_N)$. This can presumably lead to mixed coupling terms in the normal form beyond pairwise interactions. For weak coupling, however, we may consider $\psi_j(w_1, \ldots, w_N) \approx \psi_j^0(w_j) + \kappa\psi_j^1(w_1, \ldots, w_N)$ and for $\kappa \to 0$ we have $\psi_j(w_1, \ldots, w_N) = \psi_j^0(w_j)$. Since we here consider the uncoupled oscillators to be identical, the local coordinate transforms $\psi_j^0 = \psi$ coincide for all $j = 1, \ldots, N$, which results in $\Psi(W) \approx \big(\psi(w_1), \ldots, \psi(w_N)\big)$. Hence, the pairwise coupling assumption of the underlying dynamics, i.e. $\boldsymbol{g}_k(\boldsymbol{X}) = \sum_j \boldsymbol{g}(\boldsymbol{x}_k, \boldsymbol{x}_j)$, is directly inherited by the reduced dynamics as $g_k(W) = \sum_j g(w_k, w_j)$; see also Lemma A.6 in Appendix A.3. In turn, one can concentrate on the (reduced) dynamics of a single oscillator, identify the effect of the interaction with another one, and extend the result to the full network of coupled oscillators. Kuramoto's reduction technique is based upon the uncoupled, single oscillator dynamics and subsequently explores deviations induced through the coupling in a perturbative approach. The second technique first aims at identifying the correct local coordinate transform $\boldsymbol{x}_k = \psi(w_k)$ for a single oscillator, and then applies ψ also to the coupling terms. Applying either of the techniques thus leads to the (reduced) coupling function $g(w_j, w_k) = \sum_{a,b,c,d} w_j^a \bar{w}_j^b w_k^c \bar{w}_k^d$ with both resonant and non-resonant monomials $w_j^a \bar{w}_j^b w_k^c \bar{w}_k^d$. By using the arguments in Section 6.3.3*, one can discard all but the resonant monomials, which results in the approximate network Hopf normal form (6.10).

7.1. Kuramoto's reductive perturbation approach

For the system (5.5), recall that one can focus on two coupled oscillators $\boldsymbol{x}, \boldsymbol{x}' \in \mathbb{R}^n$ that evolve according to

$$\dot{\boldsymbol{x}} = \boldsymbol{f}(\boldsymbol{x};\,\mu) + \kappa\ \boldsymbol{g}(\boldsymbol{x}, \boldsymbol{x}') \tag{7.1}$$

and an analogous expression holds for $\boldsymbol{x}'$. For symmetry reasons, it suffices to consider only the dynamics of $\boldsymbol{x}$. The stable fixed point solution $\boldsymbol{x} = \boldsymbol{0}$ undergoes a Hopf bifurcation at $\mu = 0$, giving rise to stable limit-cycle oscillations with amplitude $R = \mathcal{O}(\varepsilon)$ where $\varepsilon = \sqrt{\mu}$. We will only consider $\mu > 0$ and small coupling strengths $0 \leq |\kappa| \ll \mu \ll 1$. We further substitute $\kappa \mapsto \varepsilon^2\kappa$, which indicates the smallness of κ compared to μ. The dynamics (7.1) hence reads

$$\dot{\boldsymbol{x}} = \boldsymbol{f}(\boldsymbol{x};\,\varepsilon^2) + \varepsilon^2\kappa\ \boldsymbol{g}(\boldsymbol{x}, \boldsymbol{x}')\ .$$

The time-asymptotic behavior of $\boldsymbol{x}(t)$ can be described similar to (4.7), but now subject to the coupling with the other oscillator $\boldsymbol{x}'(t)$:

$$\begin{aligned}\boldsymbol{x} &= \boldsymbol{x}_0(w, \bar{w}, \phi) + \boldsymbol{\rho}(w, \bar{w}, w', \bar{w}', \phi)\ ,\\ \dot{w} &= f(w, \bar{w}) + \kappa g(w, \bar{w}, w', \bar{w}')\ .\end{aligned} \tag{7.2}$$

$\boldsymbol{x}_0(t)$ denotes the solution (4.6) of the uncoupled linearized dynamics. The complex amplitude $w = w(\tau)$ evolves on the slower time scale $\tau = \varepsilon^2 t$ and according to the *amplitude equation* (7.2). The functions $\boldsymbol{\rho}, f, g$ are to be determined perturbatively, i.e., by considering a 'small' deviation from the first solution $\boldsymbol{x} = \boldsymbol{x}_0$ and expanding $\boldsymbol{\rho}, f, g$ around it. The explicit form of $f(w, w')$ in lowest order was already given in (4.8) & (4.9). Note that the dependence on the bifurcation parameter μ is only respected at first order, but neither in the nonlinear nor in the coupling terms. To derive the coupling function $g(w, \bar{w}, w', \bar{w}')$, we consider two cases.

First, we assume the coupling $\boldsymbol{g}(\boldsymbol{x}, \boldsymbol{x}')$ to be *linear*. Then, the coupling can be either diffusive or direct (non-diffusive), i.e $\boldsymbol{g} = \boldsymbol{g}_{\text{diff}}$ or $\boldsymbol{g} = \boldsymbol{g}_{\text{dir}}$, respectively, which yields

$$\left.\begin{array}{rcl}\boldsymbol{g}_{\text{diff}}(\boldsymbol{x}, \boldsymbol{x}') &=& \hat{\boldsymbol{D}}(\boldsymbol{x}' - \boldsymbol{x})\\ \boldsymbol{g}_{\text{dir}}(\boldsymbol{x}, \boldsymbol{x}') &=& \hat{\boldsymbol{D}}\boldsymbol{x}'\end{array}\right\} \Longrightarrow \left\{\begin{array}{rcl} g_{\text{diff}}(w, w') &=& \gamma(w' - w)\\ g_{\text{dir}}(w, w') &=& \gamma w'\end{array}\right. , \tag{7.3}$$

with $\gamma = \boldsymbol{v}\hat{\boldsymbol{D}}\boldsymbol{u}$ and $\hat{\boldsymbol{D}} \in \mathbb{R}^{n\times n}$, see also [177]. In line with (6.10), a second-order amplitude equation for weakly coupled oscillators near a supercritical Hopf bifurcation point with linear coupling $\kappa\gamma w'$ obeys the form

$$\dot{w} = \alpha w - \beta|w|^2 w + \kappa\big(\gamma w' + \delta\bar{w}w'^2\big) \tag{7.4}$$

with the complex coupling constants $\gamma \in \mathbb{C}$, as given in (7.3), and

$$\delta = 2\boldsymbol{v}\boldsymbol{n}_2\left(\bar{\boldsymbol{u}}, (\hat{\boldsymbol{L}}_0 - 2i\omega_0\boldsymbol{I})^{-1}\hat{\boldsymbol{D}}(\hat{\boldsymbol{L}}_0 - 2i\omega_0\boldsymbol{I})^{-1}\boldsymbol{n}_2(\boldsymbol{u},\boldsymbol{u})\right) . \tag{7.5}$$

Second, for *nonlinear* couplings $\boldsymbol{g}(\boldsymbol{x},\boldsymbol{x}') = \sum_{j,k\geq 0}\boldsymbol{G}_{jk}(\boldsymbol{x},\boldsymbol{x}')$, only the parameter δ in (7.4) changes to

$$\begin{aligned}\delta = {} & 2\boldsymbol{v}\boldsymbol{n}_2\Big(\bar{\boldsymbol{u}}, \big(\hat{\boldsymbol{L}}_0 - 2i\omega_0\boldsymbol{I}\big)^{-1}\Big[\boldsymbol{G}_{01}\big(\hat{\boldsymbol{L}}_0 - 2i\omega_0\boldsymbol{I}\big)^{-1}\cdot\boldsymbol{n}_2(\boldsymbol{u},\boldsymbol{u}) - \boldsymbol{G}_{02}(\boldsymbol{u},\boldsymbol{u})\Big]\Big) \\ & - \boldsymbol{v}\boldsymbol{G}_{11}\big(\bar{\boldsymbol{u}}, \big(\hat{\boldsymbol{L}}_0 - 2i\omega_0\boldsymbol{I}\big)^{-1}\boldsymbol{n}_2(\boldsymbol{u},\boldsymbol{u})\big) + \boldsymbol{v}\boldsymbol{G}_{12}(\bar{\boldsymbol{u}},\boldsymbol{u},\boldsymbol{u}) ,\end{aligned} \tag{7.6}$$

where $\boldsymbol{G}_{01}$ is the matrix corresponding to direct linear coupling, that is, $\boldsymbol{G}_{01} = \hat{\boldsymbol{D}}$, see (7.3), and $\boldsymbol{G}_{jk}$ are nonlinear coupling terms of order $j+k$ as defined in Appendix A.2.2. For linear coupling all $\boldsymbol{G}_{jk}$ vanish except for $\boldsymbol{G}_{01}$. In this case, we retrieve (7.5).

7.2. Poincaré's nonlinear transform approach

Using a series of subsequent nonlinear transforms, the reduction approach presented in this section aims at identifying the local coordinate transform ψ for the Hopf normal form of a single oscillator and applying ψ to the full network. Again, we consider the dynamics (7.1) of two weakly coupled oscillators as in the previous subsection, and strive for reduced dynamics of the form

$$\dot{w} = f(w) + \kappa\, g(w,w') = \alpha w - \beta|w|^2 w + \kappa\left(\gamma w' + \delta\bar{w}w'^2\right) .$$

We restrict our case to only two dimensions $\boldsymbol{x} = (x,y), \boldsymbol{x}' = (x',y') \in \mathbb{R}^2$. Using a projection method, the case of n-dimensional dynamical systems follows analogously, see [Chapter 5, 82] for details. As said, the strategy to obtain the reduced network dynamics consists of two steps:

(i) Following the reduction technique outlined in Section 4.3.2 for a single oscillator $\boldsymbol{x}(t)$, we can rewrite the uncoupled dynamics $\dot{\boldsymbol{x}} = \boldsymbol{f}(\boldsymbol{x};\mu)$ in complex form (4.10) for a complex-valued variable $z(t) \in \mathbb{C}$, and then establish a *Poincaré transformation* (4.11),

$$z = \psi(w) = w + \sum_{a+b\geq 2} h_{ab} w^a \bar{w}^b ,$$

in order to achieve the (individual) Hopf normal form $\dot{w} = \alpha w - \beta|w|^2 w + \mathcal{O}^4(z)$.

(ii) We apply the same set of transforms to the coupling function $\boldsymbol{g}(\boldsymbol{x},\boldsymbol{x}')$ in order to derive the corresponding coupling function $g(w,w')$ in the w-dynamics. First, we rewrite $\boldsymbol{g}(\boldsymbol{x},\boldsymbol{x}')$ in complex form, that is,

$$\boldsymbol{g}(\boldsymbol{x},\boldsymbol{x}') \quad\longmapsto\quad \tilde{g}(z,z') = \tilde{g}(z,\bar{z},z',\bar{z}') ,$$

where the transformation in the complex plane is again determined by the eigenvectors of the Jacobian $\boldsymbol{L} = \nabla\boldsymbol{f}(\boldsymbol{x})$. Then, we use the previously identified Poincaré transformation $z = \psi(w)$ for expressing $\tilde{g}(z,\bar{z},z',\bar{z}')$ in terms of w and w' as

$$\tilde{g}(z,\bar{z},z',\bar{z}') \quad\overset{\psi}{\longmapsto}\quad g(w,\bar{w},w',\bar{w}') = \sum_{a+b+c+d\geq 0} g_{abcd} w^a \bar{w}^b w'^c \bar{w}'^d ,$$

where we expanded $g(w,w') = g(w,\bar{w},w',\bar{w}')$ as a formal power series. As mentioned above, we do not need to calculate all of the coupling coefficients g_{abcd}. Those that contribute dominantly to the first and second harmonics of the phase model, respectively, are

$$\begin{aligned} g_{0010} &= \tilde{g}_{0010} \\ g_{0120} &= \tfrac{1}{2}\Big(\tilde{g}_{0120} - h_{11}\tilde{g}_{0020} - h_{01}\overline{\tilde{g}_{0002}} + h_{20}\tilde{g}_{0110} + \overline{h_{02}}\tilde{g}_{0101} \\ &\qquad - h_{11}h_{20}\tilde{g}_{0010} - h_{11}\overline{h_{02}}\tilde{g}_{0001} - |h_{02}|^2\overline{\tilde{g}_{0010}} - h_{20}h_{02}\overline{\tilde{g}_{0001}}\Big) ,\end{aligned}$$

where $\tilde{g}_{abcd}$ are the coefficients of the respective power series of $\tilde{g}(z,\bar{z},z',\bar{z}')$, h_{ab} are those of the Poincaré transformation (4.11), and the overline denotes complex conjugation. Further coefficients of third order are $g_{2100}, g_{2001}, g_{0120}, g_{0021}, g_{1110}, g_{1011}$. All the coefficients g_{abcd} can be indicated in terms of the original coupling $\boldsymbol{g}(\boldsymbol{x},\boldsymbol{x}')$. The resulting expressions, however, become rather lengthy so that we refrain from computing them explicitly but note that the method can be implemented in algorithmic form. The computational details can be found in Appendix A.3. Importantly, due to the near-identity character of the Poincaré transformation (4.11), the linear terms of $g(w,w')$ coincide with those of $\tilde{g}(z,z')$. This means, in case of (direct) linear coupling $\tilde{g}(z,z') = \gamma z'$ we can immediately infer the coefficient g_{0010} as above. Nonlinear coupling terms g_{abcd} with $a+b+c+d > 1$, by contrast, become more involved as they incorporate the intertwined effects of higher order terms in the original coupling as well as in the Poincaré transformation.

7.3. The connection between analytic reduction techniques

The different normal form reduction techniques outlined above aim at distilling the network Hopf normal form from the underlying network dynamics. Both presented techniques only lead to an approximate network Hopf normal form as the reduced coupling terms do not comply with the required symmetry assumptions. Kuramoto's reductive perturbation approach and Poincaré's nonlinear transform approach are similar in nature as they both start off the uncoupled oscillator dynamics and subsequently characterize the coupling effects of the full network. However, an important difference is that there is a prevailing and inherent dependence of all terms on the bifurcation parameter μ following the Poincaré approach, whereas in the Kuramoto approach this μ-dependence is discarded for all nonlinear terms. Evaluating the resulting expressions in the Poincaré approach at the bifurcation point, $\mu = 0$, however, will reveal much resemblance between the two reduction techniques.

In Section 4, a third alternative to derive the Hopf normal form of a single oscillator was introduced as *Takens' reduction via Lie brackets*. Similar to *Poincaré's reduction via nonlinear transforms*, it also identifies a local coordinate transform akin to the Poincaré transformation above. This coordinate transform allows for extending the *Takens approach* to a network level in the same way as in the Poincaré approach in the previous sub-section. However, *Takens' reduction via Lie brackets* respects the dependence on the bifurcation parameter only in linear terms — as in *Kuramoto's reductive perturbation*. Therefore, Takens' approach for an oscillator network can be regarded as an intermediate reduction technique between the Poincaré and the Kuramoto approaches. For this reason, we refrain from listing it here as a third alternative to reduce the network Hopf normal form of second order. Notably, the strength of Takens' approach is the computation of Hopf normal forms of arbitrary high order $M \geq 1$, yet considering higher-order Hopf normal forms on a network level is beyond the scope of this report.

All three reduction techniques are also closely related to each other although they consider different forms of the underlying dynamics as a starting point. Restricting our considerations again to two real dimensions, *Kuramoto's reductive perturbation* can be applied to an arbitrary form of the dynamics

$$\dot{x}_k = \boldsymbol{f}(\boldsymbol{x}_k; \mu) + \kappa \sum_{j=1}^{N} C_{kj} \boldsymbol{g}(\boldsymbol{x}_k, \boldsymbol{x}_j) \, .$$

Takens' reduction via Lie brackets explicitly requires the (linearized) dynamics about the fixed point $\boldsymbol{x} = \boldsymbol{0}$, that is, $\dot{\boldsymbol{x}} = \boldsymbol{L}\boldsymbol{x}$ with $\boldsymbol{L} = \boldsymbol{L}(\mu) = \nabla \boldsymbol{f}(\boldsymbol{x}; \mu)\big|_{\boldsymbol{x}=\boldsymbol{0}}$, to be given in Jordan real form

$$\boldsymbol{L}(\mu) \mapsto \boldsymbol{J}(\mu) = \begin{pmatrix} \varrho(\mu) & -\omega(\mu) \\ \omega(\mu) & \varrho(\mu) \end{pmatrix}$$

with real-valued $\varrho(\mu), \omega(\mu) \in \mathbb{R}$. For *Poincaré's reduction via nonlinear transforms*, the dynamics have to be formulated in terms of complex variables $z_k \in \mathbb{C}$ via the transformation

$$\boldsymbol{x} = z\boldsymbol{u}(\mu) + \bar{z}\bar{\boldsymbol{u}}(\mu)$$

with $\boldsymbol{u}(\mu)$ being the right eigenvector of the Jacobian $\boldsymbol{L}(\mu)$ corresponding to the eigenvalue $\lambda(\mu) = \varrho(\mu) + i\omega(\mu)$. This transformation in the complex plane establishes a linear relation between $\boldsymbol{x}$ and the real and imaginary parts of $z = z_R + iz_I$. In particular, (z_R, z_I) are the coordinates of $\boldsymbol{x}$ in the (real) eigenbasis of $\boldsymbol{L}(\mu)$ composed by $\big\{2\mathrm{Re}\big(\boldsymbol{u}(\mu)\big), -2\mathrm{Im}\big(\boldsymbol{u}(\mu)\big)\big\}$. That is, we recover the same transformation of the linearized dynamics into its canonical Jordan real form as in *Takens' reduction via Lie brackets*.

8. Networks of Brusselators

The Brusselator is a theoretical model of oscillating chemical reactions. It comprises four hypothetical chemical reactions and has been developed by the Brussels school around Ilya Prigogine and René Lefever [67,190–192] – hence the name. For a long time, reports on oscillating chemical reactions were facing harsh skepticism. Despite the strong interest in biological and biochemical oscillations in the 1950s and 60s, the discovery of oscillatory patterns in a closed chemical system by Belousov [193] in 1951 had to be meticulously reproduced and investigated for years by Zhabotinsky [194] until the nowadays so famous Belousov–Zhabotinsky reaction found its way into the scientific community [195]; for an overview of oscillating chemical reactions see also [12,21,196]. In a way, the Belousov–Zhabotinsky reaction was conceived as a manageable model of more complex systems, which simultaneously bore a close analogy to biology: Strogatz describes this analogy where "propagating waves of oxidation […] annihilate upon collision just like waves of excitation in neural or cardiac tissue. […] spiral waves are now an ubiquitous feature of chemical, biological, and physical excitable media" [21]. The original Belousov–Zhabotinsky reaction, which involves more than twenty elementary reaction steps, could effectively be rewritten in three differential equations. From a similar perspective, one can regard the Brusselator as a simplified chemical oscillator, which can be described in two differential equations. Despite its ability to exhibit oscillatory dynamics, as found in the Belousov–Zhabotinsky reaction, the Brusselator is a mere hypothetical model and is not based on a particular chemical reaction. Nonetheless, it serves as an exquisite example to apply the arsenal of phase reduction techniques because it exhibits a supercritical Hopf bifurcation. In particular, we consider on the phase dynamics of complex networks of coupled Brusselators, thereby building on and generalizing earlier network models [177,190,197–199].

8.1. Single node dynamics

The chemical reactions of the Brusselator are given in terms of

$$A \xrightarrow{k_a} X \tag{8.1a}$$

$$B + X \xrightarrow{k_b} Y + C \tag{8.1b}$$

$$2X + Y \xrightarrow{k_c} 3X \tag{8.1c}$$

$$X \xrightarrow{k_d} D\,, \tag{8.1d}$$

which add up to $A + B \to C + D$. Each of the reactions (8.1)a–d) has a rate constant k_a to k_d. Assuming that the chemicals A and B are in vast excess, their concentrations stay constant while the products C and D are constantly removed. The concentrations of the autocatalytic reactants X and Y will respond sensitively to already weak perturbations. They will reach an oscillatory state when the overall reaction is far from an equilibrium solution. (8.1) can thus be considered a thermodynamically open system with the following rate equations for the (dimensionless) concentrations $x = [X]$ and $y = [Y]$

$$\begin{aligned} \dot{x} &= k_a[A] - k_b[B]x + k_c x^2 y - k_d x \\ \dot{y} &= k_b[B]x - k_c x^2 y \end{aligned} \tag{8.2}$$

with free parameters $k_a[A]$, $k_b[B]$, k_c and k_d. The rate equations (8.2) can be understood from the reactions (8.1) as follows: Reaction a) leads to an increase of concentration x, which is proportional to the product of the rate k_a and the concentration $[A]$ of chemical A. Likewise, reaction d) decreases concentration x at rate k_d. Whenever the two chemicals B and X are involved in reaction b), concentration y increases proportional to the rate k_b times the concentrations of B and X and, simultaneously, concentration x decreases of the same amount. Reaction c) can be understood in the same manner, only that this reaction leads to an increase in x and a (balanced) decrease in concentration y.

8.2. Coupled Brusselators

We consider a network of Brusselators by coupling multiple nodes $\boldsymbol{x}_k = (x_k, y_k) \in \mathbb{R}^2$, $k = 1, \ldots, N$. For the sake of illustration, we fix the rate constants $k_c = k_d = 1$ and consider $a = k_a[A], b = k_b[B] \in \mathbb{R}^+$ as possible bifurcation parameters. Our *Brusselator network model* reads

$$\begin{aligned} \dot{x}_k &= a - (b+1)x_k + x_k^2 y_k \; + \kappa\, g_{k,x}(x_1, \ldots, x_N, y_1, \ldots, y_N) \\ \dot{y}_k &= b x_k - x_k^2 y_k \qquad\qquad\; + \kappa\, g_{k,y}(x_1, \ldots, x_N, y_1, \ldots, y_N) \end{aligned} \tag{8.3}$$

for some weak coupling strength $0 \leq |\kappa| \ll 1$ and with coupling functions $g_{k,x}, g_{k,y} : \mathbb{R}^{2N} \to \mathbb{R}$.[26]

Without coupling, $\kappa = 0$, every node has a stable fixed point at $(x_0, y_0) = (a, b/a)$, which undergoes a supercritical Hopf bifurcation at $b = 1 + a^2$. Introducing the new variables $\tilde{x}_k = x_k - x_0$ and $\tilde{y}_k = y_k - y_0$, we can shift the fixed point to the origin, $(\tilde{x}_0, \tilde{y}_0) = (0, 0)$. When restricting the form of the coupling to be the sum of pairwise interactions between nodes $\tilde{\boldsymbol{x}}_k, \tilde{\boldsymbol{x}}_j$, $k \neq j$, the dynamics (8.3) becomes

$$\begin{aligned} \dot{x}_k &= (b-1)x_k + a^2 y_k + \frac{b}{a}x_k^2 + 2a x_k y_k + x_k^2 y_k \; + \frac{\kappa}{N}\sum_{j=1}^{N} C_{kj} g_x(\boldsymbol{x}_k, \boldsymbol{x}_j) \\ \dot{y}_k &= -b x_k - a^2 y_k - \frac{b}{a}x_k^2 - 2a x_k y_k - x_k^2 y_k \qquad + \frac{\kappa}{N}\sum_{j=1}^{N} C_{kj} g_y(\boldsymbol{x}_k, \boldsymbol{x}_j)\,. \end{aligned} \tag{8.4}$$

Here, we omitted the tildes for the sake of readability and assumed the coupling terms $\boldsymbol{g} = (g_x, g_y)$ to be identical across nodes. The adjacency matrix $\boldsymbol{C} = \{C_{kj}\}$ specifies the connectivity between nodes $\boldsymbol{x}_k$ and $\boldsymbol{x}_j$. We define the bifurcation parameter as

$$\mu = \frac{b}{1+a^2} - 1 \tag{8.5}$$

and aim at transforming the dynamics (8.4) into Jordan real form, that is, the linearized dynamics with Jacobian $\boldsymbol{L}(\mu)$ around the fixed point $(0, 0)$ is of the form

$$\begin{pmatrix} \dot{x}_k \\ \dot{y}_k \end{pmatrix} = \begin{pmatrix} \varrho(\mu) & -\omega(\mu) \\ \omega(\mu) & \varrho(\mu) \end{pmatrix} \begin{pmatrix} x_k \\ y_k \end{pmatrix}.$$

[26] In practice, coupling between (electro-) chemical oscillators can be realized by introducing particular elements in the originating electrical circuit that connects the various network nodes. Adding, e.g., capacitors or resistors allows for chemical or electrical based coupling, respectively, cf. Section 10.2.1 for a discussion on different coupling functions and see the work by Hudson, Kiss and co-workers for practical implementation [200–203].

To do so, we use the transformation matrix

$$\boldsymbol{T}(\mu) = \frac{1}{2(1+\mu)(1+a^2)} \begin{pmatrix} -\left(\mu + a^2(2+\mu)\right) & \sqrt{4a^2 - \mu^2(1+a^2)^2} \\ 2(1+\mu)(1+a^2) & 0 \end{pmatrix} , \tag{8.6}$$

where $\sqrt{4a^2 - \mu^2(1+a^2)^2}/2 = \omega(\mu)$ is the emergent frequency of the oscillatory dynamics for $\mu \geq 0$ and $\omega_0 = \omega(0) = a$.[27] The to-be-analyzed system then reads

$$\dot{\boldsymbol{x}}_k = \boldsymbol{L}(\mu)\boldsymbol{x}_k + \boldsymbol{T}^{-1}\boldsymbol{N}_1(\boldsymbol{T}\boldsymbol{x}_k;\mu) + \boldsymbol{T}^{-1}\boldsymbol{N}_2(\boldsymbol{T}\boldsymbol{x}_k;\mu) + \frac{\kappa}{N}\sum_{j=1}^{N} C_{kj}\boldsymbol{T}^{-1}\boldsymbol{g}(\boldsymbol{T}\boldsymbol{x}_k, \boldsymbol{T}\boldsymbol{x}_j) \tag{8.7}$$

with linear part

$$\boldsymbol{L}(\mu) = \frac{1}{2}\begin{pmatrix} \mu(1+a^2) & -\sqrt{4a^2 - \mu^2(1+a^2)^2} \\ \sqrt{4a^2 - \mu^2(1+a^2)^2} & \mu(1+a^2) \end{pmatrix}$$

and nonlinearities

$$\boldsymbol{N}_1(\boldsymbol{x};\mu) = \begin{pmatrix} (1+\mu)(1+a^2) & 2a & 0 \\ -(1+\mu)(1+a^2) & -2a & 0 \end{pmatrix}\begin{pmatrix} x^2 \\ xy \\ y^2 \end{pmatrix} \quad \text{and} \quad \boldsymbol{N}_2(\boldsymbol{x};\mu) = \begin{pmatrix} 0 & 1 & 0 & 0 \\ 0 & -1 & 0 & 0 \end{pmatrix}\begin{pmatrix} x^3 \\ x^2y \\ xy^2 \\ y^3 \end{pmatrix} .$$

8.3. Identifying the Hopf normal form

To prepare the different reduction techniques, in particular Kuramoto's reductive perturbation and Poincaré's nonlinear transform approach, we first specify the parameters that are independent of the coupling; see also [12,204].

Kuramoto's reductive perturbation. Following Section 7.1, the normal form parameters α, β in (7.4),

$$f(w, \bar{w}) = \alpha w - \beta |w|^2 w ,$$

can be identified as

$$\alpha = \tfrac{1}{2}\mu\left(1 + a^2\right) + ia \quad \text{and} \quad \beta = \tfrac{1}{2}\left(1 + \frac{2}{a^2} + i\frac{4 - 7a^2 + 4a^4}{3a^3}\right) . \tag{8.8}$$

Note that β is independent of the bifurcation parameter μ, whereas α depends on μ. Hence, varying μ may strongly affect the normal form. The coupling parameters of order $\mathcal{O}(\kappa)$ can be computed using the expressions above once the type of coupling has been established.

Poincaré's reduction via nonlinear transforms. In a similar way, one can compute the (uncoupled part of the) normal form according to the reduction approach via nonlinear transforms as in Section 7.2. The Poincaré transformation can subsequently be employed to bring also the coupling terms into the desired form. In contrast to *Kuramoto's reductive perturbation approach*, no assumptions on the smallness of the bifurcation parameter μ have to be imposed since we do not discard the dependence of nonlinear terms on μ. While this improves the accuracy by making both α and β depend on μ, it yields equations that are too lengthy to report. Therefore, we will compare the different reduced phase dynamics numerically and graphically.

8.4. Comparing analytic and numerical phase reductions

Considering one Brusselator as an integral element of a network of coupled oscillators, every oscillator is subject to perturbations from the respective other nodes. The initial step is to investigate how (the phase dynamics of) an individual Brusselator reacts to perturbations. For this, we determine the phase sensitivity function $\boldsymbol{Z}$. We can explicitly compute $\boldsymbol{Z}$ either analytically from the reduced Hopf normal form (8.8), or numerically from the original dynamics (8.7) by employing the computational schemes outlined in Sections 3.3 and 3.4. The analytically derived phase sensitivity function is sinusoidal and reads

$$\boldsymbol{Z}(\theta) = \frac{1}{R}\begin{pmatrix} -\sin\theta - c_2\cos\theta \\ -c_2\sin\theta + \cos\theta \end{pmatrix} , \quad \text{where } R^2 = \frac{\mathrm{Re}(\alpha)}{\mathrm{Re}(\beta)} \text{ and } c_2 = \frac{\mathrm{Im}(\beta)}{\mathrm{Re}(\beta)} , \tag{8.9}$$

with α and β determined either along *Kuramoto's reductive perturbation approach* or along the *reduction approach via nonlinear transforms*. The Hopf normal form reduction imposes circular symmetry on the limit cycle, leading to the characteristic shape of $\boldsymbol{Z}$ irrespective of the size of the bifurcation parameter μ. By contrast, the numerically computed phase sensitivity function $\boldsymbol{Z}$ may exhibit higher harmonics for growing distances from the Hopf bifurcation point.

[27] Note that for $a \geq 0$ and $|\mu| \ll 1$, $\boldsymbol{T}(\mu)$ can only become singular when $\mu = a = 0$. In this case, $\det\big(\boldsymbol{T}(0)\big) = 0$, and the Jacobian $\boldsymbol{L}(0) = \boldsymbol{0}$ vanishes, too.

8.4.1. Linear coupling

A comparison of the different phase sensitivity functions provides only limited insight about the network's phase dynamics. Arguably more important is the shape of the entire phase interaction function H, which also accounts for the type of coupling. For our network of Brusselators, we first consider global and linear diffusive coupling between oscillators[28]

$$C_{kj}\boldsymbol{g}(\boldsymbol{x}_k, \boldsymbol{x}_j) = \begin{pmatrix} x_j - x_k \\ d(y_j - y_k) \end{pmatrix} \tag{8.10}$$

with some coupling constant $d \in \mathbb{R}$, cf. [177]; $d \geq 0$ 'weights' the coupling between y_j and y_k relative to that between x_j and x_k.

In the following, we briefly sketch how collective dynamics of weakly and linearly coupled Brusselators can be predicted with the help of reduced phase models when varying the parameters a, d, and μ. We will focus on the boundaries between stability and instability of the fully synchronized state and of the (balanced) two cluster state. These boundaries are described in terms of the amplitudes a_n, b_n of the first ($n = 1$) and second ($n = 2$) harmonics of the phase interaction function (5.7),

$$H(\psi) = \sum_{n\geq 0} a_n \cos(n\psi) + b_n \sin(n\psi) \,.$$

Analytic phase reductions. Recall that the sought-for dynamics (6.10) reads

$$\dot{w}_k = \alpha w_k - \beta |w_k|^2 w_k + \frac{\kappa}{N} \sum_{j=1}^{N} C_{kj} \left[\gamma w_j + \delta \bar{w}_k w_j^2\right] \,.$$

This means that the parameters γ and δ remain to be specified. Using *Kuramoto's reductive perturbation approach* for the Brusselator network with linear coupling (8.10), we find

$$\begin{aligned} \gamma &= \frac{1}{2} + \frac{d}{2} + i\,\frac{a}{2}(1+d) \,, \\ \delta &= -\frac{4 + a^2(2-10d) + d + a^4(-2+7d)}{9a^4} - i\,\frac{4 + a^2(2-11d) + 2a^4(-1+d) + 5d}{9a^3} \,. \end{aligned} \tag{8.11}$$

By combining (8.8) and (8.11), we obtain

$$\begin{aligned} c_1 &= \frac{\mathrm{Im}(\gamma)}{\mathrm{Re}(\gamma)} = \frac{-a(1-d)}{1+d} \,, \\ c_2 &= \frac{\mathrm{Im}(\beta)}{\mathrm{Re}(\beta)} = \frac{4 - 7a^2 + 4a^4}{6a + 3a^3} \,, \\ c_3 &= \frac{\mathrm{Im}(\delta)}{\mathrm{Re}(\delta)} = \frac{a\left[4 + a^2(2-11d) + 2a^4(-1+d) + 5d\right]}{4 + a^2(2-10d) + d + a^4(-2+7d)} \,, \end{aligned} \tag{8.12}$$

where the constant radius is given by

$$R = \mu\sqrt{\frac{a^2(1+a^2)}{2+a^2}} \,. \tag{8.13}$$

From here we can derive the amplitudes a_1, a_2, b_1, and b_2 of H, cf. Section 4.4.

Analogously, one can derive the amplitudes of the phase interaction function H along *Poincaré's reduction via nonlinear transforms*. Although the parameters $\alpha, \beta, \gamma, \delta$ are the main contributors to the reduced phase dynamics, the nonlinear transform approach allows to include corrective coupling terms g_{klmn} apart from $\gamma = g_{0010}$ and $\delta = g_{0120}$, see Section 7.2. Since the nonlinear transform approach also employs parameter-dependent transformations at every order, the resulting amplitudes a_1, a_2, b_1, and b_2 can be expected more accurate than those obtained with the reductive perturbation approach above. As said, the explicit parameter-dependent expressions of a_1, a_2, b_1, and b_2 are quite lengthy and, therefore, we compare the outcome of these two phase reduction techniques graphically. To do so, we determined the stability boundaries of the synchronized state and of the balanced two cluster state in the a–d plane for a fixed radius of the limit cycle oscillations that emerged through the supercritical Hopf bifurcation, thereby following the presentation of Kori and co-workers in [177]. We consider oscillations with radius $R = 0.1$ and $R = 0.4$. These values correspond to the distance μ from the Hopf bifurcation point through the relation (8.13). By increasing a from 1 to 3, μ decreases from 0.49 to 0.14

[28] Approximate linear coupling schemes have also been realized in experiments with electro-chemical oscillators, see, e.g., [177,205], which underlines the relevance of this comparably simple type of coupling.

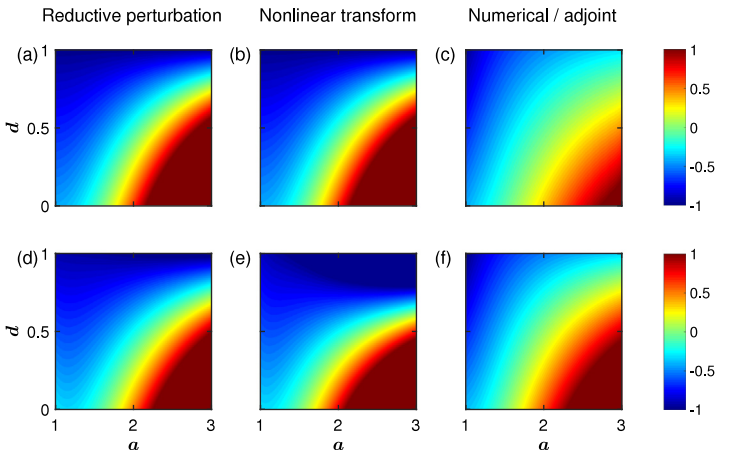

Fig. 8.1. Stability of the globally synchronized state of the network of linearly coupled Brusselators is determined through the phase interaction function H. If $\mathrm{sgn}(\kappa)H'(0) > 0$, the synchronized state is stable, otherwise unstable. In line with the subsequent analysis, we use $\kappa < 0$ and show $-H'(0)$ color coded in the a–d plane for (a–c) small-amplitude oscillations, $R = 0.1$, i.e. near the Hopf bifurcation point, and for (d–f) large-amplitude oscillations, $R = 0.4$, further away from the Hopf point. A change of stability occurs at $H'(0) = 0$ (green), between positive (red) and negative (blue) areas. The phase interaction function is reduced via (a, d) Kuramoto's reductive perturbation approach, (b, e) Poincaré's nonlinear transform approach, and (c, f) the direct numerical method.

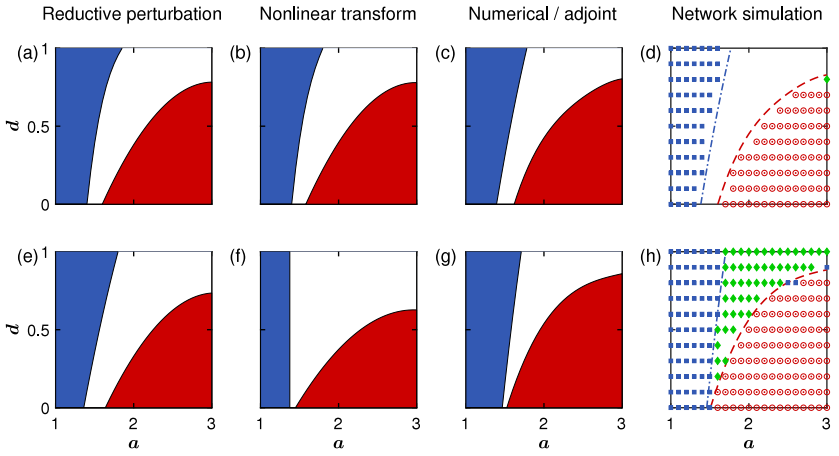

Fig. 8.2. Stable globally synchronized states (red) and stable balanced two-cluster states (blue) of the network of linearly coupled Brusselators in the a–d plane for (a–d) small-amplitude, and for (e–h) large-amplitude oscillations with $R = 0.1$ and $R = 0.4$, respectively. The (negative) coupling strength is set at $\kappa = -0.001$. Results are obtained via (a, e) Kuramoto's reductive perturbation approach, (b, f) Poincaré's nonlinear transform approach, and (c, g) the direct numerical method, and compared against (d, h) simulations of the full network of $N = 30$ weakly coupled Brusselators. In the full network, also stable three-cluster states occurred (green). The dashed and dashed–dotted lines represent the boundaries of synchronization and two-cluster regions, respectively, using the numerical method.

for large-amplitude oscillations, $R = 0.4$, and from 0.12 to 0.035 for $R = 0.1$, respectively. The parameter d is varied in the interval $[0, 1]$. The stability of the synchronized state can be directly assessed using the derivative $H'(0)$ of the phase interaction function H, cf. Section 5.3.3. The results are given in Fig. 8.1. In brief, as $H'(0)$ changes signs, the synchronized state switches from stable to unstable depending on the sign of the coupling κ. Recall that the stability boundary of the synchronized state can be given by $\{b_1 + 2b_2 = 0\}$ and the one of the two cluster state by $\{b_2 = 0\}$ for the Hopf normal form network dynamics (6.10). The parameter regions where the fully synchronized and the two cluster states are stable are depicted in Fig. 8.2 for the reductive perturbation (panels a and e) and the nonlinear transforms approaches (b and f).

The differences between the two analytic normal form reductions are barely visible for small-amplitude oscillations, both in the $H'(0)$- and in the cluster plots. Increasing the radius of oscillation leads to a minor reduction in size of the synchronization region (depicted in red) for both reduction techniques. The boundary indicating the emergence of a stable (anti-phase) two cluster state (blue) is slightly bent following the reductive perturbation approach, but becomes a straight line in the nonlinear transform approach.

Numerical phase reductions. We determined the properties of the Brusselator's limit cycle, its phase sensitivity function $\boldsymbol{Z}$ and the phase interaction function H numerically using either of the reduction techniques presented in Section 6.2.[29] After extracting the amplitudes of the first and second harmonics of H, we identified the stability boundaries of the fully synchronized and two cluster states, respectively. The results are summarized in Fig. 8.1 (panels c, f) and Fig. 8.2 (panels c, g). When comparing the network predictions to those based on the analytic techniques, we found that for small-amplitude oscillations the agreement appeared almost perfect and the stability boundaries are nearly identical. However, for large-amplitude oscillations, the different techniques diverged significantly. While the synchronization region shrank according to the analytic techniques, it enlarged following the numerical reduction. The boundary for the two cluster state slightly rectified but it did not match either of the other two predicted lines.

Network simulations. To test whether the predictions based on the reduced phase models actually recover the original network dynamics, we simulated the dynamics of $N = 30$ Brusselators coupled with some weak strength $\kappa = -0.001$. The results are shown in Fig. 8.2 (panels d, h). For both small- and large-amplitude oscillations, the analytic as well as the numeric phase reduction techniques performed sufficiently well. Yet, the numerical phase reduction outperformed the analytic approaches for large-amplitude oscillations. This holds for synchronization as well as for two-cluster regions. While both analytic techniques underestimated synchronization (smaller red area), the reductive perturbation approach slightly overestimated the two-cluster region and the nonlinear transform approach underestimated it. Moreover, the network simulations revealed a large area where a three-cluster state is stable for large-amplitude oscillations, Fig. 8.2 (panel h). By construction, none of the phase reduction techniques was able to detect this. More details about the numeric implementations can be found in Appendix B.1.

8.4.2. Nonlinear coupling

An arguably more appealing problem is that of nonlinear coupling. To illustrate this, one can add an additional coupling term $\boldsymbol{g}_{\text{syn}}$ of the form

$$\boldsymbol{g}_{\text{syn}}(\boldsymbol{x}_k, \boldsymbol{x}_j) = \hat{\boldsymbol{g}}(\boldsymbol{x}_k)\boldsymbol{S}(\boldsymbol{x}_j) \quad \text{for all } k \neq j = 1, \dots, N,$$

which may resemble a chemical synapse, see also Section 10.2.1. The function $\boldsymbol{S} = (S_x, S_y)$ is usually of sigmoidal shape, which we simplify as a polynomial of some degree $n \in \mathbb{N}$ – this can be thought of as, e.g., a truncated Taylor expansion of a sigmoidal function. As a particular example we choose the nonlinear coupling of the form[30]

$$\boldsymbol{g}(\boldsymbol{x}_k, \boldsymbol{x}_j) = \boldsymbol{g}_{\text{diff}}(\boldsymbol{x}_k, \boldsymbol{x}_j) + \hat{\boldsymbol{g}}(\boldsymbol{x}_k)\boldsymbol{S}(\boldsymbol{x}_j) = \begin{pmatrix} x_j - x_k + g_1 x_j^2 + g_2 x_k x_j + g_3 x_k x_j^2 + g_4 x_k^2 x_j \\ d(y_j - y_k) \end{pmatrix} \tag{8.14}$$

with coupling parameter d as in the linear case above. The new nonlinear coupling terms are scaled by $g_j \in \mathbb{R}, j = 1, \dots, 4$. Here, we already anticipate that for *Kuramoto's reductive perturbation approach*, the term $g_4 x_k^2 x_j$ will not influence the resulting phase model because $x_k^2 x_j$ is a resonant monomial.

Analytic phase reductions. Equivalent to the case of linear coupling, we display the predictions about synchronization in Fig. 8.3 and about two cluster states in Fig. 8.4. The fixed coupling parameter values are

$$g_1 = 0.3, \quad g_2 = -0.2, \quad g_3 = 0.35, \quad g_4 = 0.3$$

while d is varied in the interval $[0, 1]$. Again, the analytic predictions of network states for small-amplitude oscillations are almost identical. However, for large-amplitude oscillations the differences between the two analytic techniques appear more pronounced when compared to the linear coupling case. Following *Poincaré's nonlinear transform approach*, the synchronization region is enlarged and by the same token the two cluster state region shrinks, consisting of an almost parallel band on the left and of a second, small triangular region in the top right corner of the a–d plane. The boundaries predicted by the reductive perturbation method hardly change when increasing the radius R of the limit cycle.

Numerical phase reductions. As in the linear coupling case, we employed the numerical phase reduction technique to determine the stability boundaries of the synchronized and two cluster states. The results are summarized in Fig. 8.3 (panels c, f) and Fig. 8.4 (panels c, g). Remarkably, the predictions for small-amplitude oscillations and close to the Hopf bifurcation point agreed with those of the analytic reduction techniques. For the large-amplitude oscillations, the predictions of the numerically reduced phase model resembled those of the nonlinear transform approach: The synchronization regions grow, the two cluster region shrinks. Strikingly, the triangular region in the top right corner has almost fully disappeared.

---

[29] In particular, we employ the direct numerical method presented in Section 3.3.

[30] Expanding both $\hat{\boldsymbol{g}} = (g_x, g_y)$ and $\boldsymbol{S} = (S_x, S_y)$ as power series in $\boldsymbol{x}_k = (x_k, y_k)$ and $\boldsymbol{x}_j = (x_j, y_j)$, respectively, we will consider in the following only non-zero x-components of the particular form

$$g_x(\boldsymbol{x}_k) = 1 + a_1 x_k + a_2 x_k^2 + \mathcal{O}^3(x_k) \quad \text{and} \quad S_x(\boldsymbol{x}_j) = b_1 x_j + b_2 x_j^2 + b_3 x_j^3 + \mathcal{O}^4(x_j)\ .$$

In order to obtain (8.14), we choose the non-vanishing coefficients

$$a_1 = g_2/g_1, \quad a_2 = g_4/g_1, \quad b_1 = g_1, \quad b_2 = g_1 g_3/g_2.$$

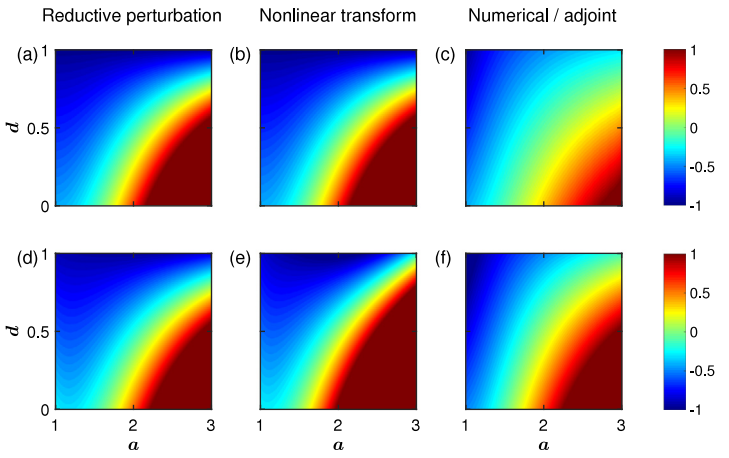

Fig. 8.3. Stability of the globally synchronized state of the network of nonlinearly coupled Brusselators is determined through the phase interaction function H. If $\mathrm{sgn}(\kappa)H'(0) > 0$, the synchronized state is stable, otherwise unstable. In line with the subsequent analysis, we use $\kappa < 0$ and show $-H'(0)$ color coded in the a–d plane for (a–c) small-amplitude oscillations, $R = 0.1$, i.e. near the Hopf bifurcation point, and for (d–f) large-amplitude oscillations, $R = 0.4$, further away from the Hopf point. A change of stability occurs at $H'(0) = 0$ (green), between positive (red) and negative (blue) areas. The phase interaction function is reduced via (a, d) Kuramoto's reductive perturbation approach, (b, e) Poincaré's nonlinear transform approach, and (c, f) the direct numerical method.

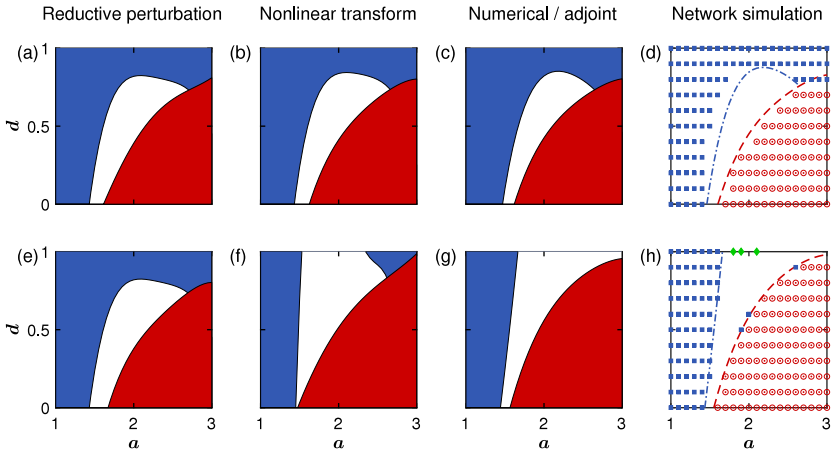

Fig. 8.4. Stable globally synchronized states (red) and stable balanced two-cluster states (blue) of the network of nonlinearly coupled Brusselators in the a–d plane for (a–d) small-amplitude, and for (e–h) large-amplitude oscillations with $R = 0.1$ and $R = 0.4$, respectively. The (negative) coupling strength is set at $\kappa = -0.001$. Results are obtained via (a, e) Kuramoto's reductive perturbation approach, (b, f) Poincaré's nonlinear transform approach, and (c, g) the direct numerical method, and compared against (d, h) simulations of the full network of $N = 30$ weakly coupled Brusselators. In the full network, also stable three-cluster states occurred (green). The dashed and dashed–dotted lines represent the boundaries of synchronization and two-cluster regions, respectively, using the numerical method.

Network simulations. As before, we simulated the dynamics of $N = 30$ weakly coupled ($\kappa = -0.001$) Brusselators but now employing the nonlinear coupling scheme. The results are depicted in Fig. 8.4 (panels d, h). We believe that they speak for themselves as the reading agrees with the results for the case of linear coupling. Again, we refer to Appendix B.1 for more details about the numerical implementation.

8.5. Other analytic phase reduction techniques

8.5.1. Isochrons, Floquet eigenvectors, and $S_N \times S^1$-symmetry

The first alternative analytic phase reduction techniques comprise of *Winfree's reduction via isochrons* and *Kuramoto's reduction via Floquet eigenvectors* for a single oscillator and *Ashwin & Rodrigues' reduction via* $S_N \times S^1$*-symmetry* for a network in Hopf normal form. As demonstrated in Section 6.3.2, all these techniques yield the same reduced phase model provided that the network of coupled Brusselators has been put in Hopf normal form.

Table 8.1
Phase models derived with different reduction techniques for linear coupling and near the Hopf bifurcation, $\mu = 0.0417$. The oscillators' natural frequency is ω, and a_n, b_n are the amplitudes of the Fourier components of the phase interaction function H. Symbols $+/-$ denote the sign of each amplitude. Their quantity corresponds to their influence on the dynamics, with $+++$ representing dominant contributions of order 1, while $0^{+/-}$ corresponds to amplitudes $\leq 10^{-3}$. Parameters are $(a, d) = (2.55, 0.65)$. Exact numerical values can be found in Appendix B.1.

Approach	ω	a_1	b_1	a_2	b_2
Reductive perturbation	2.537	$---$	$+$	0^+	0^-
Nonlinear transform	2.524	$---$	$+$	$+$	$-$
Direct averaging	$\times$	$\times$	$\times$	$\times$	$\times$
Numerical/adjoint	2.474	$++$	$+$	0^-	0^-

Table 8.2
Phase models derived with different reduction techniques for linear coupling and away from the Hopf bifurcation, $\mu = 0.1670$. The notation is the same as in Table 8.1. Parameters are $(a, d) = (2.55, 0.65)$. Exact numerical values can be found in Appendix B.1.

Approach	ω	a_1	b_1	a_2	b_2
Reductive perturbation	2.348	$---$	$+$	$++$	$--$
Nonlinear transform	1.832	$---$	$++$	$++$	$--$
Direct averaging	$\times$	$\times$	$\times$	$\times$	$\times$
Numerical/adjoint	2.671	$+++$	$++$	$-$	$-$

8.5.2. Haken's reduction via averaging

When introducing polar coordinates $\boldsymbol{x}_k = (x_k, y_k) = \big(R_k \cos(\Omega t + \phi_k), R_k \sin(\Omega t + \phi_k)\big)$ with $\Omega = \mathrm{Im}\big(\lambda_1(0)\big)$, one can realize that the right-hand side of (8.7) is of order $\mathcal{O}(R_k)$. Assuming that $0 \leq \mu \ll 1$, i.e. close to the Hopf bifurcation, the amplitude $R_k \ll 1$ is small and we may consider to apply Haken's averaging to (8.7) as outlined in Section 3.5. For simplicity, we approximate all nonlinear terms in (8.7) by the corresponding expressions at the Hopf point, $\mu = 0$, that is, one can use $\boldsymbol{T}(0), \boldsymbol{N}_1(\boldsymbol{x}; 0), \boldsymbol{N}_2(\boldsymbol{x}; 0)$. Averaging over one period $T = 2\pi/\Omega$ yields the approximate phase and amplitude dynamics

$$\dot{\phi}_k = 1 + \frac{a}{8(1+a^2)} R_k^2 + \mathcal{O}(\kappa)$$
$$\dot{R}_k = R_k \left[-a + \mu - \frac{3a^2}{8(1+a^2)} R_k^2 \right] + \mathcal{O}(\kappa) \,,$$

where $\mathcal{O}(\kappa)$ denotes the coupling terms. However, the uncoupled dynamics of the phase deviations ϕ_k is too large for slight deviations from the offset frequency at the Hopf point. Moreover, the amplitude dynamics R_k does not exhibit a non-trivial fixed point solution unless $0 < a \leq \mu \ll 1$ is very small, which stands in clear contrast to the well-established supercritical Hopf bifurcation character of the Brusselator. Apparently, applying an ad-hoc averaging in the current setting may yield spurious results.

8.6. Remarks

We analyzed the collective dynamics of a network of weakly coupled Brusselators with respect to (stable) synchronized, incoherent, and balanced two-cluster states. Numerical phase reduction techniques are perfectly able to detect the correct dynamical regimes as revealed by full network simulations. Analytic phase reduction techniques, by contrast, capture the actual collective dynamics only in a close neighborhood to the Hopf bifurcation point. This holds across linear and nonlinear coupling schemes.

For illustration, we fixed the parameter value $a = 2.55$ and investigated numerically the resulting phase model in terms of the frequency term and the Fourier coefficients of first and second harmonics of the reduced phase interaction function H. For linear coupling and close to the Hopf bifurcation point, the analytic reduction techniques do not only capture the correct collective dynamics, but they also provide the same order of amplitudes as obtained by numerical methods, see Table 8.1. Away from the Hopf point, the reduction techniques still perform considerably well, but slightly incorrect estimations of the first and second harmonics result in different predictions: according to the reductive perturbation approach a too strong second harmonic forces the phase dynamics into an incoherent state, whereas both the nonlinear transform approach and the numerical reduction correctly capture synchronization of the network, cf. Fig. 8.2 and Table 8.2.

Nonlinear coupling, by contrast, affects the performance more. For small-amplitude oscillations, the differences in sign of the b_2 values in Table 8.3 may be due to numerical artifacts, so that the (wrongly) predicted incoherent state by the nonlinear transform approach has to be considered with care in contrast to the correct prediction of a stable two-cluster state by the reductive perturbation approach and the numerical reduction. For large-amplitude oscillations, however, the phase reduction techniques diverge as shown in Fig. 8.4. Since the nonlinear transform approach respects the parameter-dependence in the normal form reduction, it outperforms the reductive perturbation approach and largely retrieves the results of the numeric reduction technique, see Table 8.4, where the amplitudes of first and second harmonics agree.

Table 8.3
Phase models derived with different reduction techniques for nonlinear coupling and near the Hopf bifurcation, $\mu = 0.0417$. The oscillators' natural frequency is ω, and a_n, b_n are the amplitudes of the Fourier components of the phase interaction function H. Symbols $+/-$ denote the sign of each amplitude. Their quantity corresponds to their influence on the dynamics, with $+++$ representing dominant contributions of order 1, while $0^{+/-}$ corresponds to amplitudes $\leq 10^{-3}$. Parameters are $(a, d) = (2.55, 0.75)$. Exact numerical values can be found in Appendix B.1.

Approach	ω	a_1	b_1	a_2	b_2
Reductive perturbation	2.537	$---$	$--$	0^+	0^+
Nonlinear transform	2.524	$---$	$--$	$+$	0^-
Direct averaging	$\times$	$\times$	$\times$	$\times$	$\times$
Numerical/adjoint	2.474	$++$	$-$	0^-	0^+

Table 8.4
Phase models derived with different reduction techniques for nonlinear coupling and away from the Hopf bifurcation, $\mu = 0.1670$. The notation is the same as in Table 8.3. Parameters are $(a, d) = (2.55, 0.75)$. Exact numerical values can be found in Appendix B.1.

Approach	ω	a_1	b_1	a_2	b_2
Reductive perturbation	2.345	$---$	$--$	$+$	0^+
Nonlinear transform	1.832	$---$	$++$	$++$	$-$
Direct averaging	$\times$	$\times$	$\times$	$\times$	$\times$
Numerical/adjoint	2.671	$+++$	$++$	$-$	$-$

We would like to add a final remark on phase reductions of the Brusselator. While we concentrated on the mere rate equations (of the mean field), there also exists a natural spatio-temporal extension of the Brusselator model into a two-component reaction–diffusion system. The Brusselator as a reaction–diffusion system allows for so-called chemical waves and other pattern formation, such as, e.g., traveling fronts or rotating spirals in an extended medium [12]. Not only is it possible to define a phase for rhythmic patterns in extended media, but also to derive the corresponding phase dynamics from the underlying spatio-temporal dynamics, as has been successfully demonstrated by Nakao, Kawamura and co-workers [151,154,164]. This strategy may be used to determine a meaningful phase dynamics of periodic fluid flows [206]. It has been extended to reduce the phase dynamics of limit cycle solutions to general partial differential equations [207]. In the same way, the phase dynamics of collective oscillations of globally coupled noisy elements may be derived, given that these oscillations are solutions to a Fokker–Planck equation [150,208]. We refer the interested reader to the literature for more details about phase reduction of oscillatory spatio-temporal dynamics, and stick here to non-extended systems.

9. Networks of Wilson–Cowan neural masses

As a second example for a network of coupled oscillators, we use the Wilson–Cowan neural mass model as a representative example for a smooth neural oscillator.[31] In their pioneering work, Wilson and Cowan derived a firing rate model for a neural population consisting of N_e excitatory and N_i inhibitory neurons [68,69]. Denoting the firing rate of a single excitatory (inhibitory) neuron by $e_n(i_n)$, the corresponding mean firing rates of the excitatory and inhibitory parts of the population are the averages $E = (1/N_e)\sum_{n=1}^{N_e} e_n$ and $I = (1/N_i)\sum_{n=1}^{N_i} i_n$, respectively. The firing rate of a single neuron is given as the number of spikes per time. A neuron elicits a spike whenever the sum over all of its inputs exceeds a certain threshold θ_n. We assume that every neuron receives inputs from all other neurons within the population. Every excitatory neuron receives some additional external input p_n, whose average is given by $P = (1/N_e)\sum_{n=1}^{N_e} p_n$. For a particular (unimodal) distribution of threshold values θ_n across the population, one can assign a sigmoidal activation function[32] $\mathcal{S}$ to the population dynamics [68]. Without loss of generality, we choose $\mathcal{S}[x] = 1/(1 + \mathrm{e}^{-x})$ and denote the population-specific threshold values by Θ_E and Θ_I for the excitatory and inhibitory parts, respectively. Then, the coarse-grained dynamics of the mean firing rates of a neural population obeys the form

$$\begin{aligned} \mu_E \dot{E} &= -E(t) + [1 - r_E E]\,\mathcal{S}\left[a_E\left(c_{EE}E - c_{IE}I - \Theta_E + P\right)\right] , \\ \mu_I \dot{I} &= -I(t) + [1 - r_I I]\,\mathcal{S}\left[a_I\left(c_{EI}E(t) - c_{II}I - \Theta_I\right)\right] . \end{aligned} \tag{9.1}$$

The coupling parameters c_{kj} with $k, j \in \{E, I\}$ indicate the strength of interaction between the different parts within the population, and a_E, a_I define the slopes of the transfer function $\mathcal{S}$. The terms $[1 - r_E E]$ and $[1 - r_I I]$ represent the refractory dynamics of the excitatory and inhibitory parts, respectively. They track the period of time during which the corresponding cells are incapable of being stimulated after an activation. We will neglect this term and set $r_E = r_I = 0$, thereby following Pinto and co-workers [210], who showed that the refractory terms effectively rescale the parameters of

[31] By smooth we refer to the smooth limit-cycle trajectory in the two-dimensional coordinate plane as in case of the Wilson–Cowan model. By contrast, integrate-and-fire models present an example for non-smooth neural oscillators, as the reset mechanism leads to discontinuities along the trajectory.

[32] Other names for the activation function $\mathcal{S}$ are transfer or gain function. The introduction of $\mathcal{S}$ may alternatively be motivated starting from a single neuron level and along an ergodicity argument, as the time average of individual, saturating firing rates equals the population average [209].

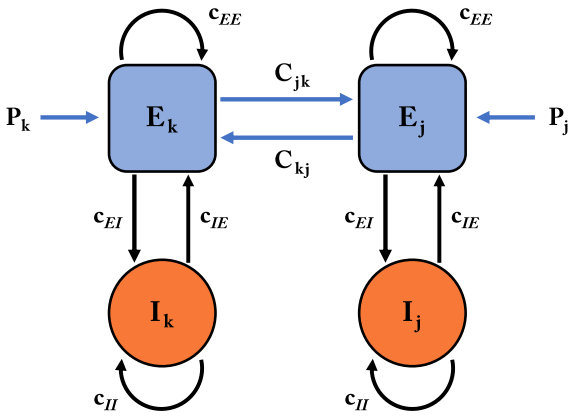

Fig. 9.1. Network of two coupled Wilson–Cowan neural masses. Each neural population k consists of excitatory and inhibitory parts (E_k and I_k), which are internally coupled with strengths c_{ij}, $i, j \in \{E, I\}$. Moreover, the population receives an external input P_k. Interaction between two neural masses k, j occurs via their respective excitatory parts only, where C_{kj} denotes the connectivity whether node k receives input from node j.

the nonlinear transfer function $\mathcal{S}$. For the sake of simplicity, we further consider the time scales $\mu_E = \mu_I = 1$. Depending on the choice of parameters, this model can exhibit rich dynamics such as self-sustained oscillations and multi-stability, see, e.g., [46,68,211]. Here, we restrict the parameter values to the dynamical regime in which every (E, I) population displays stable limit cycle oscillations.

To build a cortical network model, we connect N different (E_k, I_k) populations of excitatory and inhibitory neurons, $k = 1, \ldots, N$, via their excitatory parts [32,33,212]; see Fig. 9.1 for illustration. The neural mass dynamics of node k reads

$$\begin{aligned} \dot{E}_k &= -E_k + \mathcal{S}\left[a_E\left(c_{EE}E_k - c_{IE}I_k - \Theta_E + P_k + \frac{\kappa}{N}\sum_{j=1}^{N} C_{kj}E_j\right)\right] \\ \dot{I}_k &= -I_k + \mathcal{S}\left[a_I\left(c_{EI}E_k - c_{II}I_k - \Theta_I\right)\right] \ . \end{aligned} \tag{9.2}$$

$0 \leq \kappa \ll 1$ denotes the overall coupling strength and $\boldsymbol{C} = \{C_{kj}\}_{k,j}$ is an adjacency matrix indicating structural connectivity between two cortical regions k and j. The population specific average input P_k to the respective excitatory subpopulations may vary across the different cortical regions.

9.1. Single node dynamics

As in the case of the Brusselator, first we discuss the dynamics of a single unit using dynamics (9.2) without coupling, i.e. for $\kappa = 0$. Following [32,33], we fix several parameters to physiologically motivated values

$$a_E = 1.2,\ a_I = 2,\ c_{EE} = c_{EI} = 10,\ c_{IE} = 6,\ c_{II} = 1,\ \Theta_E = 2.5,\ \Theta_I = 3.5\ , \tag{9.3}$$

unless stated otherwise. Furthermore, we consider P_k to represent external inputs. Taking P_k as the bifurcation parameter results in the bifurcation diagram depicted in Fig. 9.2.[33]

9.2. Coupled Wilson–Cowan neural masses

We are interested in the dynamics of a network of coupled Wilson–Cowan neural masses of the form (9.2). The interplay between the excitatory and inhibitory parts of a single neural mass is governed by the coupling setup sketched in Fig. 9.1. We couple distinct neural masses only via their excitatory parts, which can be justified as an appropriate rescaling of the population-internal coupling parameters c_{kj} may compensate for inputs to the inhibitory parts. The adjacency matrix $\boldsymbol{C} = \{C_{kj}\}$ defines structural links between the different neural masses. While the coupling term in (9.2) of interconnected neural masses appears natural when compared to the internal coupling structure of a single neural mass, it deserves some discussion.

In Wilson and Cowan's original work [68], the sigmoid function was constructed in such a way that in the absence of external influences the baseline activity state $(E_k, I_k) = (0, 0)$ is a fixed point. In our formulation, where we follow [32,46,168], however, the sigmoid function takes on a slightly different form and a zero fixed point solution is

[33] Despite the lack of symmetry, one can realize the resemblance with Hoppensteadt and Izhikevich's bifurcation diagram [Fig. 2.12,46] with $\Theta_{E,I}$ as key parameters, as well as with the derivation by Borisyuk and Kirillov [211], who used $P = P_k$ and $c_3 = c_{EI}$ as key parameters.

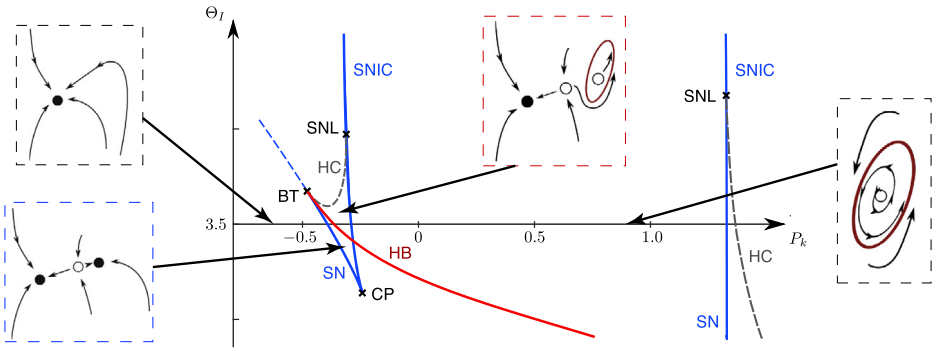

Fig. 9.2. Bifurcation diagram of the uncoupled Wilson–Cowan model (9.2) with respect to the bifurcation parameter P_k. By increasing P_k, one can find four qualitatively different dynamical regimes possible; see inlets — filled (empty) dots: stable (unstable) fixed points, red: stable limit cycle. A saddle–node (SN) bifurcation at $P_k \approx -0.3937$ initiates bistability of two stable fixed-points. The stable fixed point emerging from the SN bifurcation undergoes a supercritical Hopf bifurcation (HB) at $P_k \approx -0.3663$, while the saddle point coincides with the other stable fixed point and disappears in another SN bifurcation at $P_k \approx -0.2914$. Up to the SN bifurcation at $P_k \approx 1.3272$ away from the stable limit-cycle. The latter is the unique attractor of the dynamics. The collision of the saddle point with the limit-cycle in a homoclinic bifurcation (HC) at $P_k \approx 1.3648$ terminates the oscillatory regime. BT — Bogdanov–Takens point, CP — cusp point, SNL — saddle–node loop bifurcation, SNIC — saddle–node on invariant cycle bifurcation.

no longer feasible. Hence, external perturbations through mutual interaction have a non-trivial impact: If we assume that all neural masses reside in a stationary state with mean (excitatory) firing rate $E_k^0 > 0$ in the absence of coupling, then as soon as we increase the coupling strength, $\kappa > 0$, all neural masses will experience a sudden perturbation of strength $\kappa \sum_j C_{kj} E_j > 0$ even if they are all identical. Not the small relative distance $x_j := E_j - E_j^0$ to the fixed point, but its absolute value E_j drives the network dynamics. For this reason, we use a direct coupling in form of

$$\frac{\kappa}{N} \sum_{j=1}^{N} C_{kj} E_j \quad \longmapsto \quad \frac{\kappa}{N} \sum_{j=1}^{N} C_{kj} \left(E_j - E_j^0 \right) =: \frac{\kappa}{N} \sum_{j=1}^{N} C_{kj} x_j \,, \tag{9.4}$$

where E_j^0 is the unstable fixed point solution of neural mass (E_j, I_j) in the absence of coupling. In general, $E_j^0 = E_j^0(P_j)$ depends on the heterogeneous input $P_j = P_H + \mu$, where P_H denotes the value of external input at the supercritical Hopf bifurcation, cf. Fig. 9.2. We can thus assume the deviation $E_j - E_j^0(P_H + \mu) =: x_j = x_j(\mu)$ to depend on the distance μ from the Hopf bifurcation. When expanding E_j^0 around P_H, that is, for $E_j^0(P_H + \mu) = E_j^0(P_H) + \mathcal{O}(\mu)$ with $\tilde{E}_j^0 := E_j^0(P_H)$, the coupling term (9.4) reduces to

$$\frac{\kappa}{N} \sum_{j=1}^{N} C_{kj} \left(E_j - \tilde{E}_j^0 \right) + \mathcal{O}(\kappa\mu) \,. \tag{9.5}$$

Consequently, we replace the coupling term in the dynamics (9.2) by

$$\frac{\kappa}{N} \sum_{j=1}^{N} C_{kj} E_j = \frac{\kappa}{N} \sum_{j=1}^{N} C_{kj} \left(x_j + E_j^0 \right) \quad \longmapsto \quad \frac{\kappa}{N} \sum_{j=1}^{N} C_{kj} \tilde{x}_j \tag{9.6}$$

with $\tilde{x}_j = x_j(0) = E_j - \tilde{E}_j^0$. In the following, we will consider the Wilson–Cowan dynamics (9.2) with coupling (9.6) and discard the tildes for conciseness.

9.3. Identifying the Hopf normal form

The choice of model parameters guaranteed oscillatory dynamics of the (uncoupled) Wilson–Cowan neural masses close to a supercritical Hopf bifurcation. At the Hopf bifurcation, stable oscillations emerge around an unstable fixed point and the eigenspectrum of the linearized dynamics shows the specific features of this type of bifurcation: the Jacobian of the (uncoupled) Wilson–Cowan dynamics (9.2) evaluated at the unstable fixed point (E_j^0, I_j^0) has a pair of complex conjugate eigenvalues with negative real part, which corresponds to the distance $\mu = P_j - P_H$ from the Hopf bifurcation point. Changing the parameter P_j leads to a different position (and size and shape) of the limit cycle as well as to a different position of the fixed point, that is, $\left(E_j^0(\mu), I_j^0(\mu)\right) := \left(E_j^0(P_H + \mu), I_j^0(P_H + \mu)\right)$. We express the dynamics in terms of the deviations $x_k(\mu) = E_k - E_k^0 = E_k - E_k^0(\mu)$ and $y_k(\mu) = I_k - I_k^0 = I_k - I_k^0(\mu)$ around the unstable fixed points. Effectively, we shift the fixed point such that the Hopf bifurcation occurs at the origin in phase and parameter space. The transformed

system with coupling (9.6) reads

$$\begin{aligned}\dot{x}_k &= -\left(x_k + E_k^0(\mu)\right) + \mathcal{S}\Big[a_x\Big(c_1\left(x_k + E_k^0(\mu)\right) - c_2\left(y_k + I_k^0(\mu)\right) - \Theta_x + \mu + \frac{\kappa}{N}\sum_{j=1}^{N} C_{kj}x_j\Big)\Big] \\ \dot{y}_k &= -\left(y_k + I_k^0(\mu)\right) + \mathcal{S}\left[a_y\left(c_3\left(x_k + E_k^0(\mu)\right) - c_4\left(y_k + I_k^0(\mu)\right) - \Theta_y\right)\right] ,\end{aligned} \tag{9.7}$$

where we changed the notation of the parameters: $(a_E, a_I, c_{EE}, c_{IE}, c_{EI}, c_{II}, \Theta_E, \Theta_I) \mapsto (a_x, a_y, c_1, c_2, c_3, c_4, \Theta_x, \Theta_y)$. Since $(E_k^0(\mu), I_k^0(\mu))$ solves (9.7), one can simplify the transformed dynamics for weak coupling $0 \leq \kappa \ll 1$ and sufficiently small $\mu \ll 1$ by Taylor expanding the sigmoid function $\mathcal{S}$ around the fixed point:

$$\begin{aligned}\dot{x}_k &= -x_k + \sum_{n=1}^{\infty}\frac{1}{n!}\mathcal{S}^{(n)}\left[\chi_{x,k}\right]\cdot a_x^n\Big(c_1x_k - c_2y_k + \frac{\kappa}{N}\sum_{j=1}^{N}C_{kj}x_j\Big)^n \\ \dot{y}_k &= -y_k + \sum_{n=1}^{\infty}\frac{1}{n!}\mathcal{S}^{(n)}\left[\chi_{y,k}\right]\cdot a_y^n\left(c_3x_k - c_4y_k\right)^n .\end{aligned} \tag{9.8}$$

In (9.8) we abbreviated

$$\begin{aligned}\chi_{x,k} &= \chi_{x,k}(\mu) = a_x\left(c_1E_k^0(\mu) - c_2I_k^0(\mu) - \Theta_x + \mu\right) \\ \chi_{y,k} &= \chi_{y,k}(\mu) = a_y\left(c_3E_k^0(\mu) - c_4I_k^0(\mu) - \Theta_y\right) .\end{aligned}$$

and $\mathcal{S}^{(n)}$ refers to the nth derivative of $\mathcal{S}$. Unfortunately, the sigmoidal shape of the original dynamics (9.2) does not allow for a simplified form of $(E_k^0(\mu), I_k^0(\mu))$ in μ, but one can find numerically a polynomial fit

$$\begin{aligned}E_k^0(\mu) &= E_k^0(0) + \mu\vartheta_E + \mathcal{O}^2(\mu) \\ I_k^0(\mu) &= I_k^0(0) + \mu\vartheta_I + \mathcal{O}^2(\mu) ,\end{aligned}$$

where $\left(E_k^0(0), I_k^0(0)\right)$ denotes the fixed point at the Hopf bifurcation, which corresponds to $(x_k, y_k) = 0$. At this point, the Jacobian of the dynamics (9.2), or (9.7), has purely complex eigenvalues $\pm i\omega_0$. When discarding higher-order terms in μ and κ, we have

$$\begin{aligned}\dot{x}_k &= -x_k + \sum_{n=1}^{\infty}\frac{1}{n!}\left(\mathcal{S}^{(n)}\left[\chi_x\right] + \mu\mathcal{S}^{(n+1)}\left[\chi_x\right]a_x\left(c_1\vartheta_E - c_2\vartheta_I + 1\right)\right)\cdot a_x^n\left(c_1x_k - c_2y_k\right)^n \\ &\quad + \kappa\sum_{m=0}^{\infty}\frac{1}{m!}\mathcal{S}^{(m+1)}\left[\chi_x\right]\cdot a_x^{m+1}\left(c_1x_k - c_2y_k\right)^m\cdot\sum_{j=1}^{N}\frac{C_{kj}}{N}x_j + \mathcal{O}^2(\mu) + \mathcal{O}^2(\kappa) + \mathcal{O}(\kappa\mu) \\ \dot{y}_k &= -y_k + \sum_{n=1}^{\infty}\frac{1}{n!}\left(\mathcal{S}^{(n)}\left[\chi_y\right] + \mu\mathcal{S}^{(n+1)}\left[\chi_y\right]a_y\left(c_3\vartheta_E - c_4\vartheta_I\right)\right)\cdot a_y^n\left(c_3x_k - c_4y_k\right)^n + \mathcal{O}^2(\mu) ,\end{aligned} \tag{9.9}$$

where $\chi_x = \chi_{x,k}(\mu = 0)$ and $\chi_y = \chi_{y,k}(\mu = 0)$.

Considering from now on only weak coupling,[34] we truncate the Taylor expansion in (9.9) at third order. With

$$S_{xn} = \frac{1}{n!}S^{(n)}\left[\chi_{x,k}\right]a_x^n \quad \text{and} \quad S_{yn} = \frac{1}{n!}S^{(n)}\left[\chi_{y,k}\right]a_y^n ,$$

we can rewrite the dynamics (9.9) as

$$\begin{aligned}\dot{x}_k &= f_1(x_k, y_k) + \kappa\, g_k(\boldsymbol{X}) + \mathcal{O}^2(\kappa) , \\ \dot{y}_k &= f_2(x_k, y_k) ,\end{aligned} \tag{9.10}$$

[34] At this point, we would like to add that in the limit of weak coupling, only monomials of the form $x_k^a y_k^b x_j^c$ with $c = 0$ or $c = 1$ appear in the coupling term for the kth neural mass. That is, the coupling effect from another neural mass j is at most linear and of order $\mathcal{O}(x_j)$. Still, the mixed terms $x_k^a y_k^b x_j^c$ may lead to nonlinear coupling effects. One may ask: When do these nonlinear coupling effects invoke non-negligible phase–amplitude interactions? Or, what is the upper boundary for the weak coupling approximation? To the best of our knowledge, as of yet there is no general answer to this question, cf. Section 6.1. Stronger coupling, or strong perturbations, induce amplitude effects. But at which critical value of κ these amplitude modulations fail to admit a unique phase description of the single units, remains an open problem. Strikingly, the critical value is exceeded by far when oscillatory states lose stability and eventually cease to exist. Such a scenario has been coined amplitude death, which has attracted much attention in the literature. Analytic results about such coupling induced effects are limited to very small network sizes of a few coupled oscillators. For larger network sizes amplitude death states elude analytical tractability, but their occurrence in networks of coupled oscillators is reported in numerical studies [213–217].

where for $\boldsymbol{X} = (\boldsymbol{x}_1, \ldots, \boldsymbol{x}_N)$ and $\boldsymbol{x}_k = (x_k, y_k)$ the functions f_1, f_2 and g_k are given as

$$
\begin{aligned}
f_1(x,y) &= -x + S_{x1}(c_1 x - c_2 y) + S_{x2}(c_1^2 x^2 - 2c_1 c_2 xy + c_2^2 y^2) + S_{x3}(c_1 x - c_2 y)^3 \ , \\
f_2(x,y) &= -y + S_{y1}(c_3 x - c_4 y) + S_{y2}(c_3^2 x^2 - 2c_3 c_4 xy + c_4^2 y^2) + S_{y3}(c_3 x - c_4 y)^3 \ , \\
g_k(\boldsymbol{X}) &= S_{x1}\bar{x}_k + 2S_{x2}(c_1 x_k - c_2 y_k)\bar{x}_k + 3S_{x3}(c_1 x_k - c_2 y_k)^2 \bar{x}_k \ .
\end{aligned}
$$

The bar $\bar{\cdot}_k$ denotes the (weighted) average, $\bar{x}_k = \frac{1}{N}\sum_{j=1}^{N} C_{kj} x_j$. In more compact form, we have for weak non-diffusive coupling between two Wilson–Cowan nodes $\boldsymbol{x} = (x, y)$ and $\boldsymbol{x}' = (x', y')$ the dynamics

$$
\dot{\boldsymbol{x}} = \boldsymbol{J}\boldsymbol{x} + \boldsymbol{f}\,(\boldsymbol{x}; \mu) + \kappa\ \boldsymbol{g}\left(\boldsymbol{x}, \boldsymbol{x}'\right) \ , \tag{9.11}
$$

with

$$
\boldsymbol{f}(\boldsymbol{x}; \mu) = \boldsymbol{N}_1 \begin{pmatrix} x^2 \\ xy \\ y^2 \end{pmatrix} + \boldsymbol{N}_2 \begin{pmatrix} x^3 \\ x^2 y \\ xy^2 \\ y^3 \end{pmatrix} \quad \text{and} \quad \boldsymbol{g}(\boldsymbol{x}, \boldsymbol{x}'; \mu) = \left[\boldsymbol{G}_1 + \boldsymbol{G}_2 \begin{pmatrix} x & 0 \\ y & 0 \end{pmatrix} + \boldsymbol{G}_3 \begin{pmatrix} x^2 & 0 \\ xy & 0 \\ y^2 & 0 \end{pmatrix} \right] \begin{pmatrix} x' \\ y' \end{pmatrix} .
$$

In these expressions, we abbreviated the matrices

$$
\begin{aligned}
\boldsymbol{J} &= \begin{pmatrix} -1 + S_{x1}c_1 & -S_{x1}c_2 \\ S_{y1}c_3 & -1 - S_{y1}c_4 \end{pmatrix}, \quad \boldsymbol{N}_1 = \begin{pmatrix} S_{x2}c_1^2 & -2S_{x2}c_1c_2 & S_{x2}c_2^2 \\ S_{y2}c_3^2 & -2S_{y2}c_3c_4 & S_{y2}c_4^2 \end{pmatrix}, \\
\boldsymbol{N}_2 &= \begin{pmatrix} S_{x3}c_1^3 & -3S_{x3}c_1^2c_2 & 3S_{x3}c_1c_2^2 & -S_{x3}c_2^3 \\ S_{y3}c_3^3 & -3S_{y3}c_3^2c_4 & 3S_{y3}c_3c_4^2 & -S_{y3}c_4^3 \end{pmatrix}, \\
\boldsymbol{G}_1 &= S_{x1}\begin{pmatrix} 1 & 0 \\ 0 & 0 \end{pmatrix}, \quad \boldsymbol{G}_2 = 2S_{x2}\begin{pmatrix} c_1 & -c_2 \\ 0 & 0 \end{pmatrix}, \quad \boldsymbol{G}_3 = 3S_{x3}\begin{pmatrix} c_1^2 & -2c_1c_2 & c_2^2 \\ 0 & 0 & 0 \end{pmatrix} .
\end{aligned}
$$

Similar to the Brusselator model, also here the Jacobian $\boldsymbol{J} = \boldsymbol{J}(\mu)$ is not in Jordan real form. Using the eigenvectors associated with eigenvalues $\lambda(\mu) = \varrho(\mu) \pm i\omega(\mu)$ where $\omega(0) = \omega_0$, we can transform $\boldsymbol{J}$ such that

$$
\boldsymbol{L} = \boldsymbol{T}^{-1}\boldsymbol{J}\boldsymbol{T} = \begin{pmatrix} \varrho & -\omega \\ \omega & \varrho \end{pmatrix} . \tag{9.12}
$$

Finally, we can rewrite (9.11) as

$$
\dot{\boldsymbol{x}} = \boldsymbol{L}\boldsymbol{x} + \boldsymbol{T}^{-1}\boldsymbol{f}\,(\boldsymbol{T}\boldsymbol{x}; \mu) + \kappa\,\boldsymbol{T}^{-1}\boldsymbol{g}\left(\boldsymbol{T}\boldsymbol{x}, \boldsymbol{T}\boldsymbol{x}'\right) \ , \tag{9.13}
$$

The dynamics (9.13) exhibits qualitatively the same behavior as (9.11) but due to the Jordan real form of (9.12) the circular symmetry of the limit cycle is now induced on the full dynamics. Eq. (9.13) can be extended to the full network dynamics as in (9.10).

Our pre-processing is mandatory for bringing the Wilson–Cowan dynamics (9.2) into Hopf normal form. Analogously to Section 8.4, we apply *Kuramoto's reductive perturbation approach* and *Poincaré's reduction via nonlinear transforms* to the (truncated) Wilson–Cowan network dynamics (9.11)/(9.13) to obtain the parameter values α, β, γ and δ of the corresponding network Hopf normal form (6.10),

$$
\dot{w}_k = \alpha w_k - \beta |w_k|^2 w_k + \frac{\kappa}{N}\sum_{j=1}^{N} C_{kj}\left[\gamma w_j + \delta \bar{w}_k w_j^2\right] \ .
$$

Next, we can reduce a phase model and infer the network dynamics based on the shape of the resulting phase interaction function H. The so-obtained phase dynamics along either of the two analytic phase reduction techniques will be compared against the numerically reduced phase dynamics as well as against the phase model obtained through Haken's averaging approach, which yields a Kuramoto-like phase model.

9.4. Haken's reduction via averaging

The Wilson–Cowan dynamics allows for a meaningful reduction along Haken's averaging approximation. Given the dynamics (9.13) in Jordan real form, one can capitalize on the (nearly) circular shape of oscillations and insert the ansatz $\boldsymbol{x}_k = (x_k, y_k) = (R_k \cos(\Omega t + \phi_k), R_k \sin(\Omega t + \phi_k))$, a so-called *van der Pol transformation*, where R_k, ϕ_k are amplitude and phase (deviations) of the oscillations at node k, which are slowly varying with respect to the (mean) frequency Ω. We define the central frequency Ω via the eigenvalues at the Hopf point, that is, $\Omega = \omega(0)$. In this way, we obtain an analytic form of the phase dynamics $\dot{\theta}_k = \Omega + \dot{\phi}_k$ without a laborious transformation into Hopf normal form. However, as we step over a careful Hopf normal form reduction, one ought to realize that the resulting phase model is only an approximate description of the actual phase dynamics. Nonetheless, the smaller the amplitude of oscillations, the more accurate the phase model.

Near the onset of oscillations through a supercritical Hopf bifurcation, $R_k \ll 1$ is small and, thus, the right-hand side of (9.13) is at least of order $\mathcal{O}(R_k)$. Given the slower time scales of R_k and ϕ_k, one can average over one cycle $T = 2\pi/\Omega$. In line with [212], this direct averaging of the dynamics (9.13) yields the dynamics of the phase variable $\theta_k = \Omega t + \phi_k$

$$\dot{\theta}_k = \varpi_k + \sum_{j=1}^{N} D_{kj} \sin(\theta_j - \theta_k + \Delta_{kj}) \tag{9.14}$$

with $\varpi_k = \omega_k + \mathcal{O}(R_k)$; we used the following expressions:

$$\begin{aligned}
&D_{kj} = \frac{\kappa}{2N} S_{x1} \Lambda_k C_{kj} \frac{R_j}{R_k} , \qquad \Delta_{kj} = \tan^{-1}(\rho_k) , \\
&\Lambda_k^2 = 1 + \rho_k^2 , \qquad \rho_k = \omega_k^{-1}(S_{x1}c_1 + S_{y1}c_4) , \\
&\omega_k^2 = \det \boldsymbol{J} - (\operatorname{tr} \boldsymbol{J})^2/4 = S_{x1}S_{y1}c_2c_3 - (S_{x1}c_1 + S_{y1}c_4)^2/4 .
\end{aligned}$$

Note that ω_k is the imaginary part of the eigenvalue of $\boldsymbol{J}$. Near the Hopf bifurcation, we can hence safely assume that $\omega_k \approx \Omega$. Note further that since $S_{x1}, S_{y1}, c_1, c_4, \omega_k \geq 0$, we have $\rho_k \geq 0$ and $\Delta_{kj} \in (0, \pi/2)$. Therefore, (9.14) resembles the Kuramoto–Sakaguchi model (5.8) with phase lag $|\Delta_{kj}| \leq \pi/2$, so that we can expect a transition to full synchronization if the coupling strength κ exceeds a critical value $\kappa_c = \kappa_c(\delta)$, where δ denotes the width of distribution of the natural frequency terms ω_k. In case that the setup of a Wilson–Cowan neural mass is fully symmetric, that is, in particular $c_1 = -c_4$, we find for the resulting phase dynamics that $\rho_k \to 0$, and we retrieve the conventional Kuramoto model.

The here-presented averaging of the Wilson–Cowan network dynamics yields the phase dynamics (9.14), whose phase interaction function only consists of first harmonics. The absence of higher harmonics hampers complex network dynamics such as, e.g., clustering effects. This is in remarkable contrast to the other phase models that have been derived from dynamics in Hopf normal form. The main reason is that the Hopf normal form reduction induces circular symmetry also on the coupling function g_x and the corresponding transformation leads to resonant monomials of first and third order.[35] On the other hand, the direct averaging approach does not employ transformations aimed at establishing resonant monomials. In fact, the coupling of the dynamics (9.13) remains linear in $\boldsymbol{x}'$ and all nonlinear coupling terms eventually average out at zero. Irrespective of this, however, the direct averaging along Haken's method stands out for its simplicity and its potential to be applied in a straightforward way.

9.5. Analytic and numerical phase reductions

The ultimate goal of any of the phase reduction techniques introduced above is to simplify the network dynamics of coupled oscillators, here, of (weakly) coupled Wilson–Cowan neural masses, in terms of a corresponding phase model (5.6),

$$\dot{\theta}_k = \omega + \frac{\kappa}{N} \sum_{j=1}^{N} C_{kj} H\left(\theta_k - \theta_j\right) .$$

For simplicity, we consider all nodes to be identical, in particular, they have the same natural frequency $\omega_k = \omega$, and that they are globally, or all-to-all, coupled with adjacency values $C_{kj} = 1$ for all $j \neq k$. The factor $1/N$ is for convenience and ensures that the phase model is well-behaved in the limit $N \to \infty$. The phase interaction function $H(\psi)$ admits a representation as a Fourier series (5.7),

$$H(\psi) = \sum_{n \geq 0} a_n \cos(n\psi) + b_n \sin(n\psi) = a_0 + a_1 \cos(\psi) + b_1 \sin(\psi) + a_2 \cos(2\psi) + b_2 \sin(2\psi) + \cdots .$$

In the following, we will highlight that phase reduction can, in general, be highly parameter-sensitive. Close to particular bifurcation curves in parameter space, the obtained phase model coincides with analytic predictions about the associated normal form. With growing distance to the bifurcation boundaries, however, higher harmonics in the reduced phase model emerge that give rise to non-trivial and complex collective behavior. Subsequently, we will compare the results of the analytic phase reduction techniques (*Kuramoto's reductive perturbation*, *Poincaré's reduction via nonlinear transforms* and *Haken's averaging* – the latter here denoted as *direct averaging*) with those of numerical phase reduction techniques (here we complement the findings of the *adjoint method* using XPPAUT with those of the *direct method*; as both reduction techniques show consistent results, we will refer to them interchangeably as the *numerical/adjoint method*). We will consider the dynamics close to the Hopf bifurcation, i.e. for small $\mu \ll 1$. After that, we will treat the case of larger distances, i.e. further away from the Hopf point. To anticipate, analytically derived phase dynamics will diverge from the numerically established ones and one may wonder which technique reveals the true collective behavior of the oscillatory network.

[35] Recall that the third order monomial most significant for the coupling term in the phase dynamics is nonlinear in the respective other oscillator $\boldsymbol{x}'$.

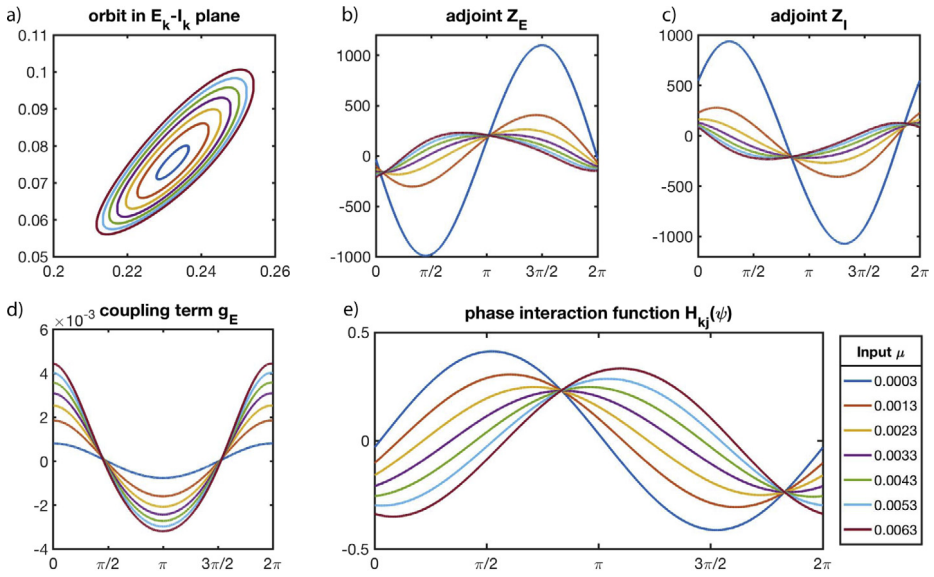

Fig. 9.3. Computing the phase interaction function: (a) Trajectory of the Wilson–Cowan dynamics in phase space, (b,c) numerically determined phase sensitivity function $\boldsymbol{Z} = (Z_E, Z_I)$ as solutions to the adjoint problem, (d) coupling term evaluated at the limit cycle, and (e) phase interaction function H for different input value parameters $P_k \in (-0.366, -0.36)$ corresponding to values $\mu \in (0.0003, 0.0063)$. As shown in (a), the limit cycle solution of the underlying (and uncoupled) Wilson–Cowan model changes its shape. Its amplitude grows monotonically. The shape of the phase sensitivity function deviates from the initial shape, and higher harmonics seem to occur; see panels (b) and (c) – we refer to the two components of the phase sensitivity function as adjoints, underlying the here-applied numerical reduction technique. The phase interaction function depends on both the phase sensitivity function and the coupling term and absorbs their variation (e). At a particular parameter value P_k, the derivative of H at the origin, $H'(0)$, changes signs. While a network of identical and globally coupled units will fully synchronize if $H'(0) > 0$, this state loses stability if $H'(0)$ becomes negative. Hence, a small parameter change at about $P_k = -0.364$ will cause qualitatively different network behavior — when using XPPAUT, the change from $H'(0) > 0$ to $H'(0) < 0$ already appears at $P_k = -0.3658$ and not at $P_k = -0.364$, which we derived using the adjoint solver implemented in Matlab.

9.5.1. Parameter-sensitivity of phase reduction

Synchronization transition. Close to a bifurcation boundary in parameter space, one can capitalize on center manifold and normal form theory to distill characteristic features of the underlying dynamics, which allows for a qualitative description of the observed behavior [64]. As demonstrated in Section 4.4, for dynamics close to a (supercritical) Hopf bifurcation, the phase sensitivity function $\boldsymbol{Z}$ has the characteristic purely sinusoidal form $-\sin(\theta)$. Moreover, the coupling function $\boldsymbol{g}(\boldsymbol{x}, \boldsymbol{x}')$ when evaluated at the respective limit cycles $\boldsymbol{x}^c, \boldsymbol{x}'^c$ that are (in a leading order approximation) circular near the Hopf bifurcation, takes on a form proportional to $1 + \cos(\theta)$. The resulting phase interaction function H of the corresponding phase model thus becomes

$$H(\psi) \propto \frac{1}{2\pi} \int_0^{2\pi} -\sin(\theta) \cdot \big[1 + \cos(\theta + \psi)\big] d\theta = \tfrac{1}{2} \sin(\psi) \,.$$

Consequently, the slope of H at $\psi = 0$ is positive ($H'(0) = 1/2$) so that coupled (identical) oscillators that are all very close to a Hopf bifurcation, are expected to perfectly synchronize with each other.

This result holds in theory exactly at the Hopf bifurcation, $\mu = 0$, and in practice also in the immediate vicinity of the Hopf bifurcation. An obvious question is how far this 'immediate vicinity' can be stretched. Slightly increasing the distance $\mu > 0$ from the Hopf bifurcation point, will change the shape of the limit cycle and thus also lead to different properties of the corresponding phase dynamics. In Fig. 9.3 we illustrate how such a parameter change affects the Wilson–Cowan dynamics and the reduced phase model. The slope of the phase interaction function H switches from positive to negative at a parameter value as small as $0 < \mu < 0.01$, and the network state will transition from synchronization to incoherence. Hence, we can conclude that phase reduction is highly parameter-sensitive.

Emergence of higher harmonics. Already for small parameter changes, higher harmonics occur in the phase sensitivity function $\boldsymbol{Z}$ and/or in the coupling term. Higher harmonics will eventually find their way also in the phase interaction function H and may thus affect the (predictions about the) collective behavior of the network. The occurrence of higher harmonics is not restricted to the example of a Hopf bifurcation, but may be found across any kind of bifurcation. In fact, this phenomenon is not a peculiar feature of the Wilson–Cowan neural mass model, but appears generic across neural oscillator models, see, e.g., Figure 4 in [64]. There, Brown and co-workers already reported changing phase sensitivity functions $\boldsymbol{Z}$, but did not explicitly point to a specific parameter-sensitivity.

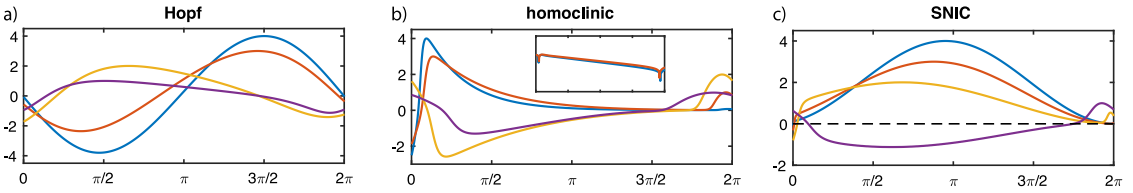

Fig. 9.4. Phase sensitivity functions (numerically computed via the adjoint method) quickly diverge from the analytically predicted shape, which are sinusoidal (Hopf), exponential (homoclinic) and cosinusoidal/non-negative (SNIC), and exhibit non-negligible higher harmonics. Phase sensitivity function are normalized in amplitude. Colors represent the distance to the respective bifurcation points in parameter space: $\mu = 1/10000$ (blue), $\mu = 1/1000$ (red), $\mu = 1/100$ (yellow), $\mu = 1/10$ (violet). Insets for the homoclinic bifurcations show the first two graphs in log-scale and display exponential decay. The model parameters can be found in Appendix B.2.

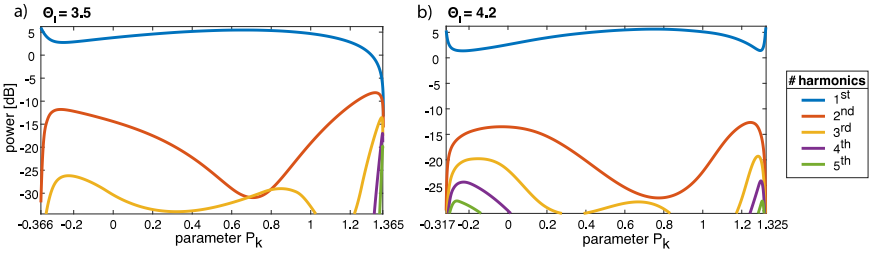

Fig. 9.5. Higher harmonics in the phase sensitivity function of the Wilson–Cowan neural mass model for varying input P_k. (a) Input P_k such that oscillations emerge through a supercritical Hopf bifurcation and cease through a homoclinic bifurcation. (b) Oscillations both emerge and cease through a SNIC bifurcation; cf. Fig. 9.2.

Extending the analysis in Fig. 9.3, we numerically determined the adjoint solution for the phase sensitivity function $\boldsymbol{Z}$ of the Wilson–Cowan dynamics and investigated how its shape changed when further increasing the input parameter P_k from the three generic types of bifurcation: the Hopf, homoclinic and SNIC bifurcations appear for different parameter values in the Wilson–Cowan model, cf. Fig. 9.2. Increasing the distance from the respective bifurcation points in parameter space from $\mu = 1/10000$ to $\mu = 1/10$, Fig. 9.4 illustrates how quickly the shape of the phase sensitivity function changes and higher harmonics occur.

We also analyzed the reduced phase sensitivity functions $\boldsymbol{Z}$ in Fourier space to account for the occurrence of higher harmonics. To do so, we varied the input parameter P_k between two bifurcation boundaries where the Wilson–Cowan dynamics exhibit stable limit-cycle oscillations, see Fig. 9.2. Fig. 9.5 (panel a) shows the power of the first five harmonics for parameter values where oscillations emerge via a Hopf and cease through a homoclinic bifurcation. Although the first harmonics is the dominant one for all parameter values P_k, the analysis remains quite insightful. Directly on the Hopf bifurcation at $P_k \approx -0.3663$, the first harmonics is not only dominant, but also exclusive: the amplitudes of the second and higher harmonics converge to zero faster than exponentially. This is perfectly in line with the analytically predicted purely sinusoidal shape of the phase sensitivity function $\boldsymbol{Z}$. On the other side, the nature of the homoclinic bifurcation becomes also apparent. All harmonics tend to a non-vanishing constant amplitude, giving rise to the exponential character of the bifurcation, cf. [64] for more theoretical arguments. Between these oscillation boundaries, higher harmonics have a non-negligible effect on the phase sensitivity function $\boldsymbol{Z}$ and must not be discarded. This becomes even more striking when investigating the phase sensitivity function $\boldsymbol{Z}$ near SNIC bifurcations, Fig. 9.5 (panel b). While higher harmonics vanish directly on the bifurcation points and thereby allow the phase sensitivity function $\boldsymbol{Z}$ to take the known (co-)sinusoidal shape $1 - \cos(\theta)$, off these bifurcation points but in their immediate vicinity the amplitudes of the higher harmonics contribute to the shape beyond mere higher-order corrections. Consequently, a careful investigation of particular parameter regions and the corresponding dynamical regimes as well as their respective bifurcation boundaries is indispensable for a meaningful phase reduction. Emerging higher harmonics in the phase sensitivity function $\boldsymbol{Z}$ away from bifurcation boundaries and nonlinear coupling terms will mutually interact and catalyze, thus generate rich and highly non-trivial network effects.

9.5.2. Near the Hopf point

In order to compare the different phase reduction techniques, we here consider the input parameter in close vicinity of the Hopf bifurcation point. The resulting Fourier coefficients of the reduced phase interaction function H are summarized in Table 9.1 for an exemplary small parameter value. For typical parameter choices very near the Hopf bifurcation, all the four phase reduction techniques properly recover the natural frequencies as well as the dominant first harmonics with a strong positive sinusoidal component. Both analytic and numerical reduction techniques reveal that the amplitudes of the second harmonics are smaller by three orders of magnitude than the first harmonics. Therefore, the different phase

Table 9.1
Phase models derived with different reduction techniques in very close to the Hopf bifurcation ($\mu = 0.0013$). The oscillators' natural frequency is ω, and a_n, b_n are the amplitudes of the Fourier components of the phase interaction function H. Symbols $+/-$ denote the sign of each amplitude. Their quantity corresponds to their influence on the dynamics, with $+++$ representing dominant contributions of order 1, while $0^{+/-}$ corresponds to amplitudes $\leq 10^{-3}$. Exact numerical values can be found in Appendix B.2.

Approach	ω	a_1	b_1	a_2	b_2
Reductive perturbation	0.701	$---$	$+++$	0^-	0^+
Nonlinear transform	0.701	$---$	$+++$	0^-	0^+
Direct averaging	0.701	$---$	$++$	0	0
Numerical/adjoint	0.701	$--$	$+++$	0^-	0^+

Table 9.2
Phase models derived with different reduction techniques away from the Hopf bifurcation, $\mu = 0.1663$. The notation is the same as in Table 9.1, and exact values can be found in Appendix B.2.

Approach	ω	a_1	b_1	a_2	b_2
Reductive perturbation	0.73	$---$	$+++$	$--$	$++$
Nonlinear transform	1.02	$--$	$++$	$-$	$+$
Direct averaging	1.33	$--$	$++$	0	0
Numerical/adjoint	0.94	$--$	$--$	$-$	$-$

models are qualitatively identical close to the Hopf bifurcation. The closer we choose the input parameter near the Hopf point, the more "accurate" becomes the numerical method: the phase interaction function H resembles a pure sine curve, cf. Fig. 9.3 (panel e). However, the analytic methods, *Kuramoto's reductive perturbation* and *Poincaré's nonlinear transform approach*, which build upon a normal form reduction, retain a dominant cosine component. To conclude, the different phase reduction techniques lead to consistent results close to the Hopf bifurcation boundary in that the resulting phase models are qualitatively identical[36] (although quantitative differences occur, cf. Appendix B.2 for numerical values).

9.5.3. Away from the Hopf point

The qualitative agreement close to the Hopf point no longer holds when the individual oscillatory dynamics are further away. For larger distances, $\mu \gg 0$, the different reduction techniques start to diverge from each other and quantitative differences have a qualitative impact as shown in Table 9.2. Remarkably, only the *numerical/adjoint method* captures the change of slope of the phase interaction function H, whose derivative at $\psi = 0$ is dominated by b_1 as has been illustrated in Fig. 9.3. *Poincaré's reduction via nonlinear transforms* does not yield the correct sign of b_1, but the amplitudes of the first and second harmonics, at least in terms of orders of magnitude, coincide with the *numerical/adjoint method*. While *Kuramoto's reductive perturbation* overestimates the second harmonics, by construction *Haken's averaging* does not contain any higher harmonics; we refer to Appendix B.2 for exact numerical values. Strong first harmonics of the phase interaction function H amplify the coupling and thus result in faster (de-)synchronization, depending on the sign of the sinusoidal component. Second and higher harmonics may play a crucial role for clustering. An over- or underestimation of the amplitudes of higher harmonics may hence lead to erroneous multiple- or one-cluster effects, respectively.

9.6. Numerical methods

The farther one moves away from particular bifurcation boundaries, the more the reduced phase models may diverge. Naturally, one seeks a phase reduction technique that reliably recovers the (collective) behavior of the original (network) dynamics. Recall that the accuracy of analytic phase reduction techniques scales with the distance to the bifurcation point due to the normal form reduction inherent to these two-step reduction approaches. By contrast, numerical phase reduction techniques may not suffer this shortcoming and retain the accuracy across parameter space. For this reason, numerical phase reduction appears a promising candidate to capture the dynamics of the underlying high-dimensional oscillator networks. In the following, we will demonstrate that this is indeed the case.

Following the literature on the agreement between network dynamics and their reduced phase dynamics, we use a network of identical Wilson–Cowan neural masses with parameters given by Hoppensteadt and Izhikevich [46] or by Hlinka and Coombes [168]; see Appendix B.2 for the values. Moreover, we set $\Theta_E + P_k \mapsto P_k$ and $\Theta_I \mapsto Q_k$ and consider the inputs P_k and Q_k to the excitatory and inhibitory parts of neural mass k as bifurcation parameters. As illustrated in Fig. 9.6, the colored regions represent parameter values (P_k, Q_k) at which the Wilson–Cowan model exhibits self-sustained stable limit-cycle oscillations. This region falls into the analytically determined Hopf bifurcation boundaries, see, e.g., [46],

[36] The Hopf normal forms obtained with the normal form reductions may be further transformed into the *topological* Hopf normal form, leading to a purely sinusoidal phase interaction function H. The corresponding transformation, however, requires a rescaling of time, after which a direct comparison with the other reduction methods appears more difficult. For this reason, we stick to the *Poincaré Hopf normal form* along the analytic phase reduction techniques throughout this report. We refer to [Theorem 3.4, 82] for more details on the transformation into the *topological Hopf normal form* $w' = (\tilde{\alpha} + i)w + l_1(\tilde{\alpha})|w|^2 w + \mathcal{O}^4(|w|)$ with $w \in \mathbb{C}$ and $l_1(\tilde{\alpha}) \in \mathbb{R}$ denotes the *first Lyapunov coefficient*.

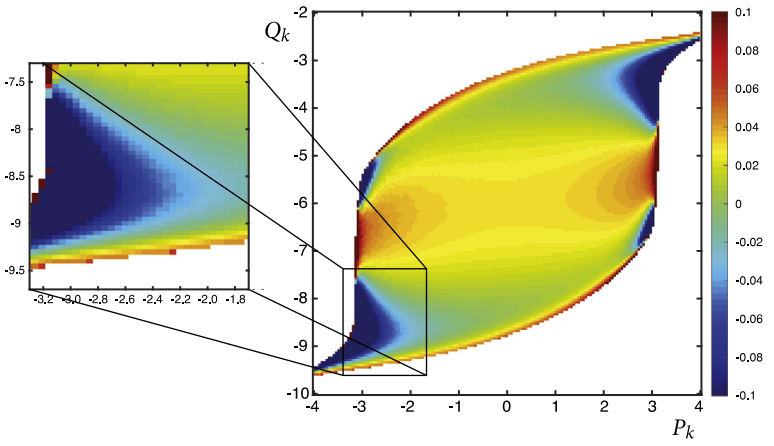

Fig. 9.6. Oscillatory regime of the Wilson–Cowan neural mass model using the same parameters as in [168]. The color coding indicates the derivative of the phase interaction function H at $\psi = 0$ determining the stability of the fully synchronized solution: if $H'(0) > 0$ the fully synchronized solution is stable, and unstable otherwise. In view of the results in Section 9.5, we used the numerical/adjoint reduction method to generate this figure.

for a more detailed bifurcation analysis. Hlinka and Coombes investigated this Wilson–Cowan network model with respect to its functional connectivity. They showed that the predictions based on the derivative of the numerically reduced phase interaction function H agreed almost perfectly with the synchronization properties of the original network, cf. their Figures 6 and 7. However, they reported small parameter regions, see, e.g., the inset in Fig. 9.6, in which their predictions did not match the actual dynamics [168]. We confirm their analysis and extend their findings in one of these parameter regions by exploiting the reduced phase model in more detail. As we will show, our extended insights using numerical phase reduction allow for predicting the collective behavior beyond the incoherence–synchronization transition and even cluster states can be detected reliably.[37]

To show that higher harmonics of the phase interaction function H capture collective behavior when the fully synchronized solution is no longer stable, we zoomed in into the corresponding parameter region; see the inset in Fig. 9.6. The Hopf bifurcation occurs at the lower boundary between oscillatory (colored) and stationary behavior (white region). Positive values of $H'(0)$ predict synchronized oscillations, irrespective of the other (even) Fourier components. Moving upwards in parameter space by increasing the parameter Q_k, leads to a change of signs, $H'(0)$ becomes negative and the fully synchronized state is no longer stable.

Considering only first and second harmonics in the phase model with positive coupling strength, the possible network states can be divided into three dynamical regimes: (i) the fully synchronized solution (one-cluster state) is stable if $b_1 > 0$ and $b_1 \gg |b_2|$, (ii) the incoherent solution (anti-cluster state) is stable if $b_1 < 0$ and $b_2 < 0$ with $|b_1| \gg |b_2|$, and (iii) the (balanced) two-cluster state is stable if $b_1 < 0$ and $b_2 > 0$; see Section 5.3.3 and [177]. Analyzing the numerically reduced phase interaction function H with respect to higher harmonics, we find that all of the three possible states above can be realized. When fixing the parameter $P_k = -3$, we find at $Q_k = -9.3$ that $b_1 > 0$ (stable one-cluster state), at $Q_k = -8.9$ that $b_1 < 0$ and $b_2 < 0$ (stable anti-cluster state), and at $Q_k = -8.7$ that $b_1 < 0$ and $b_2 > 0$ (stable two-cluster state); for the exact numerical values we refer to Appendix B.2. To test these predictions for the different parameter values, we used the *direct method* and simulated a network of $N = 30$ Wilson–Cowan neural masses with global coupling strength $\kappa = 0.15$. The simulations displayed the predicted fully synchronized solution, an anti-cluster state, i.e. incoherence, and a stable two-cluster state, respectively; see Fig. 9.7. Interestingly, the other phase reduction techniques did not only fail to predict the existence of two-cluster states, but they also missed the change of stability of the fully synchronized solution; cf. Table 9.2.

9.7. Remarks

Phase reduction is a powerful tool to analyze the collective behavior of bio-physiologically realistic network models such as coupled Wilson–Cowan neural masses. Reduced phase models can properly predict the transition from incoherence to synchronization of oscillatory networks, and even complex collective behavior such as two-cluster states can

[37] As mentioned above and according to the reduced phase model, the network will synchronize close to the Hopf bifurcation boundaries as anticipated from the topological Hopf normal form. In general, global synchronization of coupled (identical) oscillators can be expected if the slope of the phase interaction function H at the origin is positive, that is, if $H'(0) > 0$. Hlinka and Coombes [168] also assessed the synchronization properties of the original Wilson–Cowan model in terms of mean phase coherence and correlation and found a good agreement with the predictions based on $H'(0)$, see Fig. 9.6.

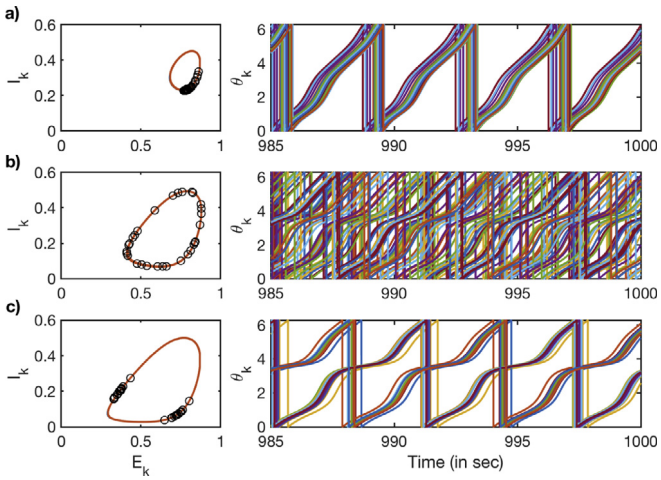

Fig. 9.7. Non-trivial network dynamics of $N = 30$ coupled Wilson–Cowan neural masses. The different network states (a) global synchronization, (b) incoherence, and (c) a balanced two-cluster state were predicted by the reduced phase model using the numerical/adjoint method. Shown are final ($T_{\text{end}} = 1000$ s) conditions ('o') on the uncoupled limit cycle (left column) and the extracted phases (right) for the last 15 seconds. We fixed the coupling strength at $\kappa = 0.15$ and the simulations started from uniformly distributed initial conditions along the uncoupled limit cycle. Parameter values of (P_k, Q_k) are (a) $(-3, -9.3)$, (b) $(-3, -8.9)$ and (c) $(-3, -8.7)$.

be inferred. However, phase reduction is highly parameter-sensitive and a careful analysis with respect to underlying dynamical regimes and bifurcation boundaries ought to precede the derivation of a phase model.

Close to bifurcation boundaries of the supercritical Hopf bifurcation, all the different phase reduction techniques yield consistent results. There are, however, striking differences between the reduced phase models already at reasonably small distances $\mu \ll 1$ from the Hopf bifurcation point. One may wonder which reduced phase models indeed describe the phase dynamics of oscillator networks and capture the actual collective behavior. Analytic phase reduction techniques have shortcomings unless parameters are considered in direct vicinity of the Hopf bifurcation. Possible inaccuracies can be traced back to the inherent normal form reduction in these two-step phase reduction methods. Moreover, analytic reduction techniques may lead to different results although all normal form reductions have the same background, cf. Section 4.1. While *Poincaré's reduction via nonlinear transforms* accounts for the full dependence on the bifurcation parameter μ, *Kuramoto's reductive perturbation* neglects this accuracy by approximating nonlinear terms with the corresponding expressions evaluated at $\mu = 0$ in the subsequent reduction steps, leading to possibly different results. Numerical reduction techniques, by contrast, bear the potential to accurately describe the respective phase dynamics, and predictions about the actual network dynamics can readily be drawn from the reduced phase model. We highlighted the potential of phase reduction with extensive simulations of the Wilson–Cowan network.

10. Discussion

The reduction of a network of interacting oscillatory systems into a network of coupled phase oscillators facilitates the analysis of the collective, macroscopic network dynamics. Complex oscillatory networks typically stand out for high-dimensional, nonlinear dynamics on both the network and the nodal level. As explained, by looking at the phase dynamics one drastically reduces this dimensionality while keeping the option to infer (the stability of) network states and to predict collective behavior. Usefulness and strength of a model (here, the reduced phase model) may be judged by its predictive power. Quantifying this can be a challenge. Models are built on assumptions, which restrict their applicability and range of use. Beyond this range, however, a model can lose its validity and the actual dynamics can significantly diverge from model predictions.

All the listed phase reduction techniques to derive a phase model dwell on assumptions. First, they require a certain degree of homogeneity among the dynamics of the network's nodes. Moreover, we assumed a static pairwise coupling structure and thereby ignored that the form, structure and dynamics of the coupling between nodes may also, and decisively, influence the collective behavior. Then, we considered phase reductions only for deterministic, autonomous systems without delay. In principle, reduction techniques can be generalized to cope with delay, noise and time-varying input, at least to some extent. Last but not least, most, if not all, of the phase reduction techniques rely on the theory of weakly coupled oscillators [46]: Every node of the original network has to exhibit stable limit cycle oscillations in the absence of coupling to other nodes, and the coupling strength has to be sufficiently weak so that amplitude effects can largely be neglected. That is, the dynamics of each node remains close to the respective unperturbed limit cycle solution while (and despite of) interacting with other nodes. More recently, several phase reduction techniques have been refined and extended so that the assumptions inherent to the theory of weakly coupled oscillators might be loosened, at least to certain degree.

10.1. Beyond nearly identical oscillators

We assumed that the coupled nonlinear oscillators are (nearly) identical. By this, differences in the individual, uncoupled dynamics $\dot{\boldsymbol{x}}_k = \boldsymbol{f}_k(\boldsymbol{x}_k)$ could be subsumed under the coupling terms so that the function $\boldsymbol{f}_k = \boldsymbol{f}$ coincided for all oscillators, $k = 1, \ldots, N$. This simplification enabled us to predict the collective behavior solely by evaluating the phase interaction function H. Admittedly, the assumption of identical nodes is often inaccurate. This is particularly true when modeling realistic networks of biophysiological, chemical, or neuronal oscillators. Understanding, however, the potential as well as limitations of phase reductions for networks of identical oscillators, is essential for tackling an even more complex setup of physically meaningful heterogeneous networks.

The theory on phase reductions generally holds for heterogeneous oscillators as long as their frequencies are either ϵ-close or pairwise commensurable [46,167]. Yet, practical application becomes more cumbersome because the phase dynamics have to be retrieved for each oscillator individually. There are approaches to assess (the stability of) synchronized network or cluster states of heterogeneous oscillators, e.g., along an extended master stability function formalism for nearly identical systems [218–220]. There, the degree of heterogeneity has to be small so that predictions about the collective behavior are possible. When heterogeneity of a network only affects the natural frequencies and leaves the phase interaction functions identical, the resulting phase oscillator network can be treated in terms of heterogeneous Kuramoto-like oscillators. A major advantage of this kind of coupled phase oscillator models is that they typically give rise to only a few macroscopic variables, which in addition often allow for an intuitive interpretation [221], as does, e.g., the Kuramoto order parameter. The Watanabe–Strogatz [222] and Ott–Antonsen theories [170,223] are paramount examples how macroscopic variables may serve to describe the network behavior [224], see also [225] for a recent review.

10.2. Beyond pairwise coupling

The coupling dynamics of interacting nonlinear oscillators is a research theme in itself, and we do not dare to even intend to treat this subject thoroughly. Already the interaction between two units, let alone multivariate coupling schemes, can take too many forms, is too diverse and may feature too distinct dynamics, so that most of the times realistic coupling scenarios are approximated by simpler terms to render a network analysis feasible. In our case, we have heavily dwelled on a static pairwise coupling structure. This facilitates the derivation of the phase model insofar as it is sufficient to consider the phase dynamics of only two coupled oscillators.

10.2.1. Coupling functions

When confronted with interacting systems, it is important to identify the type of coupling between them, especially given the role of coupling dynamics in shaping non-trivial network behavior. As we briefly noted in our Brusselator example, Section 8, for systems with dynamics $\dot{x} = f(x) + g(x, y)$ the character of the coupling can be *direct*, $g(x, y) = g(y)$, *diffusive*, $g(x, y) = g(y - x)$, *reactive*, $g(x, y) = (\epsilon + i\beta)g(x - y)$, *conjugate*, $g(x, y) = g(x - Py)$, as a *chemical synapse*, $g(x, y) = g(x)S(y)$ with $S(\cdot)$ of sigmoidal shape, or *environmental*, $g(x, y) = \epsilon \int_0^t \mathrm{e}^{-\kappa(t-s)}(x(s) + y(s))ds$; see the recent review [226] and the references therein. One may further distinguish between *linear* and *nonlinear* coupling, depending on the order of $g(x, y)$. While the original dynamics of interacting systems exhibit one or more coupling functions of the types above, their counterpart in the corresponding and reduced phase model often boils down to either a diffusive phase coupling term $\tilde{g}(\theta_x, \theta_y) = \tilde{g}(\theta_x - \theta_y)$ or to a pulse–response coupling of the form $\tilde{g}(\theta_x, \theta_y) = P(\theta_y)R(\theta_x)$. These two phase coupling functions can be ascribed to physically distinct mechanisms. The first one is also referred to as electrotonic or gap junction coupling, which is based on voltage differences between cells in electrical contact. The latter relates to impulse coupling, or in a rather neuroscientific context, to spike-triggered synaptic transmission via the release of neurotransmitters across a synaptic cleft. How coupling terms of the original dynamics translate into the particular phase coupling functions, depends both on the characteristics of the underlying dynamical system as well as on the strength of interaction. The pulse–response coupling, as established by Winfree in his original work [73], appears to be the more general form of phase interactions where the coupling term is the product of the external perturbation $P(\theta_y)$ through the other oscillator with the response $R(\theta_x)$ of the perturbed oscillator, the latter commonly referred to as the phase response function. Averaging procedures, however, can be applied if the perturbations and/or coupling strength are sufficiently weak, in which case a diffusive phase coupling term can be recovered again. There are other exceptions where an averaging procedure is possible when, e.g., multiple strong pulses are dispersed around the cycle, cf. [55].

10.2.2. Dynamic coupling

We are fully aware that models of interconnected nonlinear oscillators often feature rather complex coupling terms with individual dynamics. This is particularly true for neural oscillators [54,57,227]. Keyword here is *event driven* coupling. For instance, let two neurons be connected via a chemical synapse. When the presynaptic neuron elicits a spike, an action potential travels along the axon and provokes the release of neurotransmitters at the synapse. This in turn leads to a temporary change of the membrane potential of the postsynaptic neuron with characteristic finite rise and fall times. Taken together, event driven coupling can be defined as the time-resolved interaction between nodes (e.g., neurons) that is triggered through a particular event (e.g., the spiking of the presynaptic neuron). This transient dynamical process can be described mathematically with a linear differential operator that has a given response (or Green's function).

When allowing for this kind of complex coupling, the corresponding network model becomes more detailed and high-dimensional. Still, the theory outlined in Sections 3, 4, 6 and 7 also applies in this case and a proper phase model may be reduced. The coupling functions in the reduced phase model, however, are now time-dependent and may become arbitrarily difficult. Sometimes, these reduced coupling functions can be approximated and continue to provide an accurate model of the underlying system, see, e.g., [228]. We discourage, however, from ad hoc approximations without a sensitive assessment of both the full dynamics and the reduced, or simplified, phase dynamics. In Section 9, we first analyzed the parameter range in which the nonlinear, sigmoidal coupling function in the Wilson–Cowan neural mass model can be adequately approximated by polynomial terms, and we employed the analytic reduction techniques for these parameters.

10.3. Beyond deterministic, autonomous and non-delayed dynamics

We ignored that the self-sustained limit cycle dynamics may also be subject to noisy and time-dependent perturbations, or to time-delayed coupling with other oscillators. How will such inputs affect the oscillators dynamics, their phase description and eventually the network behavior?

10.3.1. Stochastic and time-varying systems

Exemplarily, we reconsider the Wilson–Cowan neural mass model (9.2) with population-specific input P_k that combines both a stochastic term and a deterministic time-varying term,

$$P_k = \xi_k(t) + P_0\big[1 + A_k \sin(\omega_{p,k} t + \phi_{0,k})\big] \,. \tag{10.1}$$

The deterministic term oscillates sinusoidally with amplitude A_k, frequency $\omega_{p,k}$ and phase shift $\phi_{0,k}$. $\xi_k(t)$ is an arbitrary noise term. When restricting it to white Gaussian noise, the noise characteristics are given by $\langle \xi_k(t) \rangle = 0$ and $\langle \xi_k(t)\xi_l(s) \rangle = 2D^2\delta_{kl}\delta(t-s)$, where $\langle \cdot \rangle$ denotes averaging over the realizations of ξ_k, and $D \geq 0$ scales the noise intensity. Both noise and time-variability can lead to more complex dynamics and may complicate the phase reduction to great extent.

Periodic forcing without noise, i.e. $A_k > 0$ and $D = 0$, may already lead to quasi-periodic oscillations of the single neural masses. Quasi-periodic oscillations can also be caused by the time-delay structure, see Section 10.3.2, or by unidirectional coupling [229]. Phase reduction techniques for weakly connected quasi-periodic Wilson–Cowan oscillators have been proposed by Izhikevich [230], and further extended by Demirt and co-workers [231]. The application to networks of weakly coupled Wilson–Cowan neural masses where time-periodic input is inducing quasi-periodic oscillations at the single node level, however, is still missing and requires further investigation. Likewise, non-autonomous input functions may generate chaotic oscillations. While a phase can be defined for chaotic oscillators [232], to the best of our knowledge, no phase reduction approach has been attempted for weakly coupled chaotic oscillators.

Recently, several studies have extended the deterministic Wilson–Cowan model by a noisy component [233–238]. The origin of an additional noise term can be motivated in various ways: intrinsic fluctuations in neural activity, microscopic randomness in neural connectivity, or stochastic perturbations due to finite-size effects; see [239,240] and the references therein. There is still an ongoing discussion about stochastic descriptions of meso-scale neural populations, see, e.g., the recently proposed model by Schwalger and co-workers [241]. We here aim at revising briefly how one can rigorously describe a network model of stochastic Wilson–Cowan neural masses in terms of their phase dynamics. We consider noisy external input $P_k(t) = P_{0,k} + \varepsilon\xi_k(t)$ to the external part of the kth Wilson–Cowan population and omit further state-dependencies, i.e. the dynamics of interest read

$$\dot{E}_k = -E_k + S\left[a_E\left(c_{EE}E_k - c_{IE}I_k - \Theta_E + P_{0,k} + \frac{\kappa}{N}\sum_{l=1}^{N} C_{kl}E_l\right) + \varepsilon\xi_k(t)\right] \tag{10.2a}$$

$$\dot{I}_k = -I_k + S\left[a_I\left(c_{EI}E_k - c_{II}I_k - \Theta_I\right)\right] \,. \tag{10.2b}$$

We assume that the noise is weak, i.e. $\varepsilon \ll 1$ is sufficiently small, and, as before, we consider the parameter regime exhibiting self-sustained oscillations when $\kappa = 0 = \varepsilon$. Limit cycle oscillations will be perturbed both by noise and by the other weakly coupled Wilson–Cowan populations in the same manner. The effects of noisy perturbations crucially depend on the phase sensitivity function $\boldsymbol{Z}$ of the Wilson–Cowan neural mass, and a reduced dynamics is favorable. Therefore, it appears legitimate to linearize around the noise term such that we arrive at the dynamics (10.2)a) of the excitatory part now given by

$$\begin{aligned}
\dot{E}_k &= -E_k + S\left[a_E\left(c_{EE}E_k - c_{IE}I_k - \Theta_E + P_{0,k} + \frac{\kappa}{N}\sum_{l=1}^{N} C_{kl}E_l(t)\right)\right] + \varepsilon\sigma_k\xi_k(t) + \mathcal{O}(\kappa\varepsilon, \varepsilon^2) \,, \\
\sigma_k &= \sigma_k(E_k, I_k) = S\left[a_E\left(c_{EE}E_k - c_{IE}I_k - \Theta_E + P_{0,k}\right)\right] + \mathcal{O}(\kappa) \,.
\end{aligned} \tag{10.3}$$

Note that the multiplicative character of the noise becomes evident as $\xi_k(t)$ appears in the sigmoidal transfer function $S\big[\cdot\big]$ in (10.2). Again, the aim is to deduce the phase dynamics of the network of coupled Wilson–Cowan neural masses with noisy input. Noise may lead to strongly irregular oscillations, such that an extended phase description for stochastic

oscillators is needed as has been suggested alternatively by Schwabedal and Pikovsky [242] and Thomas and Lindner [243]. In the case of weak noise, these strong irregularities may not arise, and we can rely on phase reduction methods for stochastic limit-cycle oscillators with both additive and multiplicative noise [244–247]. The main focus in these references lies on the synchronization of a network by common (white and colored) noise, but not necessarily on a phase description where both coupling and noise terms affect the oscillators' phase dynamics. Nonetheless, the work provides important insight into the subtleties of phase reduction that arise due to (distinct) characteristic time scales of both the noise and the deterministic dynamics [164].

Let τ_ξ and τ_ρ denote the characteristic correlation time of the noise and the relaxation time of the amplitude $\boldsymbol{\rho}$ of the limit cycle, respectively. For simplicity, we assume τ_ρ to be independent of the phase θ. When the dynamics converges towards the limit cycle solution instantaneously, we can assume the "phase limit" $\tau_\rho \to 0$ as before. In the case of white noise, one can also consider the limit $\tau_\xi \to 0$. In general, however, both τ_ξ and τ_ρ are finite. If we ignore the coupling for a moment, then the general form of the phase dynamics associated to (10.2) reads [246]

$$\dot{\theta}_k = \left[\omega_k + \frac{\varepsilon^2}{1+(\tau_\xi/\tau_\rho)} Y(\theta_k)\right] + \varepsilon Z(\theta_k)\xi_k(t) \tag{10.4}$$

in the Stratonovich interpretation [248]. In (10.4) the natural frequency ω_k of the oscillator may vary even when driven by white noise. Although this variation is of order $\mathcal{O}(\varepsilon^2)$, it is of the same intensity as effects due to additional forcing, or coupling, and might therefore not be neglected [164]. In order to derive the actual expressions of $Z(\theta_k) = Z_k(\theta_k)$ and $Y(\theta_k) = Y_k(\theta_k)$, it is important to define phase and amplitude coordinates θ_k, $\boldsymbol{\rho}_k$ in a vicinity of the (unperturbed) limit cycle solution $\left(E_k^c(t), I_k^c(t)\right) = \left(E_k^c(\theta_k), I_k^c(\theta_k)\right)$. We find

$$Z_k(\theta_k) = \boldsymbol{Z}_k \cdot \begin{pmatrix} \sigma_k(E_k, I_k) \\ 0 \end{pmatrix}\Big|_{(E_k,I_k)=(E_k^c,I_k^c)},$$

where $\boldsymbol{Z}_k$ is the phase sensitivity function of the (deterministic and uncoupled) neural mass k. The expression $Y_k(\theta_k)$ is more complicated and crucially depends on the amplitude dynamics $\boldsymbol{\rho}_k$ evaluated on the limit cycle. For the general forms of $Z_k(\theta_k)$ and $Y_k(\theta_k)$, we refer to [245,246]. Note, however, that in the limit of weak coupling, $0 < \kappa \ll 1$, we arrive at

$$\dot{\theta}_k = \omega_k + \frac{\varepsilon^2}{1+(\tau_\xi/\tau_\rho)} Y_k(\theta_k) + \frac{\kappa}{N}\sum_{j=1}^{N} H_{kj}(\theta_j - \theta_k) + \varepsilon Z_k(\theta_k)\xi_k(t) \tag{10.5}$$

with H_{kj} the usual phase interaction function introduced earlier; for the underlying theory see [12,146,147,208,249,250]. For the practical application of an analytic reduction it is again advantageous to first cast the dynamics (10.2) into Hopf normal form, determine the phase sensitivity function $\boldsymbol{Z}$ and the relaxation time τ_ρ of the amplitude dynamics, and subsequently apply a phase reduction resulting into (10.5).[38]

The phase reduction of the stochastic Wilson–Cowan neural mass network is based on strong assumptions on the weakness of perturbations through coupling and noise. The recent extensions to strongly perturbed limit cycle oscillators [251] dwell on the separation of a slow but large-amplitude component and weak fluctuations of the perturbation. Therefore, they seem rather adequate to model weakly coupled oscillators with changing background activity [252]. Although not explicitly mentioned, the incorporation of noise appears to be straightforward. External input functions, both deterministic and stochastic, may lead to complex collective behavior, such as the onset of collective oscillations [150] or stochastic, i.e. noise-induced, synchronization [244,247]. However, a comprehensive theory for the reduction of stochastic and nonautonomous systems in terms of phase (and amplitude) dynamics is still being sought for and remains in the focus of current research.

10.3.2. Systems with delay

Complex networks often stand out for a realistic network structure, or topology. An important feature of complex network topology, which we largely ignored in the presentation of phase reduction techniques, is the incorporation of a transmission rate, that is, the time needed for the signal of node k to travel to and perturb or affect node j. Up to now, we only considered infinitely fast, or instantaneous, interactions between oscillators. In general, however, one ought to take also the (transient) dynamics of signal propagation into account, which can mainly, and sufficiently well, be approximated by an additional delay structure.

Incorporating delays between cortical regions or spatial kernels leads to far more intricate coupling dynamics, see, e.g., [253], and the following subsection. Friston popularized Volterra series to model inherent nonlinear interactions when also taking neuronal transients into account, i.e. the recent history of neural activity of connected neuronal populations [254]. Phase reduction strategies have been extended recently to cope with time-varying external perturbations [251,252,255], which hints at ways how to tackle dynamically more intricate coupling terms. However, a thorough

[38] When the amplitude dynamics towards the limit cycle is much faster than the correlation time τ_ξ of the noise, or when the limit cycle is sufficiently robust against amplitude perturbations, then the ratio τ_ξ/τ_ρ can be assumed to tend to infinity and the term with $Y_k(\theta)$ will vanish. In this case, the phase reduction to $\dot{\theta}_k = \omega_k + \varepsilon Z_k(\theta_k)\xi_k(t)$ is of the same (non-stochastic) nature as the 'standard' phase reduction method considered above [246].

analysis of complex coupling functions and their translation into phase models is beyond the scope of this review. Yet, we trust that our results can help to construct particular phase coupling terms, which especially becomes important for the modeling of (neural) cross-frequency interactions [256,257].

We briefly revisit the phase reduction theory for delay-coupled systems. As in the previous subsection, we exemplarily focus on the Wilson–Cowan mass model. Delays may occur both within a single neural mass and between distinct neural masses. Usually, the (internal) interactions are assumed to be considerably fast compared to the typical transmission speed across cortical regions. Therefore, delays within each neural mass can be neglected so that only delays in the coupling between different neural masses generate a global (cortical) delay structure. Such delay structure can be neurobiologically motivated when, e.g., inferred from diffusion spectrum imaging. Once axonal pathways have been identified, the Euclidean distances between connected brain regions and physiologically realistic conduction velocities provide an estimate on the delays τ_{kl} between nodes k, l. The network dynamics with time-delay read

$$\dot{E}_k = -E_k + S\left[a_E\left(c_{EE}E_k - c_{IE}I_k - \Theta_E + P_k + \frac{\kappa}{N}\sum_{l=1}^{N} C_{kl}E_l(t-\tau_{kl})\right)\right] \tag{10.6a}$$

$$\dot{I}_k = -I_k + S\left[a_I\left(c_{EI}E_k - c_{II}I_k - \Theta_I\right)\right] \ . \tag{10.6b}$$

Assuming the time delays τ_{kl} to be of the same order of magnitude as the period T_k of oscillation of each of the neural masses, they will manifest as model-dependent phase shifts $\Delta_{kl} = (2\pi/T_k)\tau_{kl}$ in the coupling function of the reduced phase dynamics:

$$\dot{\theta}_k = \omega_k + \kappa\sum_{l=1}^{N} H(\theta_l - \theta_k - \Delta_{kl}) \ ; \tag{10.7}$$

for the derivation see, e.g., [33,35,39,212]. Intuitively, this phase shift can be explained within the theory of weakly coupled oscillators: Given that $\kappa \ll 1$ is small, the time-delayed coupling term corresponds to a phase-shifted point on the (uncoupled) limit cycle. When expanding the phase interaction function H in Fourier space, the phase shifts Δ_{kl} will effectively shape the amplitudes of the odd and even harmonics, i.e. of the sine and cosine components, respectively, which may affect the collective dynamics of the network. In fact, prior studies that respected transmission delays in phase oscillator networks have reported elaborate synchronization dynamics [258–262].

When a phase shift-approximation as above is no longer adequate and τ represents the time of propagation of the signal from one neuron to another, the dynamics of the corresponding delay-differential equations become more complex. Indeed, delayed dynamical systems are infinite-dimensional, and thus present a serious mathematical challenge. Numerical tools have been developed such as DDE-BiFTOOL [263,264], which can be used to investigate the dynamical properties of coupled systems with delay. Coombes and Laing [265] applied the methods to a single Wilson–Cowan population with multiple time delays. Time delays influence the creation of oscillations as well as the form of the limit-cycle. Even quasi-periodic orbits can emerge, as has been shown for a slightly different version of a Wilson–Cowan population with delays [266]. How coupling, with and without delays, to other Wilson–Cowan populations further shapes the oscillatory properties of the single neural masses has not been answered, yet.

The incorporation of time delays may lead to oscillations around an otherwise stable fixed point solution. Phase reduction techniques have been extended to tackle these delay-induced oscillations [164,267,268]. The theoretical framework developed there has yet to be generalized to analyze weakly coupled delay-induced limit-cycle oscillators. It remains open whether reduction techniques can be applied to deduce a phase model when oscillations are not necessarily delay-induced but strongly affected by the delay: if delays lead to very strong amplitude effects, a ‘standard’ phase reduction goes along with the loss of (too much) information so that alternative ways have to be found.

10.4. Beyond weak coupling

The reduction of phase dynamics from a network of coupled oscillators retains its mathematical justification as long as the theory of weakly coupled oscillators can be evoked. However, no rigorous definition of weak coupling exists, nor a concrete limit of the coupling strength at which the character of interaction switches from weak to strong. Usually, phase reduction is achieved with the tacit understanding that each isolated system already displays stable limit cycle oscillations, which is a necessary condition for the theory of weakly coupled oscillators. In some cases, however, it is the coupling between systems that induces oscillations. Smale was among the first to investigate the emergence of oscillations via a Hopf bifurcation due to diffusive coupling [269]. On the other hand, coupling between systems can also make oscillations cease. Revoking the example of coupled Wilson–Cowan neural masses, Ermentrout and Kopell reported this kind of oscillation death for a chain of oscillatory nodes [54], and Daffertshofer and van Wijk found similar behavior in a heterogeneous network [33].

Coupling-induced effects only occur for reasonably large coupling strengths. Then, an identification of the phase dynamics as within the theory of weak coupling may no longer be possible. While sufficiently weak coupling ensures that the shape and the frequency of the limit-cycle orbits remain almost unchanged, strong coupling leads to non-negligible

amplitude effects. These can destabilize synchronized states, cause (amplitude and thus) oscillation death or collective chaos, and a phase reduction has only been proposed for quite restrictive assumptions; see [251] and the references therein. The theory of weakly coupled oscillators additionally requires that the actual trajectories of the oscillators are always close to the isolated limit-cycle solution and typically instantaneous relaxation back to the limit cycle after a perturbation is assumed. By this one can rely on the linear dynamics around limit cycles, yielding a straightforward yet comprehensive (isochronal) description as outlined in Section 2. However, non-linear effects may occur when moving away from the direct proximity to the limit cycle, rendering a phase reduction spurious.

There are at least two possible approaches to improve phase reductions for oscillatory dynamics with 'stronger' perturbations. A first one is to consider higher order approximations to the isochronal dynamics in order to construct so-called higher order phase sensitivity functions, see, e.g., [270,271]. However, there are also potential pitfalls when applying such a phase reduction. The presence of nearby invariant structures (e.g., saddle points or invariant manifolds) or strong forcing moving the oscillator out of the limit cycle's basin of attraction $\mathcal{B}(\mathcal{C})$ are but a few possible obstacles. The second one is to use phase–amplitude descriptions of the oscillatory dynamics. By appropriate coordinate transformations, these phase–amplitude descriptions can be either *non-isochronal*, in which case the reduced phase and amplitude dynamics may also hold outside of the basin of attraction $\mathcal{B}(\mathcal{C})$, or *isochronal*, when the reduced dynamics is only valid within $\mathcal{B}(\mathcal{C})$. Given the potential of these kinds of extended phase reduction, we will revise various techniques in Section 11.

10.5. Uniqueness of normal forms

A final point of discussion concerns normal forms, which are an important ingredient for analytic phase reduction techniques. Given the plethora of derivation schemes as mentioned in Section 4.1, it appears obvious to ask whether they all result into the same, unique normal form. Needless to say, uniqueness of normal forms can, in general, not be guaranteed, at least not for 'classic' normal forms, which we have used throughout this report. Classic normal forms are usually simple enough to become solvable and can be truncated at a given degree. This leaves the question of asymptotic validity. That is, is a normal form in terms of a (formal) series, or a truncated normal form, a reasonably good approximation of the original dynamics? In fact, quite detailed error analyses can be found in the literature [77,272,273]. Murdock presents several error estimates in [Chapter 5, 77], among which there is a basic theorem that allows to estimate an asymptotic error (depending on the order of truncation and on the initial distance) if (a) the matrix of the linear term is *semi-simple* and has all its eigenvalues on the imaginary axis, and (b) if the semi-simple normal form style is used, see [Lemma 5.3.6,77]. A *normal form style* is connected with the choice of a complementary subspace $\mathcal{H}_k$ of the image of a homological operator applied to a particular vector space $\mathcal{P}_k$, as shown in Section 4.1. The operator is associated with the Jacobian, that is, with the linear term of the dynamics. In the case that the Jacobian is semi-simple[39], e.g., in the case of a Hopf bifurcation, there is only one useful choice of $\mathcal{H}_k$ as the kernel of the operator applied to $\mathcal{P}_k$, which is the *semi-simple normal form style*[40]. Fixing a normal form style, however, does not necessarily determine a unique normal form [77]. The main reason is that all higher order terms in the normal form are normalized with respect to the linear term only, i.e. the normal form satisfies a condition which is defined through the Jacobian. A more complete normalization, by contrast, builds on a series of normalizations: first the quadratic term is normalized with respect to the linear one, then the cubic term is normalized with respect to the sum of the linear and quadratic terms, etc. The resulting *higher-level normal forms* require more advanced calculations, see, e.g., [85,276]. The actual ideas of these fully normalized normal forms go back to Belitskii [277] and the work by Baider and co-workers [278,279]. One can find alternative notions for higher-level normal forms in the literature like *hypernormal forms*, *simplest normal forms*, or *unique normal forms*. Higher-level normal forms can differ for distinct normal form styles applied, but uniqueness may be established within a fixed normal form style.

11. Outlook

There exists a variety of extended phase and phase–amplitude reduction techniques. A thorough review of all of them would certainly amount to a second volume of this report. Still, we want to briefly gather and revise those techniques that can be readily used to derive an improved description of the phase dynamics of a single oscillator. Our aim is to provide an overview over different approaches and to aid create a unifying language of and perspective on the topic. This will, as we believe, be very beneficial for extending phase–amplitude reductions to networks, so that the derivation of the phase dynamics of complex oscillatory networks can be standardized and improved further.

Given oscillatory dynamics with a periodic orbit, an appropriate coordinate transformation into a phase–amplitude model can allow for a convenient definition of a phase variable along the limit cycle and of amplitude variables that can be associated with the distance from the limit cycle. Such coordinate transformations preserve the dimensionality of the system under study. If, for instance, some amplitude variables turn out to be negligible and can be discarded, the derivation of the (truncated) phase–amplitude model indeed becomes a phase–amplitude *reduction*. Alternatively, the description of the phase dynamics can be improved through an *augmented phase reduction*. It is closely related to

[39] An $n \times n$ matrix $\boldsymbol{A}$ is called semi-simple if it is diagonizable with diagonal entries $\lambda_1, \ldots, \lambda_n \in \mathbb{C}$, otherwise $\boldsymbol{A}$ is non-semi-simple.

[40] For non-semi-simple Jacobians, the mainly used styles are the adjoint operator or inner product normal form popularized by Elphick and co-workers [274], and the $\mathrm{sl}(2, \mathbb{R})$ normal form due to Cushman and Sanders [275].

phase–amplitude reductions, but instead of capitalizing on non-isochronal phase and amplitude coordinates, augmented phase reduction builds on the concept of isochrons and isostables for a periodic orbit. Similar to the notion of isochrons as level sets of the same asymptotic phase value, *isostables* are defined as a set of initial conditions that have the same relaxation rate towards the attracting limit cycle [280]. An isostable represents an amplitude degree of freedom, which in addition is independent of the phase and of other amplitude degrees of freedom. Both isochrons and isostables can be understood from a unified perspective via the spectral properties of the Koopman operator [280–282].

In the following, we first introduce two approaches to phase–amplitude reduction. Then, we turn to the augmented phase reduction and also revise an approach how to increase the accuracy of phase–amplitude reductions beyond a leading order approximation of the phase and isostable dynamics, which is called a *second-order phase reduction*. Last, we sketch three methods that exploit the full global properties of isochrons and isostables, giving rise to another class of extended phase reduction techniques along *global isochrons and isostables*.

11.1. Phase–amplitude reductions

Here, we present two phase–amplitude reduction techniques that are based on coordinate transformations of the oscillatory dynamics. The new coordinate system is such that one coordinate, corresponding to the axis that points in the direction of the tangent vector along the periodic orbit, indicates the phase, whereas the other coordinates denote transversal variables, giving the notion of distance from the limit cycle. The first method was established by Ermentrout and Kopell [53–55] and became popular as it resembles a phase reduction in the limit of "infinite attraction". The second one upholds the full phase–amplitude description through the setting of a moving orthonormal system. The underlying theory was detailed by Hale [283], see also [167,284], and has been put forward as a phase–amplitude description by Wegdwood and co-workers in [285]. It generalizes Ermentrout & Kopell's reduction approach in that it respects the amplitude dynamics beyond leading order. The resulting interaction functions in the phase(-amplitude) model thus comprise both phase and amplitude effects from the other oscillators.

11.1.1. Ermentrout & Kopell's reduction

The reduction method by Ermentrout and Kopell [53–55] is based upon a coordinate transformation $\boldsymbol{x}_k = \mathcal{T}_k(\theta_k, \boldsymbol{\rho}_k)$ of the oscillatory dynamics in terms of phase and amplitude variables. For a network of coupled oscillators, it is possible to apply the transformation $\mathcal{T}_k$ to every node, leading to network dynamics whose evolution is governed by differential equations for the interacting phases and amplitudes of the respective nodes. In the limit of "infinite attraction", that is, if the amplitude variables tend to vanish infinitely fast, the phase–amplitude description reduces to a phase model of the oscillator network. We briefly sketch the coordinate transformation $\mathcal{T}_k$ for a single oscillator, and subsequently extend the phase–amplitude description first to two, and then to multiple coupled oscillators.

Single oscillator. We consider an oscillator $\dot{\boldsymbol{x}}_k = \boldsymbol{f}_k(\boldsymbol{x}_k), \boldsymbol{x}_k \in \mathbb{R}^n$, with an asymptotically stable limit cycle solution $\boldsymbol{x}_k^c(t)$ with period T_k and frequency $\omega_k = 2\pi/T_k$. The coordinate transformation $\mathcal{T}_k$ is such that it maps $\boldsymbol{x}_k$ to variables $\theta_k \in \mathbb{S}^1$ and $\boldsymbol{\rho}_k \in \mathbb{R}^{n-1}$. The phase θ_k parametrizes $\boldsymbol{x}_k^c$ along the limit cycle $\mathcal{C}$ and the amplitudes $\boldsymbol{\rho}_k$ are normal coordinates in a neighborhood of $\mathcal{C}$, with $\boldsymbol{\rho}_k = 0$ directly on it. Ermentrout and Kopell [55] chose the transform $\mathcal{T}_k$ of the form

$$\boldsymbol{x}_k(t) = \mathcal{T}_k\left(\theta_k(t), \boldsymbol{\rho}_k(t)\right) = \boldsymbol{x}_k^c\left(\theta_k(t)\right) + \boldsymbol{M}_k\big(\theta_k(t)\big)\boldsymbol{\rho}_k(t) + \mathcal{O}^2(\boldsymbol{\rho}_k)\,, \tag{11.1}$$

where $\boldsymbol{M}_k(\theta)$ is an $n \times (n-1)$-matrix and normalized such that it fulfills

$$\begin{aligned} \boldsymbol{M}_k(\theta)^\intercal \boldsymbol{M}_k(\theta) &= \boldsymbol{I}_{(n-1)\times(n-1)} \\ \left[\partial_\theta \boldsymbol{x}_k^c(\theta)\right]^\intercal \boldsymbol{M}_k(\theta) &= \boldsymbol{0}_{1\times(n-1)}\,. \end{aligned} \tag{11.2}$$

Here, $\partial_\theta = d/d\theta$ denotes the derivative with respect to θ. For small $|\boldsymbol{\rho}_k| \ll 1$, one can express the dynamics $\dot{\boldsymbol{x}}_k = \boldsymbol{f}_k(\boldsymbol{x}_k)$ in the phase and amplitude variables as

$$\begin{aligned} \dot{\theta}_k &= \omega_k + f_{1,k}(\theta_k, \boldsymbol{\rho}_k) + \mathcal{O}^2(\boldsymbol{\rho}_k) \\ \dot{\boldsymbol{\rho}}_k &= \boldsymbol{A}_k(\theta_k)\boldsymbol{\rho}_k + o(\boldsymbol{\rho}_k)\,. \end{aligned} \tag{11.3}$$

The function $f_{1,k}(\theta_k, \boldsymbol{\rho}_k) = \mathcal{O}(\boldsymbol{\rho}_k)$ is defined such that $f_{1,k} \to 0$ for $\boldsymbol{\rho}_k \to 0$. On the limit cycle we retrieve $\dot{\theta}_k = \omega_k$. With the Jacobian $\boldsymbol{L}_k(\theta) = \nabla \boldsymbol{f}(\boldsymbol{x})\big|_{\boldsymbol{x}=\boldsymbol{x}_k^c(\theta)}$ of $\boldsymbol{f}$ evaluated at the limit cycle $\boldsymbol{x}_k^c$, and abbreviating $\varsigma_k(\theta) = \left|\partial_\theta \boldsymbol{x}_k^c(\theta)\right|^2$, the functions $f_{1,k} : \mathbb{S}^1 \times \mathbb{R}^{n-1} \to \mathbb{S}^1$ and $\boldsymbol{A}_k : \mathbb{S}^1 \to \mathbb{R}^{(n-1)\times(n-1)}$ can be found [55] as

$$\begin{aligned} f_{1,k}(\theta, \boldsymbol{\rho}) &= \frac{\omega_k}{\varsigma_k(\theta)}\left[\partial_\theta \boldsymbol{x}_k^c(\theta)\right]^\intercal \left[\boldsymbol{L}_k(\theta) + \boldsymbol{L}_k(\theta)^\intercal\right]\boldsymbol{M}_k(\theta)\boldsymbol{\rho} \\ \boldsymbol{A}_k(\theta) &= \omega_k\left[\boldsymbol{M}_k(\theta)^\intercal \boldsymbol{L}_k(\theta)\boldsymbol{M}_k(\theta) + \left[\partial_\theta \boldsymbol{M}_k(\theta)\right]^\intercal \boldsymbol{M}_k(\theta)\right]\,. \end{aligned} \tag{11.4}$$

In the case of a two-dimensional system $\boldsymbol{x}_k \in \mathbb{R}^2$ with limit cycle solution $\boldsymbol{x}_k^c(t) = (u_k(t), v_k(t))$, we have $\varsigma_k = \left|\partial_\theta \boldsymbol{x}_k^c(\theta)\right|^2 = \left[\partial_\theta u_k(\theta)\right]^2 + \left[\partial_\theta v_k(\theta)\right]^2$ and so the 2×1-matrix $\boldsymbol{M}_k(\theta)$ becomes the vector $\left(\partial_\theta v_k(\theta), -\partial_\theta u_k(\theta)\right)/\sqrt{\varsigma_k(\theta)}$, which fulfills the required normalization conditions (11.2).

Coupled oscillators. The approach above can naturally be extended to networks of coupled oscillators by using coordinate transformations $\mathcal{T}_k$ for every node $k = 1, \dots, N$ of the network. For simplicity, we will consider two coupled nearly-identical oscillators $\boldsymbol{x}_k, \boldsymbol{x}_j$ with dynamics

$$\dot{\boldsymbol{x}}_k = \boldsymbol{f}(\boldsymbol{x}_k) + \kappa\, \boldsymbol{g}_k(\boldsymbol{x}_k, \boldsymbol{x}_j)\,, \quad \boldsymbol{x}_k \in \mathbb{R}^n, \tag{11.5}$$

and show explicitly how the network extension can be achieved — note that the case $\dot{\boldsymbol{x}}_k = \boldsymbol{f}(\boldsymbol{x}_k) + \kappa/N \sum_{j=1}^{N} \boldsymbol{g}_k(\boldsymbol{x}_k, \boldsymbol{x}_j)$ follows analogously for $N > 2$. Moreover, we briefly revisit the derivation of the phase interaction function H for two coupled oscillators $k \neq j$ with strongly attracting limit cycles as in [55]. Considering (11.5), we search for solutions of the form $\boldsymbol{x}_k(t) = \boldsymbol{x}^c(t) + \kappa\, \boldsymbol{u}_k(t)$, where $\boldsymbol{x}^c(t)$ denotes the T-periodic limit cycle solution of $\dot{\boldsymbol{x}} = \boldsymbol{f}(\boldsymbol{x})$ with frequency $\omega = 2\pi/T$, and $\boldsymbol{u}_k$ is such that it converges to zero for solutions on the limit cycle $\boldsymbol{x}(t) = \boldsymbol{x}^c(t)$.[41] We apply the coordinate transformation $\mathcal{T}$ given by (11.1) to both oscillators, which yields the corresponding dynamics in phase and amplitude variables

$$\begin{aligned} \dot{\theta}_k &= \omega + f_1(\theta_k, \boldsymbol{\rho}_k) + \kappa\; h_k(\theta_k, \theta_j) + \mathcal{O}(|\boldsymbol{\rho}_k, \boldsymbol{\rho}_j|) \\ \dot{\boldsymbol{\rho}}_k &= \boldsymbol{A}(\theta_k)\boldsymbol{\rho}_k + \kappa\; \boldsymbol{d}_k(\theta_k, \theta_j) + \mathcal{O}(|\boldsymbol{\rho}_j|) + o(|\boldsymbol{\rho}_k|) \end{aligned} \tag{11.6}$$

with the functions f_1 and $\boldsymbol{A}$ given in (11.4) as well as

$$\begin{aligned} h_k(\theta_k, \theta_j) &= \frac{\omega}{\varsigma(\theta_k)} \big[\partial_\theta \boldsymbol{x}^c(\theta)\big]^\intercal \boldsymbol{g}_k\big(\boldsymbol{x}^c(\theta_k), \boldsymbol{x}^c(\theta_j)\big) \\ \boldsymbol{d}_k(\theta_k, \theta_j) &= \omega \boldsymbol{M}(\theta_k)^\intercal \boldsymbol{g}_k\big(\boldsymbol{x}^c(\theta_k), \boldsymbol{x}^c(\theta_j)\big)\,. \end{aligned} \tag{11.7}$$

Note that (11.6) with (11.7) are general and hold for any coupling strength $\kappa \in \mathbb{R}$ at leading order in $\boldsymbol{\rho}_k$ and $\boldsymbol{\rho}_j$, the latter approximation allows us to evaluate the coupling terms $\boldsymbol{g}_k$ at the respective limit cycles. In the case of weak coupling, $0 \leq \kappa \ll 1$, and in the limit of strong, or 'infinite', attraction, $\boldsymbol{\rho}_k \to 0$, one can apply averaging as detailed in Section 5.2. This leads to the phase dynamics of the two coupled oscillators

$$\dot{\theta}_k = \omega + \kappa\, H_k(\theta_k - \theta_j)$$

with the phase interaction function[42]

$$H_k(\theta_k - \theta_j) = \frac{1}{2\pi} \int_0^{2\pi} \omega \varsigma(\phi + \theta_k)^{-1} \big[\partial_\theta \boldsymbol{x}^c(\phi + \theta_k)\big]^\intercal \boldsymbol{g}_k\big(\boldsymbol{x}^c(\phi + \theta_k), \boldsymbol{x}^c(\phi + \theta_j)\big) d\phi\,. \tag{11.8}$$

If allowing for finite attraction to the limit cycle while keeping the weak coupling limit $0 \leq \kappa \ll 1$, the normal coordinates $\boldsymbol{\rho}_k$ stay κ-close to the limit cycle. Then, we can introduce $\boldsymbol{\rho}_k = \kappa \boldsymbol{s}_k$, and (11.6) becomes

$$\begin{aligned} \dot{\theta}_k &= \omega + \kappa \left\{ \boldsymbol{b}(\theta_k)\boldsymbol{s}_k + \varsigma(\theta_k)^{-1} \big[\partial_\theta \boldsymbol{x}^c(\theta)\big]^\intercal \boldsymbol{g}_k\big(\boldsymbol{x}^c(\theta_k), \boldsymbol{x}^c(\theta_j)\big) \right\} + \mathcal{O}^2(\kappa)\,, \\ \dot{\boldsymbol{s}}_k &= \boldsymbol{A}(\theta_k)\boldsymbol{s}_k + \omega \boldsymbol{M}(\theta_k)^\intercal \boldsymbol{g}_k\big(\boldsymbol{x}^c(\theta_k), \boldsymbol{x}^c(\theta_j)\big) + \mathcal{O}(\kappa)\,, \end{aligned} \tag{11.9}$$

with $\boldsymbol{b}(\theta_k) = \omega \varsigma(\theta_k)^{-1} \big[\partial_\theta \boldsymbol{x}^c(\theta)\big]^\intercal \left[\boldsymbol{L}(\theta_k) + \boldsymbol{L}(\theta_k)^\intercal\right] \boldsymbol{M}(\theta_k)$. In order to determine the phase interaction function H_k for finite $\boldsymbol{\rho}_k$, we have to take the additional term $\boldsymbol{b}(\theta_k)\boldsymbol{s}_k$ into account when applying averaging as in (11.8). Having defined the slower time scale $\tau = \kappa t$, we seek for solutions

$$\boldsymbol{x}_k(t) = \boldsymbol{x}^c\,(\theta_k) + \kappa\, \boldsymbol{u}_k(t, \tau, \kappa) \quad \text{with} \quad \theta_k(\tau) = t + \phi_k(\tau)\,. \tag{11.10}$$

$\boldsymbol{u}_k$ depends on both t and τ, whereas $\phi_k = \phi_k(\tau)$ are slowly-varying phase deviations from the natural frequency, which we set to $\omega = 1$ without loss of generality. As detailed in Appendix A.6, the 'amplitude-corrected' phase dynamics turns out to be

$$\dot{\theta}_k = 1 + \kappa\, \tilde{H}_k(\theta_k - \theta_j) = 1 + \frac{\kappa}{2\pi} \int_0^{2\pi} \big[\varsigma(t)^{-1} \partial_\theta \boldsymbol{x}^c(t) \boldsymbol{\varrho}(t)\big]^\intercal \boldsymbol{g}_k\big(\boldsymbol{x}^c(t + \theta_k), \boldsymbol{x}^c(t + \theta_j)\big) dt \tag{11.11}$$

with the additional, 'corrective' term $\boldsymbol{\varrho}(t)$ when compared to (11.8). For more details, we also refer to [55]. Finally, the phase dynamics (11.11) can be extended to a network of more than two coupled oscillators as

$$\dot{\theta}_k = 1 + \frac{\kappa}{N} \sum_{j=1}^{N} C_{kj} \tilde{H}_k(\theta_k - \theta_j)$$

with C_{kj} representing the connectivity between nodes $k \neq j$.

---

[41] The to-be-presented approach can thus be considered a formal perturbation expansion. It dwells on the Fredholm alternative.

[42] An alternative proof to establish the phase equations for oscillatory networks is given by Hoppensteadt and Izhikevich in [Theorem 9.1, 46]. They focus on the phase dynamics of (11.6) and use normal form theory as presented in Section 4.1 to describe perturbations P off the invariant manifold of (the product of) hyperbolic limit cycles. Ad-hoc they interpret their choice $P \equiv 0$ as an 'infinite attraction' to the invariant manifold and thus link their result to Ermentrout and Kopell's work.

11.1.2. Wegdwood et al.'s reduction

The phase–amplitude reduction approach by Wegdwood, Lin, Thul and Coombes [285] is a generalization of Ermentrout and Kopell's approach presented above in that the assumption of infinitely fast attraction to the limit cycle is loosened. The to-be-reduced phase and amplitude dynamics go beyond the linear order approximation of the amplitude dynamics, and thus provide a full phase–amplitude description, which is valid for arbitrarily large coupling strengths $\kappa \in \mathbb{R}$. As before, we will first revisit the theory for a single oscillator and subsequently consider the phase–amplitude dynamics of an oscillator network.

Single oscillator. We consider an oscillator $\dot{\boldsymbol{x}} = \boldsymbol{f}(\boldsymbol{x}), \boldsymbol{x} \in \mathbb{R}^n$, with an asymptotically stable limit cycle solution $\boldsymbol{x}^c(t)$ with period T and frequency $\omega = 2\pi/T$. The coordinate transformation $\mathcal{T}$ is such that it maps $\boldsymbol{x}$ to variables $\theta \in \mathbb{S}^1$ and $\boldsymbol{\rho} \in \mathbb{R}^{n-1}$. Via this coordinate transformation, a moving orthonormal system is created with one axis pointing in the direction of a unit tangent vector along the periodic orbit, $\boldsymbol{\xi}(\theta) = \partial_\theta \boldsymbol{x}^c(\theta) \big/ \left|\partial_\theta \boldsymbol{x}^c(\theta)\right|$ with $\partial_\theta = d/d\theta$ as before. The remaining coordinate axes form the columns of an $n \times (n-1)$ matrix $\boldsymbol{M}$. Any point $\boldsymbol{x}$ can then be expressed in terms of its phase.[43] θ and its amplitude $\boldsymbol{\rho}$, analogously to (11.1), as

$$\boldsymbol{x} = \mathcal{T}(\theta, \boldsymbol{\rho}) = \boldsymbol{x}^c(\theta) + \boldsymbol{M}(\theta)\boldsymbol{\rho} \,, \tag{11.12}$$

where $|\boldsymbol{\rho}|$ is the Euclidean distance from the limit cycle. We can project the oscillatory dynamics onto the moving orthonormal system in order to obtain the phase and amplitude dynamics

$$\begin{aligned} \dot{\theta} &= \omega + f_1(\theta, \boldsymbol{\rho}) \\ \dot{\boldsymbol{\rho}} &= \boldsymbol{A}(\theta)\boldsymbol{\rho} + \boldsymbol{f}_2(\theta, \boldsymbol{\rho}) \end{aligned} \tag{11.13}$$

with

$$\omega^{-1} f_1(\theta, \boldsymbol{\rho}) = -\boldsymbol{h}(\theta, \boldsymbol{\rho})^\intercal \partial_\theta \boldsymbol{M}(\theta)\boldsymbol{\rho} + \boldsymbol{h}^\intercal(\theta, \boldsymbol{\rho})\big[\boldsymbol{f}\left(\boldsymbol{x}^c(\theta) + \boldsymbol{M}(\theta)\boldsymbol{\rho}\right) - \boldsymbol{f}\left(\boldsymbol{x}^c(\theta)\right)\big], \tag{11.14a}$$

$$\omega^{-1} \boldsymbol{f}_2(\theta, \boldsymbol{\rho}) = -\boldsymbol{M}(\theta)^\intercal \partial_\theta \boldsymbol{M}(\theta)\boldsymbol{\rho} f_1(\theta, \boldsymbol{\rho}) + \boldsymbol{M}(\theta)^\intercal\big[\boldsymbol{f}\left(\boldsymbol{x}^c(\theta) + \boldsymbol{M}(\theta)\boldsymbol{\rho}\right) - \boldsymbol{f}\left(\boldsymbol{x}^c(\theta)\right) - \boldsymbol{L}(\theta)\boldsymbol{M}(\theta)\boldsymbol{\rho}\big], \tag{11.14b}$$

$$\boldsymbol{h}(\theta, \boldsymbol{\rho}) = \left[\left|\partial_\theta \boldsymbol{x}^c(\theta)\right| + \boldsymbol{\xi}(\theta)^\intercal \partial_\theta \boldsymbol{M}(\theta)\boldsymbol{\rho}\right]^{-1} \boldsymbol{\xi}(\theta), \tag{11.14c}$$

$$\boldsymbol{A}(\theta) = \omega \boldsymbol{M}(\theta)^\intercal\big[-\partial_\theta \boldsymbol{M}(\theta) + \boldsymbol{L}(\theta)\boldsymbol{M}(\theta)\big] \,. \tag{11.14d}$$

Again, $\boldsymbol{L}(\theta) = \nabla \boldsymbol{f}(\boldsymbol{x})\big|_{\boldsymbol{x}=\boldsymbol{x}^c(\theta)}$ is the Jacobian evaluated on the limit cycle. Note the overall similarity between (11.13) & (11.3) and (11.14) & (11.4). As before, $f_1(\theta, \boldsymbol{\rho})$ is such that it vanishes for $|\boldsymbol{\rho}| \to 0$, by which we retrieve the unperturbed phase dynamics on the limit cycle, $\dot{\theta}^c = \omega$. For non-vanishing $\boldsymbol{\rho}$, the function $f_1(\theta, \boldsymbol{\rho})$ captures the *shear* of the oscillatory dynamics, that is, it determines whether and how the distance to the limit cycle accelerates or decelerates the phase dynamics [285,286]. The matrix $\boldsymbol{A}(\theta)$ indicates for each phase θ the rate of attraction to or repulsion from the limit cycle. Moreover, the function $\boldsymbol{h}$ given by (11.14c) plays the role of satisfying a normalization condition similar to (11.2). More details on the derivation of (11.13) can be found in the Appendix of [285].

In contrast to Ermentrout & Kopell's reduction, (11.13) is not truncated at any particular order but provides the exact dynamics of the non-isochronal phase–amplitude coordinates. The validity of (11.13) is not restricted to the basin of attraction of the limit cycle. Yet, it may no longer hold when the coordinate transformation (11.12) breaks down, which will happen if the determinant of the Jacobian of the transformation vanishes, i.e. when $\det\left(\partial \boldsymbol{x}/\partial\theta \;\; \partial \boldsymbol{x}/\partial \boldsymbol{\rho}\right) = 0$. This cannot occur on the limit cycle, where $|\boldsymbol{\rho}| = 0$, but may be the case for some $|\boldsymbol{\rho}| = k_0 > 0$. Thus, k_0 sets an upper limit for the distance from the limit cycle up to which the phase–amplitude dynamics (11.13) provide an accurate description.

Coupled oscillators. In a next step, we apply the coordinate transformation (11.12) to two coupled oscillators of the form $\dot{\boldsymbol{x}}_k = \boldsymbol{f}(\boldsymbol{x}_k) + \kappa\, \boldsymbol{g}_k(\boldsymbol{x}_k, \boldsymbol{x}_j)$ with $\kappa \neq 0$ not necessarily small. Then, the phase–amplitude dynamics in $(\theta_k, \boldsymbol{\rho}_k)$ for oscillator $\boldsymbol{x}_k \in \mathbb{R}^n$ becomes

$$\begin{aligned} \dot{\theta}_k &= \omega + f_1(\theta_k, \boldsymbol{\rho}_k) + \kappa\, \omega \boldsymbol{h}(\theta_k, \boldsymbol{\rho}_k)^\intercal \boldsymbol{g}_k\Big(\boldsymbol{x}^c(\theta_k) + \boldsymbol{M}(\theta_k)\boldsymbol{\rho}_k, \boldsymbol{x}^c(\theta_j)\boldsymbol{M}(\theta_j)\boldsymbol{\rho}_j\Big) \\ \dot{\boldsymbol{\rho}}_k &= \boldsymbol{A}(\theta_k)\boldsymbol{\rho}_k + \boldsymbol{f}_2(\theta_k, \boldsymbol{\rho}_k) + \kappa\, \omega \boldsymbol{M}(\theta_k)^\intercal \boldsymbol{B}(\theta_k, \boldsymbol{\rho}_k)\boldsymbol{g}_k\Big(\boldsymbol{x}^c(\theta_k) + \boldsymbol{M}(\theta_k)\boldsymbol{\rho}_k, \boldsymbol{x}^c(\theta_j) + \boldsymbol{M}(\theta_j)\boldsymbol{\rho}_j\Big) \end{aligned} \tag{11.15}$$

with

$$\boldsymbol{B}(\theta, \boldsymbol{\rho}) = \boldsymbol{I}_n - \partial_\theta \boldsymbol{M}(\theta)\boldsymbol{\rho}\boldsymbol{h}(\theta, \boldsymbol{\rho})^\intercal \;;$$

[43] We assume that the phase variable $\theta \in [0, 2\pi)$ as opposed to $\theta \in [0, T)$ in [285]. This results in a rescaling of the subsequently reduced phase and amplitude dynamics by the frequency ω.

see [285] for more details. The dynamics (11.15) allow for setting up a phase–amplitude model of an oscillator network $\dot{\boldsymbol{x}}_k = \boldsymbol{f}(\boldsymbol{x}_k) + \kappa/N \sum_{j=1}^{N} C_{kj}\boldsymbol{g}(\boldsymbol{x}_k, \boldsymbol{x}_j)$ in the form

$$\begin{aligned} \dot{\theta}_k &= \omega + f_1(\theta_k, \boldsymbol{\rho}_k) + \frac{\kappa}{N}\sum_{j=1}^{N} C_{kj} H_1(\theta_k, \theta_j, \boldsymbol{\rho}_k, \boldsymbol{\rho}_j) \\ \dot{\boldsymbol{\rho}}_k &= \boldsymbol{A}(\theta_k)\boldsymbol{\rho}_k + \frac{\kappa}{N}\sum_{j=1}^{N} C_{kj} \boldsymbol{H}_2(\theta_k, \theta_j, \boldsymbol{\rho}_k, \boldsymbol{\rho}_j) \end{aligned} \tag{11.16}$$

with appropriate phase and amplitude interaction functions H_1 and $\boldsymbol{H}_2$, respectively, corresponding to the coupling terms in (11.15). These interaction functions also depend on the amplitude variables $\boldsymbol{\rho}_k$, $\boldsymbol{\rho}_j$ of the respective oscillators. In order to compare the network description (11.15) with Ermentrout & Kopell's reduction approach of the previous subsection, one may assume weak coupling $\kappa \ll 1$ and the dynamics being close to the limit cycle so that $\boldsymbol{\rho}_k = \kappa \boldsymbol{s}_k$. Inserting this in (11.15), Taylor-expanding the dynamics about $\boldsymbol{s}_k = \boldsymbol{0}$ and discarding higher order corrections, results in (11.9). Here, it is important to note that the function $\boldsymbol{f}_2$ as defined in (11.14b) satisfies $\boldsymbol{f}_2(\theta, \boldsymbol{0}) = 0$ as well as $\partial \boldsymbol{f}_2(\theta, \boldsymbol{0})/\partial \boldsymbol{\rho} = 0$.

Wedgwood et al.'s approach is a generalization of the reduced phase–amplitude dynamics by Ermentrout and Kopell. As of yet, however, there are hardly any network studies that rely on the phase–amplitude network description (11.16). It will be interesting to apply such an approach for detecting synchronization phenomena in strongly coupled complex oscillatory networks.

11.2. Augmented phase reductions

Alternatively to the previous phase–amplitude reductions in non-isochronal phase and amplitude coordinates, reduced phase models may be improved by employing the concept of isochrons and isostables. While isochrons represent the phase degree of freedom, isostables represent the remaining amplitude degrees of freedom as they define a set of initial conditions that have the same relaxation rate towards the attracting limit cycle [280]. Since every isostable is independent of the phase and of other amplitude degrees of freedom, augmented phase reduction is computationally more efficient and therefore might be an attractive alternative for phase–amplitude descriptions. To the best of our knowledge, there is yet no extension to coupled oscillators, so that we here stick to single oscillators.

11.2.1. Wilson & Moehlis' approach via isostables

The concept of isochrons – assigning an asymptotic, or *isochronal*, phase to any point in the basin of attraction of a stable limit cycle, see Section 2 – has proven successful to establish a counterpart for stable fixed points, building on so-called isostables [280], see also [287,288]. *Isostables* were originally introduced as sets of points in phase space that converge toward a fixed point simultaneously. In [289], Wilson and Moehlis adapted the notion of isostable coordinates for use with periodic orbits.

We consider a single oscillator with dynamics $\dot{\boldsymbol{x}} = \boldsymbol{f}(\boldsymbol{x})$, $\boldsymbol{x} \in \mathbb{R}^n$, and periodic orbit $\boldsymbol{x}^c(t)$ with period T and frequency $\omega = 2\pi/T$. Then, we choose a point $\boldsymbol{x}_0 = \boldsymbol{x}^c(0)$ on the limit cycle and denote the corresponding isochron by $\mathcal{I}_0$. In the vicinity of $\boldsymbol{x}_0$, one can analyze the dynamics by a Poincaré map P on $\mathcal{I}_0$,

$$P\colon \mathcal{I}_0 \to \mathcal{I}_0; \quad \boldsymbol{x} \mapsto P(\boldsymbol{x}) = \phi(T, \boldsymbol{x}) \,,$$

where ϕ represents the unperturbed flow of the system. This map has $\boldsymbol{x}_0$ as a fixed point and the linearized dynamics on the isochron $\mathcal{I}_0$ around $\boldsymbol{x}_0$ read

$$P(\boldsymbol{x}) = \boldsymbol{x}_0 + \boldsymbol{J}(\boldsymbol{x} - \boldsymbol{x}_0) + \mathcal{O}^2(|\boldsymbol{x} - \boldsymbol{x}_0|) \tag{11.17}$$

with Jacobian $\boldsymbol{J} = dP/d\boldsymbol{x}\big|_{\boldsymbol{x}=\boldsymbol{x}_0}$. If $\boldsymbol{J}$ is diagonalizable with $\boldsymbol{V} \in \mathbb{R}^{n\times n}$ a matrix with columns of unit length eigenvectors $\boldsymbol{v}_i$ associated with eigenvalues λ_i for $i = 1, \ldots, n$, the latter are the Floquet multipliers of the periodic orbit. Hence, at least one λ_i is equal to one: $\lambda_n = 1$. For every non-trivial Floquet multiplier λ_i, $i < n$, Wilson and Moehlis define isostable coordinates as

$$\psi_i(\boldsymbol{x}) = \lim_{j\to\infty}\left[\boldsymbol{e}_i^{\mathsf{T}}\boldsymbol{V}^{-1}\big(\phi(t_{\mathcal{I}}^j, \boldsymbol{x}) - \boldsymbol{x}_0\big)\mathrm{e}^{-\log(\lambda_i)t_{\mathcal{I}}^j/T}\right] . \tag{11.18}$$

Here, $t_{\mathcal{I}}^j$ is the jth return time to the isochron $\mathcal{I}_0$ under the flow ϕ and $\boldsymbol{e}_i$ is the unit vector in the ith direction. The term $\boldsymbol{e}_i^{\mathsf{T}}\boldsymbol{V}^{-1}$ is a left eigenvector of the Jacobian $\boldsymbol{J}$ which selects for an appropriate component of $\big(\phi(t_{\mathcal{I}}^j, \boldsymbol{x}) - \boldsymbol{x}_0\big)$ in the basis of eigenvectors of $\boldsymbol{J}$. Using the definition of isochrons, it can be shown [290] that this term multiplied by $\mathrm{e}^{-\log(\lambda_i)t_{\mathcal{I}}^j/T}$ converges to a scalar when $j \to \infty$, which we then call the isostable coordinate. The dynamics of the isostables $\psi_i(\boldsymbol{x})$ and of the *isostable response curves* $\boldsymbol{I}_i(t) = \nabla\psi_i(\boldsymbol{x})\big|_{\boldsymbol{x}=\boldsymbol{x}^c(t)}$ can be found as

$$\dot{\psi}_i = k_i\psi_i \,, \tag{11.19a}$$

$$\frac{d\boldsymbol{I}_i(t)}{dt} = \Big(k_i Id - \boldsymbol{L}(t)^{\intercal}\Big)\boldsymbol{I}_i(t)\,, \tag{11.19b}$$

where $k_i = \log(\lambda_i)/T$ are the Floquet exponents, $\boldsymbol{L}(t) = \nabla \boldsymbol{f}(\boldsymbol{x})\big|_{\boldsymbol{x}=\boldsymbol{x}^c(t)}$ is the Jacobian of the oscillatory dynamics and Id denotes the identity matrix in $\mathbb{R}^{n\times n}$; see [289] and also [291]. To ensure uniqueness of the isostable response curves, we require, additionally to the T-periodicity, that $\nabla\psi_i(\boldsymbol{x})\big|_{\boldsymbol{x}=\boldsymbol{x}_0}\cdot\boldsymbol{v}_i = 1$. For a (weakly) perturbed oscillator $\dot{\boldsymbol{x}} = \boldsymbol{f}(\boldsymbol{x}) + \kappa\,\boldsymbol{p}(t)$, we thus obtain the phase and isostable dynamics along the lines of Section 2 as

$$\begin{aligned}\dot\theta &= \omega + \kappa\,\boldsymbol{Z}(\theta)\cdot\boldsymbol{p}(t)\,,\\ \dot\psi_i &= k_i\psi_i + \kappa\,\boldsymbol{I}_i(\theta)\cdot\boldsymbol{p}(t)\,,\quad \text{for } i = 1,\dots,n-1,\end{aligned} \tag{11.20}$$

which we refer to as the *augmented phase reduction*. Note that the additional isostable dynamics do not lead to a correction of the phase dynamics, as the latter is independent of ψ_i. Below, we will show how (11.20) can be extended such that the additional knowledge about the relaxation dynamics toward the periodic orbit does indeed lead to improved phase dynamics. In practice, isostable coordinates ψ_i with sufficiently small Floquet multipliers λ_i can be ignored: any perturbation in this direction rapidly decays, and can be assumed to vanish. This leads indeed to a reduction of the n-dimensional system (11.20) to a lower-dimensional system with those isostables discarded whose Floquet multipliers are sufficiently small.[44]

11.2.2. Shirasaka, Kurebayashi & Nakao's approach via the Koopman operator

Isochrons and isostables may be understood from a unified point of view of the spectral properties of the *Koopman (composition) operator* [280,281]. Capitalizing on the Koopman operator theory, Shirasaka et al. [282] developed an alternative approach that leads to the augmented phase reduction (11.20). Considering the same setting as before, the Koopman operator U^t is a linear operator that describes the evolution of a function defined on the phase space, called an observable $f\colon\mathbb{R}^n\to\mathbb{C}$. It is defined as $U^t f(\boldsymbol{x}) = f\circ\phi(t,\boldsymbol{x})$, where $\circ$ denotes the composition of functions and ϕ is the flow associated with the dynamics $\dot{\boldsymbol{x}} = \boldsymbol{f}(\boldsymbol{x})$, $\boldsymbol{x}\in\mathbb{R}^n$. It can be shown [293,294] that U^t has eigenfunctions $s_i(\boldsymbol{x})$ associated with eigenvalues k_i, $i = 1,\dots,N$, that is,

$$U^t s_i(\boldsymbol{x}) = \mathrm{e}^{k_i t}s_i(\boldsymbol{x})\,, \tag{11.21}$$

where $k_i = \log(\lambda_i)/T$ with $T = 2\pi/\omega$ the period of the limit cycle solution $\boldsymbol{x}^c(t)$ of $\dot{\boldsymbol{x}} = \boldsymbol{f}(\boldsymbol{x})$, and λ_i the Floquet multipliers as in the previous sub-section. By convention, we set $\lambda_n = 1$ so that $k_n = i\omega$. Note that the k_i correspond to the *characteristic exponents* of the limit cycle and thus reflect the spectral property of the system. Assuming that $\boldsymbol{f}$ is twice continuously differentiable, the eigenfunctions s_i are continuously differentiable and exist on the whole basin of attraction, which underlines the isochronal character of the augmented phase reduction. When introducing amplitudes of the state $\boldsymbol{x}$ of the system by $\psi_i(\boldsymbol{x}) \equiv \mathrm{Re}\big(s_i(\boldsymbol{x})\big)$ for $i = 1,\dots,n-1$, then

$$\dot\psi_i = k_i\psi_i$$

holds, as in (11.19a). We set the phase of $\boldsymbol{x}$ as $\theta(\boldsymbol{x}) \equiv \arg\big(s_n(\boldsymbol{x})\big) \in [0, 2\pi)$. Because of $k_n = i\omega$, we have $\dot\theta = \omega$. This definition coincides with that of the asymptotic phase, see Section 2. With this, we retrieve isochrons as level sets of θ and isostables as level sets of $|\psi_i|$.

For a perturbed system of the form $\dot{\boldsymbol{x}} = \boldsymbol{f}(\boldsymbol{x}) + \kappa\,\boldsymbol{p}(t)$, the corresponding phase and amplitude dynamics can be found as

$$\begin{aligned}\dot\theta &= \omega + \kappa\,\boldsymbol{Z}\big(\theta,\psi_1,\dots,\psi_{n-1}\big)\cdot\boldsymbol{p}(t)\,,\\ \dot\psi_i &= k_i\psi_i + \kappa\,\boldsymbol{I}_i\big(\theta,\psi_1,\dots,\psi_{n-1}\big)\cdot\boldsymbol{p}(t)\,,\quad \text{for } i = 1,\dots,n-1,\end{aligned} \tag{11.22}$$

where $\boldsymbol{Z} = \nabla\theta$ and $\boldsymbol{I}_i = \nabla\psi_i$ denote the phase sensitivity function and the isostable response functions, respectively. Note that $\boldsymbol{Z}$ and $\boldsymbol{I}_i$ are evaluated at the state vector $\boldsymbol{x} \cong \big(\theta,\psi_1,\dots,\psi_{n-1}\big)$ when written in phase–amplitude coordinates. For small perturbations with $|\kappa| \ll 1$, one can approximate (11.22) by evaluating the phase sensitivity and the isostable response functions at the limit cycle (where $\psi_1 = \cdots = \psi_{n-1} = 0$), which yields (11.20),

$$\begin{aligned}\dot\theta &= \omega + \kappa\,\boldsymbol{Z}(\theta)\cdot\boldsymbol{p}(t)\,,\\ \dot\psi_i &= k_i\psi_i + \kappa\,\boldsymbol{I}_i(\theta)\cdot\boldsymbol{p}(t)\,,\quad \text{for } i = 1,\dots,n-1,\end{aligned}$$

when neglecting terms of order κ^2.

[44] As to the computation of the isostable response functions $\boldsymbol{I}_i(\theta)$, standard approaches comprise direct or adjoint methods: Similar to determine the phase sensitivity function $\boldsymbol{Z}$, one can either perturb the oscillatory dynamics at various phases and records the corresponding changes, see also [289], or one can solve the adjoint problem associated with (11.19b), cf. [289,291]. There are, however, numerical subtleties to obtain an accurate solution. The direct method suffers from the common numerical artifacts when considering infinitesimal perturbations $|\boldsymbol{p}| \to 0$. The adjoint method dwells on the integration of (11.19b) backward in time, which may lead to an unstable periodic solution [282,292]. Alternatively, the computation of $\boldsymbol{I}_i(\theta)$ can be formulated as a boundary value problem to be solved with Newton iteration, see also Section 11.3.1 and [Section 4.1,292] for details. This approach is similar to the algorithms for computing the phase sensitivity function $\boldsymbol{Z}$ as proposed by Govaerts and Sautois [98] and implemented in MatCont [99].

In order to compute the isostable response functions $\boldsymbol{I}_i$ evaluated at the limit cycle, Shirasaka et al. propose a bi-orthogonalization method. In fact, they present their theory for transient dynamics $\boldsymbol{x}^*(t)$ that start far from, but eventually approach the attracting limit cycle solution $\boldsymbol{x}^c(t)$, see [282] for more details. A first observation is that $\boldsymbol{Z}(\theta) = \boldsymbol{Z}\big(\boldsymbol{x}^c(t)\big)$ and $\boldsymbol{I}_i(\theta) = \boldsymbol{I}_i\big(\boldsymbol{x}^c(t)\big)$ are the left eigenvectors of the monodromy matrix $\partial\phi(T,\boldsymbol{x})/\partial\boldsymbol{x}\big|_{\boldsymbol{x}=\boldsymbol{x}^c(t)}$, which are also called the *adjoint covariant Lyapunov vectors* [295–297]. Next, one can introduce logarithmic amplitudes $\tilde{\psi}_i(\boldsymbol{x}) = \log\big(|\psi_i(\boldsymbol{x})|\big)$ for $i = 1, \ldots, n-1$. By convenience, $\tilde{\psi}_n(\boldsymbol{x}) = \theta(\boldsymbol{x})$. The calculation of the gradients $\nabla\tilde{\psi}_i$ of the logarithmic amplitudes is very similar to the conventional phase reduction, and $\boldsymbol{Z}$ and $\boldsymbol{I}_i$ can be readily inferred from $\nabla\tilde{\psi}_i$ by rescaling and normalizing according to

$$\boldsymbol{I}_i\big(\boldsymbol{x}^*(t)\big)\cdot\boldsymbol{f}\big(\boldsymbol{x}^*(t)\big) = k_i\psi_i \quad \text{and} \quad \boldsymbol{Z}\big(\boldsymbol{x}^*(t)\big)\cdot\boldsymbol{f}\big(\boldsymbol{x}^*(t)\big) = \omega\,. \tag{11.23}$$

The resulting adjoint equations for $\nabla\tilde{\psi}_i$ are [282]

$$\frac{d\nabla\tilde{\psi}_i\big(\boldsymbol{x}^*(t)\big)}{dt} = -\Big[\nabla\boldsymbol{f}(\boldsymbol{x})\big|_{\boldsymbol{x}=\boldsymbol{x}^*(t)}\Big]^{\mathsf{T}}\nabla\tilde{\psi}_i\big(\boldsymbol{x}^*(t)\big)\,, \tag{11.24}$$

which are to be solved with an appropriate end condition that can approximately be taken as $\nabla\tilde{\psi}_i\big(\boldsymbol{x}^*(\tau)\big) \parallel \boldsymbol{I}_i(\theta)\big|_{\theta=\theta^*}$ for some final $t = \tau$ and $\theta = \theta^*$. Furthermore, the proposed numerical method relies on bi-orthogonal dual vectors $\boldsymbol{\gamma}_i$ of $\nabla\tilde{\psi}_i$, i.e. $\boldsymbol{\gamma}_i\big(\boldsymbol{x}^*(t)\big)\cdot\nabla\tilde{\psi}_j\big(\boldsymbol{x}^*(t)\big) = \delta_{ij}$. The vectors $\boldsymbol{\gamma}_i$ satisfy

$$\dot{\boldsymbol{\gamma}}_i\big(\boldsymbol{x}^*(\tau)\big) = \nabla\boldsymbol{f}(\boldsymbol{x})\big|_{\boldsymbol{x}=\boldsymbol{x}^*(t)}\boldsymbol{\gamma}_i\big(\boldsymbol{x}^*(\tau)\big)\,, \tag{11.25}$$

and can thus be regarded as the covariant Lyapunov vectors extended to transient regimes. The resulting bi-orthogonalization method for computing the phase and amplitude dynamics

$$\begin{aligned}\dot{\theta} &= \omega + \kappa\,\boldsymbol{Z}\big(\boldsymbol{x}^*(t)\big)\cdot\boldsymbol{p}(t)\,,\\ \dot{\psi}_i &= k_i\psi_i + \kappa\,\boldsymbol{I}_i\big(\boldsymbol{x}^*(t)\big)\cdot\boldsymbol{p}(t)\,, \quad \text{for } i = 1,\ldots,n-1,\end{aligned}$$

of some (transient) dynamics $\boldsymbol{x}^*(t)$ during a time span $t \in (0,\tau)$ comprises the following steps:

(a) evaluate the adjoint Lyapunov vectors on the limit cycle and the Floquet exponents k_i;
(b) calculate the bi-orthogonal dual vectors $\boldsymbol{\gamma}_i\big(\boldsymbol{x}^*(0)\big)$ at the initial time $t = 0$ from $\nabla\tilde{\psi}_i\big(\boldsymbol{x}^*(0)\big)$, the latter can be obtained by a direct numerical simulation and using Fourier averages, see also Section 11.3.2;
(c) obtain $\boldsymbol{Z}\big(\boldsymbol{x}^*(t)\big)$ along the transient $\boldsymbol{x}^*(t), t \in (0,\tau)$ by backward integration of (11.24) with an appropriate end condition at $t = \tau$ as mentioned above;
(d) obtain the dual vector $\boldsymbol{\gamma}_n\big(\boldsymbol{x}^*(t)\big)$ for $t \in (0,\tau)$ by forward integration of (11.25);
(e) obtain $\nabla\tilde{\psi}_1\big(\boldsymbol{x}^*(t)\big)$ by backward integration of (11.24) while subtracting relatively an unstable mode $\boldsymbol{Z}\big(\boldsymbol{x}^*(t)\big)$;
(f) obtain the dual vector $\boldsymbol{\gamma}_1\big(\boldsymbol{x}^*(t)\big)$ by forward integration of (11.25) while subtracting relatively an unstable mode $\boldsymbol{\gamma}_n\big(\boldsymbol{x}^*(t)\big)$;
(g) perform (e) and (f) consecutively to obtain $\nabla\tilde{\psi}_i\big(\boldsymbol{x}^*(t)\big)$ and $\boldsymbol{\gamma}_i\big(\boldsymbol{x}^*(t)\big)$ for $i = 2,\ldots,n-1$ (note that all relatively unstable modes should be subtracted during integration);
(h) obtain $\boldsymbol{Z}\big(\boldsymbol{x}^*(t)\big)$ and $\boldsymbol{I}_i\big(\boldsymbol{x}^*(t)\big)$ normalized with respect to (11.23).

In practice, isostables associated with Floquet multipliers λ_i close to zero can be approximately assumed to vanish so that it suffices to consider only the first $1 \leq m \ll n-1$ modes. The bi-orthogonalization method for transient dynamics off the limit cycle provides the (infinitesimal) phase and amplitude responses on the limit cycle by default. As said, $\boldsymbol{Z}(\theta)$ and $\boldsymbol{I}_i(\theta)$ are the adjoint covariant Lyapunov vectors (left eigenvectors of the monodromy matrix), and can be obtained by *QR-decomposition* methods [295,297] or by *spectral dichotomy* approaches [298,299], yielding the desired augmented phase reduction (11.20).

11.2.3. Wilson & Ermentrout's second-order phase reduction

Augmented phase reduction provides a powerful framework for improving the accuracy of reduced phase dynamics of oscillatory systems. Although the phase dynamics decouple from the isostable dynamics, augmented phase reduction is beneficial: By keeping track of the isostable coordinates, one can ensure that their magnitude remains limited and the reduced phase dynamics hence valid. Compared to the phase–amplitude reduction in Section 11.1, however, it is desirable to use the knowledge about the isostable dynamics in order to correct the phase dynamics away from the direct vicinity of the limit cycle. By employing a second-order approximation of the phase and isostable dynamics, one can achieve an improved augmented phase reduction where the phase and isostable dynamics are mutually dependent. Wilson and Ermentrout presented the corresponding theory in [290], which we will briefly sketch here. The underlying idea is to consider the dynamics about the limit cycle not in linear, but in second order. Given a system $\dot{\boldsymbol{x}} = \boldsymbol{f}(\boldsymbol{x})$ with a T-periodic limit cycle solution $\boldsymbol{x}^c(t)$, we consider an infinitesimal perturbation $\Delta\boldsymbol{x}$ to the periodic orbit $\boldsymbol{x}^c(t)$ at time $t = 0$. The

transient dynamics $\boldsymbol{x}(t) = \boldsymbol{x}^c(t) + \boldsymbol{u}(t)$ due to the perturbation can be given by second-order approximation

$$\dot{\boldsymbol{u}}(t) = \boldsymbol{L}(t)\boldsymbol{u} + \frac{1}{2}\begin{bmatrix} \boldsymbol{u}^\intercal \boldsymbol{H}_1(t) \\ \boldsymbol{u}^\intercal \boldsymbol{H}_2(t) \\ \vdots \\ \boldsymbol{u}^\intercal \boldsymbol{H}_n(t) \end{bmatrix} \boldsymbol{u} + \mathcal{O}^3(|\boldsymbol{u}|) \tag{11.26}$$

with $\boldsymbol{L}(\theta) = \nabla \boldsymbol{f}(\boldsymbol{x})\big|_{\boldsymbol{x}=\boldsymbol{x}^c(t)}$ and $\boldsymbol{H}_i(t)$ the ith component of the Hessian matrix $\nabla\big(\nabla \boldsymbol{f}(\boldsymbol{x})\big)\big|_{\boldsymbol{x}=\boldsymbol{x}^c(t)}$ of second partial derivatives evaluated at the limit cycle. The phase shift due to the initial perturbation $\Delta\boldsymbol{x}$ at $t = 0$ may be written as

$$\Delta\theta = \boldsymbol{Z}(t)\Delta\boldsymbol{x} + \tfrac{1}{2}\Delta\boldsymbol{x}^\intercal \boldsymbol{H}_{\theta,\boldsymbol{x}^c(t)}\Delta\boldsymbol{x} + \mathcal{O}^3(|\Delta\boldsymbol{x}|)\,, \tag{11.27}$$

where $\boldsymbol{Z}(t) = \nabla \boldsymbol{\Theta}(\boldsymbol{x})\big|_{\boldsymbol{x}=\boldsymbol{x}^c(t)}$ is the phase sensitivity function and $\boldsymbol{H}_{\theta,\boldsymbol{x}^c(t)}$ denotes the Hessian matrix of second derivatives of the asymptotic phase map $\boldsymbol{\Theta}$ evaluated at $\boldsymbol{x}^c(t)$. For infinitesimal perturbations we thus have

$$\frac{\partial\theta}{\partial\boldsymbol{x}} = \frac{\partial\boldsymbol{\Theta}}{\partial\boldsymbol{x}} = \boldsymbol{Z}(\theta) + \boldsymbol{H}_{\theta,\boldsymbol{x}^c(\theta)}\Delta\boldsymbol{x} + \mathcal{O}^2(|\Delta\boldsymbol{x}|)\,. \tag{11.28}$$

Likewise, we find the gradient of the isostable coordinates in a second-order approximation as

$$\frac{\partial\psi_i}{\partial\boldsymbol{x}} = \boldsymbol{I}_i(\theta) + \boldsymbol{H}_{\psi_i,\boldsymbol{x}^c(\theta)}\Delta\boldsymbol{x} + \mathcal{O}^2(|\Delta\boldsymbol{x}|) \quad \text{for } i = 1,\ldots,n-1, \tag{11.29}$$

where $\boldsymbol{H}_{\psi_i,\boldsymbol{x}^c(\theta)}$ is the Hessian matrix of ψ_i evaluated at $\boldsymbol{x}^c(t)$. In the vicinity of the limit cycle solution, one can use Floquet theory [300,301] and write

$$\Delta\boldsymbol{x}(t) = \sum_{j=1}^{n} c_j e^{k_j t}\boldsymbol{q}_j(t)$$

with k_j the Floquet exponents from before, $\boldsymbol{q}_j(t)$ are T-periodic vectors, and c_j are appropriately chosen to satisfy initial conditions. With the definition of isostables (11.18) it is possible to show [290] that $c_j = \psi_j$ so that $\Delta\boldsymbol{x}$ can be given in terms of phase and isostable coordinates:

$$\Delta\boldsymbol{x}(\theta,\psi_1,\ldots,\psi_{n-1}) = \sum_{j=1}^{n-1}\psi_j\boldsymbol{p}_j(\theta)\,, \tag{11.30}$$

where $\boldsymbol{p}_j\big(\theta(0)+\omega t\big) = \boldsymbol{q}_j(t)$ with frequency $\omega = 2\pi/T$. By using $d\theta/dt = \partial\theta/\partial\boldsymbol{x}\cdot d\boldsymbol{x}/dt$, we can combine (11.30) and (11.28) to obtain a second-order correction to the phase dynamics of the perturbed system $\dot{\boldsymbol{x}} = \boldsymbol{f}(\boldsymbol{x}) + \kappa\,\boldsymbol{p}(t)$. Analogously, we can use $d\psi_i/dt = \partial\psi_i/\partial\boldsymbol{x}\cdot d\boldsymbol{x}/dt$ together with (11.30) and (11.29) for a second-order correction to the isostable dynamics. This yields the *second-order augmented phase reduction*

$$\begin{aligned} \dot{\theta} &= \omega + \kappa\left\{\boldsymbol{Z}(\theta)\cdot\boldsymbol{p}(t) + \sum_{j=1}^{n-1}\Big[\boldsymbol{b}^j(\theta)\psi_j\Big]\cdot\boldsymbol{p}(t)\right\}, \\ \dot{\psi}_i &= k_i\psi_i + \kappa\left\{\boldsymbol{I}_i(\theta)\cdot\boldsymbol{p}(t) + \sum_{j=1}^{n-1}\Big[\boldsymbol{c}_i^j(\theta)\psi_j\Big]\cdot\boldsymbol{p}(t)\right\}, \end{aligned} \tag{11.31}$$

for $i = 1,\ldots,n-1$ and with vectors $\boldsymbol{b}^j$ and $\boldsymbol{c}_i^j$ given by

$$\boldsymbol{b}^j(\theta) = \boldsymbol{H}_{\theta,\boldsymbol{x}^c(\theta)}\boldsymbol{p}_j(\theta) \quad \text{and} \quad \boldsymbol{c}_i^j(\theta) = \boldsymbol{H}_{\psi_i,\boldsymbol{x}^c(\theta)}\boldsymbol{p}_j(\theta)$$

The phase dynamics of (11.31) depends on the isostable coordinates and can be understood as a second-order correction to the standard phase reduction.

In order to close the system (11.31), one has to compute the Hessian matrices $\boldsymbol{H}_{\theta,\boldsymbol{x}^c(\theta)}$ and $\boldsymbol{H}_{\psi_i,\boldsymbol{x}^c(\theta)}$ as well as the vectors $\boldsymbol{p}_j$. The latter can be approximated numerically by exploiting the linearization of the Poincaré map P given by (11.17). The matrices $\boldsymbol{H}_{\theta,\boldsymbol{x}^c(\theta)}$ and $\boldsymbol{H}_{\psi_i,\boldsymbol{x}^c(\theta)}$ can be found as solutions to adjoint problems that involve the Hessian matrices $\boldsymbol{H}_i(t)$. To be precise, denoting by Z_k the kth component of the phase sensitivity function $\boldsymbol{Z}$, $\boldsymbol{H}_{\theta,\boldsymbol{x}^c(\theta)}$ is the T-periodic solution to

$$\frac{d\boldsymbol{H}_{\theta,\boldsymbol{x}^c(\theta)}}{dt} = -\sum_{k=1}^{n}\big[Z_k(t)\boldsymbol{H}_k(t)\big] - \boldsymbol{L}(t)^\intercal\boldsymbol{H}_{\theta,\boldsymbol{x}^c(\theta)} - \boldsymbol{H}_{\theta,\boldsymbol{x}^c(\theta)}\boldsymbol{L}(t)$$

subject to the normalization condition $-\boldsymbol{L}(t)^\intercal\boldsymbol{Z}(t) = \boldsymbol{H}_{\theta,\boldsymbol{x}^c(\theta)}\boldsymbol{f}\big(\boldsymbol{x}^c(t)\big)$. Likewise, for every $i = 1,\ldots,n-1$, one can find $\boldsymbol{H}_{\psi_i,\boldsymbol{x}^c(\theta)}$ as the T-periodic solution to

$$\frac{d\boldsymbol{H}_{\psi_i,\boldsymbol{x}^c(\theta)}}{dt} = k_i\boldsymbol{H}_{\psi_i,\boldsymbol{x}^c(\theta)} - \sum_{k=1}^{n}\big[I_{i,k}(t)\boldsymbol{H}_k(t)\big] - \boldsymbol{L}(t)^\intercal\boldsymbol{H}_{\psi_i,\boldsymbol{x}^c(\theta)} - \boldsymbol{H}_{\psi_i,\boldsymbol{x}^c(\theta)}\boldsymbol{L}(t)\,,$$

which satisfies the normalization condition $\big(k_i Id - \boldsymbol{L}(t)^{\intercal}\big)\boldsymbol{Z}(t) = \boldsymbol{H}_{\psi_i,\boldsymbol{x}^c(\theta)}\boldsymbol{f}\big(\boldsymbol{x}^c(t)\big)$, where $I_{i,k}$ is the kth component of the isostable response function $\boldsymbol{I}_i(t) = \boldsymbol{I}_i\big(\boldsymbol{x}^c(t)\big)$. For the mathematical details we refer to [290]. There, one also finds a discussion about the computational effort required to obtain the matrices $\boldsymbol{H}_{\theta,\boldsymbol{x}^c(\theta)}, \boldsymbol{H}_{\psi_i,\boldsymbol{x}^c(\theta)}$. An alternative and more efficient strategy is to directly compute the terms $\boldsymbol{b}^j$ and $\boldsymbol{c}_i^j$, as recently proposed by Wilson [302].

11.2.4. Extension to coupled oscillators

Extending the phase and isostable dynamics to networks of coupled oscillators is a natural next step. In view of two coupled oscillators, $\dot{\boldsymbol{x}}_k = \boldsymbol{f}(\boldsymbol{x}_k) + \kappa\, \boldsymbol{g}_k(\boldsymbol{x}_k, \boldsymbol{x}_j)$, the perturbation term $\boldsymbol{p}$ in (11.20) or (11.31) will be replaced by the coupling term $\boldsymbol{g}_k(\boldsymbol{x}_k, \boldsymbol{x}_j)$ and the states $\boldsymbol{x}_k$ have to be expressed in terms of the respective phase and amplitude variables $(\theta_k, \psi_{1,k}, \ldots, \psi_{n-1,k})$. For the first-order augmented phase reduction (11.20) close(r) to the limit cycle, the coupling term $\boldsymbol{g}_k(\boldsymbol{x}_k, \boldsymbol{x}_j)$ can be approximately evaluated on the limit cycle with vanishing isostable coordinates, $\psi_{i,k} = 0$ for $i = 1, \ldots, n-1$, which seems in line with the linear approximation. For the second-order reduction (11.31), by contrast, the isostable dynamics $\psi_{i,k}$ and $\psi_{i,j}$ of both oscillators ought to be taken into account in the reduced phase dynamics. Such an approach resembles the phase–amplitude reductions presented earlier to great extent, and can be used to derive a network phase model similar to (11.16).

11.3. Global isochrons and isostables

Essential ingredients to determine the oscillator's response to perturbations are the phase sensitivity function $\boldsymbol{Z}$ and the isostable response functions $\boldsymbol{I}_n$ as the gradients to the phase and amplitude (isostable) coordinates. Leading order approximations of the reduced phase and isostable dynamics capitalize on phase sensitivity and isostable response functions that are evaluated at the limit cycle, on which isostable coordinates vanish. Beyond first order, it is possible to introduce a phase reduction with *global* phase sensitivity and isostable response functions as

$$\begin{aligned} \dot{\theta} &= \omega + \kappa\, \boldsymbol{Z}(\theta, \psi_1, \ldots, \psi_{n-1}) \cdot \boldsymbol{p}(t)\,, \\ \dot{\psi}_i &= k_i \psi_i + \kappa\, \boldsymbol{I}_n(\theta, \psi_1, \ldots, \psi_{n-1}) \cdot \boldsymbol{p}(t)\,, \quad \text{for } i = 1, \ldots, n-1, \end{aligned} \tag{11.32}$$

where $\boldsymbol{Z}$ and $\boldsymbol{I}_n$ are now evaluated along the full, or global, isochrons and not only in the mere vicinity of the periodic orbit. This reduction is exact in the whole basin of attraction of the limit cycle. While the to-be-presented approaches have not been extended to (weakly) coupled oscillators, we restrict their presentation to a single, weakly perturbed oscillator but remark that a possible network extension may follow the lines of Section 11.2.4.

11.3.1. Osinga et al.'s approach via a boundary value problem

The computation of isochrons dates back to the work by Winfree [19], introduced in more detail in Section 3.1. Isochrons cannot be found explicitly, except for very few examples, and numerical techniques must be employed. Knowing the (geometry of) isochrons in the whole basin of attraction of a stable limit cycle automatically leads to a full picture of the phase dynamics of a system subject to perturbations. The (numerical) computation of isochrons beyond a first local approximation in the neighborhood of the limit cycle, however, is not a trivial task. This is especially true in regions where isochrons accumulate and small perturbations have large effects, giving rise to the notion of extreme phase sensitivity. The here presented method by Osinga and co-workers to compute global isochrons, which is based on the continuation of a two-point boundary value problem, is applicable even in these regions of extreme phase sensitivity [303], see also [304].

We reconsider the linearized dynamics $\boldsymbol{x}(t) = \boldsymbol{x}^c(t) + \boldsymbol{u}(t)$ about the T-periodic orbit $\boldsymbol{x}^c(t)$ of the system $\dot{\boldsymbol{x}} = \boldsymbol{f}(\boldsymbol{x})$, that is, $\dot{\boldsymbol{u}}(t) = \boldsymbol{L}(t)\boldsymbol{u}(t)$ where $\boldsymbol{L}(t) = \nabla \boldsymbol{f}(\boldsymbol{x})\big|_{\boldsymbol{x}=\boldsymbol{x}^c(t)}$ as usual. If $\boldsymbol{u}(0)$ is tangent to an isochron, then $\boldsymbol{u}(T) = \lambda \boldsymbol{u}(0)$ with λ the Floquet multiplier for the periodic orbit. Locally, an isochron is given by the stable eigenvector of the linearization about the periodic orbit. This defines a boundary value problem and one can trace out isochrons by using different (small-magnitude) vectors in the direction $\boldsymbol{u}(0)$. In some cases, e.g., for slow–fast systems exhibiting so-called relaxation oscillations, $|\lambda|$ can be quite small and it is advantageous to define $\boldsymbol{u}(t) = \mathrm{e}^{\log(\lambda)t}\boldsymbol{w}(t)$ and $\tau = t/T$. Then, the two-point *boundary value problem* reads

$$\begin{aligned} \frac{d\boldsymbol{w}}{d\tau} &= T\big[\boldsymbol{L}(\tau) - \log(\lambda)\big]\boldsymbol{w}\,, \\ \boldsymbol{w}(1) &= \boldsymbol{w}(0)\,. \end{aligned} \tag{11.33}$$

As demonstrated in [303,304], the boundary value problem (11.33) can be solved with the numerical continuation software package AUTO [305].

11.3.2. Mauroy & Mezić's approach via Fourier averages

In contrast to identifying invariant sets, the approach by Mauroy and Mezić [306] employs the Koopman operator theory and tracks observables (or measures on a state space) to construct isochrons. Using the notation of Section 11.2.2 for the Koopman operator $U^t f(\boldsymbol{x}) = f \circ \phi(t, \boldsymbol{x})$ of an observable f and the flow ϕ associated with the dynamics $\dot{\boldsymbol{x}} = \boldsymbol{f}(\boldsymbol{x})$,

Mauroy and Mezić observed that isochrons of an T-periodic orbit $\boldsymbol{x}^c(t)$ with frequency $\omega = 2\pi/T$ are level sets of the *Fourier averages*

$$f^*_\omega(\boldsymbol{x}) = \lim_{\tau\to\infty} \frac{1}{\tau}\int_0^\tau U^t f(\boldsymbol{x}) \mathrm{e}^{-i\omega t} dt \ . \tag{11.34}$$

This follows from the fact that Fourier averages are eigenfunctions of the Koopman operator U^t. Fourier averages can be computed numerically for specific trajectories using forward integration of a set of initial condition. Isochrons can subsequently be obtained through interpolation. When considering complex-valued arguments λ_i instead of $\omega \in \mathbb{R}$, then (11.34) becomes a *Laplace average*. These play a key role for computing the isostables [307].

Furthermore, Mauroy & Mezić's approach can be used to estimate the phase sensitivity function $\boldsymbol{Z}$ and the isostable response functions $\boldsymbol{I}_i$, see [307] for the computational details. As the proposed method relies on forward integration, it is well-suited to compute phase and amplitude coordinates also in high-dimensional spaces.

11.3.3. Castejón, Guillamon & Huguet's approach via Lie symmetry

Another elegant approach to compute the phase and isostable coordinates has been proposed by Castejón, Guillamon and Huguet [291,308,309] for planar oscillatory dynamics. The stable manifold theorem [91] guarantees the existence of isochrons for a system $\dot{\boldsymbol{x}} = \boldsymbol{f}(\boldsymbol{x})$ T-periodic hyperbolically stable limit cycle solution $\boldsymbol{x}^c(t) \in \mathbb{R}^2$. Following a parameterization method [310], one can build on the existence of an analytic local diffeomorphism $K\colon \mathbb{S}^1 \times [\rho_-, \rho_+] \to \mathbb{R}^2; (\theta, \rho) \mapsto K(\theta, \rho)$ around the limit cycle and which satisfies the *invariance equation*

$$\omega\big(\partial_\theta + k\rho\partial_\rho\big)K(\theta,\rho) = \boldsymbol{f}\big(K(\theta,\rho)\big), \tag{11.35}$$

with $\omega = 2\pi/T$ the frequency and k the characteristic exponent of the limit cycle. Note that the change to phase–amplitude coordinates (θ, ρ) allows for describing the dynamics as consisting of a rigid rotation with constant velocity ω for θ and a contraction (if $k < 0$) with exponential rate $k\omega$ for ρ, that is,

$$\dot\theta = \omega \quad \text{and} \quad \dot\rho = \lambda\omega\rho$$

with associated flow $\phi\big(t, K(\theta,\rho)\big) = K\big(\theta + t\omega, \rho \mathrm{e}^{k\omega t}\big)$.

The parameterization K can be computed numerically, using, e.g., a series method [308] or a Newton method [309]. Moreover, isochrons and isostables as well as the phase sensitivity function and the isostable response function can be retrieved from the solution for K within the whole basin of attraction of the limit cycle. According to [Theorem 3.1, 308], isochrons are the orbits of a vector field $\boldsymbol{y}$ satisfying the *Lie symmetry* $[\boldsymbol{y}, \boldsymbol{f}] = \omega k \boldsymbol{y}$, which can alternatively be formulated as $\boldsymbol{y} \circ K(\theta,\rho) = \partial_\rho K(\theta,\rho)$. Isostables are the orbits of a vector field $\boldsymbol{z}$ satisfying $[\boldsymbol{z}, \boldsymbol{f}] = [\boldsymbol{f}, \boldsymbol{z}] = 0$. The global phase sensitivity and isostable response functions can then be found [291] as

$$\boldsymbol{Z}(\boldsymbol{x}) = \boldsymbol{Z}\big(K(\theta,\rho)\big) = \frac{\boldsymbol{J}\partial_\rho K(\theta,\rho)}{\big(\boldsymbol{J}\partial_\rho K(\theta,\rho)\big)^\intercal \partial_\theta K(\theta,\rho)}$$

$$\boldsymbol{I}(\boldsymbol{x}) = \boldsymbol{I}\big(K(\theta,\rho)\big) = \frac{\boldsymbol{J}\partial_\theta K(\theta,\rho)}{\big(\boldsymbol{J}\partial_\rho K(\theta,\rho)\big)^\intercal \partial_\theta K(\theta,\rho)}$$

with $\boldsymbol{J} = \begin{pmatrix} 0 & -1 \\ 1 & 0 \end{pmatrix}$. The global phase sensitivity function can readily be evaluated at the limit cycle, where $\rho = 0$. With $K(\theta, 0) = \boldsymbol{x}^c(\theta)$ and $\partial_\rho K(\theta, 0) = \boldsymbol{y}\big(K(\theta,0)\big) =: K_1(\theta)$, we then have

$$\boldsymbol{Z}(\theta) = \frac{\boldsymbol{J}K_1(\theta)}{\big(\boldsymbol{J}K_1(\theta)\big)^\intercal \boldsymbol{f}\big(\boldsymbol{x}^c(\theta)\big)} \ .$$

In [291,308], it has been shown that the adjoint method for computing the phase sensitivity function $\boldsymbol{Z}(\theta)$ and the isostable response function $\boldsymbol{I}(\theta)$ evaluated at the limit cycle, can also be extended to a neighborhood of the limit cycle. By this, the 'standard' adjoint method (Section 3.4) finds support to be applied for an accurate phase reduction beyond leading order approximations around the limit cycle.

12. Conclusion

Phase reduction is a classical, yet powerful technique for the analysis of oscillatory dynamics. The rigorous reduction to phase models allows for reformulating the dynamics of high-dimensional and analytically intractable models in a convenient way and to better understand (and control) a system's behavior. In this report our focus was on the extension of phase reduction techniques for complex oscillatory networks. Phase synchronization has become a well-established paradigm for investigating emergent phenomena and collective dynamics of complex networks. By deriving the phase dynamics of every oscillatory node of the network, including the corresponding coupling dynamics between them, one can reveal invaluable information about the entire network and readily infer the dynamic state of the network. Phase reduction thus proves auspicious and prospective for exploring, characterizing, and analyzing the dynamics of complex

oscillatory networks. There is, however, no unique method for a rigorous reduction to a phase model of networks of coupled oscillators, nor a straightforward recipe along which *the* phase dynamics should be reduced. Instead, one has to choose from a variety of different phase reduction techniques, all of which have their advantages and disadvantages. The various methods can be classified as either numerical, or analytic in nature, and stem from disciplines as different as the physics of complex systems, applied mathematics and nonlinear dynamics, as well as engineering. All in all, this renders the notion of phase dynamics somewhat ambiguous and, for any chosen technique, one ought to consider the reduced phase dynamics with care. This observation had led us to review and discuss the most prominent phase reduction techniques. With this report we aimed for creating a unified language of phase reduction applied to complex oscillatory networks by revisiting the different techniques, highlighting their similarities and differences, and pinpointing their limitations and caveats.

Not only did we shed light on the diversity of methods and the underlying methodologies, we also compared the outcome of the different reduction techniques in both qualitative and quantitative ways. We guided the presentation of our results along networks of weakly coupled, near-identical oscillators close to a Hopf bifurcation. Let us briefly recap why.

(1) The coupling strength between oscillators is assumed to be sufficiently small. This guaranteed that each oscillator's dynamics remained close to its unperturbed limit cycle and the dynamics could be assumed to relax back to the limit cycle instantaneously. Weak coupling cannot induce a bifurcation of the nodal dynamics. This allowed for disentangling the phase reduction of the oscillator network. That is, we could safely capitalize on the existing results about phase reduction for a single oscillator and readily extend these results to networks.
(2) The vicinity to a supercritical Hopf bifurcation ensured that the oscillatory dynamics could be reduced to Hopf normal form. Oscillations emerging through a Hopf bifurcation are generic. There exist abundant examples of real-life systems that can be described in this way. Nevertheless, there are other generic bifurcations that lead to oscillations, e.g., SNIC of homoclinic bifurcations. Normal forms and canonical models are available in these cases and they simplify a network analysis. Yet, the Hopf bifurcation guarantees a rigorous step-by-step normal form reduction along which the concept of isochrons can be upheld. Here, this assumption allowed for a detailed comparison between all phase reduction techniques.
(3) The coupling between oscillators was assumed to be pairwise. Together with the assumption of nearly identical oscillators, this facilitated a phase reduction of the network in so far that it sufficed to consider the phase dynamics of only two coupled oscillators and extend the results to the full network. In addition, the reduced phase interaction function exhibited all information required to infer and predict a network's phase synchronization properties. We distinguished between linear and non-linear coupling schemes. Extending settings to non-linear coupling offers application to more realistic network models. By the same token, our approach made the strengths and weaknesses of the different reduction techniques visible.

We prepared a thorough comparison between different phase reduction techniques. Insights about phase reduction of a single oscillator proved indispensable for the subsequent steps. We reviewed different approaches to derive a phase model from oscillatory dynamics in the first part of this report. Here, we introduced the distinction between numerical and analytic reduction techniques. The latter heavily rely on the generic normal form of the underlying dynamics, so that we complemented the first part with a discussion about the relation between phase reductions and normal forms. Given the role of the Hopf bifurcation for later sections, we put particular emphasis on Hopf normal form reductions and exemplified the different phase reduction techniques for a single oscillator in Hopf normal form.

Subsequently, we turned to oscillator networks. A first and important section was devoted to collective behavior of complex networks and how the concept of (phase) synchronization can be used to characterize the network dynamics. After having revisited Malkin's theorem for weakly coupled oscillators, we extended the previously established phase reduction techniques to a network of coupled oscillators in Hopf normal form. This involved a closer inspection of a network Hopf normal form, followed by a section how this network normal form can be reduced from underlying network dynamics.

We then presented a careful application of the phase reduction techniques to two exemplary network models. The first one consisted of coupled Brusselators and the second of coupled Wilson–Cowan neural masses. The two corresponding sections served to underline the differences between the techniques as well as their respective sensitivity to non-linear coupling terms, which often occur in real-life systems. Sticking to the assumptions above, we compared the different analytic and numerical approaches: Analytic techniques, which naturally split into a two-step reduction consisting of a normal form reduction and a subsequent phase reduction, have the advantage that they allow for a parameterization of the reduced phase model in terms of the original model parameters. When using numerical reduction techniques, by contrast, the link between phase model and original parameters may remain opaque unless phase reduction is extensively applied across large regions of parameter space. Numerical approaches can be used to reduce phase dynamics for almost every kind of oscillatory dynamics, whereas analytic approaches rely heavily on emerging oscillations via a particular bifurcation. However, once a system has been brought into Hopf normal form, all phase reduction techniques, including numerical approaches, result in the same reduced phase model, at least, in leading order. Notable differences between analytic approaches may emerge due to different normal form reductions whose accuracy depends on the distance to the Hopf bifurcation point. Very close to this point, the reduced phase models coincide almost perfectly for different analytic

and numerical reduction techniques. For larger distances from the bifurcation point, however, numerical techniques clearly outperform the analytic ones. A combination of both analytic and numerical reduction techniques, hence, appears unavoidable when looking for a complete picture of the emerging collective dynamics of interacting oscillators.

A brief comment is at place about the Haken approach, also coined ad-hoc averaging. This method clearly stands out for its pragmatic applicability. It allows for expressing the phase model parameters in terms of the original dynamics, in a straightforward way. The method also avoids the assumptions of the theory for weakly coupled oscillators. As long as small-amplitude oscillatory dynamics are of (or can be transformed into) circular shape, it is possible to (semi-) analytically reduce the corresponding phase dynamics — no matter whether these oscillations have emerged through a supercritical Hopf, any other or no bifurcation at all, whether they are induced by changes in coupling strength or in coupling direction, or induced by noise or delay. This approach may lack some mathematical rigor and the reduced phase dynamics have to be compared to the actual evolution of the phases. However, it can readily hint at the role of particular model parameters on the network dynamics, which can only be achieved by numerical techniques by a computationally expensive scanning of the parameter space.

A thorough comparison between different methodological approaches usually involves a quantitative account to what extent these techniques generate qualitatively equivalent results, which, in our case, are the reduced phase models. It would be desirable to present particular error estimates for each technique. When based on the original model parameters, it might be possible to set upper bounds beyond which a reduction technique can no longer be applied to determine the corresponding phase dynamics at a given (small) error. Such estimates are, however, few and far between. We hope that our inventory will serve to establish this long-needed error estimation.

As a potential way forward, we have indicated several ways of extending the presented phase reduction techniques for complex oscillatory networks. For a (better) understanding of realistic and physically meaningful, heterogeneous, and possibly time-varying networks through phase reduction, it is fundamental to consider the phenomenology of phase reduction of complex networks in rather simple setups, as considered here. Phase reduction can indeed be applied when loosening most of our main assumptions, such as homogeneity of oscillators or the pairwise coupling structure, and when including time delay as well as stochastic or time-varying inputs. We provided a brief review of phase–amplitude reductions beyond the weak coupling limit. Although we hinted at ways in which phase–amplitude models for a network of coupled oscillators may be reduced, as of yet few to no studies in this direction exist. After all, establishing a phase–amplitude description for networks is a natural next step. A unified treatment of the topic as presented here together with possible extensions can and may pave the way for an improved understanding of the collective behavior (and the control) of complex oscillatory networks through phase reduction.

Acknowledgments

We gratefully acknowledge the valuable discussions with Steven Coombes, Nicolás Deschle, Federico Devalle, Maxime Lucas, Peter McClintock, Ernest Montbrió, Hiroya Nakao, and Aneta Stefanovska. The work was supported by the ITN COSMOS program funded by the EU Horizon 2020 research and innovation programme under the Marie Skłodowska-Curie Grant Agreement No. 642563.

Appendix A. Mathematical details

A.1. Malkin's theorem for weakly coupled oscillators

Malkin's theorem states that a network of weakly coupled oscillators can conveniently be reduced into a phase model $\dot{\theta}_k = \omega_k + H(\theta_1 - \theta_k, \ldots, \theta_N - \theta_k)$ so that the collective dynamics of the network can readily be inferred from the properties of the phase interaction function H. The proof builds on a singular perturbation approach and capitalizes on the separation of time scales between the (relatively fast) natural oscillation of the independent oscillators, and their slowly accumulating phase deviations due to the weak coupling. We follow the presentation in [65]; cf. also [46]. For simplicity, we consider two weakly coupled oscillators $\boldsymbol{x}, \boldsymbol{x}' \in \mathbb{R}^n$ with dynamics

$$\dot{\boldsymbol{x}} = \boldsymbol{f}(\boldsymbol{x}) + \kappa\, \boldsymbol{g}(\boldsymbol{x}, \boldsymbol{x}'), \quad 0 \leq \kappa \ll 1; \tag{A.1.1}$$

the results naturally extend to networks of $N > 2$ coupled oscillators. The uncoupled dynamics, $\kappa = 0$, describes a T-periodic limit cycle $\mathcal{C}$. Along the corresponding trajectory $\boldsymbol{x}^c(t)$ on $\mathcal{C}$, one can define a uniformly increasing phase $\theta(t) = \omega t + \phi \mod T$, where the constants ϕ, ϕ' denote the relative phase of the oscillators $\boldsymbol{x}, \boldsymbol{x}'$, respectively. Without loss of generality, we set the natural frequency to one, $\omega = 1$. We can parametrize the limit cycle by the phase via $\boldsymbol{x}^c(t) = \boldsymbol{x}^c\big(\theta(t)\big) = \boldsymbol{x}^c\big(t + \phi\big)$. For small perturbations, or for weak coupling, the oscillator will be moved away from the limit cycle, but can be assumed to stay in its immediate vicinity, so that one can approximate the solution of (A.1.1) by $\boldsymbol{x}(t) \approx \boldsymbol{x}^c\big(t + \phi(t)\big)$. Note that the relative phase $\phi(t)$ has become a function of time t.

As said, it is convenient to define a "slow time" $\tau = \kappa t$, giving rise to the time-scale on which the coupling effects can build up. We assume that solutions $\boldsymbol{x}, \boldsymbol{x}'$ to (A.1.1) can be expressed as power-series in κ that depend on both t and τ, that is,

$$\boldsymbol{x}(t, \tau) = \boldsymbol{x}_0(t, \tau) + \kappa \boldsymbol{x}_1(t, \tau) + \mathcal{O}(\kappa^2)$$

and a corresponding expression holds for $\boldsymbol{x}'$. When substituting these expansions into (A.1.1) and using $\frac{d}{dt} = \frac{\partial}{\partial t} + \kappa \frac{\partial}{\partial \tau}$, one obtains

$$\frac{\partial \boldsymbol{x}_0}{\partial t} + \kappa \left(\frac{\partial \boldsymbol{x}_0}{\partial \tau} + \frac{\partial \boldsymbol{x}_1}{\partial t} \right) + \mathcal{O}(\kappa^2) = \boldsymbol{f}\left(\boldsymbol{x}_0 + \kappa \boldsymbol{x}_1 + \mathcal{O}(\kappa^2)\right) + \kappa\, \boldsymbol{g}\left(\boldsymbol{x}_0 + \kappa \boldsymbol{x}_1 + \mathcal{O}(\kappa^2), \boldsymbol{x}_0' + \kappa \boldsymbol{x}_1' + \mathcal{O}(\kappa^2)\right) . \tag{A.1.2}$$

After expanding the vector functions $\boldsymbol{f}$ and $\boldsymbol{g}$ in terms of κ as

$$\begin{aligned} \boldsymbol{f}\left(\boldsymbol{x}_0 + \kappa \boldsymbol{x}_1 + \mathcal{O}(\kappa^2)\right) &= \boldsymbol{f}(\boldsymbol{x}_0) + \kappa\, \nabla \boldsymbol{f}(\boldsymbol{x})\big|_{\boldsymbol{x}=\boldsymbol{x}_0} \boldsymbol{x}_1 + \mathcal{O}(\kappa^2) \\ \boldsymbol{g}\left(\boldsymbol{x}_0 + \kappa \boldsymbol{x}_1 + \mathcal{O}(\kappa^2), \boldsymbol{x}_0' + \kappa \boldsymbol{x}_1' + \mathcal{O}(\kappa^2)\right) &= \boldsymbol{g}\left(\boldsymbol{x}_0, \boldsymbol{x}_0'\right) + \mathcal{O}(\kappa) \end{aligned} \tag{A.1.3}$$

and inserting (A.1.3) into (A.1.2), we collect terms of the same order in κ. At leading order $\mathcal{O}(1)$, we find

$$\frac{\partial \boldsymbol{x}_0}{\partial t} = \boldsymbol{f}(\boldsymbol{x}_0) , \tag{A.1.4}$$

which describes the dynamics of the uncoupled oscillators. Eq. (A.1.4) implies that the relative phase ϕ is constant on the (fast) time-scale t, but evolves with respect to the slow time τ, that is, $\boldsymbol{x}_0 = \boldsymbol{x}^c\left(t + \phi(\tau)\right)$. One can use these solutions to find for the order $\mathcal{O}(\kappa)$-terms in (A.1.2) (and after shifting t appropriately)

$$\mathcal{L}\boldsymbol{x}_1 \equiv \frac{\partial \boldsymbol{x}_1}{\partial t} - \boldsymbol{L}(t)\boldsymbol{x}_1 = \boldsymbol{g}\left(\boldsymbol{x}^c(t), \boldsymbol{x}^c\left(t + \phi'(\tau) - \phi(\tau)\right)\right) - \boldsymbol{f}\left(\boldsymbol{x}^c(t)\right)\frac{d\phi}{dt} , \tag{A.1.5}$$

where $\boldsymbol{L}(t) = \nabla \boldsymbol{f}(\boldsymbol{x})\big|_{\boldsymbol{x}=\boldsymbol{x}^c(t)}$. Given the linear operator $\mathcal{L}\boldsymbol{x} \equiv \frac{\partial \boldsymbol{x}}{\partial t} - \boldsymbol{L}(t)\boldsymbol{x}$, the solvability of (A.1.5) can be proven by dwelling on the Fredholm alternative for linear differential equations with T-periodic coefficients [283]. The corresponding solvability equation requires that

$$\frac{1}{T}\int_0^T \boldsymbol{Z}(t) \cdot \left[\boldsymbol{g}\left(\boldsymbol{x}^c(t), \boldsymbol{x}^c\left(t + \phi'(\tau) - \phi(\tau)\right)\right) - \boldsymbol{f}\left(\boldsymbol{x}^c(t)\right)\frac{d\phi}{dt} \right] dt = 0 \tag{A.1.6}$$

with $\boldsymbol{Z}$ a T-periodic solution of the adjoint equation

$$\mathcal{L}^*\boldsymbol{Z} = -\frac{\partial \boldsymbol{Z}}{\partial t} - \boldsymbol{L}(t)^\intercal \boldsymbol{Z} = 0 .$$

In order to obtain uniqueness, one normalizes $\boldsymbol{Z}(t)$ according to

$$\frac{1}{T}\int_0^T \boldsymbol{Z}(t) \cdot \boldsymbol{f}\left(\boldsymbol{x}^c(t)\right)\, dt = 1 ,$$

which is equivalent to setting $\boldsymbol{Z}(0) \cdot \boldsymbol{f}\left(\boldsymbol{x}^c(0)\right) = 1$. Eventually, we can rearrange (A.1.6) and obtain the phase dynamics (in the ordinary phase variable $\theta = \omega t + \phi$ and recalling that $\tau = \kappa t$)

$$\dot{\theta} = \omega + \kappa\, H(\theta' - \theta) \quad \text{with} \quad H(\psi) = \frac{1}{T}\int_0^T \boldsymbol{Z}(t) \cdot \boldsymbol{g}(\boldsymbol{x}^c(t), \boldsymbol{x}^c\left(t + \psi\right))dt .$$

A.2. Kuramoto's reductive perturbation

A.2.1. Basic theory

Let us consider two coupled systems $\boldsymbol{x}, \boldsymbol{x}' \in \mathbb{R}^n$, whose dynamics are described by

$$\dot{\boldsymbol{x}} = \boldsymbol{f}(\boldsymbol{x}, t; \mu) + \kappa \boldsymbol{g}(\boldsymbol{x}, \boldsymbol{x}', t; \mu) \tag{A.2.1}$$

and an equivalent expression holds for $\boldsymbol{x}'$, with $\boldsymbol{f}\colon \mathbb{R}^n \to \mathbb{R}^n$, the coupling function $\boldsymbol{g}\colon \mathbb{R}^n \times \mathbb{R}^n \to \mathbb{R}^n$ with coupling strength $\kappa \in \mathbb{R}$ and a bifurcation parameter $\mu \in \mathbb{R}$. We assume $\boldsymbol{x}_0(\mu)$ a steady solution for $\kappa = 0$, i.e., $\boldsymbol{f}(\boldsymbol{x}_0(\mu); \mu) = 0$ for all μ. We set

$$\tilde{\boldsymbol{x}} = \boldsymbol{x} - \boldsymbol{x}_0 \quad \text{and} \quad \tilde{\boldsymbol{x}}' = \boldsymbol{x}' - \boldsymbol{x}_0 ,$$

and expand $\boldsymbol{f}$ around $\boldsymbol{x} = \boldsymbol{x}_0$, or around $\tilde{\boldsymbol{x}} = 0$, respectively. By omitting the tilde, we have

$$\boldsymbol{f}(\boldsymbol{x}; \mu) = \boldsymbol{n}_1(\boldsymbol{x}; \mu) + \boldsymbol{n}_2(\boldsymbol{x}, \boldsymbol{x}; \mu) + \boldsymbol{n}_3(\boldsymbol{x}, \boldsymbol{x}, \boldsymbol{x}; \mu) + \mathcal{O}(|\boldsymbol{x}|^4) ,$$

where the $\boldsymbol{n}_k$ are given by

$$\boldsymbol{n}_k(\boldsymbol{u}^{(1)}, \boldsymbol{u}^{(2)}, \ldots, \boldsymbol{u}^{(k)}; \mu) = \sum_{i_1,\ldots,i_k=1}^{n} \frac{1}{k!} \left(\frac{\partial^k F(\boldsymbol{x}; \mu)}{\partial x_{i_1} \partial x_{i_2} \ldots \partial x_{i_k}} \right)_{\boldsymbol{x}=\boldsymbol{0}} u_{i_1}^{(1)} u_{i_2}^{(2)} \ldots u_{i_k}^{(k)} \tag{A.2.2}$$

with $\boldsymbol{u}^{(j)} = \left(u_1^{(j)}, \ldots, u_n^{(j)}\right) \in \mathbb{R}^n$. Note that the $\boldsymbol{n}_k$ are symmetric in their arguments $\boldsymbol{u}^{(1)}, \ldots, \boldsymbol{u}^{(k)}$. We further expand $\boldsymbol{n}_k$ with respect to μ, e.g., $\boldsymbol{n}_1(\boldsymbol{x}; \mu) = \hat{\boldsymbol{L}}_0 \boldsymbol{x} + \mu \hat{\boldsymbol{L}}_1 \boldsymbol{x} + \ldots$, and obtain

$$\boldsymbol{f}(\boldsymbol{x}; \varepsilon^2) = \hat{\boldsymbol{L}}_0 \boldsymbol{x} + \mu \hat{\boldsymbol{L}}_1 \boldsymbol{x} + M_0 \boldsymbol{x}\boldsymbol{x} + N_0 \boldsymbol{x}\boldsymbol{x}\boldsymbol{x} + \mathcal{O}(|\boldsymbol{x}|^4) , \tag{A.2.3}$$

where $M_0\boldsymbol{u}\boldsymbol{v} = \boldsymbol{n}_2(\boldsymbol{u}, \boldsymbol{v}; \mu = 0)$ and $N_0\boldsymbol{u}\boldsymbol{v}\boldsymbol{w} = \boldsymbol{n}_3(\boldsymbol{u}, \boldsymbol{v}, \boldsymbol{w}; \mu = 0)$. We thus discard all $\mathcal{O}(\mu)$ terms in $\boldsymbol{n}_2$ and $\boldsymbol{n}_3$ in (A.2.3). Furthermore, we Taylor-expand $\boldsymbol{g}$ as

$$\boldsymbol{g}(\boldsymbol{x}, \boldsymbol{x}') = G_0 + G_{10}\boldsymbol{x} + G_{01}\boldsymbol{x}' + G_{20}\boldsymbol{x}^2 + G_{11}\boldsymbol{x}\boldsymbol{x}' + G_{02}\boldsymbol{x}'^2 + \cdots \,. \tag{A.2.4}$$

If the system undergoes a supercritical Hopf bifurcation at $\mu = 0$ (and $\kappa = 0$), the operator $\hat{\boldsymbol{L}}_0$ has a set of eigenvalues $\sigma(\hat{\boldsymbol{L}}_0) = \{\lambda^\alpha \mid \alpha = 1, \ldots, n\}$, each of which can be expanded as $\lambda^\alpha = \lambda_0^\alpha + \mu\lambda_1^\alpha + \ldots$. The Hopf bifurcation condition requires that $\lambda_0^1 = -\lambda_0^2 = i\omega_0$ are purely imaginary and that $\mathrm{Re}(\lambda_0^\alpha) > 0$ for all $\alpha > 2$. For convenience, we set $\boldsymbol{u} = \boldsymbol{u}_1$ as the right eigenvector of $\hat{L}_0$ corresponding to the eigenvalue $\lambda_0^1 = \lambda_0$, that is

$$\hat{\boldsymbol{L}}_0\boldsymbol{u} = \lambda_0\boldsymbol{u} \quad \text{and} \quad \hat{\boldsymbol{L}}_0\bar{\boldsymbol{u}} = \bar{\lambda}_0\bar{\boldsymbol{u}}$$

where $\lambda_0^2 = \bar{\lambda}_0$. Likewise, we denote by $\boldsymbol{v} = \boldsymbol{v}_1$ the left eigenvector of $\hat{\boldsymbol{L}}_0$ corresponding to the eigenvalue $\lambda_0^1 = \lambda_0$: $\boldsymbol{v}\hat{\boldsymbol{L}}_0 = \lambda_0\boldsymbol{v}$. The left and right eigenvectors fulfill $\boldsymbol{v}\bar{\boldsymbol{u}} = \bar{\boldsymbol{v}}\boldsymbol{u} = 0$. Next, we normalize them such that $\boldsymbol{v}\boldsymbol{u} = \bar{\boldsymbol{v}}\bar{\boldsymbol{u}} = 1$. In particular, we have

$$\begin{aligned}\lambda_0 &= \sigma_0 + i\omega_0 = \boldsymbol{v}\hat{L}_0\boldsymbol{u}\\ \lambda_1 &= \sigma_1 + i\omega_1 = \boldsymbol{v}\hat{L}_1\boldsymbol{u}\,.\end{aligned}$$

With this, the solution to the linearized unperturbed system, $\dot{\boldsymbol{x}} = \hat{L}_0\boldsymbol{x}$, is given by

$$\boldsymbol{x}_0(t) = w\mathrm{e}^{i\omega_0 t}\boldsymbol{u} + \bar{w}\mathrm{e}^{-i\omega_0 t}\bar{\boldsymbol{u}}\,, \tag{A.2.5}$$

where w is an arbitrary complex number, which we will refer to as the complex amplitude. For the full dynamics (A.2.1) including the perturbations, $\boldsymbol{x}(t)$ generally deviates from $\boldsymbol{x}_0(t)$. To describe the asymptotic evolution of $\boldsymbol{x}(t)$, we consider the complex amplitude w to be time dependent. In the following, we will derive the dynamics of w in the form

$$\dot{w} = f(w, \bar{w}) + \varepsilon^2\kappa g(w, \bar{w}, w', \bar{w}')\,, \tag{A.2.6}$$

where the prime ($'$) indicates the coupled oscillator.

We define $\varepsilon = \sqrt{|\mu|}$ and $\chi = \mathrm{sgn}\,\mu$ and consider $\boldsymbol{x} = \boldsymbol{x}_1 + \boldsymbol{x}_2 + \ldots$ where $\boldsymbol{x}_l = \mathcal{O}(\varepsilon^l)$. When abbreviating $\boldsymbol{n}_1(\boldsymbol{x}) = \boldsymbol{L}\boldsymbol{x}$, we have $\boldsymbol{L} = \hat{\boldsymbol{L}}_0 + \chi\varepsilon^2\hat{\boldsymbol{L}}_1 + \mathcal{O}(\varepsilon^4)$. We further introduce a scaled time $\tau = \varepsilon^2 t$ such that $\boldsymbol{x} = \boldsymbol{x}(t, \tau)$ depends both on t and τ, which should be treated as mutually independent. Then, the time derivative becomes

$$\frac{d}{dt} \to \frac{\partial}{\partial t} + \varepsilon^2\frac{\partial}{\partial\tau}\,.$$

Taken together, (A.2.3) reads

$$\begin{aligned}&\left(\frac{\partial}{\partial t} + \varepsilon^2\frac{\partial}{\partial\tau} - \hat{\boldsymbol{L}}_0 - \varepsilon^2\chi\hat{\boldsymbol{L}}_1 - \cdots\right)(\boldsymbol{x}_1 + \boldsymbol{x}_2 + \cdots) =\\ &\qquad M_0\boldsymbol{x}_1\boldsymbol{x}_1 + (2M_0\boldsymbol{x}_1\boldsymbol{x}_2 + N_0\boldsymbol{x}_1\boldsymbol{x}_1\boldsymbol{x}_1) + \mathcal{O}(\varepsilon^4)\\ &\qquad + \kappa\left[G_0 + \varepsilon\left(G_{10}\boldsymbol{x}_1 + G_{01}\boldsymbol{x}_1'\right) + \varepsilon^2\left(G_{20}\boldsymbol{x}_1\boldsymbol{x}_1 + G_{11}\boldsymbol{x}_1\boldsymbol{x}_1' + G_{02}\boldsymbol{x}_1'\boldsymbol{x}_1'\right) + \mathcal{O}(\varepsilon^3)\right]\,.\end{aligned} \tag{A.2.7}$$

For merely weak coupling, that is, $0 < \kappa \ll \mu \ll 1$, it is appropriate to assume $\kappa \mapsto \varepsilon^2\kappa$. The right-hand side of (A.2.7) becomes

$$(M_0\boldsymbol{x}_1\boldsymbol{x}_1 + \kappa G_0) + \left(2M_0\boldsymbol{x}_1\boldsymbol{x}_2 + N_0\boldsymbol{x}_1\boldsymbol{x}_1\boldsymbol{x}_1 + \varepsilon^2\kappa\left[G_{10}\boldsymbol{x}_1 + G_{01}\boldsymbol{x}'_1\right]\right) + \mathcal{O}(\varepsilon^4)\,. \tag{A.2.8}$$

The term in the first parentheses is of order $\mathcal{O}(\varepsilon^2)$ and the term in the second of order $\mathcal{O}(\varepsilon^3)$. For this particular choice of coupling parameter $\eta = \varepsilon^2\kappa$, the coupling function reduces to at most linear coupling terms. If, e.g., $\eta = \mathcal{O}(\varepsilon)$, then also quadratic terms have to be taken into account. Here, however, we constrain ourselves to linear coupling. Comparing the coefficients of different powers of ε in (A.2.7), we get a set of equations of the form

$$\left(\frac{\partial}{\partial t} - \hat{\boldsymbol{L}}_0\right)\boldsymbol{x}_\nu = \boldsymbol{B}_\nu\,, \quad \nu = 1, 2, \ldots\,, \tag{A.2.9}$$

where $\boldsymbol{B}_\nu = \mathcal{O}(\varepsilon^\nu)$ and the first $\boldsymbol{B}_\nu$'s are given by

$$\begin{aligned}\boldsymbol{B}_1 &= 0\,,\\ \boldsymbol{B}_2 &= M_0\boldsymbol{x}_1\boldsymbol{x}_1 + \varepsilon^2\kappa G_0\,,\\ \boldsymbol{B}_3 &= -\left(\varepsilon^2\frac{\partial}{\partial\tau} - \varepsilon^2\chi\hat{L}_1\right)\boldsymbol{x}_1 + 2M_0\boldsymbol{x}_1\boldsymbol{x}_2 + N_0\boldsymbol{x}_1\boldsymbol{x}_1\boldsymbol{x}_1 + \varepsilon^2\kappa\left[G_{10}\boldsymbol{x}_1 + G_{01}\boldsymbol{x}'_1\right]\,.\end{aligned} \tag{A.2.10}$$

In general, the $\boldsymbol{B}_\nu$'s are depending on $\boldsymbol{x}_{\nu'}$ with $\nu' < \nu$. Therefore, one can solve the system (A.2.9) of linear inhomogeneous differential equations subsequently. Computation can be simplified by using the following *solvability condition*.

Lemma A.1. *The solvability condition for system (A.2.9) reads*

$$\boldsymbol{v}\boldsymbol{B}_{\nu}^{(1)}(\tau)=0\ , \tag{A.2.11}$$

where $\boldsymbol{B}_{\nu}^{(1)}$ *is the first Fourier coefficient of the expansion*

$$\boldsymbol{B}_{\nu}(t,\tau)=\sum_{l=-\infty}^{\infty}\boldsymbol{B}_{\nu}^{(l)}(\tau)\mathrm{e}^{il\omega_0 t}\ . \tag{A.2.12}$$

Proof. First of all, we use the fact that

$$\int_0^{2\pi/\omega_0}\boldsymbol{v}\boldsymbol{B}_{\nu}\mathrm{e}^{-i\omega_0 t}\,dt=\int_0^{2\pi/\omega_0}\boldsymbol{v}^{\intercal}\cdot\boldsymbol{B}_{\nu}\mathrm{e}^{-i\omega_0 t}\,dt=0\ , \tag{A.2.13}$$

which we prove via

$$\begin{aligned}\int_0^{2\pi/\omega_0}\boldsymbol{v}^{\intercal}\cdot\boldsymbol{B}_{\nu}\mathrm{e}^{-i\omega_0 t}\,dt&\overset{(A.2.9)}{=}\int_0^{2\pi/\omega_0}\left[\boldsymbol{v}^{\intercal}\cdot\left(\frac{\partial}{\partial t}-\hat{L}_0\right)\boldsymbol{x}_{\nu}\right]\mathrm{e}^{-i\omega_0 t}\,dt\quad(\text{note that }\lambda_0=i\omega_0)\\&=\int_0^{2\pi/\omega_0}\left[\boldsymbol{v}\left(\lambda_0\boldsymbol{x}_{\nu}\right)-\left(\boldsymbol{v}\hat{\boldsymbol{L}}_0\right)\boldsymbol{x}_{\nu}\right]\mathrm{e}^{-i\omega_0 t}\,dt=0\ ,\end{aligned}$$

where the second equality is due to partial integration and the last due to $\boldsymbol{v}$ being the left eigenvector of $\hat{\boldsymbol{L}}_0$ corresponding to the eigenvalue λ_0.

Having a closer look at system (A.2.9), the homogeneous part suggests that the $\boldsymbol{x}_{\nu}$'s are 2π-periodic functions of $\omega_0 t$. Hence, also $\boldsymbol{B}_{\nu}=\boldsymbol{B}_{\nu}(t,\tau)$ has to be 2π-periodic, which admits the Fourier expansion (A.2.12). Substituting the latter into (A.2.13), we have

$$\int_0^{2\pi/\omega_0}\boldsymbol{v}\boldsymbol{B}_{\nu}\mathrm{e}^{-i\omega_0 t}\,dt=\sum_{l=-\infty}^{\infty}\int_0^{2\pi/\omega_0}\boldsymbol{v}\boldsymbol{B}_{\nu}^{(l)}(\tau)\mathrm{e}^{i(l-1)\omega_0 t}\,dt=0\ .$$

Evaluating all the integrals on the right-hand side, we see that all but the one where $l=1$ vanish, which leaves the solvability condition (A.2.11). □

Now, one can solve system (A.2.9) iteratively. For $\nu=1$, we have

$$\left(\frac{\partial}{\partial t}-\hat{\boldsymbol{L}}_0\right)\boldsymbol{x}_1=0\ ,$$

which provides the "neutral solution"

$$\boldsymbol{x}_1(t,\tau)=w(\tau)\boldsymbol{u}\mathrm{e}^{i\omega_0 t}+c.c. \tag{A.2.14}$$

where $w(\tau)$ is the complex amplitude and $c.c.$ stands for the complex conjugate of the foregoing part. In particular, we have $|w(\tau)|=\mathcal{O}(\varepsilon)$. As to $\nu=2$, we would like to mention first that since $\boldsymbol{x}_1\propto\mathrm{e}^{i\omega_0 t}$, the term $M_0\boldsymbol{x}_1\boldsymbol{x}_1\propto\mathrm{e}^{2i\omega_0 t}$. Due to the solvability condition (A.2.13), we know that (i) $\boldsymbol{B}_2$ has to be periodic and that (ii) the constant coupling term G_0 has to vanish as it will be averaged out. In the case that the coupling function $\boldsymbol{g}$ in (A.2.1) is explicitly time-dependent, in particular, all terms G_{jk} in (A.2.4) have to be time-dependent, we can likewise Fourier expand G_0 and see that the first two coefficients $G_0^{(0)}=G_0^{(1)}=0$ have to vanish. One can argue in the same manner that all even Fourier coefficients $G_{jk}^{(2n)}$, $n=0,1,2,\ldots$, of any coupling term G_{jk}, $j,k\in\mathbb{N}$, must be zero. In any case, $\boldsymbol{B}_2$ only contains zeroth and $\geq$ 2nd harmonics, and the same holds for $\boldsymbol{x}_2(t,\tau)$. Hence, we can write

$$\boldsymbol{x}_2(t,\tau)=\boldsymbol{V}_{+}w(\tau)^2\mathrm{e}^{2i\omega_0 t}+\boldsymbol{V}_{-}\bar{w}(\tau)^2\mathrm{e}^{-2i\omega_0 t}+\boldsymbol{V}_0|w(\tau)|^2+h.h. \tag{A.2.15}$$

where $h.h.$ stands for higher harmonics that will not be further discussed. Substituting $\boldsymbol{x}_2$ into (A.2.9) and comparing coefficients of different harmonics, we can solve the equation for the constants $\boldsymbol{V}_{\pm,0}$. We find

$$\boldsymbol{V}_{+}=\overline{\boldsymbol{V}_{-}}=-\left(\hat{\boldsymbol{L}}_0-2i\omega_0\right)^{-1}M_0\boldsymbol{u}\boldsymbol{u}\quad\text{and}\quad\boldsymbol{V}_0=-2\hat{\boldsymbol{L}}_0^{-1}M_0\boldsymbol{u}\bar{\boldsymbol{u}}\ . \tag{A.2.16}$$

For $\nu=3$, we first substitute in $\boldsymbol{x}_1$ and $\boldsymbol{x}_2$ into $\boldsymbol{B}_3$ as given in (A.2.10), and subsequently solve for the first Fourier coefficient

$$\begin{aligned}\boldsymbol{B}_3^{(1)}(\tau)=&-\left(\varepsilon^2\frac{\partial}{\partial\tau}-\varepsilon^2\chi\hat{\boldsymbol{L}}_1\right)w(\tau)\boldsymbol{u}+\left(2M_0\boldsymbol{u}\boldsymbol{V}_0+2M_0\bar{\boldsymbol{u}}\boldsymbol{V}_{+}+3N_0\boldsymbol{u}\boldsymbol{u}\bar{\boldsymbol{u}}\right)|w(\tau)|^2w(\tau)\\&+\varepsilon^2\kappa\left(G_{10}\boldsymbol{u}w(\tau)+G_{01}\boldsymbol{u}w'(\tau)\right)\ ,\end{aligned} \tag{A.2.17}$$

where we assumed no explicit dependence of $\boldsymbol{g}$ on time. Using the solvability condition (A.2.11), i.e., $\boldsymbol{v}\boldsymbol{B}_3^{(1)} = 0$, and that $\boldsymbol{v}w\boldsymbol{u} = w$, we finally arrive at the amplitude equation

$$\dot{w} = \alpha w - \beta|w|^2 w + \varepsilon^2\kappa\left(\gamma_1 w + \gamma_2 w'\right) \tag{A.2.18}$$

with complex constants

$$\begin{aligned} \alpha &= \boldsymbol{v}\varepsilon^2\chi\hat{\boldsymbol{L}}_1\boldsymbol{u}, \\ \beta &= -\left(2\boldsymbol{v}M_0\boldsymbol{u}\boldsymbol{V}_0 + 2\boldsymbol{v}M_0\bar{\boldsymbol{u}}\boldsymbol{V}_+ + 3\boldsymbol{v}N_0\boldsymbol{u}\boldsymbol{u}\bar{\boldsymbol{u}}\right), \\ \gamma_1 &= \boldsymbol{v}G_{10}\boldsymbol{u}, \\ \gamma_2 &= \boldsymbol{v}G_{01}\boldsymbol{u}\ . \end{aligned} \tag{A.2.19}$$

Returning to the original notation with the $\boldsymbol{n}_k$ and noting that the latter are linear in each of their arguments, we have

$$\beta = -2\boldsymbol{v}\boldsymbol{n}_3\left(\boldsymbol{u},\boldsymbol{u},\bar{\boldsymbol{u}}\right) + 4\boldsymbol{v}\boldsymbol{n}_2\left(\bar{\boldsymbol{u}},\hat{\boldsymbol{L}}_0^{-1}\boldsymbol{n}_2\left(\boldsymbol{u},\bar{\boldsymbol{u}}\right)\right) + 2\boldsymbol{v}\boldsymbol{n}_2\left(\boldsymbol{u},\left(\hat{\boldsymbol{L}}_0 - 2i\omega_0\right)^{-1}\boldsymbol{n}_2\left(\boldsymbol{u},\boldsymbol{u}\right)\right)\ . \tag{A.2.20}$$

As a final remark about the dot-notation in the amplitude equation (A.2.18), we replaced $\varepsilon^2\partial/\partial\tau$ by $\partial/\partial t$, such that the derivative is now taken with respect to the original time t, although $w = w(\varepsilon^2 t)$ changes only slowly.

For the initial dynamics (A.2.1), we seek for the phase dynamics of the perturbed solution $\boldsymbol{x}(t)$ from the linearized solution $\boldsymbol{x}_0(t)$. We can write $\boldsymbol{x}(t)$ as

$$\boldsymbol{x}(t) = w(t)\mathrm{e}^{i\omega_0 t}\boldsymbol{u} + \bar{w}(t)\mathrm{e}^{-i\omega_0 t}\bar{\boldsymbol{u}} + h.h. \tag{A.2.21}$$

Differentiating with respect to time t and inserting (A.2.18) gives $\dot{\boldsymbol{x}}(t) = W\mathrm{e}^{i\omega_0 t}\boldsymbol{u} + c.c. + h.h.$, where $W = \dot{w} + i\omega_0 w$ describes the full amplitude dynamics

$$\dot{w} = (\alpha + i\omega_0)w - \beta|w|^2 w + \varepsilon^2\kappa(\gamma_1 w + \gamma_2 w') \tag{A.2.22}$$

on the slower time scale, where the natural frequency ω_0 is added to the dynamics of mere amplitude deviations (A.2.18).

Following the theory of weakly coupled oscillators, the crucial assumption for the coupling constant is that

$$\eta = \varepsilon^2\kappa \quad \text{with } 0 < \kappa < \varepsilon \ll 1\ . \tag{A.2.23}$$

This allows the linear coupling term to be correct of order $\mathcal{O}(\varepsilon)$. Higher-order corrections of the coupling term up to order $\mathcal{O}(\varepsilon^3)$ have been presented by Kori and co-workers [177] and we will elaborate on them further in Appendix A.2.2. If we drop the assumption (A.2.23), we may consider nonlinear coupling terms in the phase-space dynamics (A.2.1). Furthermore, the inhomogeneities $\boldsymbol{B}_\nu$ in the reduced system (A.2.9) take more intricate forms and the derivation leading to the amplitude equation (A.2.18) has to be revised accordingly.

Remark. The here presented Reductive Perturbation Method as one possible phase reduction technique has been established by Kuramoto [12]. Another technique closely linked is the so-called Renormalization Group Method of Goldenfeld, Oono and co-coworkers [311,312]. Kunihiro demonstrated the intricate link between the two methods [313]: Kuramoto's solvability condition (A.2.11) can be circumvented by introducing an appropriately chosen constant δ such that unwanted secular terms vanish.

A.2.2. Higher-order corrections and nonlinear coupling

We here follow the theory established in the preceding section. Not only do we want to establish higher-order corrections of the coupling term up to order $\mathcal{O}(\varepsilon^3)$ as presented by Kori and co-workers [177], but also we refrain from the direct, linear coupling. Note that the results (A.2.19) for the parameters $\alpha, \beta, \gamma_{1,2}$ remain the same for nonlinear coupling. Yet, if we allow for higher-order corrections in the amplitude equation (A.2.18), that is, in

$$\dot{w} = \alpha w - \beta|w|^2 w + \varepsilon^2\kappa(\gamma w' + \delta\bar{w}w'^2)\ , \tag{A.2.24}$$

the additional parameter δ will incorporate the nonlinear effects of the underlying coupling nonlinearity in the original dynamics.

Therefore, in the notation of the preceding section we consider the coupling function

$$\begin{aligned} \boldsymbol{g}(\boldsymbol{x},\boldsymbol{x}') = {} & G_{10}\boldsymbol{x} + G_{01}\boldsymbol{x}' + G_{20}(\boldsymbol{x}) + G_{11}(\boldsymbol{x},\boldsymbol{x}') + G_{02}(\boldsymbol{x}') \\ & + G_{30}(\boldsymbol{x}) + G_{21}(\boldsymbol{x},\boldsymbol{x}') + G_{12}(\boldsymbol{x},\boldsymbol{x}') + G_{03}(\boldsymbol{x}') + \cdots\ , \end{aligned} \tag{A.2.25}$$

where the functions

$$G_{jk}(\boldsymbol{x},\boldsymbol{x}') = G_{jk}(\underbrace{\boldsymbol{x},\ldots,\boldsymbol{x}}_{j\text{ times}},\underbrace{\boldsymbol{x}',\ldots,\boldsymbol{x}'}_{k\text{ times}}) \tag{A.2.26}$$

are of order $G_{jk} = \mathcal{O}(\varepsilon^{j+k})$ for $\boldsymbol{x},\boldsymbol{x}' = \mathcal{O}(\varepsilon)$. For instance, we are interested in the effect of nonlinear coupling terms $xx', yx', x^2x', xyx', y^2x'$ when $\boldsymbol{x} = (x,y), \boldsymbol{x}' = (x',y')$ are two-dimensional. Possible examples for G_{jk} are $G_{11}(\boldsymbol{x},\boldsymbol{x}') =$

$a \cdot xx' + b \cdot yx'$ or $G_{21}(\boldsymbol{x}, \boldsymbol{x}') = c \cdot x^2x' + d \cdot xyx' + e \cdot y^2x'$ with parameters $a, \ldots, e$. More general, if we write all possible products of $(x, y), (x', y')$ of order $j + k$ as a vector

$$(x, y)^j * (x', y')^k := \begin{pmatrix} x^j x'^k, x^{j-1} y x'^k, \ldots, y^j x'^k, x^j x'^{k-1} y', \ldots, \ldots, y^j y'^k \\ x^j x'^k, x^{j-1} y x'^k, \ldots, y^j x'^k, x^j x'^{k-1} y', \ldots, \ldots, y^j y'^k \end{pmatrix}^\intercal ,$$

we can rewrite the coupling terms G_{jk} as

$$G_{jk}\left((x, y), (x', y')\right) = \boldsymbol{G}_{jk}\left[(x, y)^j * (x', y')^k\right] \tag{A.2.27}$$

with $\boldsymbol{G}_{jk}$ a $2 \times (j + 1)(k + 1)$-matrix. In particular, $\boldsymbol{G}_{10}$ and $\boldsymbol{G}_{01}$ are quadratic, 2×2-matrices.

As before, we denote by $\boldsymbol{x}_0(t)$ the solution to the linearized unperturbed system $\dot{\boldsymbol{x}} = \hat{\boldsymbol{L}}_0 \boldsymbol{x}$. The general solution, though, will be of the form

$$\boldsymbol{x} = \boldsymbol{x}_0(w, \bar{w}, \theta) + \boldsymbol{\rho}(w, \bar{w}, w', \bar{w}', \theta) \ \in \mathbb{R}^n , \tag{A.2.28}$$

with $w \in \mathbb{C}$ following the dynamics (A.2.6). For convenience, we rewrite the dynamics as

$$\dot{\boldsymbol{x}} = \hat{\boldsymbol{L}}_0 \boldsymbol{x} + \varepsilon^2 \hat{\boldsymbol{L}}_1 \boldsymbol{x} + \boldsymbol{n}_2(\boldsymbol{x}, \boldsymbol{x}) + \boldsymbol{n}_3(\boldsymbol{x}, \boldsymbol{x}, \boldsymbol{x}) + \varepsilon^2 \kappa \ \boldsymbol{g}(\boldsymbol{x}, \boldsymbol{x}') , \tag{A.2.29}$$

$$\dot{w} = \mathcal{W}(w, \bar{w}, w', \bar{w}') . \tag{A.2.30}$$

The functions $\mathcal{W}$ and $\boldsymbol{\rho}$ have to be determined perturbatively, as outlined in the preceding section. Note also that $\mathcal{W}$ is free from $\theta = \theta(t)$. If we insert the ansatz (A.2.28) into (A.2.29) and use (A.2.30), we find

$$\mathcal{L}_0 \boldsymbol{\rho} = \mathcal{W} \exp(i\theta)\boldsymbol{u} + \bar{\mathcal{W}} \exp(-i\theta)\bar{\boldsymbol{u}} + \boldsymbol{b}(w, \bar{w}, w', \bar{w}', \theta) , \tag{A.2.31}$$

with the operator $\mathcal{L}_0 = \left(\hat{\boldsymbol{L}}_0 - \omega_0 \frac{\partial}{\partial \theta}\right)$, the right eigenvector $\boldsymbol{u}$ of $\hat{\boldsymbol{L}}_0$ corresponding to the eigenvalue $i\omega_0$, and where

$$\boldsymbol{b} = -\varepsilon^2 \hat{L}_1 \boldsymbol{x} - \boldsymbol{n}_2(\boldsymbol{x}, \boldsymbol{x}) - \boldsymbol{n}_3(\boldsymbol{x}, \boldsymbol{x}, \boldsymbol{x}) - \varepsilon^2 \kappa \ G(\boldsymbol{x}, \boldsymbol{x}') + \mathcal{W} \frac{\partial \boldsymbol{\rho}}{\partial w} + \bar{\mathcal{W}} \frac{\partial \boldsymbol{\rho}}{\partial \bar{w}} + \mathcal{W}' \frac{\partial \boldsymbol{\rho}}{\partial w'} + \bar{\mathcal{W}}' \frac{\partial \boldsymbol{\rho}}{\partial \bar{w}'} . \tag{A.2.32}$$

Regarding (A.2.31) formally as an inhomogeneous linear differential equation for $\boldsymbol{\rho}(\theta)$ where the right-hand side is the inhomogeneous part, we solve it by first expanding $\boldsymbol{\rho}(\theta)$ and $\boldsymbol{b}(\theta)$ as

$$\boldsymbol{\rho}(\theta) = \sum_{l=-\infty}^{\infty} \boldsymbol{\rho}^{(l)} \exp(il\theta) , \quad \boldsymbol{b}(\theta) = \sum_{l=-\infty}^{\infty} \boldsymbol{b}^{(l)} \exp(il\theta) . \tag{A.2.33}$$

Then, we use that $\exp(i\theta)\boldsymbol{u}$ and its complex conjugate are by construction the zero eigenvectors of the operator $\mathcal{L}_0$, i.e. $\mathcal{L}_0(\exp(i\theta)\boldsymbol{u}) = \mathcal{L}_0(\exp(-i\theta)\bar{\boldsymbol{u}}) = 0$. Since the left-hand side of (A.2.31) does not contain any of these zero-eigenvector components due to the action of $\mathcal{L}_0$, we require that these components are canceled also on the right-hand side — this is the solvability condition corresponding to (A.2.11) in the preceding section. Inserting the expansions (A.2.33) into (A.2.31) and comparing the first coefficients in the basis $\{\exp(il\theta) \mid l \in \mathbb{Z}\}$, the solvability condition reads

$$\mathcal{W} = -\boldsymbol{v}\boldsymbol{b}^{(1)} , \tag{A.2.34}$$

where $\boldsymbol{v}$ is the left eigenvector of $\hat{\boldsymbol{L}}_0$ corresponding to the eigenvector $i\omega_0$. For completeness, we find for the other coefficients

$$\boldsymbol{\rho}^{(l)} = \left(\hat{\boldsymbol{L}}_0 - il\omega_0\right)^{-1} \boldsymbol{b}^{(l)} , \quad (l \neq \pm 1) , \tag{A.2.35}$$

$$\boldsymbol{\rho}^{(1)} = \left(\hat{\boldsymbol{L}}_0 - i\omega_0\right)^{-1} \left(\boldsymbol{b}^{(1)} + \mathcal{W}\boldsymbol{u}\right) , \tag{A.2.36}$$

$$\boldsymbol{\rho}^{(-1)} = \left(\hat{\boldsymbol{L}}_0 + i\omega_0\right)^{-1} \left(\boldsymbol{b}^{(-1)} + \bar{\mathcal{W}}\bar{\boldsymbol{u}}\right) . \tag{A.2.37}$$

Furthermore, we expand $\boldsymbol{\rho}^{(l)}$ and $\boldsymbol{b}^{(l)}$ in powers of ε:

$$\boldsymbol{\rho}^{(l)} = \sum_{\nu=2}^{\infty} \varepsilon^\nu \tilde{\boldsymbol{\rho}}_\nu^{(l)} = \sum_{\nu=2}^{\infty} \boldsymbol{\rho}_\nu^{(l)} , \quad \boldsymbol{b}^{(l)} = \sum_{\nu=2}^{\infty} \varepsilon^\nu \tilde{\boldsymbol{b}}_\nu^{(l)} = \sum_{\nu=2}^{\infty} \boldsymbol{b}_\nu^{(l)} . \tag{A.2.38}$$

Correspondingly, we have

$$\boldsymbol{\rho} = \sum_{\nu=2}^{\infty} \varepsilon^\nu \tilde{\boldsymbol{\rho}}_\nu = \sum_{\nu=2}^{\infty} \boldsymbol{\rho}_\nu , \quad \boldsymbol{b} = \sum_{\nu=2}^{\infty} \varepsilon^\nu \tilde{\boldsymbol{b}}_\nu = \sum_{\nu=2}^{\infty} \boldsymbol{b}_\nu . \tag{A.2.39}$$

In a similar way, we expand $\mathcal{W}$. Since we are close to a Hopf bifurcation, the only resonant terms in $w, \bar{w}$ are of the form $|w|^n w$ with $n = 0, 1, 2, \ldots$; see Section 6.3.3 in the main text and [75,82]. Since $w, w' = \mathcal{O}(\varepsilon)$ and based on our previous

reasoning, the only mixed terms with non-negligible effect on the amplitude dynamics (A.2.6) are of odd powers in ε. This justifies an expansion of the form

$$\mathcal{W} = \sum_{\nu=1}^{\infty} \varepsilon^{2\nu+1} \tilde{\mathcal{W}}_{2\nu+1} = \sum_{\nu=1}^{\infty} \mathcal{W}_{2\nu+1} \,. \tag{A.2.40}$$

Taken together, we have $\mathcal{W}_\nu = \mathcal{O}(\varepsilon^\nu)\,(\nu \geq 3)$, $\boldsymbol{b}_\nu, \boldsymbol{\rho}_\nu = \mathcal{O}(\varepsilon^\nu)\,(\nu \geq 2)$, and $\boldsymbol{x}_0 = \mathcal{O}(\varepsilon)$. Next, to calculate $\mathcal{W}_\nu$, we need expressions for $\boldsymbol{b}_\mu$ with $1 \leq \mu \leq \nu$. After substituting all the expansions above into (A.2.32), we can compare terms of same order in ε. By respecting the symmetry of the $\boldsymbol{n}_k$ in their arguments, we find

$$\boldsymbol{b}_2 = -\boldsymbol{n}_2(\boldsymbol{x}_0, \boldsymbol{x}_0) \,, \tag{A.2.41}$$

$$\boldsymbol{b}_3 = -\varepsilon^2 \hat{\boldsymbol{L}}_1 \boldsymbol{x}_0 - 2\boldsymbol{n}_2(\boldsymbol{x}_0, \boldsymbol{\rho}_2) - \boldsymbol{n}_3(\boldsymbol{x}_0, \boldsymbol{x}_0, \boldsymbol{x}_0) - \kappa\varepsilon^2 \left(G_{10}\boldsymbol{x}_0 + G_{01}\boldsymbol{x}_0'\right) \,, \tag{A.2.42}$$

$$\begin{aligned}\boldsymbol{b}_4 = {} & -\varepsilon^2 \hat{\boldsymbol{L}}_1 \boldsymbol{\rho}_2 - 2\boldsymbol{n}_2(\boldsymbol{x}_0, \boldsymbol{\rho}_3) - \boldsymbol{n}_2(\boldsymbol{\rho}_2, \boldsymbol{\rho}_2) - 3\boldsymbol{n}_3(\boldsymbol{x}_0, \boldsymbol{x}_0, \boldsymbol{\rho}_2) \\ & - \kappa\varepsilon^2 \Big[G_{10}\boldsymbol{\rho}_2 + G_{01}\boldsymbol{\rho}_2' + G_{20}(\boldsymbol{x}_0, \boldsymbol{x}_0) + G_{11}(\boldsymbol{x}_0, \boldsymbol{x}_0') + G_{02}(\boldsymbol{x}_0', \boldsymbol{x}_0')\Big] \,,\end{aligned} \tag{A.2.43}$$

$$\begin{aligned}\boldsymbol{b}_5 = {} & -\varepsilon^2 \hat{\boldsymbol{L}}_1 \boldsymbol{\rho}_3 - 2\boldsymbol{n}_2(\boldsymbol{x}_0, \boldsymbol{\rho}_4) - 2\boldsymbol{n}_2(\boldsymbol{\rho}_2, \boldsymbol{\rho}_3) - 3\boldsymbol{n}_3(\boldsymbol{x}_0, \boldsymbol{x}_0, \boldsymbol{\rho}_3) - 3\boldsymbol{n}_3(\boldsymbol{x}_0, \boldsymbol{\rho}_2, \boldsymbol{\rho}_2) \\ & + \mathcal{W}_3 \frac{\partial \boldsymbol{\rho}_2}{\partial w} + \bar{\mathcal{W}}_3 \frac{\partial \boldsymbol{\rho}_2}{\partial \bar{w}} + \mathcal{W}_3' \frac{\partial \boldsymbol{\rho}_2}{\partial w'} + \bar{\mathcal{W}}_3' \frac{\partial \boldsymbol{\rho}_2}{\partial \bar{w}'} \\ & - \kappa\varepsilon^2 \Big[G_{10}\boldsymbol{\rho}_3 + G_{01}\boldsymbol{\rho}_3' + 2G_{20}(\boldsymbol{x}_0, \boldsymbol{\rho}_2) + G_{11}(\boldsymbol{x}_0, \boldsymbol{\rho}_2') + G_{11}(\boldsymbol{\rho}_2, \boldsymbol{x}_0') + 2G_{02}(\boldsymbol{x}_0', \boldsymbol{\rho}_2')\Big] \\ & - \kappa\varepsilon^2 \Big[G_{30}(\boldsymbol{x}_0, \boldsymbol{x}_0, \boldsymbol{x}_0) + G_{21}(\boldsymbol{x}_0, \boldsymbol{x}_0, \boldsymbol{x}_0') + G_{12}(\boldsymbol{x}_0, \boldsymbol{x}_0', \boldsymbol{x}_0') + G_{03}(\boldsymbol{x}_0', \boldsymbol{x}_0', \boldsymbol{x}_0')\Big] \,.\end{aligned} \tag{A.2.44}$$

Using the solvability condition (A.2.34), we can calculate $\mathcal{W}_3 = -\boldsymbol{v}\boldsymbol{b}_3^{(1)}$ via

$$\begin{aligned}\boldsymbol{b}_3^{(1)} &= -\varepsilon^2 \hat{\boldsymbol{L}}_1 \boldsymbol{x}_0^{(1)} - 2\boldsymbol{n}_2(\boldsymbol{x}_0, \boldsymbol{\rho}_2)^{(1)} - \boldsymbol{n}_3(\boldsymbol{x}_0, \boldsymbol{x}_0, \boldsymbol{x}_0)^{(1)} - \kappa\varepsilon^2 \left(G_{10}\boldsymbol{x}_0^{(1)} + G_{01}\boldsymbol{x}_0^{\prime(1)}\right) \\ &= -\varepsilon^2 \hat{\boldsymbol{L}}_1 \boldsymbol{x}_0^{(1)} - 2\boldsymbol{n}_2(\boldsymbol{x}_0^{(1)}, \boldsymbol{\rho}_2^{(0)}) - 2\boldsymbol{n}_2(\boldsymbol{x}_0^{(-1)}, \boldsymbol{\rho}_2^{(2)}) - \boldsymbol{n}_3(\boldsymbol{x}_0^{(1)}, \boldsymbol{x}_0^{(1)}, \boldsymbol{x}_0^{(-1)}) - \kappa\varepsilon^2 \left(G_{10}\boldsymbol{x}_0^{(1)} + G_{01}\boldsymbol{x}_0^{\prime(1)}\right) \,.\end{aligned} \tag{A.2.45}$$

Combining (A.2.35) and (A.2.41) results in

$$\boldsymbol{\rho}_2^{(0)} = \hat{\boldsymbol{L}}_0^{-1} \boldsymbol{b}_2^{(0)} = -2\hat{\boldsymbol{L}}_0^{-1} \boldsymbol{n}_2\left(\boldsymbol{x}_0^{(1)}, \boldsymbol{x}_0^{(-1)}\right) \,, \tag{A.2.46}$$

$$\boldsymbol{\rho}_2^{(2)} = \left(\hat{\boldsymbol{L}}_0 - 2i\omega_0\right)^{-1} \boldsymbol{b}_2^{(2)} = \left(\hat{\boldsymbol{L}}_0 - 2i\omega_0\right)^{-1} \boldsymbol{n}_2\left(\boldsymbol{x}_0^{(1)}, \boldsymbol{x}_0^{(1)}\right) \,. \tag{A.2.47}$$

Finally, noting that $\boldsymbol{x}_0^{(1)} = w\boldsymbol{u}$ and $\boldsymbol{x}_0^{(-1)} = w\bar{\boldsymbol{u}}$, we retrieve from (A.2.46)

$$\mathcal{W}_3 = \varepsilon^2\alpha - \beta|w|^2 w + \varepsilon^2\kappa\left[\gamma_{10}w + \gamma_{01}w'\right] \tag{A.2.48}$$

with

$$\alpha = \boldsymbol{v}\hat{\boldsymbol{L}}_1\boldsymbol{u} \,, \tag{A.2.49}$$

$$\beta = -3\boldsymbol{v}\boldsymbol{n}_3(\boldsymbol{u}, \boldsymbol{u}, \bar{\boldsymbol{u}}) + 4\boldsymbol{v}\boldsymbol{n}\left(\boldsymbol{u}, \hat{\boldsymbol{L}}_0^{-1}\boldsymbol{n}_2(\boldsymbol{u}, \bar{\boldsymbol{u}})\right) + 2\boldsymbol{v}\boldsymbol{n}_2\left(\bar{\boldsymbol{u}}, (\hat{\boldsymbol{L}}_0 - 2i\omega_0)^{-1}\boldsymbol{n}_2(\boldsymbol{u}, \boldsymbol{u})\right) \,, \tag{A.2.50}$$

$$\gamma_{10} = \boldsymbol{v}G_{10}\boldsymbol{u} \,, \quad \gamma_{01} = \boldsymbol{v}G_{01}\boldsymbol{u} \,. \tag{A.2.51}$$

Analogously, we determine $\mathcal{W}_5 = -\boldsymbol{v}\boldsymbol{b}_5^{(1)}$:

$$\begin{aligned}\boldsymbol{b}_5^{(1)} = {} & -\varepsilon^2 \hat{\boldsymbol{L}}_1 \boldsymbol{\rho}_3^{(1)} - 2\boldsymbol{n}_2(\boldsymbol{x}_0, \boldsymbol{\rho}_4)^{(1)} - 2\boldsymbol{n}_2(\boldsymbol{\rho}_2, \boldsymbol{\rho}_3)^{(1)} - 3\boldsymbol{n}_3(\boldsymbol{x}_0, \boldsymbol{x}_0, \boldsymbol{\rho}_3)^{(1)} - 3\boldsymbol{n}_3(\boldsymbol{x}_0, \boldsymbol{\rho}_2, \boldsymbol{\rho}_2)^{(1)} \\ & + \mathcal{W}_3 \frac{\partial \boldsymbol{\rho}_2^{(1)}}{\partial w} + \bar{\mathcal{W}}_3 \frac{\partial \boldsymbol{\rho}_2^{(1)}}{\partial \bar{w}} + \mathcal{W}_3' \frac{\partial \boldsymbol{\rho}_2^{(1)}}{\partial w'} + \bar{\mathcal{W}}_3' \frac{\partial \boldsymbol{\rho}_2^{(1)}}{\partial \bar{w}'} - \kappa\varepsilon^2 \Big[G_{10}\boldsymbol{\rho}_3^{(1)} + G_{01}\boldsymbol{\rho}_3^{\prime(1)}\Big] \\ & - \kappa\varepsilon^2 \Big[2G_{20}(\boldsymbol{x}_0, \boldsymbol{\rho}_2)^{(1)} + G_{11}(\boldsymbol{x}_0, \boldsymbol{\rho}_2')^{(1)} + G_{11}(\boldsymbol{\rho}_2, \boldsymbol{x}_0')^{(1)} + 2G_{02}(\boldsymbol{x}_0', \boldsymbol{\rho}_2')^{(1)}\Big] \\ & - \kappa\varepsilon^2 \Big[G_{30}(\boldsymbol{x}_0, \boldsymbol{x}_0, \boldsymbol{x}_0)^{(1)} + G_{21}(\boldsymbol{x}_0, \boldsymbol{x}_0, \boldsymbol{x}_0')^{(1)} + G_{12}(\boldsymbol{x}_0, \boldsymbol{x}_0', \boldsymbol{x}_0')^{(1)} + G_{03}(\boldsymbol{x}_0', \boldsymbol{x}_0', \boldsymbol{x}_0')^{(1)}\Big]\end{aligned} \tag{A.2.52}$$

Again, we have to expand the terms, which we show here for only the first line of (A.2.52) since the other terms follow equivalently,

$$\begin{aligned}\boldsymbol{n}_2(\boldsymbol{x}_0, \boldsymbol{\rho}_4)^{(1)} &= \boldsymbol{n}_2(\boldsymbol{x}_0^{(1)}, \boldsymbol{\rho}_4^{(0)}) + \boldsymbol{n}_2(\boldsymbol{x}_0^{(-1)}, \boldsymbol{\rho}_4^{(2)}) \,, \\ \boldsymbol{n}_2(\boldsymbol{\rho}_2, \boldsymbol{\rho}_3)^{(1)} &= \boldsymbol{n}_2(\boldsymbol{\rho}_2^{(2)}, \boldsymbol{\rho}_3^{(-1)}) + \boldsymbol{n}_2(\boldsymbol{\rho}_2^{(1)}, \boldsymbol{\rho}_3^{(0)}) + \boldsymbol{n}_2(\boldsymbol{\rho}_2^{(0)}, \boldsymbol{\rho}_3^{(1)}) + \boldsymbol{n}_2(\boldsymbol{\rho}_2^{(-1)}, \boldsymbol{\rho}_3^{(2)}) + \boldsymbol{n}_2(\boldsymbol{\rho}_2^{(-2)}, \boldsymbol{\rho}_3^{(3)}) \\ \boldsymbol{n}_3(\boldsymbol{x}_0, \boldsymbol{x}_0, \boldsymbol{\rho}_3)^{(1)} &= \boldsymbol{n}_3(\boldsymbol{x}_0^{(1)}, \boldsymbol{x}_0^{(1)}, \boldsymbol{\rho}_3^{(-1)}) + 2\boldsymbol{n}_3(\boldsymbol{x}_0^{(1)}, \boldsymbol{x}_0^{(-1)}, \boldsymbol{\rho}_3^{(1)}) + \boldsymbol{n}_3(\boldsymbol{x}_0^{(-1)}, \boldsymbol{x}_0^{(-1)}, \boldsymbol{\rho}_3^{(3)}) \,,\end{aligned}$$

$$\begin{aligned}\boldsymbol{n}_3(\boldsymbol{x}_0,\boldsymbol{\rho}_2,\boldsymbol{\rho}_2)^{(1)} = {}& 2\boldsymbol{n}_3(\boldsymbol{x}_0^{(1)},\boldsymbol{\rho}_2^{(2)},\boldsymbol{\rho}_2^{(-2)}) + 2\boldsymbol{n}_3(\boldsymbol{x}_0^{(1)},\boldsymbol{\rho}_2^{(1)},\boldsymbol{\rho}_2^{(-1)}) + 2\boldsymbol{n}_3(\boldsymbol{x}_0^{(1)},\boldsymbol{\rho}_2^{(0)},\boldsymbol{\rho}_2^{(0)}) \\ & + 2\boldsymbol{n}_3(\boldsymbol{x}_0^{(-1)},\boldsymbol{\rho}_2^{(2)},\boldsymbol{\rho}_2^{(0)}) + \boldsymbol{n}_3(\boldsymbol{x}_0^{(-1)},\boldsymbol{\rho}_2^{(1)},\boldsymbol{\rho}_2^{(1)})\,.\end{aligned}$$

We focus on those terms that contribute to $\kappa\varepsilon^2\bar{w}w'^2$. Following Kori et al. [177], one can exclude all terms that (a) include $\boldsymbol{\rho}_2$, (b) include $\boldsymbol{x}_0^{(1)}$, and (c) include $\boldsymbol{x}_0^{(-1)}$ twice. The remaining terms, hence, read

$$\begin{aligned}&-\varepsilon^2\hat{\boldsymbol{L}}_1\boldsymbol{\rho}_3^{(1)} - 2\boldsymbol{n}_2\left(\boldsymbol{x}_0^{(-1)},\boldsymbol{\rho}_4^{(2)}\right) \\ &-\kappa\varepsilon^2\Big[G_{10}\boldsymbol{\rho}_3^{(1)} + G_{01}\boldsymbol{\rho}'^{(1)}_3 + G_{11}\left(\boldsymbol{x}_0^{(-1)},\boldsymbol{\rho}'^{(2)}_2\right) + G_{12}\left(\boldsymbol{x}_0^{(-1)},\boldsymbol{x}'^{(1)}_0,\boldsymbol{x}'^{(1)}_0\right)\Big]\,.\end{aligned} \tag{A.2.53}$$

The first term can be neglected because the coupling term included there is linear. Further, the first two terms in brackets can also be neglected because each of them yields exclusively either $w,\bar{w}$ or $w',\bar{w}'$. Hence, the only remaining terms in $\boldsymbol{b}_5^{(1)}$ are the two between the brackets and the κ-dependent term in

$$-\boldsymbol{n}_2\left(\boldsymbol{x}_0^{(-1)},\boldsymbol{\rho}_4^{(2)}\right)\,. \tag{A.2.54}$$

As for the latter, according to (A.2.35) and (A.2.43) the κ-dependent terms in $\boldsymbol{\rho}_4^{(2)}$ are

$$\left(\hat{\boldsymbol{L}}_0 - 2i\omega_0\right)^{-1}\left(-\kappa\varepsilon^2\Big[G_{10}\boldsymbol{\rho}_2^{(2)} + G_{01}\boldsymbol{\rho}'^{(2)}_2 + G_{20}(\boldsymbol{x}_0^{(1)},\boldsymbol{x}_0^{(1)}) + G_{11}(\boldsymbol{x}_0^{(1)},\boldsymbol{x}'^{(1)}_0) + G_{02}(\boldsymbol{x}'^{(1)}_0,\boldsymbol{x}'^{(1)}_0)\Big]\right)\,. \tag{A.2.55}$$

Following the same reasoning as above, all but the second and the last terms in brackets can be ignored. Using (A.2.41), we have

$$\boldsymbol{\rho}'^{(2)}_2 = \left(\hat{\boldsymbol{L}}_0 - 2i\omega_0\right)^{-1}\left(-\boldsymbol{n}_2\left(\boldsymbol{x}'^{(1)}_0,\boldsymbol{x}'^{(1)}_0\right)\right) = -w'^2\left(\hat{\boldsymbol{L}}_0 - 2i\omega_0\right)^{-1}\boldsymbol{n}_2(\boldsymbol{u},\boldsymbol{u})\,. \tag{A.2.56}$$

Hence, (A.2.54) reduces to the κ-dependent terms

$$-2\kappa\varepsilon^2\bar{w}w'^2\boldsymbol{n}_2\Big(\bar{\boldsymbol{u}},\left(\hat{\boldsymbol{L}}_0 - 2i\omega_0\right)^{-1}\Big[G_{01}\left(\hat{\boldsymbol{L}}_0 - 2i\omega_0\right)^{-1}\boldsymbol{n}_2(\boldsymbol{u},\boldsymbol{u}) - G_{02}(\boldsymbol{u},\boldsymbol{u})\Big]\Big)\,. \tag{A.2.57}$$

In addition, we find

$$+\kappa\varepsilon^2\bar{w}w'^2\Big[G_{11}\left(\bar{\boldsymbol{u}},\left(\hat{L}_0 - 2i\omega_0\right)^{-1}\boldsymbol{n}_2(\boldsymbol{u},\boldsymbol{u})\right) - G_{12}(\bar{\boldsymbol{u}},\boldsymbol{u},\boldsymbol{u})\Big]\,. \tag{A.2.58}$$

Combining (A.2.57) and (A.2.58), we find the following expression for δ in (A.2.24):

$$\begin{aligned}\delta = {}& 2v\boldsymbol{n}_2\Big(\bar{\boldsymbol{u}},\left(\hat{\boldsymbol{L}}_0 - 2i\omega_0\right)^{-1}\Big[G_{01}\left(\hat{\boldsymbol{L}}_0 - 2i\omega_0\right)^{-1}\boldsymbol{n}_2(\boldsymbol{u},\boldsymbol{u}) - G_{02}(\boldsymbol{u},\boldsymbol{u})\Big]\Big) \\ & -vG_{11}\left(\bar{\boldsymbol{u}},\left(\hat{\boldsymbol{L}}_0 - 2i\omega_0\right)^{-1}\boldsymbol{n}_2(\boldsymbol{u},\boldsymbol{u})\right) + vG_{12}(\bar{\boldsymbol{u}},\boldsymbol{u},\boldsymbol{u})\,.\end{aligned} \tag{A.2.59}$$

Note that for linear coupling, all G_{jk} vanish but G_{01}, confirming the results by Kori et al. [177].

A.3. Poincaré's reduction via nonlinear transforms

We consider two weakly coupled two-dimensional oscillators $\boldsymbol{x} = (x,y), \boldsymbol{x}' = (x',y') \in \mathbb{R}^2$ near a supercritical Hopf bifurcation, whose general dynamics is given by

$$\dot{\boldsymbol{x}} = \boldsymbol{f}(\boldsymbol{x},t;\mu) + \kappa\ \boldsymbol{g}(\boldsymbol{x},\boldsymbol{x}',t;\mu) \tag{A.3.1}$$

and which we seek to transform into a generic normal form

$$\dot{w} = \alpha w - \beta|w|^2 w + \kappa\ h(w,w')\,, \tag{A.3.2}$$

where the complex parameters $\alpha = \alpha(\mu)$, $\beta = \beta(\mu)$ and the coupling function[45] h have to be determined subsequently. For the sake of legibility, we drop the explicit time-dependence of $\boldsymbol{f}$ and $\boldsymbol{g}$, and note that the theory also holds when allowing for time variations.

By definition and without loss of generality, the dynamics of an uncoupled unit

$$\dot{\boldsymbol{x}} = \boldsymbol{f}(\boldsymbol{x};\mu) \tag{A.3.3}$$

has for all sufficiently small $|\mu| \ll 1$ the equilibrium $(0,0)$ with eigenvalues

$$\lambda_{1,2}(\mu) = \varrho(\mu) \pm i\omega(\mu)\,, \tag{A.3.4}$$

[45] In this section we denote the coupling function of the resulting Hopf normal form by h and thereby deviate from the general notation g.

where $\varrho(0) = 0$ and $\omega(0) = \omega_0 > 0$. The first Lyapunov coefficient $l_1(0) = -\mathrm{Re}\ \beta(0)/\omega(0)$, which depends on the properties of the function $\boldsymbol{f}$, does not vanish and $\varrho'(0) \neq 0$. In particular, we can rewrite (A.3.3) as

$$\frac{d}{dt}\begin{pmatrix} x \\ y \end{pmatrix} = \boldsymbol{L}(\mu)\begin{pmatrix} x \\ y \end{pmatrix} + \boldsymbol{F}\left(\begin{pmatrix} x \\ y \end{pmatrix}; \mu\right) \quad \text{with} \quad \boldsymbol{L}(\mu) = \begin{pmatrix} a_{11}(\mu) & a_{12}(\mu) \\ a_{21}(\mu) & a_{22}(\mu) \end{pmatrix} , \tag{A.3.5}$$

where we further set $\sigma(\mu) = \mathrm{tr}\ \boldsymbol{L}(\mu)$ and $\Delta(\mu) = \det\ \boldsymbol{L}(\mu)$, such that

$$\lambda_{1,2}(\mu) = \tfrac{1}{2}\left[\sigma(\mu) \pm \sqrt{\sigma(\mu)^2 - 4\Delta(\mu)}\right] . \tag{A.3.6}$$

The Hopf bifurcation assumption translates into $\sigma(0) = 0$ and $\Delta(0) = \omega_0^2 > 0$. For small $|\mu|$, one can introduce

$$\varrho(\mu) = \tfrac{1}{2}\sigma(\mu), \quad \omega(\mu) = \tfrac{1}{2}\sqrt{4\Delta(\mu) - \sigma(\mu)^2} \tag{A.3.7}$$

and set $\lambda_1 = \lambda$, $\lambda_2 = \bar{\lambda}$. As can already be anticipated, the parameter α in (A.3.2) is exactly the eigenvalue λ.

Next,we couple the unit $\boldsymbol{x} = (x, y)$ to another identical one, $\boldsymbol{x}' = (x', y')$, that is, $\boldsymbol{f} = \boldsymbol{f}'$, via the coupling function $\boldsymbol{g}(\boldsymbol{x}, \boldsymbol{x}')$ and with coupling strength $\kappa \in \mathbb{R}$. In general, $\boldsymbol{g}$ depends on both the control parameter μ and the coupling strength κ. Since $|\kappa| \ll 1$ is sufficiently small, we can assume that the coupling function depends on κ only up to first order. The system of interest reads

$$\dot{\boldsymbol{x}} = \boldsymbol{f}(\boldsymbol{x}; \mu) + \kappa\tilde{\boldsymbol{g}}(\boldsymbol{x}, \boldsymbol{x}'; \mu) + \mathcal{O}(\kappa^2) , \tag{A.3.8}$$

where $\tilde{\boldsymbol{g}} = \boldsymbol{g} + \mathcal{O}(\kappa)$. In the following we omit the tilde. While common normal form transforms merely consider single units, the following lemmata along the line of Chapter 3, Lemmata 3.3 – 3.6, in [82] are adapted to take the full, coupled system (A.3.8) into account. By subsequently applying the theory outlined in this section, we can derive the transformed equations in Hopf normal form and thereby allow for a reduction of the dynamics onto the center manifold where we provide also the exact transformations of the nonlinear terms in the coupling function $\boldsymbol{g}$. To start with, we first rewrite the dynamics in complex form.

Lemma A.2. *By introducing a complex variable $z \in \mathbb{C}$, system (A.3.8) can be written for sufficiently small $|\mu|$ as a single equation:*

$$\dot{z} = \lambda(\mu)z + \tilde{f}(z, \bar{z}; \mu) + \kappa\tilde{g}(z, \bar{z}, z', \bar{z}'; \mu) + \mathcal{O}(\kappa^2) , \tag{A.3.9}$$

where $\tilde{f}, \tilde{g} = \mathcal{O}(|z|^2)$ are smooth functions of $(z, \bar{z}; \mu)$, and $(z, \bar{z}, z', \bar{z}'; \mu)$, respectively. Note that z refers to unit $\boldsymbol{x}$ and z' represents $\boldsymbol{x}'$.

Proof. As we assume $\boldsymbol{x}$ and $\boldsymbol{x}'$ being identical in the uncoupled case, $\kappa = 0$, the following reasoning applies to both $\boldsymbol{x}$ and $\boldsymbol{x}'$. Let $\boldsymbol{u}(\mu) = (u_1(\mu), u_2(\mu))^\intercal \in \mathbb{C}^2$ be a right eigenvector of $\boldsymbol{L}(\mu)$ corresponding to the eigenvalue $\lambda(\mu)$: $\boldsymbol{L}(\mu)\boldsymbol{u}(\mu) = \lambda(\mu)\boldsymbol{u}(\mu)$, and let $\boldsymbol{v}(\mu) = (v_1(\mu), v_2(\mu)) \in \mathbb{C}^{1\times 2}$ be the corresponding left eigenvector: $\boldsymbol{v}(\mu)\boldsymbol{L}(\mu) = \lambda(\mu)\boldsymbol{v}(\mu)$. We assume $\boldsymbol{u}$, $\boldsymbol{v}$ are normalized such that $\boldsymbol{v}(\mu)\boldsymbol{u}(\mu) = v_1(\mu)u_1(\mu) + v_2(\mu)u_2(\mu) = 1$. Every vector $\boldsymbol{x} \in \mathbb{R}^2$ can be uniquely represented for any small $|\mu|$ as

$$\boldsymbol{x} = z\boldsymbol{u}(\mu) + \bar{z}\bar{\boldsymbol{u}}(\mu) \tag{A.3.10}$$

for some complex z and provided the eigenvectors are specified. Then, $z = v(\mu)\boldsymbol{x}$. A rigorous justification can be found in [Lemma 3.3,82]. By vector calculus we find that

$$\begin{aligned} \dot{z} &= \boldsymbol{v}(\mu)\dot{\boldsymbol{x}} = \boldsymbol{v}(\mu)\left[\boldsymbol{L}(\mu)\boldsymbol{x} + \boldsymbol{F}(\boldsymbol{x}; \mu) + \kappa\boldsymbol{g}(\boldsymbol{x}, \boldsymbol{x}'; \mu) + \mathcal{O}(\kappa^2)\right] \\ &= \boldsymbol{v}(\mu)\boldsymbol{L}(\mu)\boldsymbol{x} + \boldsymbol{v}(\mu)\boldsymbol{F}\left(z\boldsymbol{u}(\mu) + \bar{z}\bar{\boldsymbol{u}}(\mu); \mu\right) + \kappa\,\boldsymbol{v}(\mu)g\left(z\boldsymbol{u}(\mu) + \bar{z}\bar{\boldsymbol{u}}(\mu), z'\boldsymbol{u}(\mu) + \bar{z}'\bar{\boldsymbol{u}}(\mu); \mu\right) + \mathcal{O}(\kappa^2) \\ &= \lambda(\mu)z + \tilde{f}(z, \bar{z}; \mu) + \kappa\tilde{g}(z, \bar{z}, z', \bar{z}'; \mu) + \mathcal{O}(\kappa^2) , \end{aligned} \tag{A.3.11}$$

where $\boldsymbol{F}$ denotes the nonlinear part of the function $\boldsymbol{f}(\boldsymbol{x}; \mu) = \boldsymbol{L}(\mu)\boldsymbol{x} + \boldsymbol{F}(\boldsymbol{x}; \mu)$. □

One can write $\tilde{f}$ as a formal Taylor series in the two complex variables z and $\bar{z}$:

$$\tilde{f}(z, \bar{z}; \mu) = \sum_{k+l\geq 2} \frac{1}{k!l!} f_{kl}(\mu) z^k \bar{z}^l , \tag{A.3.12}$$

where

$$f_{kl}(\mu) = \frac{\partial^{k+l}}{(\partial z)^k(\partial\bar{z})^l} v(\mu)\boldsymbol{f}\left(z\boldsymbol{u}(\mu) + \bar{z}\bar{\boldsymbol{u}}(\mu); \mu\right)\Big|_{z=0}$$

for $k + l \geq 2$, $k, l = 0, 1, \ldots$.

Remark. Suppose at $\mu = 0$ the function $\boldsymbol{f}(\boldsymbol{x}, 0)$ in (A.3.8) is represented as

$$\boldsymbol{f}(\boldsymbol{x}, 0) = \tfrac{1}{2}\boldsymbol{B}(\boldsymbol{x}, \boldsymbol{x}) + \frac{1}{6}\boldsymbol{C}(\boldsymbol{x}, \boldsymbol{x}, \boldsymbol{x}) + \mathcal{O}(\|x\|^4) ,$$

where $\boldsymbol{B}(\boldsymbol{p}, \boldsymbol{q})$ and $\boldsymbol{C}(\boldsymbol{p}, \boldsymbol{q}, \boldsymbol{r})$ are symmetric multilinear vector functions of $\boldsymbol{p}, \boldsymbol{q}, \boldsymbol{r} \in \mathbb{R}^2$. In coordinates, we have

$$\boldsymbol{B}_i(\boldsymbol{p}, \boldsymbol{q}) = \sum_{j,k=1}^{2} \left.\frac{\partial^2 f_i(\boldsymbol{\xi}, 0)}{\partial \xi_j \partial \xi_k}\right|_{\boldsymbol{\xi}=0} p_j q_k , \quad i = 1, 2,$$

and

$$\boldsymbol{C}_i(\boldsymbol{p}, \boldsymbol{q}, \boldsymbol{r}) = \sum_{j,k,l=1}^{2} \left.\frac{\partial^3 f_i(\boldsymbol{\xi}, 0)}{\partial \xi_j \partial \xi_k \partial \xi_l}\right|_{\boldsymbol{\xi}=0} p_j q_k r_l , \quad i = 1, 2 .$$

Then,

$$\boldsymbol{B}(z\boldsymbol{u} + \bar{z}\bar{\boldsymbol{u}}, z\boldsymbol{u} + \bar{z}\bar{\boldsymbol{u}}) = z^2\boldsymbol{B}(\boldsymbol{u}, \boldsymbol{u}) + 2z\bar{z}\boldsymbol{B}(\boldsymbol{u}, \bar{\boldsymbol{u}}) + \bar{z}^2\boldsymbol{B}(\bar{\boldsymbol{u}}, \bar{\boldsymbol{u}}) , \tag{A.3.13}$$

where $\boldsymbol{u} = \boldsymbol{u}(0), \boldsymbol{v} = \boldsymbol{v}(0)$. Hence, the Taylor coefficients f_{kl} of the quadratic terms in $\tilde{f}(z, \bar{z}, 0)$, i.e. $k + l = 2$, can be expressed by

$$f_{20} = \boldsymbol{v}\boldsymbol{B}(\boldsymbol{u}, \boldsymbol{u}), \quad f_{11} = \boldsymbol{v}\boldsymbol{B}(\boldsymbol{u}, \bar{\boldsymbol{u}}), \quad f_{02} = \boldsymbol{v}\boldsymbol{B}(\bar{\boldsymbol{u}}, \bar{\boldsymbol{u}}) . \tag{A.3.14}$$

Similar calculations with $\boldsymbol{C}$ give

$$f_{21} = \boldsymbol{v}\boldsymbol{C}(\boldsymbol{u}, \boldsymbol{u}, \bar{\boldsymbol{u}}) . \tag{A.3.15}$$

The following two lemmata are key to transform system (A.3.8) into Hopf normal form. In fact, both are polynomial coordinate transformations whose coefficients depend smoothly on μ. The proofs of the respective lemma use their inverse transformations, which are again smoothly dependent on μ but not necessarily polynomial. However, we will not provide the proofs here but refer to [Chapter 3.5, 82]. In some neighborhood of the origin $\boldsymbol{x} = (0, 0)$, these transformations are *near-identical* due to their linear parts.

Lemma A.3 (*Lemma 3.4 [82]*)**.** *The equation*

$$\dot{z} = \lambda z + \frac{f_{20}}{2}z^2 + f_{11}z\bar{z} + \frac{f_{02}}{2}\bar{z}^2 + \mathcal{O}(|z|^3) , \tag{A.3.16}$$

where $\lambda = \lambda(\mu) = \varrho(\mu) + i\omega(\mu), \varrho(0) = 0, \omega(0) = \omega_0 > 0$, and $f_{kl} = f_{kl}(\mu)$, can be transformed by an invertible parameter-dependent change of complex coordinate

$$z = w + \frac{h_{20}}{2}w^2 + h_{11}w\bar{w} + \frac{h_{02}}{2}\bar{w}^2$$

for all sufficiently small $|\mu|$, into an equation without quadratic terms:

$$\dot{w} = \lambda w + \mathcal{O}(|w|^3).$$

Lemma A.4 (*Lemma 3.5 [82]*)**.** *The equation*

$$\dot{z} = \lambda z + \frac{f_{30}}{6}z^3 + \frac{f_{21}}{2}z^2\bar{z} + \frac{f_{12}}{2}z\bar{z}^2 + \frac{f_{03}}{6}\bar{z}^3 + \mathcal{O}(|z|^4) , \tag{A.3.17}$$

where $\lambda = \lambda(\mu) = \varrho(\mu) + i\omega(\mu), \varrho(0) = 0, \omega(0) = \omega_0 > 0$, and $f_{kl} = f_{kl}(\mu)$, can be transformed by an invertible parameter-dependent change of complex coordinate

$$z = w + \frac{h_{30}}{6}w^3 + \frac{h_{21}}{2}w^2\bar{w} + \frac{h_{12}}{2}w\bar{w}^2 + \frac{h_{03}}{6}\bar{w}^6$$

for all sufficiently small $|\mu|$, into an equation with only one cubic term:

$$\dot{w} = \lambda w + c_1 w^2\bar{w} + \mathcal{O}(|w|^4),$$

where $c_1 = c_1(\mu) = f_{21}/2$.

Combining these two lemmata yields the *Poincaré normal form for the Hopf bifurcation*, cf. [Lemma 3.6,82].

Lemma A.5. *The equation*

$$\dot{z} = \lambda z + \sum_{2 \le k+l \le 3} \frac{1}{k!l!} f_{kl} z^k \bar{z}^l + \kappa\tilde{g}(z, \bar{z}, z', \bar{z}'; \mu) + \mathcal{O}(|Z|^4, \kappa^2) , \tag{A.3.18}$$

with $Z = (z, z')$, and where $\lambda = \lambda(\mu) = \varrho(\mu) + i\omega(\mu)$, $\varrho(0) = 0$, $\omega(0) = \omega_0 > 0$, and $f_{kl} = f_{kl}(\mu)$, and where $\tilde{\tilde{g}}$ denotes $\tilde{g}$ truncated after cubic terms, can be transformed by an invertible parameter-dependent change of complex coordinate, smoothly depending on the parameter,

$$z = \psi(w) = w + \frac{h_{20}}{2}w^2 + h_{11}w\bar{w} + \frac{h_{02}}{2}\bar{w}^2 + \frac{h_{30}}{6}w^3 + \frac{h_{12}}{2}w\bar{w}^2 + \frac{h_{03}}{6}\bar{w}^3 \,, \tag{A.3.19}$$

for all sufficiently small $|\mu|$, into an equation with only one cubic term:

$$\dot{w} = \lambda w - \beta w^2\bar{w} + \kappa\, h(w, \bar{w}, w', \bar{w}') + \mathcal{O}(|W|^4, \kappa^2), \tag{A.3.20}$$

with $W = (w, w')$, and where $\beta = \beta(\mu) = -c_1(\mu)$ is given by

$$c_1 = \frac{f_{20}f_{11}(2\lambda + \bar{\lambda})}{2|\lambda|^2} + \frac{|f_{11}|^2}{\lambda} + \frac{|f_{02}|^2}{2(2\lambda - \bar{\lambda})} + \frac{f_{21}}{2} \,, \tag{A.3.21}$$

and h has only polynomial components of degree lower than or equal to 3, i.e. h is of the form

$$h(w, \bar{w}, w', \bar{w}') = \sum_{0\le k+l+m+n\le 3} h_{klmn} w^k \bar{w}^l w'^m \bar{w}'^n \,, \tag{A.3.22}$$

where for $k + l + m + n = 0$ we have $h_{klmn} = \tilde{g}_{klmn}$ with the latter being the Taylor coefficients of $\tilde{g}$, and if $\tilde{g}$ has no constant term, i.e. $\tilde{g}_{0000} = 0$, then $h_{klmn} = \tilde{g}_{klmn}$ holds also for $k + l + m + n = 1$.

Proof. The first part of the proof is a combination of the previous two lemmata. We apply the first lemma to (A.3.18) in order to remove the quadratic terms. Then, we can apply the second lemma and arrive at the amplitude equation as wanted. Note that by the first transformation the coefficients of the cubic and higher order terms may have changed. Therefore, the coefficients of the inverse transforms as given in the proofs for the two lemmata as in [82] are no longer valid in our scenario. Once the two subsequent near-identity transforms have been established, we can also apply them to the coupling term. Indeed, the near-identity character leaves the linear terms unchanged such that $h_{klmn} = g_{klmn}$ at order $\mathcal{O}(|Z|, |W|)$.

The idea of finding the coefficients in (A.3.20) breaks down to identifying the coefficients a_{jk} of a local inverse transform up to order $\mathcal{O}(|w|^4)$:

$$w = \psi^{-1}(z) = z + a_{20}z^2 + a_{11}z\bar{z} + z_{02}\bar{z}^2 + a_{30}z^3 + a_{21}z^2\bar{z} + a_{12}z\bar{z}^2 + a_{03}\bar{z}^3 + \cdots \,. \tag{A.3.23}$$

Inserting the forward transform (A.3.19) into (A.3.23) and evaluating the right- and left-hand sides coefficient-wise, provides the inverse coefficients a_{jk}:

$$\begin{aligned}
a_{20} &= -\frac{h_{20}}{2}, \quad a_{11} = -h_{11}, \quad a_{02} = -\frac{h_{02}}{2}, \\
a_{30} &= -\frac{h_{30}}{6} + \frac{h_{20}^2}{2} + \frac{h_{11}\bar{h}_{02}}{2}, \\
a_{21} &= \frac{3h_{20}h_{11}}{2} + |h_{11}|^2 + \frac{|h_{02}|^2}{2}, \\
a_{12} &= -\frac{h_{12}}{2} + \frac{h_{20}h_{02}}{2} + h_{11}^2 + \frac{h_{11}\bar{h}_{20}}{2} + \frac{\bar{h}_{11}h_{02}}{2}, \\
a_{03} &= -\frac{h_{03}}{6} + \frac{h_{11}h_{02}}{2} + \frac{\bar{h}_{20}h_{20}}{2} \,.
\end{aligned}$$

By differentiating the inverse transform (A.3.23) with respect to t and by using the abbreviations $f(z) = \sum_{k,l} 1/(k!l!) f_{kl} z^k \bar{z}^l$, $g(z, z') = \tilde{g}(z, \bar{z}, z', \bar{z}')$, and $f(w) = f\left(\psi(w)\right)$, $g(w, w') = g\left(\psi(w), \psi(w')\right)$, we have

$$\begin{aligned}
\dot{w} &= \tfrac{d}{dt}\psi^{-1}(z) = \dot{z} + 2a_{20}z\dot{z} + a_{11}\dot{z}\bar{z} + a_{11}z\dot{\bar{z}} + \cdots \\
&= \lambda z + f(z) + \kappa g(z, z') + 2a_{20}\left[\lambda z^2 + f(z)z + \kappa g(z, z')z\right] \\
&\quad + a_{11}\left[(\lambda + \bar{\lambda})z\bar{z} + \overline{f(z)}z + f(z)\bar{z} + \kappa(\overline{g(z, z')}z + g(z, z')\bar{z})\right] + \cdots \\
&= \lambda\psi(w) + f(w) + 2a_{20}\left[\lambda\psi(w)^2 + f(w)\psi(w)\right] + a_{11}\left[(\lambda + \bar{\lambda})\psi(w)\psi(\bar{w}) + \overline{f(w)}\psi(w) + f(w)\psi(\bar{w})\right] + \cdots \\
&\quad + \kappa\left[g(w, w') + 2a_{20}g(w, w')\psi(w) + a_{11}\left(\overline{g(w, w')}\psi(w) + g(w, w')\psi(\bar{w})\right) + \cdots\right] \\
&\overset{!}{=} \lambda w - \beta w^2\bar{w} + \kappa\, h(w, \bar{w}, w', \bar{w}') + \mathcal{O}(|w|^4) \,,
\end{aligned}$$

where we inserted the dynamics (A.3.18) in the second equality and used the forward transform (A.3.19) in the third equality. Note that we assumed that z and z' coincide in the uncoupled case $\kappa = 0$. That is why the coordinate transforms $z = \psi(w)$ and $z' = \psi'(w')$ take the same form, that is, $\psi = \psi'$. Now, by collecting terms of the same order and requiring

that all quadratic and cubic terms except for the $w\bar{w}^2$-coefficient β are zero, we can solve the last equality and find $\beta = -c_1$ as (A.3.21) and the resulting coefficients h_{jk} of the forward transform (A.3.19) as

$$
\begin{aligned}
h_{20} &= \frac{f_{20}}{\lambda}, \quad h_{11} = \frac{f_{11}}{\bar{\lambda}}, \quad h_{02} = \frac{f_{02}}{2\bar{\lambda} - \lambda}, \\
h_{30} &= \frac{f_{30}}{2\lambda} + \frac{3f_{20}^2}{2\lambda^2} + \frac{3f_{11}\bar{f}_{02}}{2|\lambda|^2}\frac{\bar{\lambda} - \lambda}{2\lambda - \bar{\lambda}}, \\
h_{21} &= \frac{f_{21}}{2\bar{\lambda}} + \frac{f_{20}f_{02}}{2\bar{\lambda}(2\bar{\lambda} - \lambda)} + \frac{f_{11}^2}{\bar{\lambda}^2} + \frac{f_{11}\bar{f}_{20}}{2\bar{\lambda}^3}(3\bar{\lambda} - 2\lambda) + \frac{\bar{f}_{11}f_{02}}{2|\lambda|^2}\frac{2\bar{\lambda} - 3\lambda}{2\bar{\lambda} - \lambda}, \\
h_{03} &= \frac{f_{03}}{3\bar{\lambda} - \lambda} + \frac{3\bar{f}_{20}f_{02}}{\bar{\lambda}(3\bar{\lambda} - \lambda)} + \frac{3f_{11}f_{02}}{(3\bar{\lambda} - \lambda)(2\bar{\lambda} - \lambda)} \, .
\end{aligned}
$$

The next step is to evaluate all terms of order κ, that is, to find the h_{klmn}'s from

$$
h(w, \bar{w}, w', \bar{w}') = g(w, w') + 2a_{20}g(w, w')\psi(w) + a_{11}\left(\overline{g(w, w')}\psi(w) + g(w, w')\psi(\bar{w})\right) + \cdots \, . \tag{A.3.24}
$$

Since $\psi(w) = \mathcal{O}(w)$, we have that $h(w, \bar{w}, w', \bar{w}') = g(w, w')$ at order $\mathcal{O}(1)$. Moreover, if $g(0, 0) = 0$, i.e. g has no constant term, then $h(w, \bar{w}, w', \bar{w}') = g(w, w')$ holds up to order $\mathcal{O}(w, w')$. We expand $\tilde{g}$ into a formal Taylor series as has been done before for $\tilde{f}$,

$$
\tilde{g}(z, \bar{z}, z, ' \bar{z}'; \mu) = \sum_{0 \le k+l+m+n} \frac{1}{k!l!m!n!}\tilde{g}_{klmn}(\mu)z^k\bar{z}^l z'^m\bar{z}'^n \, . \tag{A.3.25}
$$

Then, $g(w, w') = \tilde{g}(\psi(w), \psi(\bar{w}), \psi(w'), \psi(\bar{w}'); \mu)$ and since $\psi(w) = w + \mathcal{O}(|w|^2)$, we have that $h_{0000} = \tilde{g}_{0000}$, and if $\tilde{g}_{0000} = 0$, then

$$
h_{klmn} = \tilde{g}_{klmn} \quad \text{for } k + l + m + n = 1, \quad k, l, m, n \ge 0. \quad \square
$$

Remark. The coefficient β reduces at the bifurcation parameter value $\mu = 0$ to

$$
\beta(0) = \frac{-i}{2\omega_0}\left(f_{20}f_{11} - 2|f_{11}|^2 - \frac{1}{3}|f_{02}|^2\right) - \frac{f_{21}}{2} \, . \tag{A.3.26}
$$

Note that, together with the foregoing remark, the normal form resembles to great extent the formula derived in Kuramoto's reductive perturbation, see Appendix A.2.1, although the latter pursues an alternative way to arrive at the amplitude equation.

In the following, we will briefly state the relationship between the original coupling function $\boldsymbol{g}(\boldsymbol{x}, \boldsymbol{x}'; \mu)$ in (A.3.8) and the coupling coefficients h_{klmn} of the dynamics in Hopf normal form as in Lemma A.5. Recall from Lemma A.2 that we can write $\boldsymbol{g}(\boldsymbol{x}, \boldsymbol{x}'; \mu)$ in complex form as

$$
\tilde{g}(z, \bar{z}, z', \bar{z}'; \mu) = \boldsymbol{v}(\mu)\boldsymbol{g}(z\boldsymbol{v}(\mu) + \bar{z}\bar{\boldsymbol{v}}(\mu), z'\boldsymbol{v}(\mu) + \bar{z}'\bar{\boldsymbol{v}}(\mu); \mu) \, . \tag{A.3.27}
$$

Given a Taylor expansion of $\boldsymbol{g} = (g_1, g_2)^\intercal$ with $\boldsymbol{x} = (x, y)^\intercal, \boldsymbol{x}' = (x', y')^\intercal$,

$$
g_i(\boldsymbol{x}, \boldsymbol{x}', a) = \sum_{0 \le k+l+m+n} \frac{1}{k!l!m!n!}g_{klmn}^{(i)}(a)x^k y^l x'^m y'^n, \quad \text{for } i = 1, 2 \, , \tag{A.3.28}
$$

there exists a mapping

$$
\left\{\left(g_{klmn}^{(1)}, g_{klmn}^{(2)}\right)\right\} \mapsto \left\{\tilde{g}_{klmn}\right\}
$$

from the coupling coefficients $g_{klmn}^{(i)}$ of the original dynamics (A.3.8) to those of the complex-valued coupling function (A.3.25). To be precise, substituting $\boldsymbol{x} = (zu_1(\mu) + \bar{z}\bar{u}_1(\mu), zu_2(\mu) + \bar{z}\bar{u}_2(\mu))^\intercal$ and an equivalent expression for $\boldsymbol{x}'$ into (A.3.28), we have

$$
\begin{aligned}
\tilde{g}(z, z', \bar{z}, \bar{z}'; \mu) &= \sum_{i=1}^{2} v_i(\mu)g_i(zu(\mu) + \bar{z}\bar{u}(\mu), z'u(\mu) + \bar{z}'\bar{u}(\mu); \mu) \\
&= \sum_{i=1}^{2} \sum_{0 \le k+l+m+n} \frac{1}{k!l!m!n!}v_i(\mu)g_{klmn}^{(i)}(\mu)\left\{[zu_1(\mu) + \bar{z}\bar{u}_1(\mu)]^k\,[zu_2(\mu) + \bar{z}\bar{u}_2(\mu)]^l\right. \\
&\qquad \left. \cdot\left[z'u_1(\mu) + \bar{z}'\bar{u}_1(\mu)\right]^m\left[z'u_2(\mu) + \bar{z}'\bar{u}_2(\mu)\right]^n\right\}
\end{aligned}
$$

Using the binomial theorem, $(a+b)^n = \sum_{k=0}^{n} \binom{n}{k} a^k b^{n-k}$, we can simplify the equation to

$$\begin{aligned}\tilde{g}(z,z',\bar{z},\bar{z}';\mu) = &\sum_{0\le k+l+m+n} \Big\{ \frac{1}{k!l!m!n!} \left(\sum_{i=1}^{2} v_i(\mu) g^{(i)}_{klmn}(\mu) \right) \cdot \Big[\sum_{a=0}^{k} \sum_{b=0}^{l} \sum_{c=0}^{m} \sum_{d=0}^{n} \binom{k}{a}\binom{l}{b}\binom{m}{c}\binom{n}{d} \\ &\cdot \left(u_1^{a+c} \bar{u}_1^{k+m-a-c} u_2^{b+d} \bar{u}_2^{l+n-b-d}\right) z^{a+b} \bar{z}^{k+l-a-b} z'^{c+d} \bar{z}'^{m+n-c-d} \Big] \Big\} \\ \overset{!}{=} &\sum_{0\le k+l+m+n} \frac{1}{k!l!m!n!} \tilde{g}_{klmn}(\mu) z^k \bar{z}^l z'^m \bar{z}'^n \ .\end{aligned}$$

Note that $\boldsymbol{u} = \boldsymbol{u}(\mu)$ depends on the parameter μ, which we have omitted for the sake of simplicity. Comparing the sums in the first equation and collecting coefficients of the same order leads to the correct expressions for $\tilde{g}_{klmn}$ of the second equation.

With the coefficients $\tilde{g}_{klmn}$ at hand, one can apply the forward transform (A.3.19) to the coupling function (A.3.25) as has been done at the end of Lemma A.5, and express $\tilde{g}$ in terms of w, w' as the formal power series

$$\begin{aligned} g(w,w') &= \tilde{g}\left(\psi(w), \psi(\bar{w}), \psi(w'), \psi(\bar{w}')\right) = \sum_{k+l+m+n\ge 0} \frac{1}{k!l!m!n!} \tilde{g}_{klmn} \psi(w)^k \psi(\bar{w})^l \psi(w')^m \psi(\bar{w}')^n \\ &=: \sum_{k+l+m+n\ge 0} g_{klmn} w^k \bar{w}^l w'^m \bar{w}'^n \ . \end{aligned} \tag{A.3.29}$$

Due to the near-identity character of the transform $\psi(w)$, the terms $\tilde{g}_{klmn}$ and g_{klmn} coincide for $k+l+m+n \in \{0,1\}$. For higher-order terms we find

$$\begin{aligned} g_{2000} &= \tfrac{1}{2}\tilde{g}_{2000} + \frac{h_{20}}{2}\tilde{g}_{1000} + \frac{\bar{h}_{02}}{2}\tilde{g}_{0100}, & g_{1010} &= \tilde{g}_{1010}, \quad g_{1001} = \tilde{g}_{1001}, \\ g_{0200} &= \tfrac{1}{2}\tilde{g}_{0200} + \frac{h_{02}}{2}\tilde{g}_{1000} + \frac{\bar{h}_{20}}{2}\tilde{g}_{0100}, & g_{0110} &= \tilde{g}_{0110}, \quad g_{0101} = \tilde{g}_{0101}, \\ g_{0020} &= \tfrac{1}{2}\tilde{g}_{0020} + \frac{h_{20}}{2}\tilde{g}_{0010} + \frac{\bar{h}_{02}}{2}\tilde{g}_{0001}, & g_{1100} &= \tilde{g}_{1100} + h_{11}\tilde{g}_{1000} + \bar{h}_{11}\tilde{g}_{0100}, \\ g_{0002} &= \tfrac{1}{2}\tilde{g}_{0002} + \frac{h_{02}}{2}\tilde{g}_{0010} + \frac{\bar{h}_{20}}{2}\tilde{g}_{0001}, & g_{0011} &= \tilde{g}_{0011} + h_{11}\tilde{g}_{0010} + \bar{h}_{11}\tilde{g}_{0001}, \end{aligned}$$

and some particular terms of third order

$$\begin{aligned} g_{2100} &= \tfrac{1}{2}\tilde{g}_{2100} + \left(\frac{h_{20}}{2} + \bar{h}_{11}\right)\tilde{g}_{1100} + \frac{\bar{h}_{12}}{2}\tilde{g}_{0100} \\ g_{2001} &= \tfrac{1}{2}\tilde{g}_{2001} + \frac{h_{20}}{2}\tilde{g}_{1001} + \frac{\bar{h}_{02}}{2}\tilde{g}_{0101} \\ g_{0120} &= \tfrac{1}{2}\tilde{g}_{0120} + \frac{h_{20}}{2}\tilde{g}_{0110} + \frac{\bar{h}_{02}}{2}\tilde{g}_{0101} \\ g_{0021} &= \tfrac{1}{2}\tilde{g}_{0021} + \left(\frac{h_{20}}{2} + \bar{h}_{11}\right)\tilde{g}_{0011} + \frac{\bar{h}_{12}}{2}\tilde{g}_{0001} \\ g_{1110} &= \tilde{g}_{1110} + h_{11}\tilde{g}_{1010} + \bar{h}_{11}\tilde{g}_{0110} \\ g_{1011} &= \tilde{g}_{1011} + h_{11}\tilde{g}_{1010} + \bar{h}_{11}\tilde{g}_{0101} \ . \end{aligned}$$

However, we can insert (A.3.29) into (A.3.24)

$$\begin{aligned} h(w,\bar{w},w',\bar{w}') &= \sum_{k+l+m+n\ge 0} h_{klmn} w^k \bar{w}^l w'^m \bar{w}'^n \\ &= \left(\sum_{k+l+m+n\ge 0} g_{klmn} w^k \bar{w}^l w'^m \bar{w}'^n\right) + 2a_{20}\left(\sum_{k+l+m+n\ge 0} g_{klmn} w^k \bar{w}^l w'^m \bar{w}'^n\right)\cdot \psi(w) + \cdots \ , \end{aligned} \tag{A.3.30}$$

and solve for the h_{klmn}'s. As has been shown in Section 6.3.3, we only need a particular choice of coupling coefficients, which are

$$\begin{aligned} &h_{0000} = g_{0000}, \quad h_{0010} = g_{0010} + 2a_{20}g_{0000} + a_{11}\bar{g}_{0000}, \quad h_{0001} = g_{0001} + a_{11}g_{0000} + 2a_{02}\bar{g}_{0000}, \\ &h_{2100} = g_{2100} + a_{20}\left[2g_{1100} + h_{20}g_{0100} + 2h_{11}g_{1000}\right] + a_{02}\left[2\bar{g}_{0200} + 2\bar{h}_{11}\bar{g}_{0100} + \bar{h}_{02}\bar{g}_{1000} + \bar{h}_{12}\bar{g}_{0000}\right] \\ &\qquad + a_{11}\left[g_{2000} + \bar{g}_{1100} + \bar{h}_{11}g_{1000} + \frac{\bar{h}_{02}}{2}g_{0100} + \frac{h_{20}}{2}\bar{g}_{1000} + h_{11}\bar{g}_{0100} + \frac{\bar{h}_{12}}{2}g_{0000}\right] \end{aligned}$$

$$
\begin{aligned}
&+ 3a_{30}\left[g_{0100} + 2h_{11}g_{0000}\right] + a_{21}\left[2g_{1000} + \bar{g}_{1000} + \left(h_{20} + 2\bar{h}_{11}\right)g_{0000} + 2h_{11}\bar{g}_{0000}\right]\\
&+ a_{12}\left[2\bar{g}_{0100} + \bar{h}_{02}g_{0000} + \left(h_{20} + 2\bar{h}_{11}\right)\bar{g}_{0000}\right] + 3a_{03}\bar{h}_{02}\bar{g}_{0000},\\
h_{2001} &= g_{2001} + 2a_{20}\left[g_{1001} + \frac{h_{20}}{2}g_{0001}\right] + a_{11}\left[\frac{\bar{h}_{02}}{2}g_{0001} + \bar{g}_{0110} + \frac{h_{20}}{2}\bar{g}_{0010}\right] + 2a_{02}\frac{\bar{h}_{02}}{2}\bar{g}_{0010}\\
&+ 3a_{30}g_{0001} + a_{21}\bar{g}_{0010},\\
h_{0120} &= g_{0120} + a_{11}g_{0020} + 2a_{02}\bar{g}_{0002},\\
h_{0021} &= g_{0021},
\end{aligned}
$$

and

$$
\begin{aligned}
h_{1110} &= g_{1110} + 2a_{20}\left[g_{0110} + h_{11}g_{0010}\right] + a_{11}\left[g_{1010} + \bar{h}_{11}g_{0010} + \bar{g}_{1001} + h_{11}\bar{g}_{0001}\right]\\
&+ 2a_{02}\left[\bar{g}_{0101} + \bar{h}_{11}\bar{g}_{0001}\right] + 2a_{21}g_{0010} + 2a_{12}\bar{g}_{0001},\\
h_{1011} &= g_{1011} + 2a_{20}g_{0011} + a_{11}\bar{g}_{0011}\ .
\end{aligned}
$$

In comparison with Kuramoto's reductive perturbation, see Appendix A.2.1, we find the coefficients

$$h_{0010} = g_{0010} = \tilde{g}_{0010} = v_1(\mu)g^{(1)}_{0010}u_1(\mu) + v_2(\mu)g^{(2)}_{0010}u_2(\mu)\ , \tag{A.3.31}$$

$$
\begin{aligned}
h_{0120} &= g_{0120} - h_{11}g_{0020} - h_{02}\bar{g}_{0002} \qquad\qquad (A.3.32)\\
&= \tfrac{1}{2}\Big(\tilde{g}_{0120} - h_{11}\tilde{g}_{0020} - h_{02}\overline{\tilde{g}}_{0002} + h_{20}\tilde{g}_{0110} + \bar{h}_{02}\tilde{g}_{0101}\\
&\quad - h_{11}h_{20}\tilde{g}_{0010} - h_{11}\bar{h}_{02}\tilde{g}_{0001} - |h_{02}|^2\overline{\tilde{g}}_{0010} - h_{20}h_{02}\overline{\tilde{g}}_{0001}\Big)\ .
\end{aligned}
$$

Note that the first term in parentheses, $\tilde{g}_{0120}$, can be ascribed to the coupling function G_{12}, the second and third to G_{02}, the fourth and fifth to G_{11}, and the latter four to G_{01}, as they are used in Appendix A.2.1. In particular, in case of linear coupling in the original dynamics, only the terms corresponding to G_{01} survive and (A.3.32) reduces to

$$h_{0120} = -\tfrac{1}{2}\Big(h_{11}h_{20}\tilde{g}_{0010} + h_{11}\bar{h}_{02}\tilde{g}_{0001} + |h_{02}|^2\overline{\tilde{g}}_{0010} + h_{20}h_{02}\overline{\tilde{g}}_{0001}\Big)\ . \tag{A.3.33}$$

Last but not least, we consider a network of $N > 2$ coupled oscillators $\boldsymbol{x}_k = (x_k, y_k) \in \mathbb{R}^2$, $k = 1, \ldots, N$, following the equivalent dynamics to (A.3.8),

$$\dot{\boldsymbol{x}}_k = \boldsymbol{f}(\boldsymbol{x}_k; \mu) + \kappa \boldsymbol{g}_k(\boldsymbol{x}_1, \ldots, \boldsymbol{x}_N; \mu) + \mathcal{O}(\kappa^2)\ . \tag{A.3.34}$$

The reasoning above extends to the full system dynamics (A.3.34). Especially the type of coupling between oscillators fully translates into the corresponding coupling function h_k in the reduced normal form dynamics $\dot{w}_k = \alpha w_k - \beta w_k^2\bar{w}_k + \kappa h_k(w_1, \ldots, w_N)$. In fact, we can prove the following

Lemma A.6. *Given system (A.3.34), where each uncoupled unit $\boldsymbol{x}_k$ is close to a supercritical Hopf bifurcation with $|\mu| \ll 1$ and the coupling between units is sufficiently weak, $0 < \kappa \ll |\mu| \ll 1$. If the coupling function*

$$\boldsymbol{g}_k(\boldsymbol{x}_1, \ldots, \boldsymbol{x}_N; \mu) = \hat{\boldsymbol{g}}_k(\boldsymbol{x}_1, \ldots, \boldsymbol{x}_N) := \sum_{j=1}^{N} \boldsymbol{g}_{kj}(\boldsymbol{x}_j, \boldsymbol{x}_k)$$

can be decomposed into the sum of pairwise coupling functions $\boldsymbol{g}_{kj}$, then also the coupling function h_k in the reduced Hopf normal form decomposes into pairwise interactions,

$$h_k(w_1, \ldots, w_N) = \sum_{j=1}^{N} h_{kj}(w_j, w_k)\ .$$

Proof. The demonstration of the lemma is constructive and follows closely the proof of Lemma A.5. The main assumption lies within the theory of weak coupling and can be justified in following way, see also the reasoning and proof around [Theorem 5.8, 46]: A mathematically rigorous normal form reduction of the full network may consider coordinate transforms of the form $Z = \Psi(W)$ where $Z = (z_1, \ldots, z_N)$, $W = (w_1, \ldots, w_N)$ and $\Psi = (\psi_1, \ldots, \psi_N)$ with $\psi_j = \psi_j(w_1, \ldots, w_N)$. This general transformation can presumably lead to mixed coupling terms in the normal form beyond pairwise interactions; see Section 6.3.4 for the full Hopf normal form of a network with $S_N \times S^1$-equivariance. For weak coupling, however, we may consider $\psi_j(w_1, \ldots, w_N) \approx \psi_j^0(w_j) + \kappa\psi_j^1(w_1, \ldots, w_N)$ and for $\kappa \to 0$ we have $\psi_j(w_1, \ldots, w_N) = \psi_j^0(w_j)$. Given that the uncoupled systems are all identical, the local coordinate transforms $\psi_j^0 = \psi$ coincide with (A.3.19), which results in $\Psi(W) \approx \big(\psi(w_1), \ldots, \psi(w_N)\big)$. Then, the proof of the lemma follows immediately.

For the sake of completeness, we provide the details of the proof: Recall that we identified both the normal form and coupling parameters β, h_{klmn} by inserting the local coordinate transform $\psi(w)$, see (A.3.19), into the derivative of the local

inverse transform (A.3.23) and by a subsequent comparison of coefficients. Focusing on the terms of order $\mathcal{O}(\kappa)$, we have

$$\begin{aligned}\dot{w}_k = f(w_k) + \kappa \Big[& g_k(w_1,\ldots,w_N) + 2a_{20} g_k(w_1,\ldots,w_N)\psi(w_k) \\ & + a_{11}\big(\overline{g_k(w_1,\ldots,w_N)}\psi(w_k) + g_k(w_1,\ldots,w_N)\psi(\bar{w}_k)\big) + \cdots \Big]\end{aligned} \tag{A.3.35}$$

with $f(w)$ consisting of terms that eventually become $\alpha w - \beta w^2 \bar{w} + \mathcal{O}(|w|^4)$. Recall also that the coupling function $g_k(w_1,\ldots,w_N)$ is determined from the original coupling $\hat{\boldsymbol{g}}_k$ via the transformations

$$\hat{\boldsymbol{g}}_k(\boldsymbol{x}_1,\ldots,\boldsymbol{x}_N) \longmapsto \tilde{g}_k(z_1,\ldots,z_N) \longmapsto g_k(w_1,\ldots,w_N)\,.$$

Each of these transformations respects the form of coupling. In particular, for $\hat{\boldsymbol{g}}_k(\boldsymbol{x}_1,\ldots,\boldsymbol{x}_N) = \sum_j \boldsymbol{g}_{kj}(\boldsymbol{x}_j,\boldsymbol{x}_k)$, then $\tilde{g}_k$ and eventually also g_k can be decomposed exactly into $g_k(w_1,\ldots,w_N) = \sum_j g_{kj}(w_j,w_k)$. Inserting this into (A.3.35) and given that $\psi(w_k)$ is a polynomial only in w_k, the right-hand side of (A.3.35) can be written in the form $f(w_k) + \kappa \sum_j h_{kj}(w_j,w_k)$ with

$$h_{kj}(w_j,w_k) := g_{kj}(w_j,w_k) + 2a_{20} g_{kj}(w_j,w_k)\psi(w_k) + a_{11}\left(\overline{g_{kj}(w_j,w_k)}\psi(w_k) + g_{kj}(w_j,w_k)\psi(\bar{w}_k)\right) + \cdots + \mathcal{O}(|w|^4)\,. \quad \square$$

A.4. Takens' reduction via Lie brackets

We consider a two-dimensional system $\dot{\boldsymbol{x}} = \boldsymbol{f}(\boldsymbol{x};\mu)$, $\boldsymbol{x} = (x,y) \in \mathbb{R}^2$ near a Hopf bifurcation. For a small perturbation parameter $\mu > 0$ and an equilibrium solution with eigenvalues $\pm i\omega_0 \neq 0$ at $\mu = 0$, we can shift the origin appropriately such that $\boldsymbol{x} = 0$ is the equilibrium solution undergoing a supercritical Hopf bifurcation. Furthermore, we can bring the system into Jordan real form so that the dynamics expanded as a Taylor series around $\boldsymbol{x} = 0$ reads

$$\dot{\boldsymbol{x}} = \boldsymbol{L}\boldsymbol{x} + \boldsymbol{F}_2(\boldsymbol{x}) + \boldsymbol{F}_3(\boldsymbol{x}) + \cdots + \boldsymbol{F}_r(\boldsymbol{x}) + \mathcal{O}(|\boldsymbol{x}|^{r+1}), \tag{A.4.1}$$

with

$$\begin{aligned}\boldsymbol{L} &= \boldsymbol{L}_0 + \mu\boldsymbol{L}_1 + \mathcal{O}(\mu^2) = \begin{pmatrix} 0 & -\omega_0 \\ \omega_0 & 0 \end{pmatrix} + \mu \begin{pmatrix} \beta & -\alpha \\ \alpha & \beta \end{pmatrix} + \mathcal{O}(\mu^2)\,, \\ \boldsymbol{F}_2(\boldsymbol{x}) &= \begin{pmatrix} F_{21}(\boldsymbol{x}) \\ F_{22}(\boldsymbol{x}) \end{pmatrix} = \begin{pmatrix} a_{20} & a_{11} & a_{02} \\ b_{20} & b_{11} & b_{02} \end{pmatrix} \begin{pmatrix} x^2 \\ xy \\ y^2 \end{pmatrix}\,.\end{aligned}$$

Note that for $\mu > 0$ we can introduce $\mu = \varepsilon^2$ with $0 < \varepsilon \ll 1$ and that the common asymptotic scaling $\mathcal{O}(|\boldsymbol{x}|) = \mathcal{O}(x) = \mathcal{O}(y) = \varepsilon$ is used in (A.4.1) and all subsequent series approximations. Note further that we can extend the $(n=2)$-dimensional system $\dot{\boldsymbol{x}} = \boldsymbol{f}(\boldsymbol{x};\mu)$ to the larger, $n+1$-dimensional system

$$\begin{aligned}\dot{\boldsymbol{x}} &= \boldsymbol{f}(\boldsymbol{x};\mu)\,, \\ \dot{\mu} &= 0\,.\end{aligned} \tag{A.4.2}$$

One can perform the normal form calculations in a likewise manner, requiring the coordinate transforms $\underline{\boldsymbol{P}}(\boldsymbol{x};\mu)$ to be of the form $\underline{\boldsymbol{P}}(\boldsymbol{x};\mu) = (\boldsymbol{P}(\boldsymbol{x};\mu);\mu)$. Apparently, they will leave the equation $\dot{\mu} = 0$ invariant, but transform $\dot{\boldsymbol{x}} = \boldsymbol{f}(\boldsymbol{x};\mu)$ in a μ-dependent way. Practically, the normal form computations remain the same, yet, the n-dimensional normal form system remains in normal form as μ is varied to drive the system through the bifurcation. While Poincaré's reduction via nonlinear transforms as presented in Section 4.3.2 takes the parameter dependence fully into account, Kuramoto's reductive perturbation approach, Section 4.3.1, does not consider the extended system. For illustration purposes, we stick to the non-extended system also in this section to emphasize the reduction of the higher order normal form.[46]

Now, for $\boldsymbol{w} = (w_1,w_2)^\intercal$ and $\mathcal{P}_k$ denoting the set of homogeneous polynomials of order k, the Lie bracket for system (A.4.1) with $L = \boldsymbol{L}_0\boldsymbol{x}$ and $\boldsymbol{p}_k = (p_{k1},p_{k2})^\intercal \in \mathcal{P}_k$ is given by

$$\text{ad}\, L(\boldsymbol{p}_k)(\boldsymbol{w}) = \begin{pmatrix} 0 & -\omega_0 \\ \omega_0 & 0 \end{pmatrix} \begin{pmatrix} p_{k1}(\boldsymbol{w}) \\ p_{k2}(\boldsymbol{w}) \end{pmatrix} - \begin{pmatrix} \partial p_{k1}/\partial x & \partial p_{k1}/\partial y \\ \partial p_{k2}/\partial x & \partial p_{k2}/\partial y \end{pmatrix} \begin{pmatrix} 0 & -\omega_0 \\ \omega_0 & 0 \end{pmatrix} \begin{pmatrix} w_1 \\ w_2 \end{pmatrix}\,. \tag{A.4.3}$$

For second-order normal forms, we are looking for a transformation $\boldsymbol{p}_2$ of the form $\boldsymbol{x} = \boldsymbol{w} + \boldsymbol{p}_2(\boldsymbol{w})$, where

$$\boldsymbol{p}_2(\boldsymbol{w}) = \begin{pmatrix} p_{21}(\boldsymbol{w}) \\ p_{22}(\boldsymbol{w}) \end{pmatrix} = \begin{pmatrix} \sum_{j=0}^2 c_{ij} w_1^i w_2^j \\ \sum_{j=0}^2 d_{ij} w_1^i w_2^j \end{pmatrix}\,, \quad i = 2-j\,. \tag{A.4.4}$$

[46] In this particular section the order of the normal form is indicated by the index k of the subsequent transformations $\boldsymbol{p}_k$. Compared to the general notation in all other parts of the report, $k=3$ corresponds to second-order normal forms, $k=5$ to third-order, etc.

We shall perform the Lie bracket operation (A.4.3) on each basis element of $\mathcal{P}_2$, which is given by

$$\mathcal{P}_2 = \text{span}\left\{\begin{pmatrix} w_1^2 \\ 0 \end{pmatrix}, \begin{pmatrix} w_1 w_2 \\ 0 \end{pmatrix}, \begin{pmatrix} w_2^2 \\ 0 \end{pmatrix}, \begin{pmatrix} 0 \\ w_1^2 \end{pmatrix}, \begin{pmatrix} 0 \\ w_1 w_2 \end{pmatrix}, \begin{pmatrix} 0 \\ w_2^2 \end{pmatrix}\right\} . \tag{A.4.5}$$

We find

$$\text{ad } L(\mathcal{P}_2) = \text{span}\left\{\begin{pmatrix} w_1^2 & w_1 w_2 & w_2^2 & 0 & 0 & 0 \\ 0 & 0 & 0 & w_1^2 & w_1 w_2 & w_2^2 \end{pmatrix} \cdot \boldsymbol{A}_L^2\right\} = \mathcal{P}_2 \cdot \boldsymbol{A}_L^2 , \tag{A.4.6}$$

with

$$\boldsymbol{A}_L^2 = \omega_0 \begin{pmatrix} 0 & -1 & 0 & -1 & 0 & 0 \\ 2 & 0 & -2 & 0 & -1 & 0 \\ 0 & 1 & 0 & 0 & 0 & -1 \\ 1 & 0 & 0 & 0 & -1 & 0 \\ 0 & 1 & 0 & 2 & 0 & -2 \\ 0 & 0 & 1 & 0 & 1 & 0 \end{pmatrix} .$$

For $\omega_0 > 0$ we have $\det\left(\boldsymbol{A}_L^2\right) = 8\omega_0 > 0$, that is, $\boldsymbol{A}_L^2$ is non-singular and has full rank. This implies that the image of $\mathcal{P}_2$ under ad L is the whole subspace $\mathcal{P}_2$, and therefore all second order terms can be removed by a suitable change of variables. Indeed, substituting (A.4.4) into (4.14) of the main text and using that

$$(D\boldsymbol{p}(\boldsymbol{w}))^{-1} = (\boldsymbol{I} + D\boldsymbol{p}_k(\boldsymbol{w}))^{-1} = \boldsymbol{I} - D\boldsymbol{p}_k(\boldsymbol{w}) + \mathcal{O}(|\mathbf{w}|^2) , \tag{A.4.7}$$

we have

$$\dot{\boldsymbol{w}} = \sum_{N=0}^{\infty}(-1)^N \left[D\boldsymbol{p}_2(\boldsymbol{w})\right]^N \left\{\boldsymbol{L}\boldsymbol{w} + \boldsymbol{L}\boldsymbol{p}_2(\boldsymbol{w}) + \sum_{n=2}^{\infty}\sum_{m=0}^{n} \frac{D^m \boldsymbol{F}_n(\boldsymbol{w})}{m!} \left[\boldsymbol{p}_2(\boldsymbol{w})\right]^m\right\} \tag{A.4.8}$$

$$= \boldsymbol{L}\boldsymbol{w} + \sum_{n=2}^{\tilde{N}} \boldsymbol{F}_n^{(1)}(\boldsymbol{w}) \tag{A.4.9}$$

where we truncated the Taylor series at order $\tilde{N}$ and with

$$\boldsymbol{F}_n^{(1)}(\boldsymbol{w}) = \begin{pmatrix} F_{n1}^{(1)}(\boldsymbol{w}) \\ F_{n2}^{(1)}(\boldsymbol{w}) \end{pmatrix} = \begin{pmatrix} \sum_{j=0}^{2} a_{ij}^{(1)} w_1^i w_2^j \\ \sum_{j=0}^{2} b_{ij}^{(1)} w_1^i w_2^j \end{pmatrix} , \quad n = 2, \ldots, \tilde{N},\ i = 2 - j ; \tag{A.4.10}$$

the number in the superscript parentheses refers to the index of coordinate transformations. Since the complement $\mathcal{H}_2$ of im (ad $L(\mathcal{P}_2)$) in $\mathcal{P}_2$ is $\mathcal{H}_2 = \{0\}$, we have

$$\boldsymbol{F}_2^{(1)}(\boldsymbol{w}) = \boldsymbol{F}_2(\boldsymbol{w}) + L\boldsymbol{p}_2(\boldsymbol{w}) - D\boldsymbol{p}_2(\boldsymbol{w}) \cdot L(\boldsymbol{w}) = 0 , \tag{A.4.11}$$

that is, $a_{ij}^{(1)} = b_{ij}^{(1)} = 0$ for all $i+j = 2$. Note that in order to derive $\boldsymbol{F}_2^{(1)}$ at order $\mathcal{O}(\varepsilon^2)$, we again used that $\mu = \varepsilon^2$ and that $\boldsymbol{F}_n^{(l)} = \mathcal{O}(\varepsilon^n)$ in the series representation (A.4.10). Solving now the linear algebraic equation (A.4.11) for $\boldsymbol{p}_2$ in the space $\mathcal{P}_2$, we find the coefficients c_{ij}, d_{ij} in (A.4.4) as

$$\begin{pmatrix} c_{20} \\ c_{11} \\ c_{02} \\ d_{20} \\ d_{11} \\ d_{02} \end{pmatrix} = -\left(\boldsymbol{A}_L^2\right)^{-1} \begin{pmatrix} a_{20} \\ a_{11} \\ a_{02} \\ b_{20} \\ b_{11} \\ b_{02} \end{pmatrix} = -\left(3\omega_0\right)^{-1} \begin{pmatrix} b_{20} + a_{11} + 2b_{02} \\ -2a_{20} - b_{11} + 2a_{02} \\ 2b_{20} - a_{11} + b_{02} \\ a_{20} + b_{11} - 2a_{02} \\ -2b_{20} + a_{11} + 2b_{02} \\ -2a_{20} - b_{11} - a_{02} \end{pmatrix} . \tag{A.4.12}$$

As said, the higher order normal form computations build upon each other iteratively. Hence, for the third-order normal form we are looking for a transformation $\boldsymbol{x} = \boldsymbol{w} + \boldsymbol{p}_3(\boldsymbol{w})$ with

$$\boldsymbol{p}_3(\boldsymbol{w}) = \begin{pmatrix} P_{31}(\boldsymbol{w}) \\ P_{32}(\boldsymbol{w}) \end{pmatrix} = \begin{pmatrix} \sum_{j=0}^{3} c_{ij} w_1^i w_2^j \\ \sum_{j=0}^{3} d_{ij} w_1^i w_2^j \end{pmatrix} , \quad i = 3 - j . \tag{A.4.13}$$

$\mathcal{P}_3$ is eight-dimensional and given by

$$\mathcal{P}_3 = \text{span}\left\{\begin{pmatrix} w_1^3 \\ 0 \end{pmatrix}, \begin{pmatrix} w_1^2 w_2 \\ 0 \end{pmatrix}, \begin{pmatrix} w_1 w_2^2 \\ 0 \end{pmatrix}, \begin{pmatrix} w_2^3 \\ 0 \end{pmatrix}, \begin{pmatrix} 0 \\ w_1^3 \end{pmatrix}, \begin{pmatrix} 0 \\ w_1^2 w_2 \end{pmatrix}, \begin{pmatrix} 0 \\ w_1 w_2^2 \end{pmatrix}, \begin{pmatrix} 0 \\ w_2^3 \end{pmatrix}\right\} . \tag{A.4.14}$$

Similar to (A.4.6), we find

$$\text{ad } L(\mathcal{P}_3) = \mathcal{P}_3 \cdot \boldsymbol{A}_L^3 \tag{A.4.15}$$

with

$$\boldsymbol{A}_L^3 = \omega_0 \begin{pmatrix} 0 & -1 & 0 & 0 & -1 & 0 & 0 & 0 \\ 3 & 0 & -2 & 0 & 0 & -1 & 0 & 0 \\ 0 & 2 & 0 & -3 & 0 & 0 & -1 & 0 \\ 0 & 0 & 1 & 0 & 0 & 0 & 0 & -1 \\ 1 & 0 & 0 & 0 & 0 & -1 & 0 & 0 \\ 0 & 1 & 0 & 0 & 3 & 0 & -2 & 0 \\ 0 & 0 & 1 & 0 & 0 & 2 & 0 & -3 \\ 0 & 0 & 0 & 1 & 0 & 0 & 1 & 0 \end{pmatrix} .$$

The vectors $\boldsymbol{e}_1 = (1, 0, 1, 0, 0, 1, 0, 1)^\intercal$ and $\boldsymbol{e}_2 = (0, -1, 0, -1, 1, 0, 1, 0)^\intercal$ are two eigenvectors corresponding to the zero eigenvalue of $\boldsymbol{A}_L^3$. Therefore, $\boldsymbol{A}_L^3$ induces a non-vanishing complementary space $\mathcal{H}_3$ given by

$$\mathcal{H}_3 = \mathcal{P}_3 \cdot \begin{pmatrix} \boldsymbol{e}_1 & \boldsymbol{e}_2 \end{pmatrix} = \text{span}\left\{ \begin{pmatrix} w_1(w_1^2 + w_2^2) \\ w_2(w_1^2 + w_2^2) \end{pmatrix}, \begin{pmatrix} -w_2(w_1^2 + w_2^2) \\ w_1(w_1^2 + w_2^2) \end{pmatrix} \right\} . \tag{A.4.16}$$

The resulting third-order normal form takes the following form

$$\begin{aligned} \dot{w}_1 &= \beta\mu w_1 - (\alpha\mu + \omega_0)w_2 + a_1 w_1(w_1^2 + w_2^2) - b_1 w_2(w_1^2 + w_2^2) + \mathcal{O}(|w_1|^5, |w_2|^5) , \\ \dot{w}_2 &= (\alpha\mu - \omega_0)w_1 + \beta\mu w_2 + a_1 w_2(w_1^2 + w_2^2) + b_1 w_1(w_1^2 + w_2^2) + \mathcal{O}(|w_1|^5, |w_2|^5) , \end{aligned} \tag{A.4.17}$$

where a_1, b_1 are to be determined. In the same manner as before, we have

$$\begin{aligned} \dot{\boldsymbol{w}} &= \sum_{N=0}^{\tilde{N}} (-1)^N \left[D\boldsymbol{p}_3(\boldsymbol{w})\right]^N \left\{ \boldsymbol{L}\boldsymbol{w} + \boldsymbol{L}\boldsymbol{p}_3(\boldsymbol{w}) + \sum_{n=2}^{\tilde{N}} \sum_{m=0}^{n} \frac{D^m \boldsymbol{F}_n(\boldsymbol{w})}{m!} \left[\boldsymbol{p}_3(\boldsymbol{w})\right]^m \right\} \\ &= \boldsymbol{L}\boldsymbol{w} + \boldsymbol{F}_2^{(1)}(\boldsymbol{w}) + \sum_{n=3}^{\tilde{N}} \boldsymbol{F}_n^{(2)}(\boldsymbol{w}) \end{aligned} \tag{A.4.18}$$

where

$$\boldsymbol{F}_n^{(2)}(\boldsymbol{w}) = \begin{pmatrix} F_{n1}^{(2)}(\boldsymbol{w}) \\ F_{n2}^{(2)}(\boldsymbol{w}) \end{pmatrix} = \begin{pmatrix} \sum_{j=0}^{2} a_{ij}^{(2)} w_1^i w_2^j \\ \sum_{j=0}^{2} b_{ij}^{(2)} w_1^i w_2^j \end{pmatrix} , \quad n = 3, \ldots, \tilde{N}, \ i = 3 - j . \tag{A.4.19}$$

Thus, we have to solve

$$\boldsymbol{F}_3^{(2)}(\boldsymbol{w}) = \boldsymbol{F}_3^{(1)}(\boldsymbol{w}) + L\boldsymbol{p}_3(\boldsymbol{w}) - D\boldsymbol{p}_3(\boldsymbol{w}) \cdot L(\boldsymbol{w}) = \mathcal{H}_3(\boldsymbol{w}) \tag{A.4.20}$$

for $\boldsymbol{p}_3$, which we can rewrite in terms of the basis functions of $\mathcal{P}_3$ as

$$\boldsymbol{A}_L^3 \cdot \boldsymbol{\xi} = \boldsymbol{F}_3^{(1)} - \mathcal{H}_3 =: \boldsymbol{\kappa} \tag{A.4.21}$$

where we used (A.4.16) to get

$$\begin{aligned} \boldsymbol{\xi} &= \{c_{30}, c_{21}, c_{12}, c_{03}, d_{30}, d_{21}, d_{12}, d_{03}\}^\intercal , \\ \boldsymbol{\kappa} &= \{a_{30}^{(1)} - a_1, a_{21}^{(1)} + b_1, a_{12}^{(1)} - a_1, a_{03}^{(1)} + b_1, b_{30}^{(1)} - b_1, b_{21}^{(1)} - a_1, b_{12}^{(1)} - b_1, b_{03}^{(1)} - a_1\}^\intercal . \end{aligned}$$

Following the procedure outlined in [116,117], we find the resulting coefficients as

$$\begin{aligned} \begin{pmatrix} a_1 \\ b_1 \end{pmatrix} &= \frac{1}{8} \begin{pmatrix} a_{12}^{(1)} + 3a_{03}^{(1)} + b_{21}^{(1)} + 3b_{03}^{(1)} \\ -a_{21}^{(1)} - 3a_{03}^{(1)} + b_{12}^{(1)} + 3b_{30}^{(1)} \end{pmatrix} , \\ \begin{pmatrix} c_{30} \\ c_{21} \\ c_{12} \\ c_{03} \end{pmatrix} &= \frac{1}{8\omega_0} \begin{pmatrix} 0 \\ 3a_{30}^{(1)} - 3a_{12}^{(1)} + b_{21}^{(1)} - b_{03}^{(1)} \\ 3a_{21}^{(1)} - 3a_{03}^{(1)} + b_{30}^{(1)} + b_{12}^{(1)} \\ 0 \end{pmatrix} , \quad \begin{pmatrix} d_{30} \\ d_{21} \\ d_{12} \\ d_{03} \end{pmatrix} = \frac{1}{4\omega_0} \begin{pmatrix} a_{30}^{(1)} + a_{12}^{(1)} - b_{21}^{(1)} - b_{03}^{(1)} \\ a_{21}^{(1)} + 3a_{03}^{(1)} + 5b_{30}^{(1)} - b_{12}^{(1)} \\ 3a_{30}^{(1)} + a_{12}^{(1)} + b_{21}^{(1)} + 5b_{03}^{(1)} \\ a_{21}^{(1)} + a_{03}^{(1)} + b_{30}^{(1)} + b_{12}^{(1)} \end{pmatrix} . \end{aligned} \tag{A.4.22}$$

Applying the same procedure, we can continue these calculations and derive the coefficients of the normal forms of order 5 and higher. Generalizing system (A.4.17), the normal form of order $(2M - 1)$ can be written as

$$\frac{d}{dt} \begin{pmatrix} w_1 \\ w_2 \end{pmatrix} = \begin{pmatrix} \beta\mu & -(\alpha\mu + \omega_0) \\ (\alpha\mu + \omega_0) & \beta\mu \end{pmatrix} \begin{pmatrix} w_1 \\ w_2 \end{pmatrix} + \sum_{j=1}^{M-1} (w_1^2 + w_2^2)^j \begin{pmatrix} a_j & -b_j \\ b_j & a_j \end{pmatrix} \begin{pmatrix} w_1 \\ w_2 \end{pmatrix} + \mathcal{O}(|\mathbf{w}|^{2M+3}) , \tag{A.4.23}$$

or in complex form for $w \in \mathbb{C}$ as

$$\dot{w} = \left[(\beta + i\alpha)\mu + i\omega_0\right] w + \sum_{j=1}^{M-1} (a_j + ib_j)|w|^{2j} w + \mathcal{O}(|w|^{2M+3}) . \tag{A.4.24}$$

For fifth order, the next coefficients can be found as

$$\begin{pmatrix} a_2 \\ b_2 \end{pmatrix} = \frac{1}{16}\begin{pmatrix} 5a_{50}^{(3)} + a_{32}^{(3)} + a_{14}^{(3)} + b_{41}^{(3)} + b_{23}^{(3)} + 5b_{05}^{(3)} \\ -a_{41}^{(3)} - a_{23}^{(3)} - a_{14}^{(3)} - a_{05}^{(3)} + 5b_{50}^{(3)} + b_{32}^{(3)} + b_{14}^{(3)} \end{pmatrix} . \tag{A.4.25}$$

The corresponding coefficients c_{ij}, d_{ij} with $i+j=5$ for the transform $\boldsymbol{p}_5(w)$ are listed in [116]. The complexity of computing the coefficients for higher order normal forms increases rapidly — determining $a_{ij}^{(3)}, b_{ij}^{(3)}$ builds recursively on $a_{ij}^{(2)}, b_{ij}^{(2)}$ and the lower order near-identity transformations $\boldsymbol{p}_k$, $k \leq 4$. It becomes necessary to implement efficient algorithms in symbolic computation software without running in danger of overflow errors due to memory storage. An arithmetic algorithm including the computation of normal forms up to order 11 has been presented in [117].

Once higher-order normal forms and their corresponding series of transformations $\boldsymbol{p}_k$ have been established, the latter can be applied to the coupling term $\kappa \boldsymbol{g}(\boldsymbol{x}, \boldsymbol{x}')$ of (4.12). For our purposes, however, it is sufficient to consider the transformed coupling up to third order. As we have illustrated the derivation of the coupling term using nonlinear transforms in great detail in Appendix A.3, we refrain here from further cumbersome calculations.

A.5. Ashwin & Rodrigues' reduction via $\boldsymbol{S_N} \times \boldsymbol{S}^1$-symmetry

Ashwin and Rodrigues consider in [74] coupled oscillators $w_k \in \mathbb{C}$, $k = 1, \ldots, N > 4$, which follow the dynamics

$$\dot{w}_k = f(w_k; \mu) + \kappa\, g(w_k, w_1, \ldots, w_{k-1}, w_{k+1}, \ldots, w_N; \mu) + \mathcal{O}(\kappa^2) , \tag{A.5.1}$$

and where the whole network respects full permutation symmetry S_N and rotational invariance S^1. Using equivariant theory, they prove their main result in terms of the following phase reduction.

Theorem A.7 (*Theorem 3.2. [74]*). *Consider system (A.5.1) with S_N-symmetry (for fixed $N > 4$) such that the N uncoupled systems ($\kappa = 0$) undergo a generic supercritical Hopf bifurcation on μ passing through $\mu = 0$. There exists $\mu_0 > 0$ and $\kappa_0 = \kappa_0(\mu)$ such that for any $\mu \in (0; \mu_0)$ and $|\kappa| < \kappa_0(\mu)$ the system (A.5.1) has an attracting C^r-smooth invariant N-dimensional torus for arbitrarily large r. On this invariant torus, the phases θ_k of the flow can be expressed as a coupled oscillator system*

$$\dot{\theta}_k = \tilde{\Omega}(\theta, \kappa) + \kappa \left(H_k^{(2)}(\theta) + H_k^{(3)}(\theta) + H_k^{(4)}(\theta) \right) \tag{A.5.2}$$

$$\begin{aligned} H_k^{(2)}(\theta) &= \frac{1}{N} \sum_{j=1}^{N} H_2(\theta_j - \theta_k) \\ H_k^{(3)}(\theta) &= \frac{1}{N^2} \sum_{j,l=1}^{N} H_{3,1}(\theta_j + \theta_l - 2\theta_k) + \frac{1}{N^2} \sum_{j,l=1}^{N} H_{3,2}(2\theta_j - \theta_l - \theta_k) \\ H_k^{(4)}(\theta) &= \frac{1}{N^3} \sum_{j,l,m=1}^{N} H_4(\theta_j + \theta_l - \theta_m - \theta_k) \end{aligned} \tag{A.5.3}$$

for fixed $0 < \mu < \mu_0$ in the limit $\kappa \to 0$, where $\tilde{\Omega}(\theta, \kappa)$ is independent of k and

$$\begin{aligned} H_2(\varphi) &= \xi_1^0 \cos(\varphi + \chi_1^0) + \mu \xi_1^1 \cos(\varphi + \chi_1^1) + \mu \xi_2^1 \cos(2\varphi + \chi_2^1) \\ H_{3,1}(\varphi) &= \mu \xi_3^1 \cos(\varphi + \chi_3^1) \\ H_{3,2}(\varphi) &= \mu \xi_4^1 \cos(\varphi + \chi_4^1) \\ H_4(\varphi) &= \mu \xi_5^1 \cos(\varphi + \chi_5^1) . \end{aligned} \tag{A.5.4}$$

The constants ξ_i^j and χ_i^j are generically non-zero. The natural frequency $\tilde{\Omega}$ of each oscillator in the reduced phase dynamics (A.5.2) is given by

$$\tilde{\Omega}(\theta, \kappa) = \Omega + \kappa\mu \left[\frac{-\vartheta_4}{\beta_R} \cos(\psi_4) - \frac{\vartheta_5}{\beta_R N^2} \sum_{j,k=1}^{N} \cos(\psi_5 + \theta_j - \theta_k) \right] \tag{A.5.5}$$

with $\Omega = \alpha_I - \mu(\beta_I/\beta_R) + \mathcal{O}(\mu^2)$. The error term truncated in (A.5.2) satisfies $\tilde{g} = \mathcal{O}(\mu^2)$ uniformly in the phases θ_k. This truncation by removing $\tilde{g}$ and $\mathcal{O}(\kappa^2)$ terms is valid over time intervals $0 < t < \tilde{t}$ where $\tilde{t} = \mathcal{O}(\kappa^{-1}\mu^{-2})$ in the limit $0 < \kappa \ll \mu \ll 1$. In particular, for any N, this approximation involves up to four interacting phases.

Before we go into detail of the proof, we first state an immediate corollary for large oscillator systems of the form (A.5.1) with $S_N \times S^1$-equivariance, where each uncoupled system is close to a supercritical Hopf bifurcation.

Corollary A.8. *In the limit of weak coupling $0 < \kappa \ll \mu \ll 1$ and for a reasonably large network size $N \gg 4$, the coupled oscillator system (A.5.2) reduces to*

$$\dot{\theta}_k = \Omega + \hat{\kappa}\varepsilon^2 \left(\frac{1}{N} \sum_{j=1}^{N} \Big[\xi_1^0 \cos\big(\theta_j - \theta_k + \chi_1^0\big) + \varepsilon^2 \xi_2^1 \cos\big(2(\theta_j - \theta_k) + \chi_2^1\big) \Big] + \mathcal{O}(\varepsilon^3) \right) \tag{A.5.6}$$

with $\Omega = \alpha_I - \varepsilon^2(\beta_I/\beta_R) + \mathcal{O}(\varepsilon^4)$ and $\varepsilon^2 = \mu$ as well as $\hat{\kappa} = \kappa\varepsilon^2$ with $\varepsilon > 0$. In particular, the phase interaction function of (A.5.6) consists of first and second harmonics with merely pairwise interactions.

Proof. For large $N \gg 4$, we can assume that $1/N = \mathcal{O}(\varepsilon)$ where $\varepsilon > 0$ is such that $\varepsilon^2 = \mu$. In the weak coupling limit, we set $\hat{\kappa} = \kappa\varepsilon^2$. The natural frequency Ω coincides with $\tilde{\Omega}$ at order $\mathcal{O}(\varepsilon^4, \hat{\kappa}\varepsilon^4)$, see also (A.5.5). The terms $H_k^{(3)}(\theta)$, $H_k^{(4)}(\theta)$ in Theorem A.7 are of order $\mathcal{O}(\hat{\kappa}\varepsilon^5)$. Moreover, the term $\mu\xi_1^1 \cos(\varphi + \chi_1^1)$ in $g_2(\theta)$ is only some higher-order correction to the first harmonics, and can thus be discarded. The remaining terms finally constitute (A.5.6). □

The proof of Theorem A.7 can be found in [74] where the authors use Theorem 3.1, which is proven in [Theorem 4.2, 189]. It is noteworthy that this Theorem 3.1 provides a thorough decomposition of the coupling function $g(w_1, \ldots, w_N; \mu)$ when given as a polynomial of degree lower than or equal to 3. In fact, any polynomial function $h\colon \mathbb{C}^N \to \mathbb{C}^N$ of degree lower than or equal to 3 with $N \geq 4$ and which respects the $S_N \times S^1$-equivariance can be written as $h = (h_1, \ldots, h_N)$ where

$$\begin{aligned} h_1(w_1, w_2, \ldots, w_N) &= \sum_{i=-1}^{11} a_i \hat{h}_i(w_1, w_2, \ldots, w_N) \\ h_2(w_1, w_2, \ldots, w_N) &= h_1(w_2, w_1, \ldots, w_N) \\ &\vdots \\ h_N(w_1, w_2, \ldots, w_N) &= h_1(w_N, w_2, \ldots, w_1) \end{aligned} \tag{A.5.7}$$

and $\hat{h}_0(w) = w_1$, $\hat{h}_1(w) = |w_1|^2 w_1$, as well as

$$\begin{aligned} &\hat{h}_{-1}(w) = \frac{1}{N}\sum_{j=1}^{N} w_j, && \hat{h}_2(w) = w_1^2 \frac{1}{N}\sum_{j=1}^{N} \bar{w}_j, && \hat{h}_3(w) = |w_1|^2 \frac{1}{N}\sum_{j=1}^{N} w_j, \\ &\hat{h}_4(w) = w_1 \frac{1}{N}\sum_{j=1}^{N} |w_j|^2, && \hat{h}_5(w) = w_1 \frac{1}{N^2}\sum_{j,k=1}^{N} w_j \bar{w}_k, && \hat{h}_6(w) = \bar{w}_1 \frac{1}{N}\sum_{j=1}^{N} w_j^2, \\ &\hat{h}_7(w) = \bar{w}_1 \frac{1}{N^2}\sum_{j,k=1}^{N} w_j w_k, && \hat{h}_8(w) = \frac{1}{N}\sum_{j=1}^{N} |w_j|^2 w_j, && \hat{h}_9(w) = \frac{1}{N^2}\sum_{j,k=1}^{N} w_j^2 \bar{w}_k, \\ &\hat{h}_{10}(w) = \frac{1}{N^2}\sum_{j,k=1}^{N} w_j |w_k|^2, && \hat{h}_{11}(w) = \frac{1}{N^3}\sum_{j,k,l=1}^{N} w_j w_k \bar{w}_l, \end{aligned} \tag{A.5.8}$$

for constants $a_i \in \mathbb{C}$, $i = -1, \ldots, 11$. Note that in order to respect the rotational invariance, no constant terms can appear. Moreover, the symmetries make all polynomial terms of degree two vanish. Now, assuming that the linear term $a_0 w_1$ and the first cubic term $a_1|w_1|^2 w_1$ are contained in $f(w_1) = \alpha w_1 - \beta|w_1|^2 w_1$ as in (A.5.1), see also (6.20), we are left with in total eleven coupling terms $a_i \hat{g}_i$ that will determine the phase interaction function of the reduced phase dynamics (A.5.2). Writing the complex constants as

$$a_j = \rho_j e^{i\phi_j} ,$$

Ashwin and Rodrigues [74] indicate instructions how to derive the desired constants ξ_i^j and χ_i^j in (A.5.4). First, one determines ϑ_j and ψ_j, $j = -1, 1, \ldots, 11$, by

$$\vartheta_j \cos(\psi_j + \phi) \coloneqq \rho_j \sin(\phi_j + \phi) - \frac{\beta_I}{\beta_R} \rho_j \cos(\phi_j + \phi) ,$$

where $\beta_I/\beta_R = C(0)/A(0)$ with $C(0) = -2\beta_I/\beta_R$ and $A(0) = -2$ with $\beta = \beta_R + i\beta_I$. Using Eq.(4.30) of [74] and abbreviating

$$\delta = \frac{C'(0)A(0) - C(0)A'(0)}{A(0)^2} = \lim_{\lambda \to 0} \frac{d}{d\lambda} \frac{C(\lambda)}{A(\lambda)} , \tag{A.5.9}$$

one can deduce

$$\begin{aligned}
\xi_1^0 &= \vartheta_{-1}, & \chi_1^0 &= \psi_{-1},\\
\xi_1^1 &= -\frac{1}{\beta_R}\sqrt{[\vartheta_2\cos(\psi_2)+\vartheta_3\cos(\psi_3)+\vartheta_8\cos(\psi_8)+\vartheta_{10}\cos(\psi_{10})+\delta\beta_R\rho_{-1}\cos(\phi_{-1})]^2+}\\
&\quad\overline{+[-\vartheta_2\sin(\psi_2)+\vartheta_3\sin(\psi_3)+\vartheta_8\sin(\psi_8)+\vartheta_{10}\sin(\psi_{10})+\delta\beta_R\rho_{-1}\sin(\phi_{-1})]^2}+\mathcal{O}(\mu),\\
\chi_1^1 &= \arctan\left(\frac{-\vartheta_2\sin(\psi_2)+\vartheta_3\sin(\psi_3)+\vartheta_8\sin(\psi_8)+\vartheta_{10}\sin(\psi_{10})+\delta\beta_R\rho_{-1}\sin(\phi_{-1})}{\vartheta_2\cos(\psi_2)+\vartheta_3\cos(\psi_3)+\vartheta_8\cos(\psi_8)+\vartheta_{10}\cos(\psi_{10})+\delta\beta_R\rho_{-1}\cos(\phi_{-1})}\right),\\
\xi_2^1 &= -\vartheta_6/\beta_R+\mathcal{O}(\mu), & \chi_2^1 &= \psi_6,\\
\xi_3^1 &= -\vartheta_7/\beta_R+\mathcal{O}(\mu), & \chi_3^1 &= \psi_7,\\
\xi_4^1 &= -\vartheta_9/\beta_R+\mathcal{O}(\mu), & \chi_4^1 &= \psi_9,\\
\xi_5^1 &= -\vartheta_{11}/\beta_R+\mathcal{O}(\mu), & \chi_5^1 &= \psi_{11}\,.
\end{aligned} \tag{A.5.10}$$

In particular, we can determine an explicit value for δ as presented in the following lemma.

Lemma A.9. *For the dynamics*

$$\dot z = \alpha z-\beta|z|^2z+\tau(z),\quad \text{where } \tau(z)=\varkappa z^4+\mathcal{O}(z^5),$$

we get an explicit value for δ as defined in (A.5.9), which reads

$$\delta = -2\frac{\varkappa_I}{\alpha_R^2}+\frac{5}{2}\frac{\varkappa_R\alpha_I}{\alpha_R^3}\,.$$

Moreover, if $\varkappa=0$, then also $\delta=0$.

Proof. In the following, we will use that $\lambda\in\mathbb{R}$ and that we can write $\tau(z)=\tau_R(z)+i\tau_I(z)$ with $\tau_{R/I}$ real-valued functions. For $x\in\mathbb{R}$, we have

$$\tau_R(x)=\varkappa_R x^4+\mathcal{O}(x^5)\quad\text{and}\quad \tau_I(x)=\varkappa_I x^4+\mathcal{O}(x^5)\,.$$

As has been defined in [74], $A(\lambda)$ and $C(\lambda)$ are given by

$$\begin{aligned}
A(\lambda) &= \frac{U_R'(R_*)}{\lambda}\quad\text{with}\quad U_R'(z)=\lambda+3\alpha z^2+\tau_R'(z)z+\tau_R(z)\\
C(\lambda) &= \frac{R_*(\lambda)B(\lambda)}{\sqrt{\lambda}}\quad\text{with}\quad B(\lambda)=\frac{2\alpha_IR_*+\tau_I'(R_*)}{\sqrt{\lambda}}
\end{aligned}$$

and $R_*=R_*(\lambda)$ is the solution of

$$0=\lambda+\alpha_RR_*^2+\tau_R(R_*^2)\quad\Longrightarrow\quad R_*^2(\lambda)=\frac{\lambda}{-\alpha_R}+\mathcal{O}(\lambda)\,.$$

That is,

$$\frac{C(\lambda)}{A(\lambda)}=\frac{2\alpha_IR_*^2+\tau_I'(R_*)R_*}{\lambda+3\alpha_RR_*^2+\tau_R'(R_*)+\tau_R(R_*)}\,.$$

Dividing by R_*^2 and substituting in the leading order of R_*^2, we find

$$\frac{C(\lambda)}{A(\lambda)}=\frac{2\alpha_I-\frac{4\varkappa_I}{\alpha_R}\lambda+\mathcal{O}(\lambda^2)}{2\alpha_R-\frac{5\varkappa_R}{\alpha_R}\lambda+\mathcal{O}(\lambda^2)}\,.$$

Hence, it follows

$$\delta=\frac{d}{d\lambda}\bigg|_{\lambda=0}\frac{C(\lambda)}{A(\lambda)}=\frac{-8\varkappa_I+10\varkappa_R\frac{\alpha_I}{\alpha_R}}{4\alpha_R^2}\,,$$

which gives the desired result. Additionally, if $\tau(z)=\mathcal{O}(z^5)$, or even $\tau\equiv0$, we have $\varkappa=0$, and therefore also $\delta=0$. □

We close this section of the *Appendix* with a few brief comments on the coupling functions g_k in the (Hopf) normal form description (A.5.1) of the full network of coupled identical systems close to a supercritical Hopf bifurcation.

Remark. If the coupling function g_k in the Hopf normal form description can be fully decomposed into the sum of pairwise interactions between oscillators, the following coupling parameters as introduced in (A.5.7) all vanish,

$$a_5=a_7=a_9=a_{10}=a_{11}=0\,.$$

The only non-vanishing coefficients of the Hopf normal form description are

$$a_{-1} = h_{0010}, \quad a_2 = h_{2001}, \quad a_3 = h_{1110}, \quad a_4 = h_{1011}, \quad a_6 = h_{0120}, \quad a_8 = h_{0021} \ .$$

This means that the constants

$$\xi_1^0, \xi_1^1, \xi_2^1 \quad \text{and} \quad \chi_1^0, \chi_1^1, \chi_2^1$$

are non-zero, which leads to the reduced phase dynamics

$$\dot{\theta}_k = \Omega + \kappa\varepsilon^2 \frac{-\vartheta_4}{\beta_R} \cos(\psi_4) + \frac{\kappa}{N} \sum_{j=1}^{N} \left[\xi_1^0 \cos(\theta_j - \theta_k + \chi_1^0) + \varepsilon^2 \left(\xi_1^1 \cos(\theta_j - \theta_k + \chi_1^1) + \xi_2^1 \cos(2(\theta_j - \theta_k) + \chi_2^1) \right) \right] \ . \tag{A.5.11}$$

Note that the coupling term in (A.5.11) consists again of the first two harmonics only: the terms $\xi_1^0 \cos(\varphi + \chi_1^0) + \varepsilon\xi_1^1 \cos(\varphi + \chi_1^1)$ can be comprised by trigonometric identities to $\xi_1 \cos(\varphi + \chi_1)$. Yet, the contribution of the second term to the (collected) first harmonic is only minor due to the magnitude being of order $\mathcal{O}(\varepsilon^2)$, and hence can be neglected. Moreover, the amplitude of the second harmonic $\cos(2\varphi + \chi_2^1)$ is $\mathcal{O}(\varepsilon^2)$, that is, of one order higher than the first harmonic. In total, the only constants that represent major contributions to the phase dynamics are ξ_1^0 and ξ_2^1, which correspond by (A.5.10) to $a_{-1} = h_{0010}$ and $a_6 = h_{0120}$, respectively — these are also the main contributors to the phase dynamics considered in Appendix A.2.2. Besides, disregarding the minor corrections of order $\mathcal{O}(\varepsilon^2)$, the natural frequency term $\Omega = \alpha_I - \alpha_R\beta_I/\beta_R$ (note that $\alpha_R = \varepsilon^2 = \mu$) coincides with the one derived in Section 6.3.2.

In general, the coupling functions g_k in the Hopf normal form description of the full network are not restricted to pairwise interactions, but they are linear combinations of the 11 terms given in (A.5.8). Deducing the respective factors in this linear combination from the underlying dynamics $\dot{\boldsymbol{x}}_k = \boldsymbol{f}(\boldsymbol{x}_k) + \kappa \boldsymbol{g}_k(\boldsymbol{x}_1, \ldots, \boldsymbol{x}_N)$ with $N \geq 4$ in a general way is beyond the scope of this report. Such a general normal form reduction would probably distort the ostensive link between the original coupling functions $\boldsymbol{g}_k$ and the normal form coupling functions g_k: The structure of pairwise interactions in the underlying dynamics, $\boldsymbol{g}_k(\boldsymbol{x}_1, \ldots, \boldsymbol{x}_N) = \sum_j \boldsymbol{g}_{kj}(\boldsymbol{x}_k, \boldsymbol{x}_j)$, may not be respected in the reduced Hopf normal form description $g_k(w_1, \ldots, w_N) \neq \sum_j g_{kj}(w_k, w_j)$.

Still, given our goal to provide a phase reduction of the underlying dynamics, it appears sufficient to concentrate on those coupling terms in the Hopf normal form that have significant contributions to the reduced phase dynamics. The independent considerations and derivations in Section 6.3.3 and Corollary A.8 suggest that for large networks in the limit of weak coupling the dominant coupling terms are indeed those stated in the previous *Remark*. As a consequence, we only need to find these coupling parameters. While a mathematically thorough network normal form reduction for large N becomes rather lengthy and hence unpractical, the approaches in Section 7 seem to provide decent approximations for the sought-for coupling parameters, as demonstrated by the numerical simulations throughout Sections 8 and 9. Nonetheless, both approaches are approximations for the following distinct reasons: Following *Kuramoto's reductive perturbation approach*, in particular cf. Appendix A.2.2, the derivation is based on mere pairwise interactions of the underlying dynamics and the subsequent reduction steps only respect the bifurcation parameter-dependence up to first order. On the other hand, following *Poincaré's nonlinear transform approach* the parameter-dependence is preserved throughout the reduction but the transformation steps are solely targeted at the Hopf normal form of a single oscillator but not at the Hopf normal form of the full network, see Appendix A.3. This latter assumption may be justified in the limit of weak coupling, see also [46], but a rigorous proof, or an error estimate, respectively, are missing.

A.6. Ermentrout & Kopell's phase–amplitude reduction

Given the significance of their pioneering work [53–55], we deem it appropriate to detail Ermentrout and Kopell's "infinite attraction" method, which is based upon a coordinate transformation $\boldsymbol{x}_k = \mathcal{T}_k(\theta_k, \boldsymbol{\rho}_k)$ of the oscillatory dynamics in terms of phase and amplitude variables and results in an amplitude-corrected phase dynamics

$$\dot{\theta}_k = \omega + \kappa \tilde{H}_k(\theta_k - \theta_j) \quad \text{with} \quad \tilde{H}_k(\psi) = \frac{1}{2\pi} \int_0^{2\pi} \tilde{\boldsymbol{Z}}(t) \cdot \boldsymbol{g}_k\big(\boldsymbol{x}^c(t + \theta_k), \boldsymbol{x}^c(t + \theta_j)\big) dt \ .$$

Here, $\tilde{\boldsymbol{Z}}(t)$ deviates from the conventional phase sensitivity function $\boldsymbol{Z}(t)$ when amplitude dynamics are ignored. In the limit of infinite attraction, however, that is, if the relaxation towards the limit cycle after a perturbation occurs instantaneously, then $\tilde{\boldsymbol{Z}}(t)$ and $\boldsymbol{Z}(t)$ will coincide.

To begin with, we consider an oscillator $\dot{\boldsymbol{x}}_k = \boldsymbol{f}_k(\boldsymbol{x}_k)$, $\boldsymbol{x}_k \in \mathbb{R}^n$, with an asymptotically stable limit cycle solution $\boldsymbol{x}_k^c(t)$ with period T_k and frequency $\omega_k = 2\pi/T_k$. The coordinate transformation $\mathcal{T}_k$ is such that it maps $\boldsymbol{x}_k$ to variables $\theta_k \in \mathbb{S}^1$ and $\boldsymbol{\rho}_k \in \mathbb{R}^{n-1}$:

$$\boldsymbol{x}_k(t) = \mathcal{T}_k\left(\theta_k(t), \boldsymbol{\rho}_k(t)\right) = \boldsymbol{x}_k^c\left(\theta_k(t)\right) + \boldsymbol{M}_k\big(\theta_k(t)\big)\boldsymbol{\rho}_k(t) + \mathcal{O}^2(\boldsymbol{\rho}_k) \ , \tag{A.6.1}$$

where $\boldsymbol{M}_k(\theta)$ is an $n \times (n-1)$-matrix and normalized such that it fulfills

$$\begin{aligned} \boldsymbol{M}_k(\theta)^\intercal \boldsymbol{M}_k(\theta) &= \boldsymbol{I}_{(n-1)\times(n-1)} \\ \left[\partial_\theta \boldsymbol{x}_k^c(\theta)\right]^\intercal \boldsymbol{M}_k(\theta) &= \boldsymbol{0}_{1\times(n-1)} \ . \end{aligned} \tag{A.6.2}$$

Here, $\partial_\theta = d/d\theta$ denotes the derivative with respect to θ. For small $|\boldsymbol{\rho}_k| \ll 1$, one can express the dynamics $\dot{\boldsymbol{x}}_k = \boldsymbol{f}_k(\boldsymbol{x}_k)$ in the phase and amplitude variables as

$$\begin{aligned} \dot{\theta}_k &= \omega_k + f_{1,k}(\theta_k, \boldsymbol{\rho}_k) + \mathcal{O}^2(\boldsymbol{\rho}_k) \\ \dot{\boldsymbol{\rho}}_k &= \boldsymbol{A}_k(\theta_k)\boldsymbol{\rho}_k + o(\boldsymbol{\rho}_k) \ . \end{aligned} \tag{A.6.3}$$

The function $f_{1,k}(\theta_k, \boldsymbol{\rho}_k) = \mathcal{O}(\boldsymbol{\rho}_k)$ is such that $f_{1,k} \to 0$ for $\boldsymbol{\rho}_k \to 0$, so that on the limit cycle we retrieve $\dot{\theta}_k = \omega_k$. With the Jacobian $\boldsymbol{L}_k(\theta) = \nabla \boldsymbol{f}(\boldsymbol{x})\big|_{\boldsymbol{x}=\boldsymbol{x}_k^c(\theta)}$ of $\boldsymbol{f}$ evaluated at the limit cycle $\boldsymbol{x}_k^c$, and abbreviating $\varsigma_k(\theta) = \left|\partial_\theta \boldsymbol{x}_k^c(\theta)\right|^2$, the functions $f_{1,k} : \mathbb{S}^1 \times \mathbb{R}^{n-1} \to \mathbb{S}^1$ and $\boldsymbol{A}_k : \mathbb{S}^1 \to \mathbb{R}^{(n-1)\times(n-1)}$ can be found [55] as

$$\begin{aligned} f_{1,k}(\theta, \boldsymbol{\rho}) &= \frac{\omega_k}{\varsigma_k(\theta)} \left[\partial_\theta \boldsymbol{x}_k^c(\theta)\right]^\intercal \left[\boldsymbol{L}_k(\theta) + \boldsymbol{L}_k(\theta)^\intercal\right] \boldsymbol{M}_k(\theta)\boldsymbol{\rho} \\ \boldsymbol{A}_k(\theta) &= \omega_k \left[\boldsymbol{M}_k(\theta)^\intercal \boldsymbol{L}_k(\theta) \boldsymbol{M}_k(\theta) + \left[\partial_\theta \boldsymbol{M}_k(\theta)\right]^\intercal \boldsymbol{M}_k(\theta)\right] \ . \end{aligned} \tag{A.6.4}$$

We now consider two coupled nearly-identical oscillators $\boldsymbol{x}_k, \boldsymbol{x}_j$ with dynamics

$$\dot{\boldsymbol{x}}_k = \boldsymbol{f}(\boldsymbol{x}_k) + \kappa\, \boldsymbol{g}_k(\boldsymbol{x}_k, \boldsymbol{x}_j) \ , \quad \boldsymbol{x}_k \in \mathbb{R}^n. \tag{A.6.5}$$

Specifically, we search for solutions of the form

$$\boldsymbol{x}_k(t) = \boldsymbol{x}^c(t) + \kappa\, \boldsymbol{u}_k(t) \ , \tag{A.6.6}$$

where $\boldsymbol{x}^c(t)$ denotes the T-periodic limit cycle solution of $\dot{\boldsymbol{x}} = \boldsymbol{f}(\boldsymbol{x})$ with frequency $\omega = 2\pi/T$, and $\boldsymbol{u}_k$ is such that it converges to zero for solutions on the limit cycle $\boldsymbol{x}(t) = \boldsymbol{x}^c(t)$. Applying the coordinate transformation $\mathcal{T}$ as introduced in (A.6.1) to both oscillators yields the corresponding dynamics in phase and amplitude variables

$$\begin{aligned} \dot{\theta}_k &= \omega + f_1(\theta_k, \boldsymbol{\rho}_k) + \kappa\ h_k(\theta_k, \theta_j) + \mathcal{O}(|\boldsymbol{\rho}_k, \boldsymbol{\rho}_j|) \\ \dot{\boldsymbol{\rho}}_k &= \boldsymbol{A}(\theta_k)\boldsymbol{\rho}_k + \kappa\ \boldsymbol{d}_k(\theta_k, \theta_j) + \mathcal{O}(|\boldsymbol{\rho}_j|) + o(|\boldsymbol{\rho}_k|) \end{aligned} \tag{A.6.7}$$

with the functions f_1 and $\boldsymbol{A}$ as given in (A.6.4) and

$$\begin{aligned} h_k(\theta_k, \theta_j) &= \frac{\omega}{\varsigma(\theta_k)} \left[\partial_\theta \boldsymbol{x}^c(\theta)\right]^\intercal \boldsymbol{g}_k\big(\boldsymbol{x}^c(\theta_k), \boldsymbol{x}^c(\theta_j)\big) \\ \boldsymbol{d}_k(\theta_k, \theta_j) &= \omega \boldsymbol{M}(\theta_k)^\intercal \boldsymbol{g}_k\big(\boldsymbol{x}^c(\theta_k), \boldsymbol{x}^c(\theta_j)\big) \ . \end{aligned} \tag{A.6.8}$$

Note that (A.6.7) with (A.6.8) are general and hold for any coupling strength $\kappa \in \mathbb{R}$ at leading order in $\boldsymbol{\rho}_k$ and $\boldsymbol{\rho}_j$, the latter approximation allows us to evaluate the coupling terms $\boldsymbol{g}_k$ at the respective limit cycles.

In the weak coupling limit $0 \leq \kappa \ll 1$ while allowing for finite attraction to the limit cycle, the normal coordinates $\boldsymbol{\rho}_k$ are κ-close to the limit cycle. We can thus introduce $\boldsymbol{\rho}_k = \kappa \boldsymbol{s}_k$, and (A.6.7) becomes

$$\begin{aligned} \dot{\theta}_k &= \omega + \kappa \left\{\boldsymbol{b}(\theta_k)\boldsymbol{s}_k + \varsigma(\theta_k)^{-1}\left[\partial_\theta \boldsymbol{x}^c(\theta)\right]^\intercal \boldsymbol{g}_k\big(\boldsymbol{x}^c(\theta_k), \boldsymbol{x}^c(\theta_j)\big)\right\} + \mathcal{O}^2(\kappa) \ , \\ \dot{\boldsymbol{s}}_k &= \boldsymbol{A}(\theta_k)\boldsymbol{s}_k + \omega \boldsymbol{M}(\theta_k)^\intercal \boldsymbol{g}_k\big(\boldsymbol{x}^c(\theta_k), \boldsymbol{x}^c(\theta_j)\big) + \mathcal{O}(\kappa) \ , \end{aligned} \tag{A.6.9}$$

with $\boldsymbol{b}(\theta_k) = \omega\varsigma(\theta_k)^{-1}\left[\partial_\theta \boldsymbol{x}^c(\theta)\right]^\intercal \left[\boldsymbol{L}(\theta_k) + \boldsymbol{L}(\theta_k)^\intercal\right] \boldsymbol{M}(\theta_k)$. In order to determine the phase interaction function H_k for finite $\boldsymbol{\rho}_k$, we have to take the additional term $\boldsymbol{b}(\theta_k)\boldsymbol{s}_k$ into account when applying averaging.

Before deriving the averaged solution, we first recall that we are looking for solutions of the form (A.6.6), in which $\boldsymbol{u}_k$ now additionally evolves on a slower time scale $\tau = \kappa t$, that is, we seek for solutions

$$\boldsymbol{x}_k(t) = \boldsymbol{x}^c\ (\theta_k) + \kappa\, \boldsymbol{u}_k(t, \tau, \kappa) \quad \text{with} \quad \theta_k(\tau) = t + \phi_k(\tau) \ . \tag{A.6.10}$$

Note that $\phi_k = \phi_k(\tau)$ are slowly-varying phase deviations from the natural frequency, which we set to $\omega = 1$ without loss of generality. When substituting the ansatz (A.6.10) in (A.6.5), we find at first order in κ

$$\mathcal{L}(t + \phi_k)\boldsymbol{u}_k(t, \tau, 0) \equiv \left[\frac{d}{dt} - \boldsymbol{L}(t + \phi_k)\right] \boldsymbol{u}_k(t, \tau, 0) = -\partial_\theta \boldsymbol{x}^c(t + \phi_k)\frac{\partial \phi_k}{\partial \tau} + \boldsymbol{g}_k\big(\boldsymbol{x}^c(t + \phi_k), \boldsymbol{x}^c(t + \phi_j)\big). \tag{A.6.11}$$

To solve (A.6.11) for periodic solutions $\boldsymbol{u}_k$, we rely on the Fredholm alternative, see, e.g., [283], according to which

$$\mathcal{L}(t)\boldsymbol{\xi}(t) = \boldsymbol{g}(t) \tag{A.6.12}$$

has a 2π-periodic solution $\boldsymbol{\xi}(t)$ if and only if

$$\int_0^{2\pi} \boldsymbol{\chi}(t)\boldsymbol{g}(t)dt = 0 \ , \tag{A.6.13}$$

Table B.1
Phase models derived with different reduction techniques for linear coupling and near the Hopf bifurcation, $\mu = 0.0417$. The oscillators' natural frequency is ω, and a_n, b_n are the amplitudes of the Fourier components of the phase interaction function H. Parameters are $(a, d) = (2.55, 0.65)$. Numeric values correspond to Table 8.1.

Approach	ω	a_1	b_1	a_2	b_2
Reductive perturbation	2.537	−2.0649	0.0505	0.0080	−0.0052
Nonlinear transform	2.534	−2.1146	0.0781	0.0167	−0.0111
Direct averaging	×	×	×	×	×
Numerical/adjoint	2.474	0.8302	0.0345	−0.0027	−0.0017

where $\boldsymbol{\chi}(t)$ solves the corresponding homogeneous adjoint problem

$$\mathcal{L}^*(t)\boldsymbol{\chi}(t) \equiv \left[\frac{d}{dt} - \boldsymbol{L}(t)^\intercal\right]\boldsymbol{\chi}(t) = 0\ . \tag{A.6.14}$$

We achieve uniqueness of the solution by requiring the normalization condition

$$\frac{1}{2\pi}\int_0^{2\pi} \boldsymbol{\chi}(t)\partial_\theta \boldsymbol{x}^c(t)dt = 1\ . \tag{A.6.15}$$

Hence, in order to find a solution of (A.6.11), we combine (A.6.13) and (A.6.15) to obtain

$$\frac{\partial\phi_k}{\partial\tau} = \tilde{H}_k(\phi_k - \phi_j) \equiv \frac{1}{2\pi}\int_0^{2\pi} \boldsymbol{\chi}(t)\boldsymbol{g}_k\big(\boldsymbol{x}^c(t+\phi_k), \boldsymbol{x}^c(t+\phi_j)\big)dt\ . \tag{A.6.16}$$

The function $\boldsymbol{\chi}(t)$ turns out to be

$$\boldsymbol{\chi}(t) = \left[\varsigma(t)^{-1}\partial_\theta \boldsymbol{x}^c(t)\boldsymbol{\varrho}(t)\right]^\intercal \tag{A.6.17}$$

with

$$\boldsymbol{\varrho}(t)^\intercal = \left[Q(2\pi)\left[\boldsymbol{I}_{n-1} - \boldsymbol{E}(2\pi)\right]^{-1} - Q(t)\right]\boldsymbol{E}(t)^{-1}\boldsymbol{M}(t)^\intercal\ ,$$

where $\boldsymbol{E}(t)$ is the solution to $d\boldsymbol{E}/dt = \boldsymbol{A}(t)\boldsymbol{E}$ with initial condition $\boldsymbol{E}(0) = \boldsymbol{I}_{n-1}$ and $Q(t)$ satisfies $Q(t) = \int_0^t \boldsymbol{b}(s)\boldsymbol{E}(s)ds$. Indeed, inserting the ansatz

$$\boldsymbol{\chi}(t) = \partial_\theta \boldsymbol{x}^c(t)\zeta(t) + \boldsymbol{M}(t)\boldsymbol{z}(t) \tag{A.6.18}$$

into the adjoint problem (A.6.14) with normalization (A.6.15), we find that $\zeta(t) = \varsigma(t)^{-1}$ and $\boldsymbol{z}$ satisfies $\boldsymbol{z}' = -\boldsymbol{A}(t)^\intercal\boldsymbol{z} - \boldsymbol{b}(t)^\intercal$, which eventually leads to the unique solution (A.6.17). Using (A.6.16) we thus find the 'amplitude-corrected' phase dynamics

$$\dot{\theta}_k = 1 + \kappa\,\tilde{H}_k(\theta_k - \theta_j) = 1 + \frac{\kappa}{2\pi}\int_0^{2\pi}\left[\varsigma(t)^{-1}\partial_\theta \boldsymbol{x}^c(t)\boldsymbol{\varrho}(t)\right]^\intercal \boldsymbol{g}_k\big(\boldsymbol{x}^c(t+\theta_k), \boldsymbol{x}^c(t+\theta_j)\big)dt\ . \tag{A.6.19}$$

For more mathematical details, we refer to [55].

Appendix B. Numerical details

B.1. Brusselator

For every parameter pair $(a, d) \in [1, 3] \times [0, 1]$ the network simulations ran for $T_{\text{end}} = 10^7$ seconds using the Matlab Runge–Kutta-4,5 solver with relative and absolute accuracy fixed at 10^{-8} and 10^{-10}, respectively. The oscillators were initially distributed on an unperturbed limit cycle such that the Kuramoto order parameter was close to zero. At the end of the simulation time T_{end}, the phases of the oscillators were extracted via a Hilbert transform and analyzed with respect to clustering. We applied a reformulated hierarchical cluster algorithm on a flat torus and used a segmentation index to determine phase clusters of the oscillators, see [314] for more details on the phase cluster algorithm, there for the case of K-means clustering. The resulting clusters were monitored with respect to their stability over a subsequent 10 second simulation interval of the full Brusselator network. If both intercluster stability (in terms of variances of the phase differences of the cluster centroids) and intracluster stability (in terms of variances within clusters) was given, we assigned the particular number of clusters to the parameter pair. Otherwise, we assumed the network to be incoherent. We identified incoherence with a stable n-cluster state with $n \geq 25$ as detected by the phase cluster algorithm. The following Tables B.1–B.4 provide the exact numerical values corresponding to the symbolic Tables 8.1–8.4 of Section 8.

Table B.2
Phase models derived with different reduction techniques for linear coupling and away from the Hopf bifurcation, $\mu = 0.1670$. The oscillators' natural frequency is ω, and a_n, b_n are the amplitudes of the Fourier components of the phase interaction function H. Parameters are $(a, d) = (2.55, 0.65)$. Numeric values correspond to Table 8.2.

Approach	ω	a_1	b_1	a_2	b_2
Reductive perturbation	2.348	−2.0649	0.0505	0.1285	−0.1144
Nonlinear transform	1.832	−3.2763	0.7276	0.5156	−0.5816
Direct averaging	×	×	×	×	×
Numerical/adjoint	2.671	1.3490	0.2997	−0.0579	−0.0557

Table B.3
Phase models derived with different reduction techniques for linear coupling and near the Hopf bifurcation, $\mu = 0.0417$. The oscillators' natural frequency is ω, and a_n, b_n are the amplitudes of the Fourier components of the phase interaction function H. Parameters are $(a, d) = (2.55, 0.75)$. Numeric values correspond to Table 8.3.

Approach	ω	a_1	b_1	a_2	b_2
Reductive perturbation	2.537	−2.05015	−0.2496	0.0031	+0.0000
Nonlinear transform	2.524	−2.0880	−0.2300	0.0063	−0.0001
Direct averaging	×	×	×	×	×
Numerical/adjoint	2.474	0.8378	−0.0838	−0.0010	+0.0000

Table B.4
Phase models derived with different reduction techniques for nonlinear coupling and away from the Hopf bifurcation, $\mu = 0.1670$. The oscillators' natural frequency is ω, and a_n, b_n are the amplitudes of the Fourier components of the phase interaction function H. Parameters are $(a, d) = (2.55, 0.75)$. Numeric values correspond to Table 8.4.

Approach	ω	a_1	b_1	a_2	b_2
Reductive perturbation	2.345	−2.0355	−0.2496	0.0489	0.0004
Nonlinear transform	1.832	−3.3177	0.2340	0.1728	−0.0459
Direct averaging	×	×	×	×	×
Numerical/adjoint	2.671	1.7280	0.2037	−0.0241	−0.0239

B.2. Wilson–Cowan neural mass

Throughout Section 9, we used the following version of the Wilson–Cowan neural mass model, as has been motivated around (9.4) & (9.6), where the coupling dynamics is such that only oscillatory behavior of one neural mass can exert influence on another.

$$\frac{d}{dt}E_k = -E_k + S\left[a_E\left(c_{EE}E_k - c_{IE}I_k - \Theta_E + P_k + \frac{\kappa}{N}\sum_{l=1}^{N} C_{kl}\left(E_l - E_l^0\right)\right)\right] \tag{B.2.1a}$$

$$\frac{d}{dt}I_k = -I_k + S\left[a_I\left(c_{EI}E_k - c_{II}I_k - \Theta_I\right)\right] , \tag{B.2.1b}$$

Not only does this choice cancel an additional constant input that is proportional to the coupling strength, but it also simplifies the polynomial approximation of the Wilson–Cowan dynamics in terms of the deviations $(x_k, y_k) = (E_k - E_k^0, I_k - I_k^0)$ from the unstable fixed point (E_k^0, I_k^0). This is in particular important to ease the phase reduction following either of the analytic techniques.

Numerical values for symbolic tables. In Section 9.5, we considered the parameters

$$a_E = 1.2, a_I = 2, c_{EE} = c_{EI} = 10, c_{IE} = 6, c_{II} = 1, \Theta_E = 2.5, \Theta_I = 3.5,$$

and varied the control parameter P_k. The supercritical Hopf bifurcation occurs at $P_H = -0.3663$, and we denote the distance to the Hopf point in parameter space with $\mu = P_k - P_H$. The first four Fourier coefficients of the reduced phase model

$$\dot{\theta}_k = \omega_k + \frac{\kappa}{N}\sum_{j=1}^{N} a_1\cos\left(\theta_k - \theta_j\right) + b_1\sin\left(\theta_k - \theta_j\right) + a_2\cos\left(2(\theta_k - \theta_j)\right) + b_2\sin\left(2(\theta_k - \theta_j)\right)$$

could be derived for different values of μ following the direct averaging, the numerical reduction method as well as Kuramoto's reductive perturbation and Poincaré's nonlinear transform approach. The results are presented for $\mu = 0.0003$ in Table B.5, for $\mu = 0.0013$ in Table B.6, and for $\mu = 0.1663$ in Table B.7.

Table B.5
Phase models derived with different reduction techniques infinitesimally close to the Hopf bifurcation ($\mu = 0.0003$). The oscillators' natural frequency is ω, and a_n, b_n are the amplitudes of the Fourier components of the phase interaction function H.

Approach	ω	a_1	b_1	a_2	b_2
Reductive perturbation	0.701	−0.9505	1.1555	−0.0001	0.0013
Nonlinear transform	0.701	−0.9457	1.1382	−0.0009	0.0013
Direct averaging	0.701	−0.6940	0.2140	–	–
Numerical/adjoint	0.701	−0.0472	0.3843	−0.0001	0.0002

Table B.6
Phase models derived with different reduction techniques very close to the Hopf bifurcation ($\mu = 0.0013$). The oscillators' natural frequency is ω, and a_n, b_n are the amplitudes of the Fourier components of the phase interaction function H.

Approach	ω	a_1	b_1	a_2	b_2
Reductive perturbation	0.701	−0.9505	1.1555	−0.0039	0.0013
Nonlinear transform	0.701	−0.9302	1.0830	−0.0038	0.0055
Direct averaging	0.701	−0.6886	0.2143	–	–
Numerical/adjoint	0.701	−0.3824	−0.1601	−0.0018	−0.0006

Table B.7
Phase models derived with different reduction techniques away from the Hopf bifurcation ($\mu = 0.1663$). The oscillators' natural frequency is ω, and a_n, b_n are the amplitudes of the Fourier components of the phase interaction function H.

Approach	ω	a_1	b_1	a_2	b_2
Reductive perturbation	0.728	−0.9505	1.1555	−0.2470	0.3657
Nonlinear transform	1.023	−0.4905	0.1383	−0.0604	0.0503
Direct averaging	1.330	−0.4733	0.2390	–	–
Numerical/adjoint	0.939	−0.4447	−0.2668	−0.0635	−0.0451

Table B.8
Phase models derived for different approaches at $P_k = 3, Q_k = 9.38$.

Approach	ω	a_1	b_1	a_2	b_2
Reductive perturbation	1.800	−0.3666	0.0251	−0.0006	0.0015
Nonlinear transform	1.800	−0.3675	0.0260	−0.0006	0.0015
Direct averaging	1.800	−0.1280	0.5739	–	–
Numerical/adjoint	1.800	−0.0413	0.0339	−0.0002	−0.0001

Table B.9
Phase models derived for different approaches at $P_k = 3, Q_k = 8.9$.

Approach	ω	a_1	b_1	a_2	b_2
Reductive perturbation	1.276	−0.3666	0.0251	−0.0381	0.0868
Nonlinear transform	1.263	−0.4592	0.0908	−0.0194	0.0562
Direct averaging	1.276	−0.2283	0.4600	–	–
Numerical/adjoint	1.267	−0.4436	−0.1244	−0.0077	−0.0184

Table B.10
Phase models derived for different approaches at $P_k = 3, Q_k = 8.7$.

Approach	ω	a_1	b_1	a_2	b_2
Reductive perturbation	1.078	−0.3666	0.0251	−0.0522	0.1187
Nonlinear transform	1.079	−0.4945	0.1217	−0.0191	0.0574
Direct averaging	1.078	−0.2649	0.4245	–	–
Numerical/adjoint	1.062	−0.5877	−0.2324	−0.0304	0.0135

Predicting collective behavior. For Fig. 9.7, we considered a slightly different set of parameters

$$a_E = 1, a_I = 1, c_{EE} = c_{EI} = c_{IE} = 10, c_{II} = -2, \Theta_E = 0$$

which had been considered already by Hoppensteadt and Izhikevich [46], and employed by Hlinka and Coombes [168], so that we can refrain from computing a detailed bifurcation diagram, but refer to the literature. We consider P_k and Q_k as bifurcation parameters, as mentioned above.

The numerical phase reduction technique predicts correctly the stability of the globally synchronized for parameters $(P_k, Q_k) = (-3, -9.38)$, of the incoherent state for parameters $(P_k, Q_k) = (-3, -8.9)$, and of the balanced two-cluster state for parameters $(P_k, Q_k) = (-3, -8.7)$. The numerical values of the Fourier coefficients of the numerically reduced phase interaction function H are given in Tables B.8–B.10, respectively, together with those derived along the analytic phase reduction techniques.

The corresponding network simulations for Fig. 9.7 of $N = 30$ globally coupled, identical Wilson–Cowan neural masses were initialized by choosing initial conditions on the uncoupled limit cycle such that the phase synchronization (real-valued Kuramoto order-parameter) was $R = 0.15$. The dynamics (B.2.1) was simulated with the parameter values above and coupling strength $\kappa = 0.15$ using an Euler–Maruyama scheme over $T = 1000$ s ($T = 5000$ for panels b and c), respectively, with step size $dt = 0.001$ s and noise strength $\sigma = 10^{-8}$.

References

[1] C. Huygens, Oeuvres Complètes de Christiaan Huygens, M. Nijhoff, La Haye, 1888.
[2] J. Rayleigh, The Theory of Sound, vol. 2, Macmillan, London, 1896.
[3] B. Van der Pol, Forced oscillations in a circuit with non-linear resistance, London Edinburgh Dublin Philos. Mag. J. Sci. 3 (13) (1927) 65–80.
[4] K. Wiesenfeld, P. Colet, S.H. Strogatz, Frequency locking in Josephson arrays: Connection with the Kuramoto model, Phys. Rev. E 57 (2) (1998) 1563.
[5] D.C. Michaels, E.P. Matyas, J. Jalife, Mechanisms of sinoatrial pacemaker synchronization: a new hypothesis, Circ. Res. 61 (5) (1987) 704–714.
[6] C. Liu, D.R. Weaver, S.H. Strogatz, S.M. Reppert, Cellular construction of a circadian clock: period determination in the suprachiasmatic nuclei, Cell 91 (6) (1997) 855–860.
[7] B. Ermentrout, An adaptive model for synchrony in the firefly Pteroptyx malaccae, J. Math. Biol. 29 (6) (1991) 571–585.
[8] S.-Y. Ha, E. Jeong, M.-J. Kang, Emergent behaviour of a generalized Viscek-type flocking model, Nonlinearity 23 (12) (2010) 3139.
[9] D.A. Paley, N.E. Leonard, R. Sepulchre, D. Grunbaum, J.K. Parrish, Oscillator models and collective motion, IEEE Control Syst. 27 (4) (2007) 89–105.
[10] Z. Néda, E. Ravasz, T. Vicsek, Y. Brechet, A.-L. Barabási, Physics of the rhythmic applause, Phys. Rev. E 61 (6) (2000) 6987.
[11] S. Assenza, R. Gutiérrez, J. Gómez-Gardenes, V. Latora, S. Boccaletti, Emergence of structural patterns out of synchronization in networks with competitive interactions, Sci. Rep. 1 (2011) 99.
[12] Y. Kuramoto, Chemical Oscillations, Turbulence and Waves, Springer, Berlin, 1984.
[13] K. Kaneko, I. Tsuda, Complex Systems: Chaos and Beyond: A Constructive Approach with Applications in Life Sciences, Springer Science & Business Media, 2011.
[14] N. Wiener, Cybernetics, Sci. Am. 179 (5) (1948) 14–19.
[15] M. Steriade, Cellular substrates of brain rhythms, in: E. Niedermeyer, F. Lopes Da Silva (Eds.), Electroencephalography Basic Principles, Clinical Applications, and Related Fields, Lippincott Williams & Wilkins, Philadelphia, 2005, pp. 31–84.
[16] G. Buzsáki, A. Draguhn, Neuronal oscillations in cortical networks, Science 304 (5679) (2004) 1926–1929.
[17] G. Buzsaki, Rhythms of the Brain, Oxford University Press, 2006.
[18] A. Pikovsky, M. Rosenblum, J. Kurths, J. Kurths, Synchronization: A Universal Concept in Nonlinear Sciences, vol. 12, Cambridge University Press, 2003.
[19] A.T. Winfree, The Geometry of Biological Time, vol. 12, Springer Science & Business Media, 2001.
[20] S. Strogatz, Sync: The Emerging Science of Spontaneous Order, Penguin UK, 2004.
[21] S.H. Strogatz, Nonlinear Dynamics and Chaos: With Applications to Physics, Biology, Chemistry, and Engineering, CRC Press, 2018.
[22] G.V. Osipov, J. Kurths, C. Zhou, Ensembles of Phase Oscillators, Springer, 2007.
[23] A. Arenas, A. Díaz-Guilera, J. Kurths, Y. Moreno, C. Zhou, Synchronization in complex networks, Phys. Rep. 469 (3) (2008) 93–153.
[24] L. Glass, Synchronization and rhythmic processes in physiology, Nature 410 (6825) (2001) 277.
[25] M. Rosenblum, A. Pikovsky, J. Kurths, C. Schäfer, P.A. Tass, Phase synchronization: from theory to data analysis, Handb. Biol. Phys. 4 (2001) 279–321.
[26] C.M. Gray, Synchronous oscillations in neuronal systems: mechanisms and functions, J. Comput. Neurosci. 1 (1–2) (1994) 11–38.
[27] W.A. MacKay, Synchronized neuronal oscillations and their role in motor processes, Trends Cogn. Sci. 1 (5) (1997) 176–183.
[28] F. Varela, J.-P. Lachaux, E. Rodriguez, J. Martinerie, The brainweb: phase synchronization and large-scale integration, Nature Rev. Neurosci. 2 (4) (2001) 229–239.
[29] J. Palva, S. Palva, K. Kaila, Phase synchrony among neuronal oscillations in the human cortex, J. Neurosci. 25 (15) (2005) 3962–3972.
[30] B. Schack, S. Weiss, Quantification of phase synchronization phenomena and their importance for verbal memory processes, Biol. Cybern. 92 (4) (2005) 275–287.
[31] P. Sauseng, W. Klimesch, What does phase information of oscillatory brain activity tell us about cognitive processes? Neurosci. Biobehav. Rev. 32 (5) (2008) 1001–1013.
[32] H. Schuster, P. Wagner, A model for neuronal oscillations in the visual cortex, Biol. Cybern. 64 (1) (1990) 77–82.
[33] A. Daffertshofer, B. van Wijk, On the influence of amplitude on the connectivity between phases, Front. Neuroinform. 5 (2011) 6.
[34] J. Cabral, E. Hugues, O. Sporns, G. Deco, Role of local network oscillations in resting-state functional connectivity, NeuroImage 57 (1) (2011) 130–139.
[35] R. Ton, G. Deco, A. Daffertshofer, Structure-function discrepancy: inhomogeneity and delays in synchronized neural networks, PLoS Comput. Biol. 10 (7) (2014) e1003736.
[36] J. Cabral, M.L. Kringelbach, G. Deco, Exploring the network dynamics underlying brain activity during rest, Prog. Neurobiol. 114 (Suppl. C) (2014) 102–131.
[37] J. Cabral, H. Luckhoo, M. Woolrich, M. Joensson, H. Mohseni, A. Baker, M.L. Kringelbach, G. Deco, Exploring mechanisms of spontaneous functional connectivity in MEG: How delayed network interactions lead to structured amplitude envelopes of band-pass filtered oscillations, Neuroimage 90 (Suppl. C) (2014) 423–435.
[38] R. Tasseff, A. Bheda-Malge, T. DiColandrea, C.C. Bascom, R.J. Isfort, R. Gelinas, Mouse hair cycle expression dynamics modeled as coupled mesenchymal and epithelial oscillators, PLoS Comput. Biol. 10 (11) (2014) 1–21.
[39] M. Sadilek, S. Thurner, Physiologically motivated multiplex Kuramoto model describes phase diagram of cortical activity, Sci. Rep. 5 (2015).
[40] R. Schmidt, K.J.R. LaFleur, M.A. de Reus, L.H. van den Berg, M.P. van den Heuvel, Kuramoto model simulation of neural hubs and dynamic synchrony in the human cerebral connectome, BMC Neurosci. 16 (1) (2015) 54.
[41] F. Dörfler, F. Bullo, Synchronization in complex networks of phase oscillators: A survey, Automatica 50 (6) (2014) 1539–1564.
[42] S.H. Strogatz, From Kuramoto to Crawford: exploring the onset of synchronization in populations of coupled oscillators, Physica 143D (1) (2000) 1–20.
[43] J.A. Acebrón, L.L. Bonilla, C.J. Pérez Vicente, F. Ritort, R. Spigler, The Kuramoto model: A simple paradigm for synchronization phenomena, Rev. Modern Phys. 77 (2005) 137–185.
[44] M. Breakspear, S. Heitmann, A. Daffertshofer, Generative models of cortical oscillations: neurobiological implications of the Kuramoto model, Front. Hum. Neurosci. 4 (2010).

[45] F.A. Rodrigues, T.K.D. Peron, P. Ji, J. Kurths, The Kuramoto model in complex networks, Phys. Rep. 610 (2016) 1–98.
[46] F.C. Hoppensteadt, E.M. Izhikevich, Weakly Connected Neural Networks, Springer, New York, 1997.
[47] E.M. Izhikevich, Dynamical Systems in Neuroscience, MIT Press, 2007.
[48] G.B. Ermentrout, D.H. Terman, Mathematical Foundations of Neuroscience, vol. 35, Springer, New York, 2010.
[49] J.C. Neu, Chemical waves and the diffusive coupling of limit cycle oscillators, SIAM J. Appl. Math. 36 (3) (1979) 509–515.
[50] J.C. Neu, Coupled chemical oscillators, SIAM J. Appl. Math. 37 (2) (1979) 307–315.
[51] J.C. Neu, Large populations of coupled chemical oscillators, SIAM J. Appl. Math. 38 (2) (1980) 305–316.
[52] G.B. Ermentrout, n:m phase-locking of weakly coupled oscillators, J. Math. Biol. 12 (3) (1981) 327–342.
[53] G.B. Ermentrout, N. Kopell, Frequency plateaus in a chain of weakly coupled oscillators, I, SIAM J. Math. Anal. 15 (2) (1984) 215–237.
[54] G. Ermentrout, N. Kopell, Oscillator death in systems of coupled neural oscillators, SIAM J. Appl. Math. 50 (1) (1990) 125–146.
[55] G. Ermentrout, N. Kopell, Multiple pulse interactions and averaging in systems of coupled neural oscillators, J. Math. Biol. 29 (3) (1991) 195–217.
[56] B. Ermentrout, Type I membranes, phase resetting curves, and synchrony, Neural Comput. 8 (5) (1996) 979–1001.
[57] D. Hansel, G. Mato, C. Meunier, Phase dynamics for weakly coupled Hodgkin-Huxley neurons, Europhys. Lett. 23 (5) (1993) 367.
[58] D. Hansel, G. Mato, C. Meunier, Synchrony in excitatory neural networks, Neural Comput. 7 (2) (1995) 307–337.
[59] C. Van Vreeswijk, L.F. Abbott, G. Bard Ermentrout, When inhibition not excitation synchronizes neural firing, J. Comput. Neurosci. 1 (4) (1994) 313–321.
[60] P.C. Bressloff, S. Coombes, Dynamics of strongly coupled spiking neurons, Neural Comput. 12 (1) (2000) 91–129.
[61] E.M. Izhikevich, Phase equations for relaxation oscillators, SIAM J. Appl. Math. 60 (5) (2000) 1789–1804.
[62] G. Ermentrout, D. Kleinfeld, Traveling electrical waves in cortex: Insights from phase dynamics and speculation on a computational role, Neuron 29 (1) (2001) 33–44.
[63] T.J. Lewis, J. Rinzel, Dynamics of spiking neurons connected by both inhibitory and electrical coupling, J. Comput. Neurosci. 14 (3) (2003) 283–309.
[64] E. Brown, J. Moehlis, P. Holmes, On the phase reduction and response dynamics of neural oscillator populations, Neural Comput. 16 (4) (2004) 673–715.
[65] M.A. Schwemmer, T.J. Lewis, The theory of weakly coupled oscillators, in: N.W. Schultheiss, A.A. Prinz, R.J. Butera (Eds.), Phase Response Curves in Neuroscience: Theory, Experiment, and Analysis, Springer Science & Business Media, New York, NY, 2012, pp. 3–31.
[66] N.W. Schultheiss, A.A. Prinz, R.J. Butera, Phase Response Curves in Neuroscience: Theory, Experiment, and Analysis, Springer Science & Business Media, New York, NY, 2012.
[67] P. Glansdorff, I. Prigogine, Thermodynamic Theory of Structure, Stability and Fluctuations, Wiley, 1971.
[68] H.R. Wilson, J.D. Cowan, Excitatory and inhibitory interactions in localized populations of model neurons, Biophys. J. 12 (1) (1972) 1–24.
[69] H.R. Wilson, J.D. Cowan, A mathematical theory of the functional dynamics of cortical and thalamic nervous tissue, Kybernetik 13 (2) (1973) 55–80.
[70] S. Ciliberti, O.C. Martin, A. Wagner, Innovation and robustness in complex regulatory gene networks, Proc. Natl. Acad. Sci. 104 (34) (2007) 13591–13596.
[71] I. Malkin, Methods of Poincaré and Liapunov in Theory of Non-Linear Oscillations, Gostexizdat, Moscow, 1949.
[72] I. Malkin, Some Problems in Nonlinear Oscillation Theory, vol. 541, Gostexizdat, Moscow, 1956 (in Russian).
[73] A.T. Winfree, Biological rhythms and the behavior of populations of coupled oscillators, J. Theoret. Biol. 16 (1) (1967) 15–42.
[74] P. Ashwin, A. Rodrigues, Hopf normal form with SN symmetry and reduction to systems of nonlinearly coupled phase oscillators, Physica D 325 (2016) 14–24.
[75] J. Guckenheimer, P.J. Holmes, Nonlinear Oscillations, Dynamical Systems, and Bifurcations of Vector Fields, Springer, New York, 2013.
[76] S.-N. Chow, C. Li, D. Wang, Normal Forms and Bifurcation of Planar Vector Fields, Cambridge University Press, 1994.
[77] J. Murdock, Normal Forms and Unfoldings for Local Dynamical Systems, Springer Science & Business Media, 2006.
[78] A.H. Nayfeh, The Method of Normal Forms, John Wiley & Sons, 2011.
[79] S.-N. Chow, J.K. Hale, Methods of Bifurcation Theory, vol. 251, Springer Science & Business Media, 2012.
[80] M. Han, P. Yu, Normal Forms, Melnikov Functions and Bifurcations of Limit Cycles, vol. 181, Springer Science & Business Media, 2012.
[81] H. Poincaré, R. Magini, Les méthodes nouvelles de la mécanique céleste, Il Nuovo Cimento (1895–1900) 10 (1) (1899) 128–130.
[82] Y.A. Kuznetsov, Elements of Applied Bifurcation Theory, Springer, New York, 1998.
[83] F. Takens, Normal forms for certain singularities of vector fields, Ann. Inst. Fourier 23 (2) (1973) 163–195.
[84] F. Takens, Singularities of vector fields, Publ. Math. l'IHÉS 43 (1974) 47–100.
[85] J.A. Sanders, F. Verhulst, J.A. Murdock, Averaging Methods in Nonlinear Dynamical Systems, vol. 59, Springer, 2007.
[86] N.N. Bogoliubov, I.A. Mitropol'skii, Y.A. Mitropolsky, Asymptotic Methods in the Theory of Non-Linear Oscillations, vol. 10, CRC Press, 1961.
[87] H. Haken, Advanced synergetics: Instability hierarchies of self-organizing systems and devices, in: Springer Series in Synergetics, Springer, 1983.
[88] H. Haken, Synergetics: Introduction and Advanced Topics, Springer Science & Business Media, 2013.
[89] B. Kralemann, L. Cimponeriu, M. Rosenblum, A. Pikovsky, R. Mrowka, Uncovering interaction of coupled oscillators from data, Phys. Rev. E 76 (2007) 055201.
[90] B. Kralemann, L. Cimponeriu, M. Rosenblum, A. Pikovsky, R. Mrowka, Phase dynamics of coupled oscillators reconstructed from data, Phys. Rev. E 77 (2008) 066205.
[91] J. Guckenheimer, Isochrons and phaseless sets, J. Math. Biol. 1 (3) (1975) 259–273.
[92] S. Wiggins, Normally Hyperbolic Invariant Manifolds in Dynamical Systems, vol. 105, Springer Science & Business Media, 2013.
[93] M.R. Guevara, L. Glass, M.C. Mackey, A. Shrier, Chaos in neurobiology, IEEE Trans. Syst. Man Cybern. 13 (5) (1983) 790–798.
[94] L. Cesari, Asymptotic Behavior and Stability Problems in Ordinary Differential Equations, vol. 16, Springer Berlin Heidelberg, 1971.
[95] V. Novičenko, K. Pyragas, Computation of phase response curves via a direct method adapted to infinitesimal perturbations, Nonlinear Dynam. 67 (1) (2012) 517–526.
[96] T.L. Williams, G. Bowtell, The calculation of frequency-shift functions for chains of coupled oscillators, with application to a network model of the lamprey locomotor pattern generator, J. Comput. Neurosci. 4 (1) (1997) 47–55.
[97] B. Ermentrout, Simulating, Analyzing, and Animating Dynamical Systems: A Guide to XPPAUT for Researchers and Students, SIAM, 2002.
[98] W. Govaerts, B. Sautois, Computation of the phase response curve: A direct numerical approach, Neural Comput. 18 (4) (2006) 817–847.
[99] A. Dhooge, W. Govaerts, Y.A. Kuznetsov, H.G. Meijer, B. Sautois, New features of the software MatCont for bifurcation analysis of dynamical systems, Math. Comput. Model. Dyn. Syst. 14 (2) (2008) 147–175.
[100] A.H. Nayfeh, D.T. Mook, Nonlinear Oscillations, John Wiley & Sons, 2008.
[101] D.W. Jordan, P. Smith, Nonlinear Ordinary Differential Equations: An Introduction to Dynamical Systems, vol. 2, Oxford University Press, USA, 1999.

[102] J. Hesse, J.-H. Schleimer, S. Schreiber, Qualitative changes in phase-response curve and synchronization at the saddle-node-loop bifurcation, Phys. Rev. E 95 (2017) 052203.
[103] P. Tass, Phase resetting in medicine and biology: Stochastic modelling and data analysis, in: Springer Series in Synergetics, Springer Berlin Heidelberg, 2007.
[104] M.J. Aburn, Critical Fluctuations and Coupling of Stochastic Neural Mass Models (Ph.D. thesis), University of Queensland, 2016.
[105] P. Yu, Computation of normal forms via a perturbation technique, J. Sound Vib. 211 (1) (1998) 19–38.
[106] K. Huseyin, Multiple Parameter Stability Theory and Its Applications: Bifurcations, Catastrophes, Instabilities ..., Clarendon Press, 1986.
[107] Y.-R. Liu, J.-B. L.i, Theory of values of singular point in complex autonomous differential systems, Sci. China 33 (1) (1990) 10–23.
[108] H. Chen, Y. Liu, Linear recursion formulas of quantities of singular point and applications, Appl. Math. Comput. 148 (1) (2004) 163–171.
[109] C. Van der Beek, Normal forms and periodic solutions in the theory of non-linear oscillations. existence and asymptotic theory, Int. J. Non-Linear Mech. 24 (4) (1989) 263–279.
[110] A. Leung, Q. Zhang, Higher order normal form and period averaging, J. Sound Vib. 217 (5) (1998) 795–806.
[111] A.Y. Leung, Q. Zhang, Normal form computation without central manifold reduction, J. Sound Vib. 266 (2) (2003) 261–279.
[112] P. Coullet, E.A. Spiegel, Amplitude equations for systems with competing instabilities, SIAM J. Appl. Math. 43 (4) (1983) 776–821.
[113] D. Sattinger, Topics in stability and bifurcation theory, in: Lecture Notes in Mathematics, Springer, Berlin, Heidelberg, 1973.
[114] H. Haken, Higher order corrections to generalized Ginzburg-Landau equations of non-equilibrium systems, Z. Phys. B 22 (1) (1975) 69–72.
[115] H. Haken, Synergetics: A Workshop: Proceedings of the International Workshop on Synergetics at Schloss Elmau, Bavaria, May 2–7, 1977, in: Springer Series in Synergetics, Springer-Verlag, 1977.
[116] A. Leung, Z. Qichang, C. Yushu, Normal form analysis of Hopf bifurcation exemplified by Duffing's equation, Shock Vib. 1 (3) (1994) 233–240.
[117] A. Leung, T. Ge, An algorithm for higher order Hopf normal forms, Shock Vib. 2 (4) (1995) 307–319.
[118] N. Kopell, L.N. Howard, Plane wave solutions to reaction-diffusion equations, Stud. Appl. Math. 52 (4) (1973) 291–328.
[119] M. Newman, Networks, Oxford University Press, 2018.
[120] T.G. Lewis, Network Science: Theory and Applications, John Wiley & Sons, 2011.
[121] A.-L. Barabási, et al., Network Science, Cambridge University Press, 2016.
[122] S.N. Dorogovtsev, J.F. Mendes, Evolution of Networks: From Biological Nets To the Internet and WWW, OUP Oxford, 2013.
[123] L. da F. Costa, F.A. Rodrigues, G. Travieso, P.R.V. Boas, Characterization of complex networks: A survey of measurements, Adv. Phys. 56 (1) (2007) 167–242.
[124] R. Albert, A.-L. Barabási, Statistical mechanics of complex networks, Rev. Modern Phys. 74 (1) (2002) 47.
[125] J.J. Hopfield, Neural networks and physical systems with emergent collective computational abilities, Proc. Natl. Acad. Sci. 79 (8) (1982) 2554–2558.
[126] S. Grossberg, Nonlinear neural networks: Principles, mechanisms, and architectures, Neural Netw. 1 (1) (1988) 17–61.
[127] S. Boccaletti, V. Latora, Y. Moreno, M. Chavez, D.-U. Hwang, Complex networks: Structure and dynamics, Phys. Rep. 424 (4–5) (2006) 175–308.
[128] M. Newman, A.-L. Barabási, D.J. Watts, The Structure and Dynamics of Networks, vol. 19, Princeton University Press, 2011.
[129] S. Boccaletti, G. Bianconi, R. Criado, C.I. Del Genio, J. Gómez-Gardenes, M. Romance, I. Sendina-Nadal, Z. Wang, M. Zanin, The structure and dynamics of multilayer networks, Phys. Rep. 544 (1) (2014) 1–122.
[130] M.E. Newman, The structure and function of complex networks, SIAM Rev. 45 (2) (2003) 167–256.
[131] M. Barthélemy, Spatial networks, Phys. Rep. 499 (1–3) (2011) 1–101.
[132] S.H. Strogatz, Exploring complex networks, Nature 410 (6825) (2001) 268.
[133] P. Holme, J. Saramäki, Temporal networks, Phys. Rep. 519 (3) (2012) 97–125.
[134] R. Pastor-Satorras, C. Castellano, P. Van Mieghem, A. Vespignani, Epidemic processes in complex networks, Rev. Modern Phys. 87 (3) (2015) 925.
[135] A. Barrat, M. Barthélemy, A. Vespignani, Dynamical Processes on Complex Networks, Cambridge University Press, 2008.
[136] M.A. Porter, J.P. Gleeson, Dynamical systems on networks, in: Frontiers in Applied Dynamical Systems: Reviews and Tutorials, vol. 4, Springer, 2016.
[137] S.N. Dorogovtsev, A.V. Goltsev, J.F. Mendes, Critical phenomena in complex networks, Rev. Modern Phys. 80 (4) (2008) 1275.
[138] S. Boccaletti, J. Almendral, S. Guan, I. Leyva, Z. Liu, I. Sendiña-Nadal, Z. Wang, Y. Zou, Explosive transitions in complex networks? Structure and dynamics: Percolation and synchronization, Phys. Rep. 660 (2016) 1–94.
[139] Y. Bar-Yam, Dynamics of Complex Systems, Perseus Books, Cambridge, MA, USA, 1997.
[140] S. Boccaletti, J. Kurths, G. Osipov, D. Valladares, C. Zhou, The synchronization of chaotic systems, Phys. Rep. 366 (1) (2002) 1–101.
[141] S. Fortunato, Community detection in graphs, Phys. Rep. 486 (3–5) (2010) 75–174.
[142] L.M. Pecora, F. Sorrentino, A.M. Hagerstrom, T.E. Murphy, R. Roy, Cluster synchronization and isolated desynchronization in complex networks with symmetries, Nature Commun. 5 (2014) 4079.
[143] F. Sorrentino, L.M. Pecora, A.M. Hagerstrom, T.E. Murphy, R. Roy, Complete characterization of the stability of cluster synchronization in complex dynamical networks, Sci. Adv. 2 (4) (2016) e1501737.
[144] M. Golubitsky, I. Stewart, D.G. Schaeffer, Singularities and Groups in Bifurcation Theory, vol. 2, Springer Science & Business Media, 2012.
[145] M. Golubitsky, I. Stewart, The Symmetry Perspective: From Equilibrium to Chaos in Phase Space and Physical Space, vol. 200, Springer Science & Business Media, 2003.
[146] Y. Kawamura, H. Nakao, K. Arai, H. Kori, Y. Kuramoto, Collective phase sensitivity, Phys. Rev. Lett. 101 (2008) 024101.
[147] H. Kori, Y. Kawamura, H. Nakao, K. Arai, Y. Kuramoto, Collective-phase description of coupled oscillators with general network structure, Phys. Rev. E 80 (2009) 036207.
[148] Y. Kawamura, H. Nakao, K. Arai, H. Kori, Y. Kuramoto, Phase synchronization between collective rhythms of globally coupled oscillator groups: Noisy identical case, Chaos 20 (2010) 043109.
[149] Y. Kawamura, H. Nakao, K. Arai, H. Kori, Y. Kuramoto, Phase synchronization between collective rhythms of globally coupled oscillator groups: Noiseless non-identical case, Chaos 20 (2010) 043110.
[150] Y. Kawamura, H. Nakao, Y. Kuramoto, Collective phase description of globally coupled excitable elements, Phys. Rev. E 84 (2011) 046211.
[151] Y. Kawamura, H. Nakao, Collective phase description of oscillatory convection, Chaos 23 (4) (2013) 043129.
[152] Y. Kawamura, Phase synchronization between collective rhythms of fully locked oscillator groups, Sci. Rep. 4 (2014) 4832.
[153] Y. Kawamura, H. Nakao, Phase description of oscillatory convection with a spatially translational mode, Physica D 295–296 (2015) 11–29.
[154] H. Nakao, T. Yanagita, Y. Kawamura, Phase-reduction approach to synchronization of spatiotemporal rhythms in reaction-diffusion systems, Phys. Rev. X 4 (2) (2014) 021032.
[155] H. Nakao, S. Yasui, M. Ota, K. Arai, Y. Kawamura, Phase reduction and synchronization of a network of coupled dynamical elements exhibiting collective oscillations, Chaos 28 (4) (2018) 045103.
[156] T.-W. Ko, G.B. Ermentrout, Phase-response curves of coupled oscillators, Phys. Rev. E 79 (2009) 016211.
[157] Z. Levnajić, A. Pikovsky, Phase resetting of collective rhythm in ensembles of oscillators, Phys. Rev. E 82 (2010) 056202.

[158] K. Kotani, I. Yamaguchi, L. Yoshida, Y. Jimbo, G.B. Ermentrout, Population dynamics of the modified theta model: macroscopic phase reduction and bifurcation analysis link microscopic neuronal interactions to macroscopic gamma oscillation, J. R. Soc. Interface 11 (95) (2014) 20140058.
[159] K.M. Hannay, V. Booth, D.B. Forger, Collective phase response curves for heterogeneous coupled oscillators, Phys. Rev. E 92 (2015) 022923.
[160] G. Dumont, G.B. Ermentrout, B. Gutkin, Macroscopic phase-resetting curves for spiking neural networks, Phys. Rev. E 96 (2017) 042311.
[161] G. Dumont, B. Gutkin, Macroscopic phase resetting-curves determine oscillatory coherence and signal transfer in inter-coupled neural circuits, 2018, arXiv preprint arXiv:1812.03455.
[162] A. Akao, Y. Ogawa, Y. Jimbo, G.B. Ermentrout, K. Kotani, Relationship between the mechanisms of gamma rhythm generation and the magnitude of the macroscopic phase response function in a population of excitatory and inhibitory modified quadratic integrate-and-fire neurons, Phys. Rev. E 97 (2018) 012209.
[163] D. Wilson, B. Ermentrout, Augmented phase reduction of (not so) weakly perturbed coupled oscillators, SIAM Rev. 61 (2) (2019) 277–315.
[164] H. Nakao, Phase reduction approach to synchronisation of nonlinear oscillators, Contemp. Phys. 57 (2) (2016) 188–214.
[165] S. Gherardini, S. Gupta, S. Ruffo, Spontaneous synchronisation and nonequilibrium statistical mechanics of coupled phase oscillators, Contemp. Phys. 59 (3) (2018) 229–250.
[166] L.M. Pecora, T.L. Carroll, Master stability functions for synchronized coupled systems, Phys. Rev. Lett. 80 (10) (1998) 2109.
[167] P. Ashwin, S. Coombes, R. Nicks, Mathematical frameworks for oscillatory network dynamics in neuroscience, J. Math. Neurosci. 6 (1) (2016) 2.
[168] J. Hlinka, S. Coombes, Using computational models to relate structural and functional brain connectivity, Eur. J. Neurosci. 36 (2) (2012) 2137–2145.
[169] V. Nicosia, M. Valencia, M. Chavez, A. Díaz-Guilera, V. Latora, Remote synchronization reveals network symmetries and functional modules, Phys. Rev. Lett. 110 (17) (2013) 174102.
[170] E. Ott, T.M. Antonsen, Low dimensional behavior of large systems of globally coupled oscillators, Chaos 18 (3) (2008).
[171] D.S. Goldobin, I.V. Tyulkina, L.S. Klimenko, A. Pikovsky, Collective mode reductions for populations of coupled noisy oscillators, Chaos 28 (10) (2018) 101101.
[172] M. Rosenblum, A. Pikovsky, Self-organized quasiperiodicity in oscillator ensembles with global nonlinear coupling, Phys. Rev. Lett. 98 (2007) 064101.
[173] A. Pikovsky, M. Rosenblum, Self-organized partially synchronous dynamics in populations of nonlinearly coupled oscillators, Physica D 238 (1) (2009) 27–37.
[174] M. Rosenblum, A. Pikovsky, Two types of quasiperiodic partial synchrony in oscillator ensembles, Phys. Rev. E 92 (2015) 012919.
[175] K. Okuda, Variety and generality of clustering in globally coupled oscillators, Physica D 63 (3–4) (1993) 424–436.
[176] D. Hansel, G. Mato, C. Meunier, Clustering and slow switching in globally coupled phase oscillators, Phys. Rev. E 48 (5) (1993) 3470.
[177] H. Kori, Y. Kuramoto, S. Jain, I.Z. Kiss, J.L. Hudson, Clustering in globally coupled oscillators near a hopf bifurcation: theory and experiments, Phys. Rev. E 89 (6) (2014) 062906.
[178] H. Kori, Y. Kuramoto, Slow switching in globally coupled oscillators: robustness and occurrence through delayed coupling, Phys. Rev. E 63 (4) (2001) 046214.
[179] H. Kori, Slow switching in a population of delayed pulse-coupled oscillators, Phys. Rev. E 68 (2) (2003) 021919.
[180] P. Clusella, A. Politi, M. Rosenblum, A minimal model of self-consistent partial synchrony, New J. Phys. 18 (9) (2016) 093037.
[181] M. Komarov, A. Pikovsky, Multiplicity of singular synchronous states in the Kuramoto model of coupled oscillators, Phys. Rev. Lett. 111 (20) (2013) 204101.
[182] M. Komarov, A. Pikovsky, The Kuramoto model of coupled oscillators with a bi-harmonic coupling function, Physica D 289 (2014) 18–31.
[183] C. Bick, M. Timme, D. Paulikat, D. Rathlev, P. Ashwin, Chaos in symmetric phase oscillator networks, Phys. Rev. Lett. 107 (2011) 244101.
[184] K.K. Lin, K.C.A. Wedgwood, S. Coombes, L.-S. Young, Limitations of perturbative techniques in the analysis of rhythms and oscillations, J. Math. Biol. 66 (1) (2013) 139–161.
[185] T.I. Netoff, C.D. Acker, J.C. Bettencourt, J.A. White, Beyond two-cell networks: Experimental measurement of neuronal responses to multiple synaptic inputs, J. Comput. Neurosci. 18 (3) (2005) 287–295.
[186] D. Hansel, G. Mato, B. Pfeuty, The role of intrinsic cell properties in synchrony of neurons interacting via electrical synapses, in: N.W. Schultheiss, A.A. Prinz, R.J. Butera (Eds.), Phase Response Curves in Neuroscience: Theory, Experiment, and Analysis, Springer Science & Business Media, New York, NY, 2012, pp. 361–398.
[187] I.I. Blechmann, Synchronization of Dynamical Systems (in Russian: Sinchronizatzia Dinamicheskich Sistem), Science, Moscow, 1971.
[188] C. Bick, P. Ashwin, A. Rodrigues, Chaos in generically coupled phase oscillator networks with nonpairwise interactions, Chaos 26 (9) (2016) 094814.
[189] A. Rodrigues, Bifurcations of Dynamical Systems with Symmetry (Ph.D. thesis), University of Porto, 2007.
[190] I. Prigogine, R. Lefever, Symmetry breaking instabilities in dissipative systems. II, J. Chem. Phys. 48 (4) (1968) 1695–1700.
[191] R. Lefever, G. Nicolis, Chemical instabilities and sustained oscillations, J. Theoret. Biol. 30 (2) (1971) 267–284.
[192] G. Nicolis, I. Prigogine, Self-organization in Nonequilibrium Systems. From Dissipative Structures to Order Through Fluctuations, Wiley-Interscience, New York, 1977.
[193] B.P. Belousov, Oscillations reaction and its mechanism, Sb. Ref. Radiac. Med. (1959) 145 (in Russian).
[194] A.M. Zhabotinsky, Periodical oxidation of malonic acid in solution (a study of the Belousov reaction kinetics), Biofizika 9 (1964) 306–311.
[195] R.J. Field, M. Burger, Oscillations and Traveling Waves in Chemical Systems, Wiley, 1985.
[196] I.R. Epstein, K. Kustin, P. De Kepper, M. Orbán, Oscillating chemical reactions, Sci. Am. 248 (3) (1983) 112–123.
[197] J.J. Tyson, Some further studies of nonlinear oscillations in chemical systems, J. Chem. Phys. 58 (9) (1973) 3919–3930.
[198] K. Bar-Eli, On the stability of coupled chemical oscillators, Physica D 14 (2) (1985) 242–252.
[199] A. Nandi, G. Santhosh, R.K.B. Singh, R. Ramaswamy, Effective mechanisms for the synchronization of stochastic oscillators, Phys. Rev. E 76 (2007) 041136.
[200] I.Z. Kiss, W. Wang, J.L. Hudson, Experiments on arrays of globally coupled periodic electrochemical oscillators, J. Phys. Chem. B 103 (51) (1999) 11433–11444.
[201] I.Z. Kiss, Y. Zhai, J.L. Hudson, Predicting mutual entrainment of oscillators with experiment-based phase models, Phys. Rev. Lett. 94 (2005) 248301.
[202] I.Z. Kiss, C.G. Rusin, H. Kori, J.L. Hudson, Engineering complex dynamical structures: Sequential patterns and desynchronization, Science 316 (5833) (2007) 1886–1889.
[203] M. Wickramasinghe, I.Z. Kiss, Synchronization of electrochemical oscillators with differential coupling, Phys. Rev. E 88 (2013) 062911.
[204] H.K. Sarmah, M.C. Das, T.K. Baishya, Hopf bifurcation in a chemical model, Int. J. Innov. Res. Sci. Technol. 1 (9) (2015) 23–33.
[205] Y. Zhai, I.Z. Kiss, H. Daido, J.L. Hudson, Extracting order parameters from global measurements with application to coupled electrochemical oscillators, Physica D 205 (1) (2005) 57–69, Synchronization and Pattern Formation in Nonlinear Systems: New Developments and Future Perspectives.
[206] K. Taira, H. Nakao, Phase-response analysis of synchronization for periodic flows, 2018, arXiv preprint arXiv:1804.01274.

[207] Y. Kawamura, R. Tsubaki, Phase reduction approach to elastohydrodynamic synchronization of beating flagella, Phys. Rev. E 97 (2018) 022212.
[208] Y. Kawamura, Collective phase reduction of globally coupled noisy dynamical elements, Phys. Rev. E 95 (2017) 032225.
[209] A.C. Marreiros, J. Daunizeau, S.J. Kiebel, K.J. Friston, Population dynamics: variance and the sigmoid activation function, Neuroimage 42 (1) (2008) 147–157.
[210] D.J. Pinto, J.C. Brumberg, D.J. Simons, G.B. Ermentrout, R. Traub, A quantitative population model of whisker barrels: re-examining the Wilson-Cowan equations, J. Comput. Neurosci. 3 (3) (1996) 247–264.
[211] R.M. Borisyuk, A.B. Kirillov, Bifurcation analysis of a neural network model, Biol. Cybernet. 66 (4) (1992) 319–325.
[212] A. Daffertshofer, R. Ton, B. Pietras, M.L. Kringelbach, G. Deco, Scale-freeness or partial synchronization in neural mass phase oscillator networks: Pick one of two? NeuroImage (2018).
[213] D.G. Aronson, G.B. Ermentrout, N. Kopell, Amplitude response of coupled oscillators, Physica D 41 (3) (1990) 403–449.
[214] R.E. Mirollo, S.H. Strogatz, Amplitude death in an array of limit-cycle oscillators, J. Stat. Phys. 60 (1) (1990) 245–262.
[215] A. Sen, R. Dodla, G.L. Johnston, G.C. Sethia, Amplitude death, synchrony, and chimera states in delay coupled limit cycle oscillators, in: F.M. Atay (Ed.), Complex Time-Delay Systems: Theory and Applications, Springer Berlin Heidelberg, Berlin, Heidelberg, 2010, pp. 1–43.
[216] G. Saxena, A. Prasad, R. Ramaswamy, Amplitude death: The emergence of stationarity in coupled nonlinear systems, Phys. Rep. 521 (5) (2012) 205–228.
[217] A. Koseska, E. Volkov, J. Kurths, Oscillation quenching mechanisms: Amplitude vs. oscillation death, Phys. Rep. 531 (4) (2013) 173–199.
[218] J. Sun, E.M. Bollt, T. Nishikawa, Master stability functions for coupled nearly identical dynamical systems, Europhys. Lett. 85 (6) (2009) 60011.
[219] F. Sorrentino, M. Porfiri, Analysis of parameter mismatches in the master stability function for network synchronization, Europhys. Lett. 93 (5) (2011) 50002.
[220] Y. Zhang, A.E. Motter, Identical synchronization of nonidentical oscillators: when only birds of different feathers flock together, Nonlinearity 31 (1) (2018) R1.
[221] A. Pikovsky, M. Rosenblum, Dynamics of heterogeneous oscillator ensembles in terms of collective variables, Physica D 240 (9) (2011) 872–881.
[222] S. Watanabe, S.H. Strogatz, Constants of motion for superconducting Josephson arrays, Physica 74D (3) (1994) 197–253.
[223] E. Ott, T.M. Antonsen, Long time evolution of phase oscillator systems, Chaos 19 (2) (2009).
[224] B. Pietras, A. Daffertshofer, Ott-Antonsen attractiveness for parameter-dependent oscillatory systems, Chaos 26 (10) (2016) 103101.
[225] C. Bick, M. Goodfellow, C.R. Laing, E.A. Martens, Understanding the dynamics of biological and neural oscilaltor networks through mean-field reductions: a review, 2019, ArXiv e-prints, arXiv:1902.05307.
[226] T. Stankovski, T. Pereira, P.V. McClintock, A. Stefanovska, Coupling functions: Universal insights into dynamical interaction mechanisms, 2017, arXiv preprint arXiv:1706.01810.
[227] R.D. Traub, R. Wong, Synchronized burst discharge in disinhibited hippocampal slice. I. Initiation in CA2-CA3 region, J. Neurophysiol. 49 (2) (1983) 442–458.
[228] E. Brown, J. Moehlis, P. Holmes, E. Clayton, J. Rajkowski, G. Aston-Jones, The influence of spike rate and stimulus duration on noradrenergic neurons, J. Comput. Neurosci. 17 (1) (2004) 13–29.
[229] Y. Maruyama, Y. Kakimoto, O. Araki, Analysis of chaotic oscillations induced in two coupled Wilson–Cowan models, Biol. Cybernet. 108 (3) (2014) 355–363.
[230] E.M. Izhikevich, Weakly connected quasi-periodic oscillators, FM interactions, and multiplexing in the brain, SIAM J. Appl. Math. 59 (6) (1999) 2193–2223.
[231] A. Demirt, C. Gu, J. Roychowdhury, Phase equations for quasi-periodic oscillators, in: Computer-Aided Design (ICCAD), 2010 IEEE/ACM International Conference on, IEEE, 2010, pp. 292–297.
[232] J.T.C. Schwabedal, A. Pikovsky, B. Kralemann, M. Rosenblum, Optimal phase description of chaotic oscillators, Phys. Rev. E 85 (2012) 026216.
[233] M. Benayoun, J.D. Cowan, W. van Drongelen, E. Wallace, Avalanches in a stochastic model of spiking neurons, PLoS Comput. Biol. 6 (7) (2010) e1000846.
[234] E. Wallace, M. Benayoun, W. Van Drongelen, J.D. Cowan, Emergent oscillations in networks of stochastic spiking neurons, PloS One 6 (5) (2011) e14804.
[235] G. Gigante, G. Deco, S. Marom, P. Del Giudice, Network events on multiple space and time scales in cultured neural networks and in a stochastic rate model, PLoS Comput. Biol. 11 (11) (2015) 1–23.
[236] I. Goychuk, A. Goychuk, Stochastic Wilson–Cowan models of neuronal network dynamics with memory and delay, New J. Phys. 17 (4) (2015) 045029.
[237] J.D. Cowan, J. Neuman, W. van Drongelen, Wilson–Cowan Equations for Neocortical Dynamics, J. Math. Neurosci. 6 (1) (2016) 1.
[238] C. Zankoc, T. Biancalani, D. Fanelli, R. Livi, Fluctuating hydrodynamics approximation of the stochastic Cowan-Wilson model, 2016, arXiv preprint arXiv:1611.00300.
[239] P.C. Bressloff, Spatiotemporal dynamics of continuum neural fields, J. Phys. A 45 (3) (2011) 033001.
[240] C. Kuehn, M.G. Riedler, Large deviations for nonlocal stochastic neural fields, J. Math. Neurosci. 4 (1) (2014) 1.
[241] T. Schwalger, M. Deger, W. Gerstner, Towards a theory of cortical columns: From spiking neurons to interacting neural populations of finite size, PLoS Comput. Biol. 13 (4) (2017) 1–63.
[242] J.T.C. Schwabedal, A. Pikovsky, Phase description of stochastic oscillations, Phys. Rev. Lett. 110 (2013) 204102.
[243] P.J. Thomas, B. Lindner, Asymptotic phase for stochastic oscillators, Phys. Rev. Lett. 113 (2014) 254101.
[244] J.-n. Teramae, D. Tanaka, Robustness of the noise-induced phase synchronization in a general class of limit cycle oscillators, Phys. Rev. Lett. 93 (2004) 204103.
[245] K. Yoshimura, K. Arai, Phase reduction of stochastic limit cycle oscillators, Phys. Rev. Lett. 101 (2008) 154101.
[246] J.-n. Teramae, H. Nakao, G.B. Ermentrout, Stochastic phase reduction for a general class of noisy limit cycle oscillators, Phys. Rev. Lett. 102 (2009) 194102.
[247] P.C. Bressloff, Stochastic Fokker-Planck equation in random environments, Phys. Rev. E 94 (4) (2016) 042129.
[248] C. Gardiner, Stochastic Methods: A Handbook for the Natural and Social Sciences, in: Springer Series in Synergetics, Springer Berlin Heidelberg, 2009.
[249] Y. Kawamura, H. Nakao, Y. Kuramoto, Noise-induced turbulence in nonlocally coupled oscillators, Phys. Rev. E 75 (2007) 036209.
[250] Y. Kawamura, Collective phase dynamics of globally coupled oscillators: Noise-induced anti-phase synchronization, Physica D 270 (2014) 20–29.
[251] W. Kurebayashi, S. Shirasaka, H. Nakao, Phase reduction method for strongly perturbed limit cycle oscillators, Phys. Rev. Lett. 111 (21) (2013) 214101.
[252] Y. Park, B. Ermentrout, Weakly coupled oscillators in a slowly varying world, J. Comput. Neurosci. 40 (3) (2016) 269–281.
[253] V.K. Jirsa, Neural field dynamics with local and global connectivity and time delay, Philos. Trans. R. Soc. Lond. Ser. A Math. Phys. Eng. Sci. 367 (1891) (2009) 1131–1143.
[254] K.J. Friston, The labile brain. I. Neuronal transients and nonlinear coupling, Philos. Trans. R. Soc. B 355 (1394) (2000) 215–236.

[255] K. Pyragas, V. Novičenko, Phase reduction of a limit cycle oscillator perturbed by a strong amplitude-modulated high-frequency force, Phys. Rev. E 92 (2015) 012910.
[256] V. Jirsa, V. Müller, Cross-frequency coupling in real and virtual brain networks, Front. Comput. Neurosci. 7 (2013).
[257] T. Stankovski, V. Ticcinelli, P.V. McClintock, A. Stefanovska, Neural cross-frequency coupling functions, Front. Syst. Neurosci. 11 (2017).
[258] D.H. Zanette, Propagating structures in globally coupled systems with time delays, Phys. Rev. E 62 (3) (2000) 3167.
[259] S.-O. Jeong, T.-W. Ko, H.-T. Moon, Time-delayed spatial patterns in a two-dimensional array of coupled oscillators, Phys. Rev. Lett. 89 (2002) 154104.
[260] T.-W. Ko, G.B. Ermentrout, Effects of axonal time delay on synchronization and wave formation in sparsely coupled neuronal oscillators, Phys. Rev. E 76 (2007) 056206.
[261] B. Ermentrout, T.-W. Ko, Delays and weakly coupled neuronal oscillators, Philos. Trans. R. Soc. Lond. Ser. A Math. Phys. Eng. Sci. 367 (1891) (2009) 1097–1115.
[262] S. Petkoski, A. Spiegler, T. Proix, P. Aram, J.-J. Temprado, V.K. Jirsa, Heterogeneity of time delays determines synchronization of coupled oscillators, Phys. Rev. E 94 (1) (2016) 012209.
[263] K. Engelborghs, T. Luzyanina, D. Roose, Numerical bifurcation analysis of delay differential equations using DDE-BIFTOOL, ACM Trans. Math. Softw. 28 (1) (2002) 1–21.
[264] J. Sieber, K. Engelborghs, T. Luzyanina, G. Samaey, D. Roose, DDE-BIFTOOL Manual-bifurcation analysis of delay differential equations, 2014, arXiv preprint arXiv:1406.7144.
[265] S. Coombes, C. Laing, Delays in activity-based neural networks, Philos. Trans. R. Soc. Lond. Ser. A Math. Phys. Eng. Sci. 367 (1891) (2009) 1117–1129.
[266] Z.-G. Song, J. Xu, Stability switches and double Hopf bifurcation in a two-neural network system with multiple delays, Cogn. Neurodynam. 7 (6) (2013) 505–521.
[267] V. Novičenko, K. Pyragas, Phase reduction of weakly perturbed limit cycle oscillations in time-delay systems, Physica D 241 (12) (2012) 1090–1098.
[268] K. Kotani, I. Yamaguchi, Y. Ogawa, Y. Jimbo, H. Nakao, G.B. Ermentrout, Adjoint method provides phase response functions for delay-induced oscillations, Phys. Rev. Lett. 109 (4) (2012) 044101.
[269] S. Smale, A mathematical model of two cells via Turing's equation, in: The Hopf Bifurcation and Its Applications, Springer New York, New York, NY, 1976, pp. 354–367.
[270] Ö. Suvak, A. Demir, Quadratic approximations for the isochrons of oscillators: A general theory, advanced numerical methods, and accurate phase computations, IEEE Trans. Comput.-Aided Des. Integr. Circuits Syst. 29 (8) (2010) 1215–1228.
[271] D. Takeshita, R. Feres, Higher order approximation of isochrons, Nonlinearity 23 (6) (2010) 1303.
[272] A. Bruno, W. Hovingh, C. Coleman, Local methods in nonlinear differential equations: Part I the local method of nonlinear analysis of differential equations Part II the sets of analyticity of a normalizing transformation, in: Springer Series in Soviet Mathematics, Springer Berlin Heidelberg, 1989.
[273] P.B. Kahn, Y. Zarmi, Nonlinear Dynamics: Exploration Through Normal Forms, Courier Corporation, 2014.
[274] C. Elphick, E. Tirapegui, M. Brachet, P. Coullet, G. Iooss, A simple global characterization for normal forms of singular vector fields, Physica D 29 (1–2) (1987) 95–127.
[275] R. Cushman, J.A. Sanders, Nilpotent Normal Forms and Representation Theory of sl(2, $\mathbb{R}$), Vrije Universiteit Amsterdam, Subfaculteit Wiskunde en Informatica, 1985.
[276] J. Murdock, Hypernormal form theory: foundations and algorithms, J. Differential Equations 205 (2) (2004) 424–465.
[277] G.R. Belitskii, Invariant normal forms of formal series, Funct. Anal. Appl. 13 (1) (1979) 46–47.
[278] A. Baider, Unique normal forms for vector fields and Hamiltonians, J. Differential Equations 78 (1) (1989) 33–52.
[279] A. Baider, R. Churchill, Unique normal forms for planar vector fields, Math. Z. 199 (3) (1988) 303–310.
[280] A. Mauroy, I. Mezić, J. Moehlis, Isostables, isochrons, and Koopman spectrum for the action-angle representation of stable fixed point dynamics, Physica D 261 (2013) 19–30.
[281] M. Budišić, R. Mohr, I. Mezić, Applied Koopmanism, Chaos 22 (4) (2012) 047510.
[282] S. Shirasaka, W. Kurebayashi, H. Nakao, Phase-amplitude reduction of transient dynamics far from attractors for limit-cycling systems, Chaos 27 (2) (2017) 023119.
[283] J. Hale, Ordinary differential equations, in: Pure and Applied Mathematics, Wiley-Interscience, 1969.
[284] G.S. Medvedev, Synchronization of coupled stochastic limit cycle oscillators, Phys. Lett. A 374 (15) (2010) 1712–1720.
[285] K.C. Wedgwood, K.K. Lin, R. Thul, S. Coombes, Phase-amplitude descriptions of neural oscillator models, J. Math. Neurosci. 3 (1) (2013) 2.
[286] W. Ott, M. Stenlund, From limit cycles to strange attractors, Comm. Math. Phys. 296 (1) (2010) 215–249.
[287] A.J. Roberts, Appropriate initial conditions for asymptotic descriptions of the long term evolution of dynamical systems, J. Aust. Math. Soc. Ser. B. Appl. Math. 31 (1) (1989) 48–75.
[288] S.M. Cox, A. Roberts, Initial conditions for models of dynamical systems, Physica D 85 (1) (1995) 126–141.
[289] D. Wilson, J. Moehlis, Isostable reduction of periodic orbits, Phys. Rev. E 94 (2016) 052213.
[290] D. Wilson, B. Ermentrout, Greater accuracy and broadened applicability of phase reduction using isostable coordinates, J. Math. Biol. (2017).
[291] O. Castejón, A. Guillamon, G. Huguet, Phase-amplitude response functions for transient-state stimuli, J. Math. Neurosci. 3 (1) (2013) 13.
[292] B. Monga, D. Wilson, T. Matchen, J. Moehlis, Phase reduction and phase-based optimal control for biological systems: a tutorial, Biol. Cybern. (2018).
[293] I. Mezić, Analysis of fluid flows via spectral properties of the Koopman operator, Annu. Rev. Fluid Mech. 45 (1) (2013) 357–378.
[294] Y. Lan, I. Mezić, Linearization in the large of nonlinear systems and Koopman operator spectrum, Physica D 242 (1) (2013) 42–53.
[295] P.V. Kuptsov, U. Parlitz, Theory and computation of covariant Lyapunov vectors, J. Nonlinear Sci. 22 (5) (2012) 727–762.
[296] F.L. Traversa, M. Bonnin, F. Corinto, F. Bonani, Noise in oscillators: a review of state space decomposition approaches, J. Comput. Electron. 14 (1) (2015) 51–61.
[297] A. Pikovsky, A. Politi, Lyapunov Exponents: A Tool to Explore Complex Dynamics, Cambridge University Press, 2016.
[298] G. Froyland, T. Hüls, G.P. Morriss, T.M. Watson, Computing covariant Lyapunov vectors, Oseledets vectors, and dichotomy projectors: A comparative numerical study, Physica D 247 (1) (2013) 18–39.
[299] T. Hüls, Computing stable hierarchies of fiber bundles, Discrete Contin. Dyn. Syst. Ser. B 22 (2017) 3341–3367.
[300] R. Grimshaw, Nonlinear Ordinary Differential Equations, CRC Press, Baca Raton, 1993.
[301] C.A. Klausmeier, Floquet theory: a useful tool for understanding nonequilibrium dynamics, Theor. Ecol. 1 (3) (2008) 153–161.
[302] D. Wilson, Isostable reduction of oscillators with piecewise smooth dynamics and complex floquet multipliers, Phys. Rev. E 99 (2019) 022210.
[303] P. Langfield, B. Krauskopf, H.M. Osinga, Solving Winfree's puzzle: The isochrons in the FitzHugh-Nagumo model, Chaos 24 (1) (2014) 013131.
[304] H. Osinga, J. Moehlis, Continuation-based computation of global isochrons, SIAM J. Appl. Dyn. Syst. 9 (4) (2010) 1201–1228.
[305] E.J. Doedel, AUTO: A program for the automatic bifurcation analysis of autonomous systems, Congr. Numer 30 (1981) 265–284.
[306] A. Mauroy, I. Mezić, On the use of Fourier averages to compute the global isochrons of (quasi) periodic dynamics, Chaos 22 (3) (2012) 033112.

[307] A. Mauroy, I. Mezić, Global computation of phase-amplitude reduction for limit-cycle dynamics, 2018, ArXiv e-prints, arXiv:1803.07379.
[308] A. Guillamon, G. Huguet, A computational and geometric approach to phase resetting curves and surfaces, SIAM J. Appl. Dyn. Syst. 8 (3) (2009) 1005–1042.
[309] G. Huguet, R. de la Llave, Computation of limit cycles and their isochrons: Fast algorithms and their convergence, SIAM J. Appl. Dyn. Syst. 12 (4) (2013) 1763–1802.
[310] X. Cabré, E. Fontich, R. de la Llave, The parameterization method for invariant manifolds III: overview and applications, J. Differential Equations 218 (2) (2005) 444–515.
[311] N. Goldenfeld, O. Martin, Y. Oono, Intermediate asymptotics and renormalization group theory, J. Sci. Comput. 4 (4) (1989) 355–372.
[312] N. Goldenfeld, O. Martin, Y. Oono, F. Liu, Anomalous dimensions and the renormalization group in a nonlinear diffusion process, Phys. Rev. Lett. 64 (12) (1990) 1361.
[313] T. Kunihiro, The renormalization-group method applied to asymptotic analysis of vector fields, Progr. Theoret. Phys. 97 (2) (1997) 179–200.
[314] A. Hutt, A. Daffertshofer, U. Steinmetz, Detection of mutual phase synchronization in multivariate signals and application to phase ensembles and chaotic data, Phys. Rev. E 68 (2003) 036219.